CLUSTERS OF GALAXIES

Martin R. Green

A thesis submitted for the degree of

Doctor of Philosophy in the

University of Oxford

Corpus Christi College

Oxford

December 1978

Clusters of Galaxies

Martin R. Green

Corpus Christi College
Oxford

Submitted for the degree
of Doctor of Philosophy

Michaelmas Term 1978

Abstract

The observations on which this thesis are based are of three types:

i) Spectroscopy of southern galaxies from which redshifts have been determined. These redshifts have enabled the calculation of velocity dispersions of the galaxies in five clusters of galaxies: Klemola 44, Sersic 40/6, 2354-35, A496 and the Pavo Group. Redshifts of galaxies in several other southern clusters have also been obtained.

ii) Photographic Photometry using digitised two-dimensional micro-densitometer scans of IIIaJ Schmidt plates of two southern clusters of galaxies: K44 and Sersic 40/6. Similar photometry of two other clusters, A1146 and 2354-35, is also available. Magnitudes in the B-band to a limiting isophote of 27mag/□" are obtained for all galaxies to a limiting magnitude of ~20 within a ~2Mpc (H_o = 50 km s^{-1} Mpc^{-1}) square around the cluster. Methods of distinguishing stars from galaxies are discussed.

iii) Photoelectric photometry through several circular apertures of 21 bright southern galaxies, using the B, V, R and I bands. As well as providing catalogue data for southern galaxies, these readings supply magnitude zero-points for the photographic photometry of clusters.

The results are discussed in the light of current theories of the morphology, formation and evolution of clusters of galaxies. The X-ray flux from clusters of galaxies is found to be consistent with emission by bremsstrahlung from a hot intracluster gas. Four of the clusters: Klemola 44, 2354-35, A1146 and Sersic 40/6 contain cD galaxies. These galaxies increase in ellipticity with radius and are aligned with their clusters (except A1146); such properties are predicted if cD galaxies evolve by accretion of other galaxies. It is suggested that Klemola 44 may be undergoing a phase of rapid core evolution, leading to the accretion of the core by the cD galaxy. The cluster 2354-35 may have already passed through this evolutionary stage.

Here was very fine discourses - and experiments; but I do lack philosophy enough to understand them, and so cannot remember them.

Pepys: Diary 1 March 1665

O dark dark dark. They all go into the dark,
The vacant interstellar spaces, the vacant into the vacant,

Eliot: East Coker III

Only connect....

Forster: Howards End

CONTENTS

Chapter 1 Introduction

1.1: Caveat Emptor

Based as it is on optical observations of clusters of galaxies, this thesis is perforce a biassed view. Although X-ray and radio data will be used in this study, it remains essentially an investigation of the visible properties of clusters. In the near future such a narrow approach to the subject will be less tenable as high-resolution X-ray telescopes begin to explore the distribution of gas in clusters and make possible accurate X-ray spectroscopy, but for the present only optical data provide sufficient detail.

Another restriction of the work described here is the assumption that the accepted laws of physics are applicable to the enormous length scales and extreme conditions found in extragalactic astronomy. Gravity has been verified experimentally only on the much smaller scales of the solar system and compact stellar systems. It seems quite likely that an extrapolation by 8 orders of magnitude in size may be unjustified, especially as the nature of space itself is still poorly understood. The use of units such as the Mpc conceals the vastness of the distances and leads to unwise confidence in the correctness of the physics being used.

1.2: Notation and Conventions

Normal astronomical usage has been followed where possible and notations and conventions that may not be obvious are shown in Table 1.1. The values used for H_o and q_o do not reflect any belief in their truth; the choice was made for mathematical convenience and

consistency with other workers in the field. Similarly the Ångstrom has been used as the unit of wavelength to conform to usual practice in redshift measurements.

1.3: Background

The details of the background to cluster research have already been adequately described by a number of authors. Bahcall (1977a) van den Bergh (1977a), Abell (1975) and de Vaucouleurs (1977) have given recent reviews. No attempt will be made in the present work to cover this ground once more; instead a rough outline of the history of cluster research is given in this section, and in the following section is a rather more detailed description of work in the southern hemisphere since the clusters with which the rest of this thesis is concerned lie in the southern sky.

A group of four galaxies is visible to the naked eye: M31, LMC, SMC and the Milky Way. The apparent difference between these objects resulted in their true nature remaining unrecognised until the present century. In the 19th century the great survey work of the Herschels and others showed that such nebulae were not unusual objects but that there were thousands spread across the sky. It was realised that the nebulae were distributed unevenly; von Humboldt (1866) described the major aggregations of the nebulae that had been found. Around the turn of the century Wolf was investigating these "nebelhäufen" (e.g. Wolf 1901) but little interest was aroused, if only because the true nature of the nebulae was unknown. Research was hindered by the still primitive state of astronomical photography; the human eye is ill-designed for examining faint low surface brightness objects.

Once it was clear that many of the nebulae are the "island universes" of Kant, then it was apparent that space contains a very uneven spread of these "galaxies". Shapley (1933) catalogued the clusters of galaxies that he found and was able to derive luminosity functions for them. Baade (1928) had already measured the luminosity function of the cluster now known as A1377, as had Shapley & Ames (1926) for the Virgo Cluster. Zwicky and Sinclair Smith were also studying clusters in this period and both discovered the "missing mass" problem when considering the differences between the redshifts of galaxies in the same cluster; the problem remains unsolved.

The development of the Schmidt telescope, culminating in the Palomar Sky Survey, led to a much clearer overall view of the extra-galactic Universe. In the 1950's there were the first attempts to describe the clustering of galaxies statistically; Neyman et al (1954) used the galaxy counts from Astrograph plates by Shane & Wirtanen (1967 & refs. therein). More recently Totsuji & Kihara (1969) and Peebles and co-workers in a long series of papers (Groth & Peebles 1977 & refs. therein) have used a similar approach, attempting to correlate the the positions of galaxies on the sky. Peebles has also used power spectrum analysis, an equivalent technique in the Fourier domain.

The most important result has been that galaxies are clustered on all scales up to the size of superclusters (aggregations of several groups and clusters). The two-dimensional, two-point correlation function function is given by:-

$$dP = N\,(1 + w(\theta))\,d\Omega$$

where N is the mean number of galaxies per steradian and dP is the probability of finding a second galaxy within a solid angle $d\Omega$ at angle

θ away from a randomly chosen galaxy. It is found that $w(\theta) \propto \theta^{1-\gamma}$ with $\gamma \approx 1.8$ over scales up to 20Mpc.

Theoretically, more detailed information can be derived from the correlation functions between greater numbers of galaxies, defined similarly to the two-point function, but Peebles has found that even with the three-point function the noise is large and the results are difficult to interpret.

The results of these statistical studies are especially useful when interpreting the present state of the Universe in terms of cosmological models. However, they confuse information about various parts of galaxy aggregations with each other and give no particular results for individual systems. They are certainly no replacement for the study of individual clusters which, since they are probably partially relaxed dynamical systems, are expected to be rather special regions.

The terminology and taxonomy of clusters is confused since they do not form simple discrete classes. In practice, "cluster of galaxies" has come to mean a collection of galaxies that is rich (i.e. populous) and dense enough to merit inclusion in the Abell (1958) cluster catalogue. Thus a cluster has 30 or more galaxies within 2 magnitudes of its third brightest member once a correction for background and foreground galaxies has been made. For the purposes of this definition a projected radius of ~3Mpc from the cluster centre is used as the cluster boundary, but the profiles of clusters do not show cut-offs at any particular radius. The surface density of galaxies on the sky usually varies approximately inversely with the distance from the centre, so much of the membership of a cluster may be in the outer regions.

The existence of a true "field" of galaxies that are members of no groups or clusters has been debated extensively. Part of the difficulty lies in the definition of "member", but it does seem that there are remarkably few galaxies in some regions of space (Gregory & Thompson 1978, Joeveer et al 1978).

The northern hemisphere was thoroughly catalogued by Abell (1958) and Zwicky et al (1961-8). Although not perfect these catalogues provide a solid basis for cluster research. Classification of the clusters has been by several systems, but until the relationship between the different properties of clusters is understood, these schemes must remain arbitrary and descriptive only. Galaxies and clusters are too pathological to fit neatly into elegant classification schemes without a deeper understanding of the reasons for the differences between them.

The most important classification is Abell's (1958) richness parameter, although this provides only a very approximate estimate of the cluster population. The Bautz-Morgan (1970) system of typing clusters by the comparative magnitudes of their brightest members is also often used, but it is very susceptible to contamination by field galaxies. The most useful system for classifying the morphology of clusters is the Rood-Sastry (1971) method which takes account of the distribution of galaxies in the cluster as well as the nature of the brightest member galaxies.

A distinction has often been made between rich, symmetric clusters that have a large proportion of elliptical galaxies in their populations, and loose clouds of spiral galaxies. This contrast was noted by Shapley (1933) who pointed out the analogy with globular and galactic star clusters. Abell (1965) used the contrast as a basic

method of classifying clusters, as did Oemler (1974).

The emphasis has shifted in recent years to embrace a more detailed study of the processes of evolution that may be occuring in clusters. Not only do the galaxies themselves evolve, but there are changes with time in the distribution of galaxies in the cluster caused by n-body dynamics, and the galaxies are affected by interactions with other galaxies and the gas that fills the cluster. These processes will be discussed later in this thesis.

1.4 Southern Cluster Research

Extragalactic astronomy has lagged in the South. No doubt the gap will be closed with the increase in the number of large telescopes available there. The southern photographic surveys have encouraged an increase in interest in southern objects, as have all-sky X-ray surveys.

The first extragalactic astronomy in the South was by John Herschel who led an expedition to South Africa, leaving England in 1833. He swept the sky from Cape Town and found many nebulae which he later put in his General Catalogue. Other southern nebulae found in the 19th century are listed in the Index Catalogue; most of these were discovered from above the equator. The coverage is very imperfect, particularly near the South Celestial Pole, and many bright galaxies that would have been recorded in the North do not appear in either the NGC or IC. The Shapley-Ames catalogue (1932) and its successors RCBG1 and RCBG2 have been less uneven, although basic data are lacking for many bright southern galaxies. The research of the 19th century was sufficient to show that in the South, as in the North, the nebulae

are distributed unevenly, and several clusters were found (e.g. K44, see Chap. 2).

Shapley (1933) listed several southern clusters in his catalogue; they were found in photographic surveys. As well as noting their positions he also derived their luminosity functions. Humason, Mayall & Sandage (1956) included some southern clusters in their work, but concentrated on northern clusters. The Zwicky catalogue (Zwicky et al 1961-8) is northern, as is the Uppsala catalogue of galaxies (Nilson 1973). Although the Abell (1958) catalogue and the MCG cover the northern part of the southern hemisphere, they are of lower quality in the South. All these catalogues were based on the Palomar Sky Survey. The Whiteoak Extension Survey down to $\delta = -45^{\circ}$ is of only limited value because of the high sky brightness and poor seeing resulting from the large zenith distances at which the plates were taken.

Klemola (1969), Snow(1970) and Rose (1976) were able to produce lists of southern clusters on plates taken for astrometric purposes. Klemola's and Snow's lists are mixed collections of groups and clusters; Rose's is more uniform, covering a large area of sky near the South Galactic Pole. Sérsic (1974) has also listed southern clusters.

The quality of the southern survey plates being taken by the ESO and UK Schmidt telescopes is very good. In particular, the blue sensitive IIIaJ plates from the UK Schmidt are considerably better than those taken for the Palomar Survey. Abell & Corwin are at present (1978) using these plates to compile a comprehensive southern cluster catalogue, similar to the Abell (1958) catalogue. As well as acting as the standard reference list for the cluster descriptions

and positions, this will provide a uniform nomenclature system to replace the present confusion.

Already two lists have been published of clusters found on plates of the ESO survey (Duus & Newell 1977, Braid & MacGillivray 1978). They give estimates of the richness and distances of the clusters as well as the cluster positions.

1.5: Arrangement of this thesis

Subsequent chapters describe and discuss the observations made on clusters of galaxies. The clusters examined are all in the southern sky; brief descriptions of them are given in Chap. 2.

The telescopic observations were all carried out at the Sutherland site of the SAAO. Redshift data were collected for 5 clusters: K44, S40/6, 2354-35, A496 and the Pavo Group. The methods used are outlined in Chaps. 3 and 4, and the velocities of the galaxies and the derived velocity dispersions are discussed in Chap. 5.

Photographic photometry has been carried out on 3 of these clusters, (K44, S40/6 and 2354-35), and on one other, (A1146); this work is described in Chap. 7 and the results discussed in Chap. 8. As part of this programme of cluster photometry, photoelectric readings (see Chap. 6) were made on bright galaxies in the fields of clusters; these readings were used to provide zero-points for the photographic photometry.

All the clusters examined, except the Pavo Group, have a cD-type galaxy at their centre. The final chapter attempts to review the observations in terms of the current theories of the formation of

these galaxies and the evolution of clusters. The X-ray emission of clusters and the missing-mass problem are also discussed.

Data from the observations are given in a series of 6 appendices. The first and second contain detailed data on the spectroscopic observations and the derived redshifts. The third shows finding charts for clusters and galaxies. The results of the photographic photometry, both lists of galaxy magnitudes and charts for the 4 clusters, are given in the fourth appendix. The fifth contains the photoelectric photometry results and the sixth appendix summarises the most important data available for the clusters.

Table 1.1: Notation etc.

Abbreviations:

SAAO = South African Astronomical Observatory
ESO = European Southern Observatory
RGO = Royal Greenwich Observatory
AAT = Anglo-Australian Telescope
APM = Automatic Plate Measuring System (Cambridge)

Catalogues:

2U = Giacconi et al (1972)
3U = Giacconi et al (1974)
4U = Forman et al (1978)
2A = Cooke et al (1978)
A = Abell (1958)
K = Klemola (1969)
S = Sersic (1974)
NGC = N = Dreyer (1888)
IC = I = Dreyer (1910)
MCG = Vorontsov-Velyaminov et al (1962-8)
RCBG1 = de Vaucouleurs & de Vaucouleurs (1964)
RCBG2 = de Vaucouleurs et al (1976)
SAO = Smithsonian Astrophysical Observatory (1966)

Notation:

$H_o = 50$ km s^{-1} Mpc^{-1} Hubble constant
$q_o = +1$ deceleration parameter
μ_B surface brightness in B-band
B_{27} isophotal apparent magnitude in B-band, limiting isophote $\mu_B = 27 mag/\square''$
$M_{B_{27}}$ absolute isophotal B-band magnitude
R Abell richness class
BM Bautz-Morgan morphological class.
$M_\odot, L_\odot$ Solar mas and luminosity.

Chapter 2: Descriptions of the Clusters

This chapter describes the clusters of galaxies that are investigated in the rest of this work. The most detailed descriptions are those of the 4 clusters (K44, S40/6, 2354-35 & A1146) for which there exist compatible sets of B_{27} galaxy magnitudes. Appendix IV gives lists and maps of galaxies in these clusters; finding charts for the other clusters are given in App. III. The basic data for all the clusters are tabulated in App. VI; the derivation of these data, and their interpretation, are described the rest of this work.

2.1 Klemola 44 (K44)

K44 is catalogued as $23^h45.4^m-28^o23'$ in Braid & MacGillivray (1978), where it is described as fairly distant and very rich. Duus & Newell (1977) list it as STR2345-284. Although normally known by its designation in Klemola's (1969) list of southern groups and clusters of galaxies, it was originally recorded in the late 19th century; Swift (1898) noted it as a group of 5 galaxies on the night of 1896 Sept. 14 and Howe (1899) also observed it. The Second Index Catalogue (Dreyer 1910) includes the brightest galaxies in K44 and they are also noted in the MCG. Maccacaro et al (1977) in their study of K44 used their own lettering system for the galaxies, and Chincarini et al (1978) also used their own system, but included cross-references to the MCG and IC (erroneously prefixing the IC numbers with an "N"). The designations by other workers, and those used here, are collated in Table 5.1, which lists the available redshift data for K44.

Maccacaro et al (1977) give the redshifts of galaxies in the cluster centre and show that the velocity dispersion there is

very low. Chincarini et al (1978) have found redshifts for a rather more widely spread sample of galaxies, including some several Mpc from the cluster centre. Further redshifts of galaxies in K44 have been derived in the present study and are given in App. I.

In the 2U X-ray catalogue there is a source listed at 2358-29 which may be K44. A re-analysis of the X-ray data in the 3U catalogue moved the position to 0001-31, where it was tentatively identified with a distant group (Melnick & Quintana 1975). This area of the sky was described as a "complex X-ray emitting region which we could not unravel to our complete satisfaction": (Kellogg, 1974 priv. comm.).

The Sky Survey Instrument on the Ariel V satellite found an X-ray source at the position of K44; it is listed in the 2A catalogue (Cooke et al 1978) as 2A2344-285. The 90% probability contour of the source position encloses an area including, and running South from, the cluster centre (Maccacaro et al 1977). The identification with K44 is highly probable.

Low frequency radio surveys show a source coincident with the cluster (Finlay & Jones 1973, Mills et al 1960). Maccacaro et al (1977) searched at 6cm in an area centered on I5353=g1, but found no source down to 0.12Jy, nor did the Parkes survey find the cluster at 11cm. Crawford has, however, discovered a 1Jy, 75cm source consistent with the position of I5358=g2 (priv. comm. in Maccacaro et al 1977).

The photographic photometry of K44 is based on a ~56 arcmin square scan of a IIIaJ Schmidt plate of the cluster. This was centered on

g28 which is assumed to be the centre of the cluster. The coordinates of the scan were rotated by 0.8^{o} to E-W orientation and scaled to arcsecs by reference to 4 SAO stars in the scan area. The origin of the coordinates is $23^{h}44^{m}59.3^{s}$ $-28^{o}24'10''$ (1950); consistency of the SAO star positions suggests an accuracy of $\pm 1.5''$ in the measured galaxy positions.

Two Schmidt plates of K44 were available (Table 7.1); the cluster was scanned on plate J3730, which is deep but has only moderate seeing (full width at half intensity = 6"). The final visual check on the star-galaxy sorting was carried out on plate J3466 which has rather better seeing, but is a short exposure taken in moonlight.

A fourth magnitude star, δ Sculptoris, lies only ~18' W of the cluster centre. One of its diffraction spikes runs through the central area of K44, although not seriously contaminating any bright galaxies. Special methods were necessary to remove the brightness due to the halo of the star. Its profile was found by averaging the radial profiles at position angles of 45^{o}, 135^{o}, 225^{o} and 315^{o}, omitting any parts that passed through images on the plate. These position angles were used to avoid the diffraction spikes:  . The mean star profile was represented by a cubic spline. More than 636" from the centre of the star image the profile was less than 1% of the sky brightness and the effect on galaxy images was negligible. At distances nearer to the star the profile was subtracted from the measured brightness values, leaving uncontaminated brightnesses. The subtraction was not perfect since the star halo is slightly asymmetric, and the magnitudes derived for galaxies less than 636" from the star are not as accurate as in other regions of the scan. Photometry was not possible less than 356" from the

star due to the presence of a disk-like ghost image surrounding the position of the star.

An isophotal map of the centre of the cluster is shown in Fig. 2.1. Isophotes fainter than μ_B = 26mag/□" suggest that the background brightness has been estimated as slightly too great in this area as a consequence of the faint outer regions of the central diffuse luminosity being indistinguishable from variations in the plate sensitivity. In view of this, the extent of the diffuse luminosity is probably underestimated. Even so, it can be traced to a major diameter of >300" at μ_B = 26mag/□" and encloses the central galaxies. This luminosity is centred on I5358 = g2, which is cD in nature. Its middle has a curious morphology; the isophotes are rotated in the centre, and further out they are centered on a point 7.5" ± 1.5" to the NW of the galaxy nucleus. Chincarini et al (1978) explain this as due to the superposition of an elliptical galaxy on a cD galaxy. If this two-component model is correct then the cD would have the abnormally low central surface brightness, μ_B = 22.5mag/□". Redshift measurements on the diffuse halo and large scale plates taken in good seeing conditions are necessary to decide if their hypothesis is correct.

Surrounding the cD and embedded in its halo is a tight group of galaxies. Outside the central region the cluster is comparatively sparse and the population of K44 only justifies an Abell Richness Class of 1. The morphology of the cluster is discussed further in later chapters where it will be suggested that it is undergoing a short-lived phase of collapse.

To the South of the centre of K44 there is a group of faint images presumably those mentioned by Chincarini et al (1978). Galaxies 146 and 165 are the brightest members (B_{27} = 18.38 and 18.55). This group is probably the brightest members of a distant cluster ($z \sim 0.2$), only a few galaxies of which appear above the plate limit, but there is also a possibility that it is the faint HII regions of a nearby low surface brightness galaxy.

2.2 Sérsic 40/6 (S40/6)

This cluster derives its name from the survey of southern galaxies groups and clusters by Sérsic (1974), where it is described as a cluster of diameter 7' and with two cD galaxies. Duus & Newell (1977) list it as STR0431-616; they counted 400 galaxies in it, more than in any other cluster they examined, except Sérsic 149/10. Holmberg et al (1975) catalogue the centre galaxy as 118-IG30, mis-classifyin it as "SO+SO in contact". Vidal (1975) too claimed that the cluster does not contain a cD galaxy. In both cases the mistake was probably due to failing to use a deep enough plate; the central galaxy is a typical cD, with two nuclei (g1 and g4) and an extended halo (Fig. 2.2). It has been noted by Ekers & Ekers (1973) that D galaxies may often be mistaken for face-on SO galaxies.

An X-ray source was found by the Ariel satellite at $4^{h}.516-61^{o}.57$. The centre of the cluster lies within the 90% probability contour. This source, 2A0430-615, is noted in the 2A catalogue (Cooke et al 1978) as possibly variable, but Maccagni et al (1978), among whom are members of the Ariel group, consider the variability not significant and identify the source with the cluster. 3U0426-63 = 4U0427-61 is probably the same source, and Vidal (1975) identified

it with S40/6. A radio source, PKS0429-61, also coincides with the cluster.

The cluster lies at $b^{II}=-40^{o}$, and there is no evidence that the area is subject to abnormal obscuration. In appearance S40/6 is a typical, centrally condensed, cD cluster. The photographic photometry of the present work shows that it is slightly less rich than the Coma cluster. Maccagni et al (1978) estimated its Abell Richness Class as 2. They found a surprisingly high proportion of SO galaxies (60% within 1 Abell radius, uncorrected for field); this claim is discussed in a later chapter.

The photographic photometry was based on a scan ~34 arcmin square of a IIIaJ Schmidt plate. The lines of the scan were aligned N-S; the coordinates were rotated to the normal orientation, scaled to arcsecs and the origin was placed midway between the nuclei (g1 and g4) of the cD. The 1950 coordinates of this point and of 5 stars in the scan area were found with the Oxford plate measuring machine using SAO stars on the plate as position standards. The consistency of the star coordinates suggested that the measured positions of objects in the scan have errors of $\pm 2''$. The position of the origin of the scan coordinates is $4^{h}30^{m}32.9^{s}-61^{o}33'26''$ (1950) $\pm 2''$. S40/6 thus lies in Reticulum, the Net.

There is an obvious sub-clustering in the scan area (see map in App. IV) around g5 on the northern fringe of S40/6. The profile of this galaxy shows that it may be a cD galaxy at $z \sim 0.1$. In this case, ignoring any correction for the field of background galaxies, there are only 11 galaxies within 100" (0.24Mpc) of g5 that are no more than 4mags fainter than it. Hence the grouping cannot be a rich

cD cluster, z~0.1, but is either a sparse background cluster or a closer group, possibly associated with S40/6.

Redshifts of galaxies in S40/6 show that it has a high velocity dispersion (see Chap. 5). The redshift value found for the central cD by Vidal (1975) is consistent with that found in the present work.

2.3 A1146

A1146 is classified by Abell (1958) as Distance Class 5, Richness 4. The redshift of the central cD is 0.137 (heliocentric, Sandage et al 1976). Maccagni et al (1978) identify A1146 with the X-ray source 2A1058-226 (Cooke et al 1978), in which case it is one of the most luminous of the X-ray clusters yet found.

Carter & Godwin (1979) have carried out photographic photometry of a ~14 arcmins square area of the cluster, using a prime focus AAT plate. The B_{27} magnitudes they derived are compatible with those for S40/6, K44 and 2354-35 since they used similar, but not identical, methods. There is a slight difference in the band observed since a GG385, and not GG395, filter was used in front of the IIIaJ plate. The greater distance of A1146 necessitates larger corrections for the K-effect and isophotal contraction than for the other 3 clusters. The galactic absorption correction is also rather larger due to its low latitude ($b^{II}=-33^{o}$). Chap. 8 includes details of these corrections.

A1146 is similar to the Coma cluster and its population is no greater; a Richness Class of 3 is rather more appropriate than that of 4 assigned to it by Abell (1958). The central galaxy has a double nucleus, unresolved in the photographic photometry. Unfortunately

a redshift is available only for the central galaxy, which is a cD, so the velocity dispersion is unknown. A large telescope would be needed to obtain the velocity dispersion since the tenth brightest galaxy has B_{27} = 19.06.

2.4 2354-35

This is the least rich of the four clusters for which B_{27} data exist. Its population suggests that its Abell Richness Class would be barely 1, although it is significantly richer than Virgo. It is dominated by an extremely bright cD galaxy. This galaxy is a radio source, PKS2354-35 (Bolton & Ekers 1966), and shows 3727Å emission in its spectrum. Close to the cD is a spiral galaxy, g2, which has a redshift 2000km/s less than that of the cD, g1. If the spiral is at the distance of 2354-35, then its absolute B_{27} magnitude is $\sim$-22.8, in which case it is one of the brightest spirals known (cf. M31: M_B = -20.3, in Allen 1973). Even at the distance suggested by its redshift, g2 is very bright: $M_{B_{27}} = \sim -22.5$. No X-ray source has been found in the vicinity of the cluster, but if it has the same X-ray luminosity as K44, then it would probably not have been detected in the 2A survey (Cooke et al 1978).

The redshift of the cD galaxy was measured by Whiteoak (1972) as .0487 (heliocentric). Further redshifts for the cD and other galaxies in the cluster have been derived in the present work; the redshift value for the cD is confirmed. Photographic photometry of the cluster has been taken from Bucknell (1977); these data were found using methods similar to those described in Chap. 7.

2.5 A496

This cluster is at a low galactic latitude ($b^{II}=-36^{o}$) and may be subject to patchy obscuration as well as a high surface density of stars. No photographic photometry has been attempted on A496, but redshifts for 3 of the galaxies have been obtained by Melnick & Sargent (1977) and 3 further are derived in the present work, with one in common. Two radio galaxies lie 10' NE and 10' SE of the central cD galaxy: PKS0431-13.3 and PKS0431-13.5 respectively (Bolton & Ekers 1966). Whiteoak (1972) found the redshift of PK PKS0431-13.5 = g5 to be 0.0365 (heliocentric), ~1100km/s greater than that of the central cD galaxy. The cluster membership of these radio galaxies thus remains in doubt.

A496 is classified by Abell as Distance Class 3, Richness 1. It was detected as an X-ray source by the Ariel satellite and listed as 2A0431-136 (Cooke et al 1978). Although detected by Uhuru, it was not included in the 3U catalogue (Kellogg et al 1973, Brecher & Burbidge 1972).

2.6 Klemola 2 (K2)

Like K44, this cluster appears in the Klemola (1969) list of southern groups and clusters. Redshifts of 6 of the galaxies have been obtained and show that the cluster is the superposition of two groups of galaxies, one at z~0.0230 and the other at z~0.0194. In view of this, its lack of special interest, and its sparseness (it is less rich than the Virgo cluster), no photometry has been carried out on K2. No known X-ray or radio sources coincide with the cluster.

2.7 Pavo

This group is part of the Pavo-Indus cloud of low-redshift galaxies, which stretches from 19^h to 22^h and from -40° to -75° (de Vaucouleurs 1977). The Pavo Group is a close-knit group of both spiral and elliptical galaxies. Redshifts have been derived for the brighter galaxies by several workers, most notably Sandage (1975b), and further redshifts are given in the present work. Sandage suggests that the close pair N6872/I4970 may be background since their redshifts are nearly 1000km/s higher than the mean for the Group. The redshift of one of the Group members, I4985, has been found to be intermediate between that of this pair and the rest of the Group (App. I); in view of this, and because the pair are near the centre of the Group, it is possible that they are true members.

An X-ray source, 3U1959-69 has been identified with the Pavo Group (Melnick & Quintana 1975, Vidal 1975), but the Ariel satellite failed to find the source at the reported intensity (Cooke et al 1978). The Uhuru source position was revised to 1955-68 in the 4U catalogue (Forman et al 1978) and Jones & Forman (1978) consider the identification with the Pavo Group uncertain.

2.8 Sérsic 149/5 and Sérsic 149/10 (S149/5 & S149/10)

This is a pair of rich southern clusters. The single redshift obtained in each, z=0.0745 and z=0.0770 respectively (App. I), show that the clusters are at a similar distance and separated by ~25Mpc on the sky. They are therefore members of the same supercluster. Duus & Newell (1977) list them as 2143-575 and 2150-581.

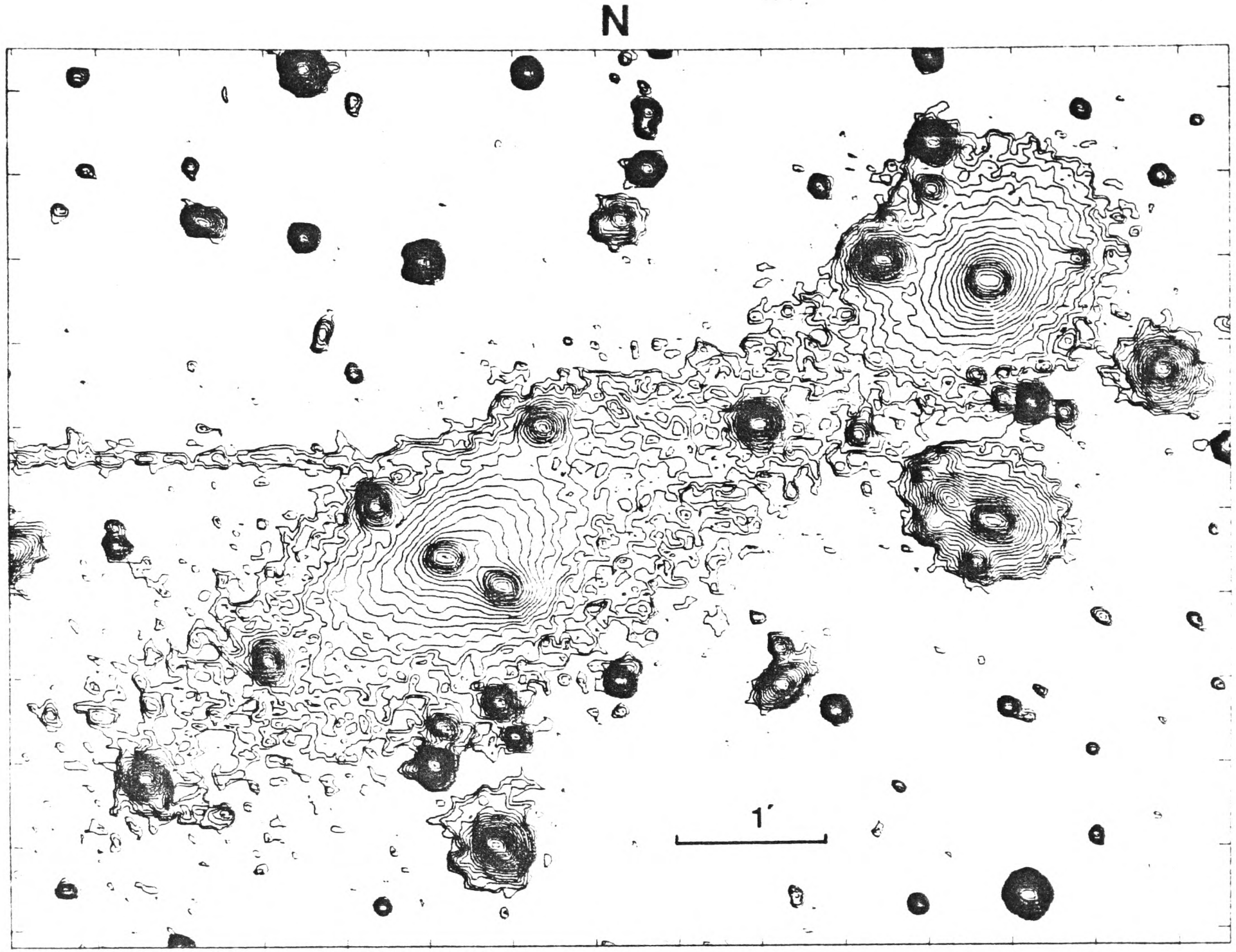

Fig. 2.1: Centre of K44

Isophotes are at $\frac{1}{4}$ mag intervals, the faintest at μ_B = 26.00 mag/□"

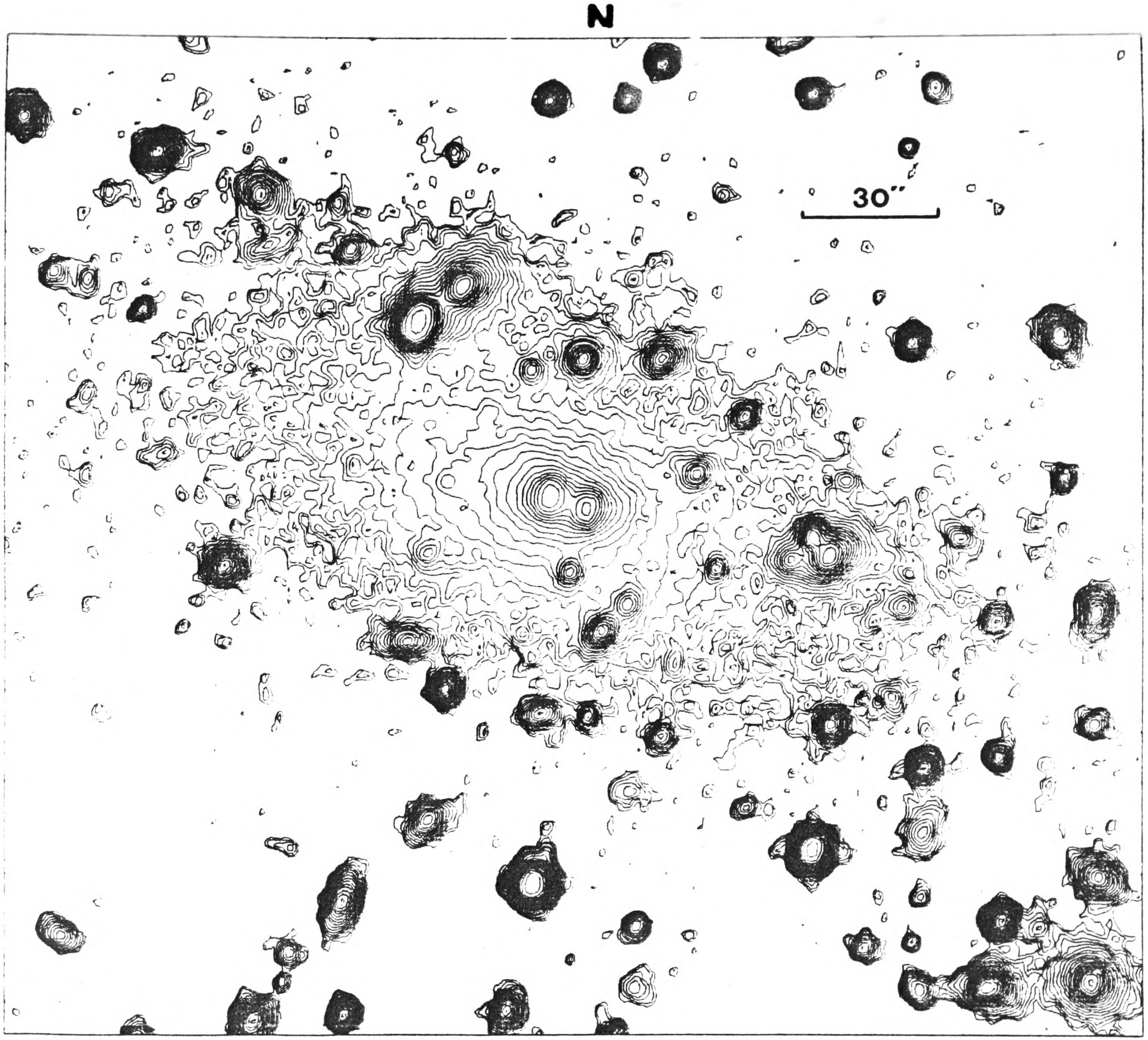

Fig. 2.2: Centre of S40/6

Isophotes at $\frac{1}{4}$ mag intervals,
the faintest at μ_B = 26.00 mag/□"

Chapter 3: Spectroscopic Observations

3.1 The Equipment

The redshift observations were carried out in two periods, each lasting a week: 1976 August 23-29 and 1977 October 11-17. Both were in "dark time" and hence only a small proportion of the spectra were taken with the moon up. No faint galaxies ($m_B \gtrsim 14$) were observed with the moon up since contamination by solar lines would have resulted in unreliable redshifts.

The telescope used was the 74" (1.9m) Radcliffe Reflector of the South African Astronomical Observatory at Sutherland; it is described in the SAAO Facilities Handbook. At the time of use it had a primitive control system, causing difficulties in acquisition, and a rather mediocre mirror coating. In compensation, the Sutherland site suffers very little from pollution of the night sky by artificial light, and has a large percentage of nights suitable for spectroscopic observations.

Fig. 3.1 shows the Image Tube Spectrograph, which was used at the Cassegrain focus of the 74". It is the twin of the RGO ITS; they are described in the Facilities Handbooks for the SAAO and RGO, and Palmer & Milsom (1972) discuss their performance and design.

Field viewing is by a pierced mirror which is also used for offset guiding, the galaxies being too faint and diffuse to guide on the slit. When the mirror is centered, the optical path is clear for

the image of the object to fall on the adjustable slit. Light from a comparison lamp can also be focussed on the slit. Behind the slit there is a prism that can be inserted in the beam to divert it to a Varo image tube; this is useful in centering faint galaxies. In the second observing period, the beam could also be diverted to an exposure meter system. This was of some help in choosing exposure times, but it was not practical to use it for centering faint galaxies due to noise in the counting rate and a long time constant.

Using Grating 1 (300 lines/mm) at an angle of $18^{o}45'$ gave a dispersion at the plate of 210Å/mm, centered at 4000Å. The detector system was an f/1.4 Maksutov-Cassegrain camera and 3-stage EMI image tube. A transfer lens is used to couple the final phosphor of the tube to the photographic plate used to record the spectrum. The 2inch square plates used had sufficient space to record up to 5 separate spectra. During the first observing period, IIaO emulsion plates, baked in air, were used; in the second period the plates were baked in a pulsed flow of nitrogen. They were developed in D19, fixed with Amfix, hardened, and dried at ambient temperature.

3.2 Observations

A slit width of 300μm = 1.8arcsecs was used; this is reduced at the tube and plate to 23μm. The resolution of the tube is 50 line-pairs/mm and of the IIaO emulsion rather better. At the dispersion used, 23μm is equivalent to 360km/s redshift at 4000Å.

Spectra can be trailed (i.e. the length of the lines increased perpendicularly to the direction of the dispersion) using coils to deflect the slit image in the tube from side to side. Trailing can also be achieved by moving the telescope itself, but this has the considerable disadvantage that for only a fraction of the exposure is any particular part of the slit on the galaxy nucleus; the result is a dilution of the galaxy spectrum by the night sky spectrum. The comparison spectrum can also be trailed; in this case the same short slit is used for it as for the galaxy and a deflection to either side of the galaxy spectrum is applied by the tube coils.

During the 1976 observing period the galaxy spectra were untrailed and air-baked IIaO plates were used. The fast emulsion and lack of trailing gave short exposure times, ~30mins. Only a few of the spectra failed to show a definite redshift, but they were rather noisy and not many lines other than CaH and K were visible since exposure long enough to overcome the noise resulted in over-exposure of the galaxy continuum. The spectra were also very vulnerable to ion-spots caused by the impact of heavy ions accelerated in the tube. These appear as dark dots and are large enough to obliterate untrailed features with which they coincide.

Tests were made on nitrogen-baked IIIaJ emulsion plates at the beginning of the second period. It was hoped that the smaller grain size would compensate for the slowness, and that measurement by a densitometer would make it possible to measure the resulting low contrast lines. In practice no significant improvement was found over IIaO, possibly due to the nitrogen baking system used, or

because the low resolution of the tube limited the quality of the plates so the fine grain was of no benefit.

In the second period, therefore, IIaO emulsion was once again used. The plates were baked in a pulsed flow of nitrogen (8hr at 60°C). The galaxy spectra were trailed electronically to aid recognition of lines and to reduce the noise. The use of trailing necessitated longer exposure times, ~55mins, but this did not reduce proportionately the number of spectra taken in a given time since acquiring the galaxies and operating the ITS was cumbersome and considerable time was needed between exposures. The spectra, despite being of fainter galaxies in general than during the first period, were of better quality. Fainter lines could be identified and there were fewer difficulties caused by ion-spots and plate flaws.

The comparison spectra were put on in both periods using a long slit with the centre masked by a dekker. The emission line spectrum of the comparison lamp thus runs down each side of the galaxy spectrum. This procedure relies on the straightness of the slit, although no evidence was found to suggest it was curved, and uses the system off-axis. The alternative was to use the short slit for comparison as well as galaxy and trail it with the tube coils. Although more convenient this was not done as there is a danger of contamination of the galaxy spectrum from persistence in the tube. Run at 30kV e.h.t., the intermediate phosphors of the tube are over-excited, and the after-glow from them is amplified by subsequent stages of the tube. The comparison spectrum follows the same path as the galaxy spectrum in the first part of the tube

and persistence of the comparison spectrum may overlay the subsequent galaxy spectrum: Moss (1976) discusses this problem. The danger of persistence from one galaxy spectrum to the next is less since the time between them is longer and the galaxy continuum is not as over-exposed as the comparison emission lines. Tests were made to check the extent of persistence from one galaxy to the next by taking exposures with the slit shutter closed while acquiring the next galaxy. These exposures show no sign of the previous galaxy continuum, although a few of the comparison lines are just visible to either side of it.

Different lamps were used in the two periods: in the first Cu/Ar and in the second He with slight Ne (not as much as in a standard He/Ne lamp). The exposure time was ~12s both before and after each galaxy exposure. Filters were used to lengthen the exposure times of the comparison and to eliminate the second-order spectrum.

The Cu/Ar lamp gives many lines, some of them blended at the low dispersion used. The He/Ne lamp produces fewer, but better lines. The lines used in the reductions, and methods of selecting and weighting them are discussed in Chap. 4.

Table 3.1 summarises the observational details of the spectroscopy and App. II lists the plates taken and the exposure times etc. The next chapter describes the derivation of the redshifts and the results are shown in App. I.

Table 3.1: Summary of Spectroscopic Observations

	1976	1977
Dates	Aug. 23-29	Oct. 11-17
Telescope	SAAO 74" (1.9m)	
Focus	Cassegrain	
Spectrograph	Image Tube Spectrograph (ITS)	
Tube	3-stage EMI	
Emulsion	Air-baked IIaO	N_2-baked IIaO
Dispersion	~210 Å/mm	
Comparison Lamp	Cu/Ar	He + slight Ne
Galaxy Trailing	No	Electronic Trail
Comparison Trailing	No	No
Exposure Times	~30mins	~55mins
At Slit:		
Slit Width	300μm = 1.8arcsecs	
Slit Length (Galaxy)	2.5mm	600μm=3.6arcsecs
Slit Length (Comparison)	2 x 5.1mm	
At Plate:		
Slit Width	23μm	
Slit Length (Galaxy)	200μm	47μm trailed to 200μm
Slit Length (Comparison)	2 x 400μm	

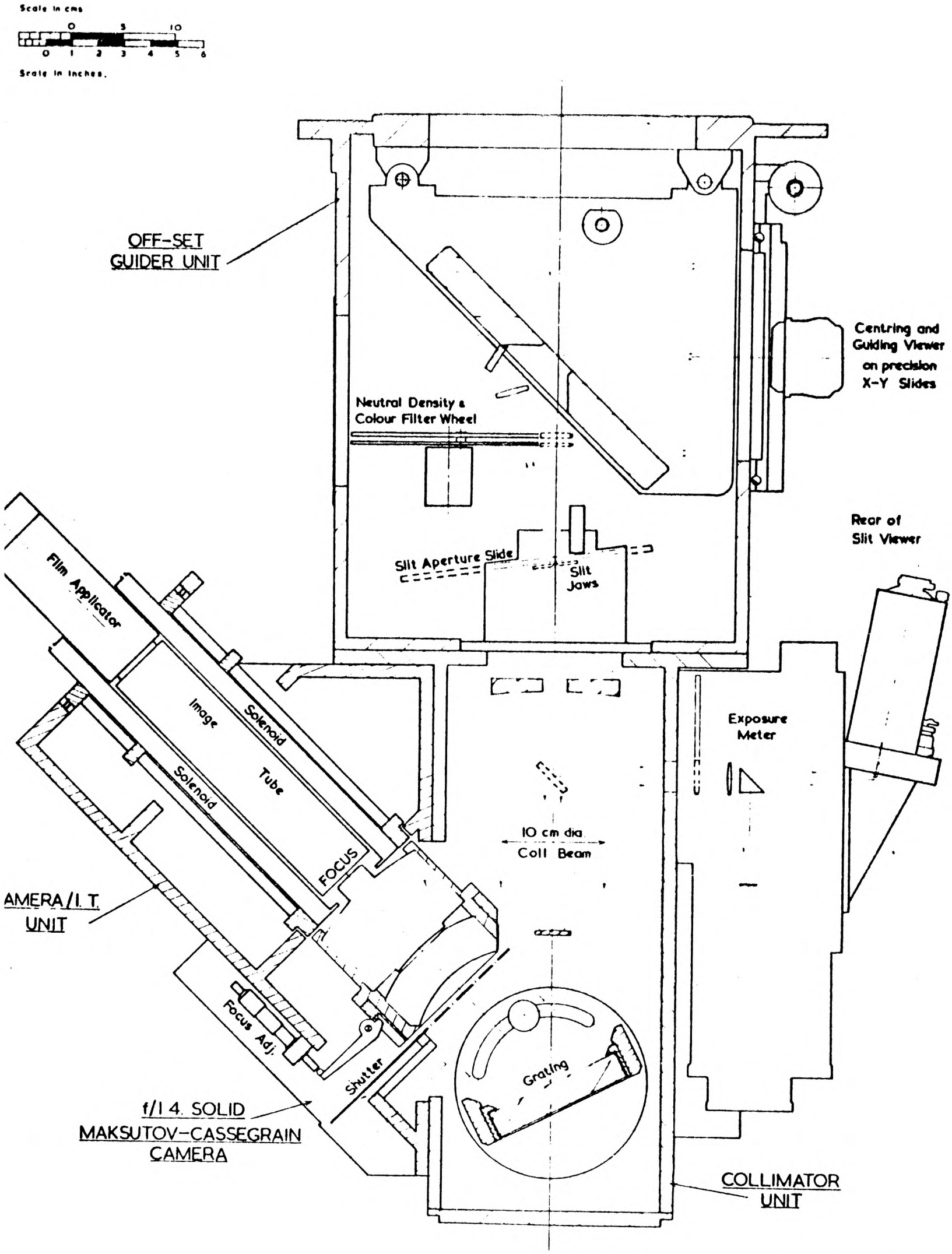

Figure 3.1: The ITS, fitted with a Spectracon Tube

Chapter 4: Measurement of the redshifts

4.1 The Abbé Comparator

The accuracy of redshifts is limited by the nature of the spectra and the spectrograph, but the measuring machine must also be accurate or it, too, will degrade the results. At a dispersion of 210Å/mm an error of 10μm in the position of the CaH or CaK line gives an error of ~150km/s in its velocity.

The Oxford modified Abbé Comparator was used to measure the spectra: it has an accuracy of ~2μm for repeated readings. Its main advantage over a travelling microscope is in displaying a densitometer scan of the line being measured as well as a magnified image; more information is thus available when deciding on the position of the centre of a line.

A full description of the Abbé and its modification is given by Gollnow (1961). The plate is placed on a massive table that can move in x and y under a microscope head, and is illuminated from beneath. A beam splitter above the head gives two separate images of the part of the plate in view. One is thrown directly on to a ground glass screen provided with a fiducial mark, so that spectral lines may be positioned on it by moving the table. The other image is swept repeatedly across a slit and dekker by the deflecting action of a revolving glass block. A photomultiplier detects the light entering the slit.

The densitometer trace from the Abbé is displayed as a deflection in the y-direction on a c.r.o. that has its time base synchronised

to the block rotation. The line profile is thus displayed on the screen. A mirror-image trace is generated electronically and displayed similarly. To make a measurement, the table is moved until the two traces of a line coincide at the chosen line centre. If the line is symmetrical, then the whole profile of the line coincides on the two traces. Alternatively, the direct image of the line on the ground glass screen can be used to find the line position.

Line asymmetries are easily seen on the c.r.o. and it is also particularly useful in identifying lines in very dense continua. The projected image is necessary since the c.r.o. trace is one-dimensional and it is often important to know whether a line goes all the way across the continuum in order to be convinced of its reality. Ion-spots, for instance, can easily be mistaken for emission lines when seen on the c.r.o.

The position of the table is measured by a Moiré fringe unit to the nearest 1μm. No attempt was made to calibrate the unit of measurement, since it is irrelevant in the reduction, but it does not differ greatly from the nominal micron. Backlash of ~2μm is present, but can be corrected for. The position is punched on to paper tape on command, and other identifying marks and comments can be punched when necessary. Position in the y-direction across the spectra is shown by a vernier scale, readable to the nearest 25μm.

The Abbé is housed in a constant temperature room, held to ±0.2K over time-scales longer than is needed to measure a plate.

Drift due to thermal and other causes is very small, amounting to less than 1μm during the measurement of most spectra.

4.2 Measurement of the Spectra

Every spectrum was measured at least twice. These measurements were fully independent, being on different days and reduced separately. The notes from the first were not referred to in the second. In the case of serious disagreement between the measurements or if the reduction showed there to be an anomaly, such as displacement of the night sky lines, then the spectrum was measured a third time.

The complete set of comparison lines were measured both above and below the galaxy spectrum before and after measurement of the galaxy spectrum: thus the comparison lines were measured four times. A short slit, the same length as the galaxy continuum width was used for all the measurements on a spectrum, and the slit width was always 18μm. Movement of the table in the y-direction is by a screw. No adjustment was necessary during the run along a set of lines since bending of the spectrum only became significant redward of 6500Å, where there are very few lines present. In any case the reduction method corrects for bending to the first order.

Single readings were taken on the comparison lines and sets of three on those of the galaxy and night sky. During the pass along the galaxy spectrum any possible lines were measured and their appearance noted. The position of a line was taken as being its

centre near its deepest part. It is not possible to use a simple objective criterion for finding the position of the centre since the lines are of different strengths and intrinsic shapes: the G-band, for instance, is a complex blend. The effect of noise and night sky interference on a line also depends on its redshift since this determines in which part of the spectrum the line falls.

Some improvement in the accuracy of redshift determinations can be made by cross-correlating the galaxy spectrum with a "standard" galaxy spectrum and finding the redshift that gives the best match (e.g. Faber & Dressler 1977). This procedure is only possible with good, calibrated plates, and can have the unfortunate effect of putting high weight on the strongest features, without regard to their quality.

4.3 Computation of the redshifts

The Oxford ICL1906A was used for the reduction of the paper tape output from the Abbé Comparator. After reading in the tapes, any obvious errors due to mis-punching or the omission of lines were corrected. The data were then rearranged in a compact form for ease of storage and reference in the computer.

The sets of comparison readings taken on the upper lines before and after measurement of the galaxy spectrum were combined to give the mean position of these lines. The readings on the comparison lines below the galaxy spectrum were treated similarly. Linear interpolation was used to combine the upper and lower readings at the y-position of the galaxy spectrum, giving a single x-position

which can be compared with the x-positions of the galaxy lines. This procedure is only correct in the absence of bending of the spectrum by S-distortion in the tube, and if the slit is not bent. The S-distortion present only gives an error of >1μm beyond 6500Å where no galaxy lines have been measured. To check the slit (or equivalently the tube deflection in the case of trailed spectra) test plates were taken in which the comparison lines were put on across the whole width of the spectrum. They showed no systematic slit curvature greater than 1μm.

Wavelengths for the comparison lines were taken from Zaidel et al (1970) and Moore (1959). The set of lines was chosen by examining the line shapes with the Abbé. Lines that were severely asymmetrical were eliminated, as were over and under-exposed lines, and blends. The tables of lines were used to pick out lines that were close blends. In practice, adopting these criteria left too few lines in some parts of the spectrum and less satisfactory lines had to be included. In particular the blue end of the Cu/Ar spectrum was under-exposed, and the green part of the same spectrum had nearly every line blended to some extent. Three of the adopted Cu/Ar lines were blends of close lines; the wavelengths assumed are similar to those found by polynomial interpolation by Moss (1976). The lines in the He/Ne spectrum were generally of good quality and nearly all were used apart from the 5875Å He line which was very over-exposed and blended with a faint Ne line.

Lines that consistently had a large residual in the reduction were also eliminated, even though this could also be explained as a

characteristic of the dispersion of the spectrograph. An "intrinsic weight", v_i, on a scale from 1 to 5 was assigned to each line in the sets on the basis of their quality. Table 4.1 shows the wavelengths and weights of the members of each set.

A polynomial was fitted to the x-positions of the comparison lines, adjusted to the y-position of the galaxy spectrum as explained above. The polynomial was calculated separately for each of the galaxy line positions, x_j. In its calculation, each line was given a weight, w_{ij}, that was the product of two factors: firstly the "intrinsic weight" of the line, v_i, and secondly an expression that was greatest for lines that were closest to the galaxy line position. In practice, a gaussian form was used for this second factor, giving a total weight:

$$w_{ij} = v_i \exp(-(x_i - x_j)^2 / x_o^2)$$

Using x_o=6000μm, this was successful in reducing the influence of poor lines and those far away when calculating the position-wavelength polynomial for a particular galaxy line.

Polynomials to the fourth or fifth powers were found to be sufficient to give a good fit to the comparison line positions. Residuals from the polynomials were usually ~0.5Å s.d., and showed no systematic effects. In the course of the reduction several criteria were used to reject comparison lines: disagreement in the measurements, abnormal tilt across the spectrum, and large (>2.5s.d.) residual from the polynomial. On average, ~2 lines per spectrum were rejected for one or more reasons; they were usually lines that had a low intrinsic weight.

If the 3727Å galaxy line had been present in the spectra of the lower velocity gal xies it would have lain outside the span of the He/Ne comparison lines, but in no case did this happen and extrapolation was never necessary.

The derived wavelengths of the galaxy lines were examined to identify the lines present. The CaH and K lines were normally definite enough to avoid any danger of grossly erroneous redshifts. Weights for the reliability of each galaxy line were assigned using the notes taken when measuring the spectra. A scale from 1 to 5 was used: generally the H and K lines were given weights of 4 or 5, the G-band 2 and other lines 1 or 2. Occasionally the NaD line merited a high weight due to its clean shape and the 3727Å emission line when strong was also assigned a high weight.

The finally adopted line wavelengths and weights were the mean of the two measuring sessions' results. If there was doubt about the reality of a line, or if it was distorted by a night-sky feature, then it was rejected. The galaxy redshift value was calculated using the weighted mean of the individual line redshifts.

The rest wavelengths used for the galaxy lines were taken from Sandage (1975a) and are listed in Table 4.2 which also shows the number of occurrences of each line, the mean residual of the line from the adopted galaxy velocity, and the error in this value. The number of occurences of a line is not an unbiassed indication of its strength in the spectra since certain lines may be hidden behind night-sky features or fall outside the range of photocathode high sensitivity.

Table 4.2 shows that the H and K lines differ significantly in the redshifts they give by ~60km/s, being measured an average of ~0.8Å too close together. There is no way of telling which one or both of them is in error, and no correction can be made. The error in the galaxy velocities if one of them is wrong by 60km/s will be rather less than 30km/s since both H and K are normally present in the spectra and usually other lines are too.

$H\eta$ also shows a significant residual in both observing periods. This line only occurs in a few of the spectra since it is strong only in late-type galaxies, and never has a high weight. Even so, it has been omitted from the redshift calculations and so also has the single occurrence of the related $H\theta$ line.

Ideally the wavelengths of the absorption lines would be calibrated using the emission line wavelengths, but it has not been possible to follow this procedure here since, apart from the planetary nebula N6818, the only emission line found is 3727Å. N6818 is of no help in calibration as it has no absorption lines. The rest wavelengths adopted are unlikely to be much (>50km/s) in error since they were derived using similar telescope-detector-measurement combinations.

The values of the redshifts calculated for the galaxies are shown in App. I, quoted in terms of the "representative velocity", $v=cz$. The values of v are corrected to the heliocentric frame; the correction is never larger than 30km/s. Many authors correct for the motion of the heliocentric frame in the galaxy and Local Group, often using the expression for the correction:

$$v_{corr.} = v_{obs.} + a \sin l^{II} \cos b^{II}$$

where a=300km/s and b^{II} and l^{II} are the revised galactic coordinates.

This practice has not been adopted here since the rotational velocity of the Galaxy is still uncertain by $\pm$20km/s and its translational velocity is rather less accurate. Measurements of the motion through the microwave background (Partridge 1974) and relative to the nearby galaxies (Rubin et al 1976) disagree even in the direction of the motion. In this confused situation it would seem unwise to apply any correction at all.

4.4 Errors

Although zero-point errors are unimportant when calculating velocity dispersions from homogeneous data, they must be included when using results from a variety of sources. In the red end of the spectrum they were investigated by finding the apparent wavelengths of four night sky lines during the measurement of the spectra. The results are shown in Table 4.3: no significant shifts are found. Blueward of 5577Å there are no bright night-sky lines visible at Sutherland, so the zero-point error must be assessed from a comparison with galaxy velocities by other authors. The listing of redshifts in App.I shows data from other sources where these are available. The comparison is made with each worker with >3 in common, and for the whole set, in Table 4.4; $\overline{V_o - V_s}$ is the mean difference between the velocities found here for the comparison objects and the mean velocities found by other workers, σ is the s.d. in the mean difference, and s.e. is the error in

the mean difference.

There is no indication of a need for a zero-point correction, and none has therefore been made. Shown in Fig. 4.1 is the variation with velocity of $V_o - \bar{V}_s$; all the comparison sample is plotted. A large zero-point error variation with velocity would be apparent as a slope in the distribution.

The comparisons, however, with previous redshift results may be misleading. The information for different redshift ranges tends to come from different sources, and this may mask the variation of zero-point error with redshift. It is also unfortunate that most velocities of southern galaxies have been found using only two telescopes: the 1.9m reflectors at Sutherland and Mount Stromlo. Rather more serious is the strong evidence presented by Sandage (1978) that optical redshifts are systematically 30km/s too low compared with 21cm redshifts. (Sandage's redshifts used in Table 4.4 and App. I. do not include his 30km/s correction). Since there is little reason to doubt the accuracy of the 21cm data, it seems likely that there is an error in the optical zero-point, perhaps due to incorrect wavelengths of the galaxy lines, or night-sky interference. It is not known if this affects distant elliptical galaxies, which form most of the sample here, as well as the nearby spirals in Sandage's sample. Meanwhile, the 29km/s error shown for the zero-point in Table 4.4 should be considered as a lower limit.

Night-sky interference arises from the blending of night-sky features with galaxy lines. Systematic differences between the optical velocities found by Humason et al (1956) and 21cm velocities in the range 1300km/s to 2500km/s have been blamed on this cause

(e.g. Roberts 1972). Simkin (1977) has shown by simulation that the H and K lines are liable to be changed in apparent velocity, by hundreds of km/s in certain circumstances, by blending with the sky features. Tifft (1978), although disagreeing with her conclusions about his work, confirmed that the 4047Å mercury line can cause serious errors in observations.

The effect is insidious in that non-linearity of the emulsion response can lead to the sky feature being almost invisible when not added to the galaxy continuum, even when fairly strong. The sky at Sutherland is less polluted by artificial light than at most sites, including that used as an example by Simkin. There is therefore probably little error from this source. To confirm this, the residual velocity of a line from the mean of all the lines of the galaxy is shown plotted against the wavelength at which the line is observed (see fig. 4.2). The complete sample of galaxies is included. If the absorption lines were being displaced by any night-sky emission lines, then a characteristic shape:

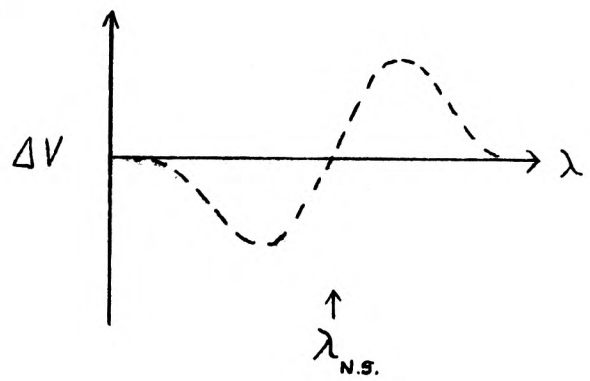

would appear in the distribution at the night sky line wavelength; there is a slight indication of this at 4047Å. Fig.4.3 shows the difference between the H and K line velocities plotted against their mean wavelengths. No anomaly is apparent, apart from $V_H - V_K$ being non-zero.

Other sources of error in the velocity determinations will be the inaccuracy of the wavelength-position calibration curve, measuring errors, and noise in the spectra. Shown in App. I is the "internal error" of the velocity for each galaxy. This is calculated as the standard error in the combination of velocities of the individual lines to derive the galaxy velocity. It should be distinguished from the "external error" in the velocity which is an estimate of the true error in the velocity. The internal error does not include the effect of systematic errors that influence all the lines; this can be the case for night-sky interference or calibration curve errors in some parts of the redshift range, as well as systematic faults in the spectroscope and measuring machine. A large proportion of the internal error is simply due to noise in the spectra; measuring errors as shown by the night-sky line velocities and by comparison between the two measures of each spectrum only amount to ~35km/s.

The internal errors are in general under-estimates of the external errors and show large statistical fluctuations because of the small number of lines measured. The dispersion, σ=146km/s, given in Table 4.4 for the difference between velocities from this work and from other sources suggests that the external errors in the galaxy velocities are ~100km/s, assuming that all sources are equally accurate. This value is similar to the ~95km/s and 108km/s found by Sandage (1978) for his own data and that of Martin (1976) respectively. The mean of the internal errors given for this sample in App. I is 63km/s, considerably smaller than the external errors.

A representative internal error is found for each galaxy by taking the mean of the internal errors of galaxies with similar quality spectra. The external error of the galaxy is then assessed as twice the representative internal error and shown in App. I as an error class (see Table 4.5). Sandage (1978) found that such a procedure was justified since the external error is greatest for galaxies with large internal errors. The normal error class for low redshift galaxies, which predominate in the comparison sample, is "a", which is in agreement with the external errors found above by comparison with other sources.

Table 4.1: Wavelengths of Comparison Lines

Copper/Argon			Helium/Neon		
λ,Å	Intrinsic Weight		λ,Å	Intrinsic Weight	
7383.98	3	Ar I	7281.35	2	He I
7272.94	3	Ar I	7065.19	5	He I
7030.26	1	Ar I	6678.15	3	He I
6871.29	3	Ar I	6506.53	3	Ne I
6416.31	5	Ar I	6402.25	5	Ne I
6173.10	1	Ar I	6334.43	2	Ne I
5912.09	4	Ar I	6266.50	3	Ne I
5860.32	2	Ar I	6143.06	5	Ne I
5739.52	3	Ar I	6096.16	4	Ne I
5650.70	2	Ar I	6074.34	2	Ne I
5606.73	5	Ar I	5764.42	1	Ne I
5558.70	3	Ar I	5047.74	2	He I
5218.20	3	Cu I	5015.68	3	He I
5187.75	4	Ar I	4921.93	4	He I
5062.07	3	Ar II	4713.14	4	He I
4965.07	2	Ar II	4685.68	3	He II
4847.90	4	Ar II	4471.48	4	He I
4806.07	4	Ar II	4387.93	5	He I
4764.89	2	Ar II	4143.76	2	He I
4657.94	4	Ar II	4120.85	1	He I
4510.73	4	Ar I	4026.19	5	He I
4400.48	2	Ar II (blend)	3964.73	5	He I
4300.10	2	Ar I	3888.65	4	He I
4131.73	4	Ar II			
4103.91	4	Ar II			
3994.81	2	Ar II			
3948.50	1	Ar I (blend)			
3928.63	1	Ar II			
3868.53	1	Ar II			
3850.57	1	Ar II			
3765.27	2	Ar II			
3560.40	2	Ar II (blend)			
3491.39	1	Ar II			
3341.77	3	Ar II			
3273.96	5	Cu I			
3247.54	5	Cu I			

Table 4.2: Line rest wavelengths and residual velocities

		1976				1977			
Line	Rest Å	Mean km/s	σ km/s	s.e. km/s	n	Mean km/s	σ km/s	s.e km/s	n
K	3933.7	21	110	16	47	57	70	13	29
H	3968.5	-23	122	18	48	-25	167	31	30
Ca I	4226.7	-113	137	69	4	370	166	96	3
G	4304.4	-48	161	35	22	-14	208	45	22
Fe I	4383.6	78	46	23	4	84	192	78	6
Mg I	5175.36	-21	130	58	5	-57	228	72	10
Ca+Fe	5268.98				0	-272	214	107	4
Na D	5892.5	83	144	33	19	-10	197	51	15
H θ	3798.6				0	29			1
H η	3835.6	-203	139	49	8	-231	208	120	3
H δ	4101.7	-83	77	44	3	76	172	86	4
H γ	4340.5				0	-213	273	158	3
H β	4863.9	-1			1	-29	356	159	5
O II (em)	3727.3	86	49	19	7	-110	196	98	4

"Mean" is the mean deviation of the line velocity from the galaxy velocity. σ and s.e. are the standard deviation and standard error of that value; the number of occurrences of the line is given under "n".

Table 4.3: Measurements on Night-Sky Lines

a) 1976 Spectra

Line	Wavelength Å	Mean vel. km/s	σ km/s	s.e. km/s	no. of spectra
OI	5577.35	-20	37	6	39
NaD	5891.94	8	57	9	37
OI	6300.23	2	39	6	39

b) 1977 Spectra

Line	Wavelength Å	Mean vel. km/s	σ km/s	s.e. km/s	no. of spectra
OI	5577.35	-22	24	5	23
NaD	5891.94	36	61	25	6
OI	6300.23	0	32	10	10
OI	6363.88	-24	42	19	5

The line velocities used are the averages of the two measurements on each spectrum.

Table 4.4: Comparisons with velocities from other sources

Reference	Galaxies in common	mean diff. $\overline{V_o - V_s}$	σ	s.e. in mean
All	25	-3	146	29
Sandage (1978)	9	-71	140	47
Chincarini et al (1978)	9	22	117	39
Maccacaro et al (1977)	5	65	236	106
Vidal (1975)	4	-102	225	113
Martin (1976)	4	-91	109	54

All values are in km/s. Galaxy 8 in K44 has been omitted ($V_o - V_s = -695$)

Table 4.5: Error classes

Error Class	Estimated external error
a	60 - 120 km/s
b	120 - 180 km/s
c	180 - 240 km/s
d	possibility of gross error

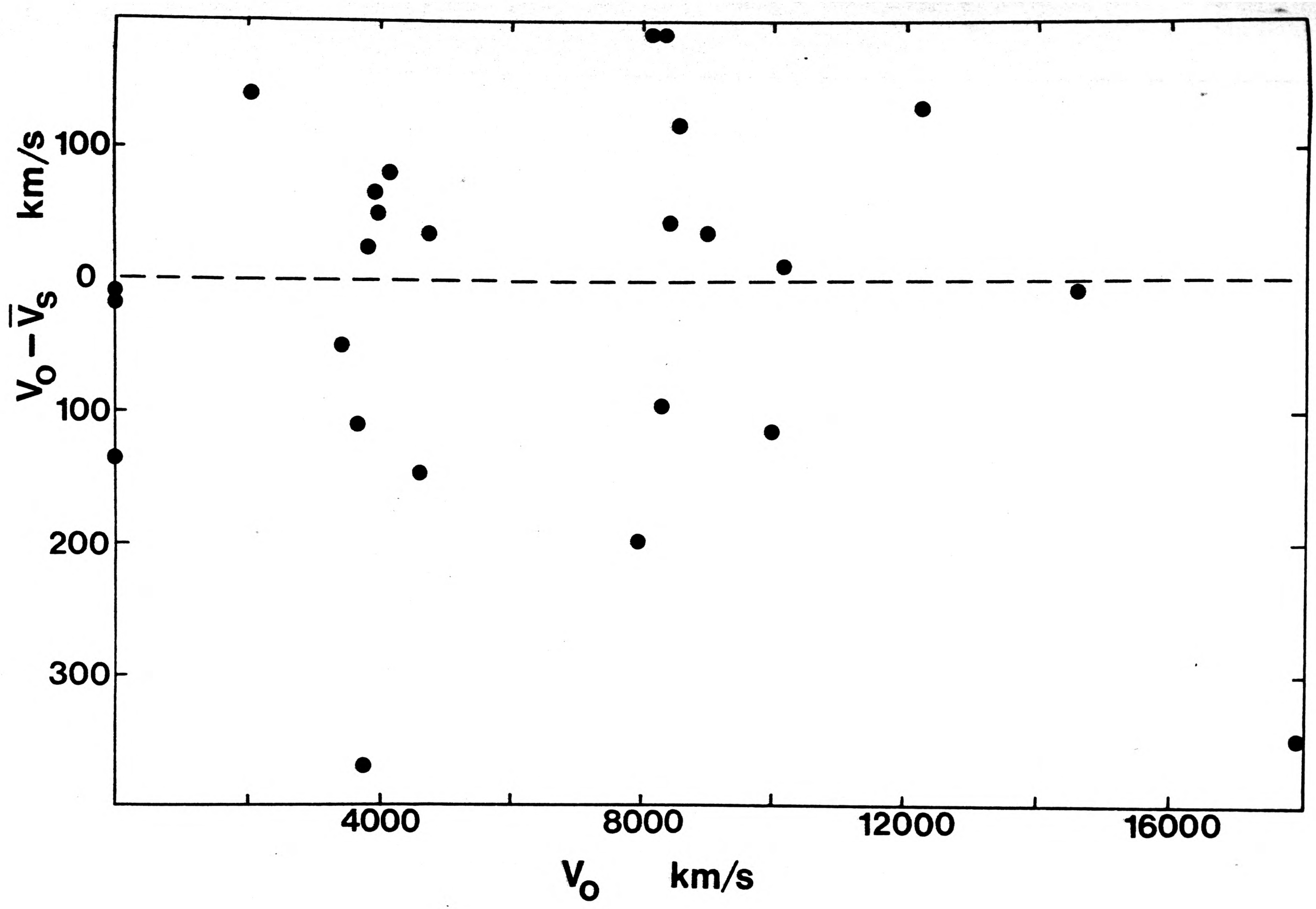

Fig. 4.1: Differences between velocities from this work and from other sources, plotted against velocity

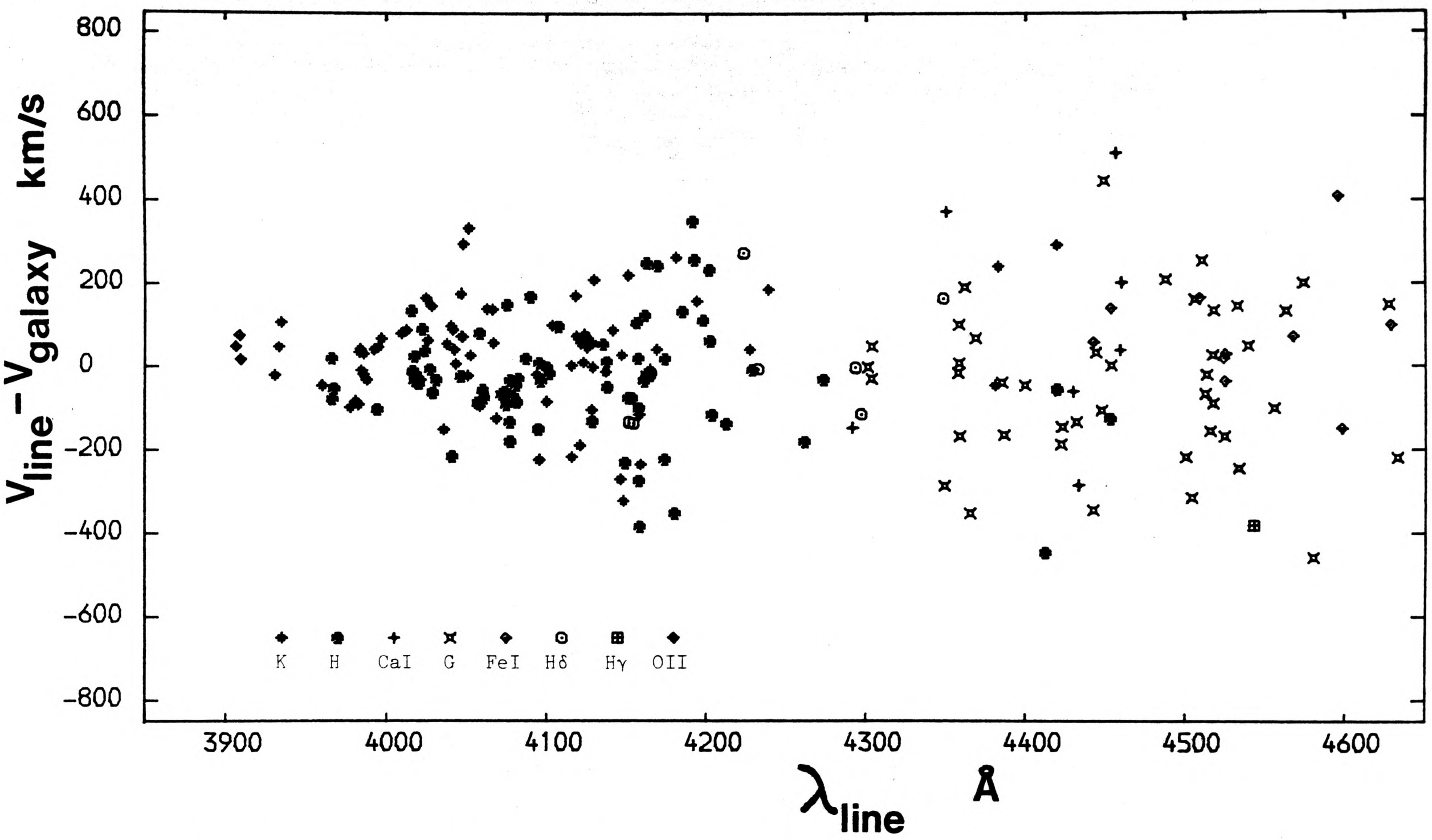

Fig. 4.2: Residuals of line velocities from galaxy velocities

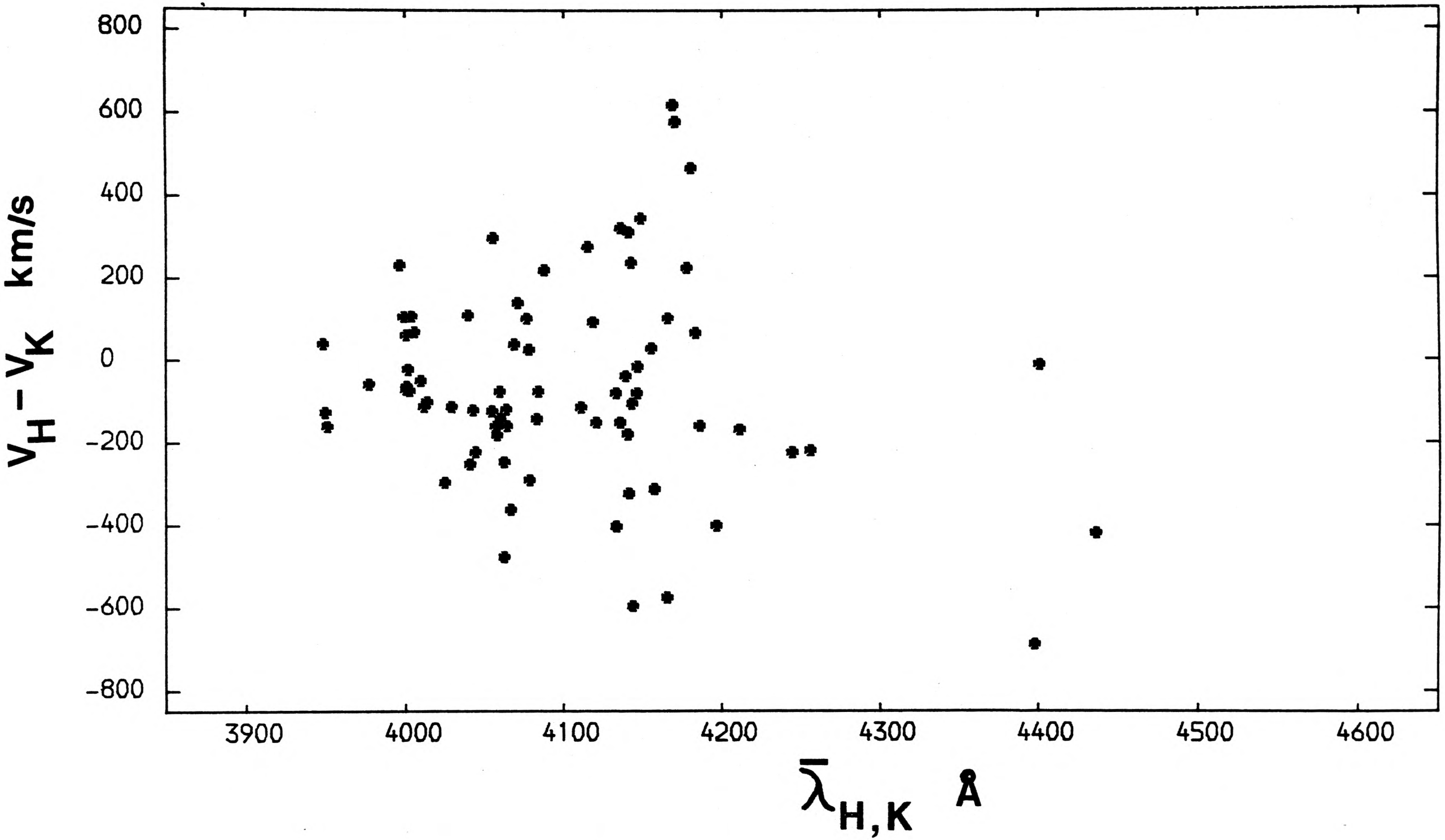

Fig. 4.3: H-K Velocity residuals against H,K mean wavelength

Chapter 5: The Velocity Dispersions

5.1: Introduction

In the future it may be possible to measure the redshifts of the bright galaxies of a cluster at the same time, using multi-aperture spectrographs, objective prism systems or, eventually, holographic techniques (Lindegren & Dravins 1978). At present, only single object spectrographs can provide the necessary accuracy; hence finding the velocity dispersion of a cluster remains expensive in telescope time and resources. A consequence is that the calculation of the velocity dispersion of a cluster must normally be carried out using the redshifts of fewer galaxies than is desirable. These galaxies are generally the brightest in the cluster since this minimises the exposure times (cf. Jones & Jones (1978) who suggest that a well-defined and rather fainter sample would be useful).

In the present work, only $\sim$10 redshifts are known in each cluster, giving no opportunity to derive any detailed conclusions about the dynamics of the clusters. A sample this small provides enough information to tentatively reject possible non-members and give a brutally simplified picture of the kinematics of the cluster. Fortunately, there has been detailed study of the velocity distribution in a few clusters, most notably Coma, and this provides some clues as to how the data should be treated.

5.2: Calculation of the Velocity Dispersions

The distribution of the velocities of galaxies in a cluster is normally assumed to be gaussian; Yahil & Vidal (1977) showed, using a large body of data from many clusters, that this assumption is reasonable. The velocities of galaxies in the Coma cluster do not differ significantly from a gaussian distribution (Gregory & Tifft 1976). However, the tails of the distribution are difficult to investigate observationally due to contamination by field galaxies; theoretically, too, it is not clear to what extent the tails will be modified by the escape of high-velocity galaxies from the cluster.

A best estimate of the underlying dispersion of the velocities in a cluster is:-

$$s^2_{obs} = \frac{\sum_i (v_i - \bar{v})^2_{obs}}{n - 1}$$

where $(v_i - \bar{v})_{obs}$ is the observed deviation of the galaxy velocity from the mean for the cluster, and n is the number of galaxies observed. Some authors use n, not (n - 1), as the denominator.

Allowance must be made for the error, e, in the measurements of the velocities. Assuming that the galaxies should have equal weight in the calculation of the mean velocity, then $(v_i - \bar{v})_{obs}$ must be corrected (Materne 1974, Rood & Dickel 1976):-

$$s^2 = \frac{\sum_i ((v_i - \bar{v})^2_{obs} - \frac{n-1}{n} e^2)}{n-1} = s^2_{obs} - e^2$$

This is the velocity dispersion that will be used in the present work; it refers only to line-of-sight velocities and should be multiplied by a projection factor, often assumed to be $3^{\frac{1}{2}}$, to give the dispersion in space. The velocities, v_i, used in these calculations are <u>not</u> representative velocities, v=cz, but are derived from the redshifts by the relativistic Doppler expression:-

$$v = c \frac{(1+z)^2 - 1}{(1+z)^2 + 1}$$

Use of the representative velocites would result in the velocity dispersions being too great by a factor (1 + z) (Faber & Dressler 1977). There is a small error, even when using the relativistic velocities, caused by calculating the deviation from the mean cluster velocity by subtraction, rather than the proper relativistic formula; it is less than 1% for the clusters considered here and has been ignored.

The velocities of galaxies in 5 clusters are shown in Table 5.1. Velocities assigned an error class of "d" in App. I are excluded as they may well be wrong. Otherwise, the velocities by all workers are given equal weight in the determination of the mean of the velocity measurements for a galaxy. One galaxy in K44 (VV19) and one in 2354-35 (X) have been included despite being outside the scan area since they are within 2Mpc projected distance from the cluster centre. Velocities are available for other galaxies in these two clusters that are more than 2Mpc from the centres; they have not been included in the calculation of the velocity dispersions, but will be discussed later in this chapter.

Fig. 5.1 shows the distribution of galaxy redshifts in the clusters.

5.3: The Exclusion of Non-members

A näive prediction of the number of non-members in the redshift samples may be made by assuming that "field" galaxies are distributed randomly in space, with a universal luminosity function. Such predictions are shown in Table 5.2; they suggest that very few non-members have been included. However, these figures are an under-estimate since:-

i) The space density of galaxies around a cluster is higher than the density in space generally (assuming that "generally" has any meaning here). This can be explained as either the membership of a supercluster by the cluster, or, equivalently, as a result of the continuous spectrum of galaxy clustering. This excess of galaxies will result in an enhancement in the number of non-members that are seen projected on to the cluster when observed.

ii) Non-members will be preferentially included in the redshift samples if they have a redshift similar to that of the cluster. Theoretical calculations (Pence 1976) of the mean redshift of "field" galaxies of different apparent magnitudes suggest that at $m_B = 16$, $\bar{z} = .03$ and at $m_B = 17$, $\bar{z} = .05$. Comparing these figures with the limiting magnitudes of the redshift samples, B_{lim}, given in Table 5.2, it can be seen that the $\bar{z}$ of non-members having magnitudes $m_B \sim B_{lim}$ is similar to that of the cluster. This happens because the "knee" part of the luminosity function found for

galaxies (Chap. 8) predominates in the observed "field" galaxies, and the redshift sample of galaxies in a cluster normally has a limiting magnitude close to the "knee".

The result of effects i) and ii) is that more non-members are likely to be found than is predicted by Table 5.2. This excess will be of galaxies with similar redshifts to that of the cluster since such galaxies are more numerous than näively predicted and have suitable apparent magnitudes for inclusion in the observed sample.

These non-members cannot be simply removed from the sample, even statistically, since the nature of the supercluster around the observed cluster is unknown. The galaxies in the supercluster may have a velocity dispersion of $\sim 10^3$ km/s (cf. the Virgo Cluster - Local Group velocity difference) and will therefore be indistinguishable on the evidence of velocity from cluster members.

Obvious background and foreground galaxies, of course, may be eliminated; it has often been the practice to remove galaxies more than 2.5σ or 3σ from the mean cluster redshift; this process does not greatly bias the derived velocity dispersions (Yahil & Vidal 1977). The remaining galaxies will be a mixture of members and galaxies from the surrounding supercluster.

5.4 Discussion of the Velocity Dispersions

It is a well known result that the velocity dispersion of groups of galaxies is much less than that in clusters; the richer a system, the greater the dispersion. The velocity dispersion ir not a single parameter for each cluster, but varies according to projected radius form the centre. Studies of Coma and A194 (Gregory & Tifft 1976,

Chincarini & Rood 1977) show that the velocity dispersion of these clusters is lowest in their centres, reaches a maximum at projected radii of 0.4Mpc in Coma and 0.8Mpc in A194, and then decreases out to at least 3Mpc. The data are difficult to interpret at greater radii, but the velocity dispersion may start to rise again. The same pattern is shown by the velocities in A1367 (Dickens & Moss 1976).

The low central velocity dispersions suggest that the centres of rich clusters are not mixed fully with the rest of the clusters but form separate bound systems. The decrease seen in the velocity dispersions at large radii can be interpreted as due to galaxies in the outer regions of the cluster following slow, radial orbits. Galaxies observed at large projected radii from the centre would then have velocities at large inclinations to the line-of-sight so their observed redshift velocities relative to the cluster as a whole would be small.

The possible increase in the velocity dispersions at very large radii may be a result of contamination by non-members. The proportion of non-members to be expected amongst the galaxies is highest in the outer areas where the surface density of cluster galaxies is low. Fast moving galaxies in the supercluster would be able to mingle with true cluster members without being bound to the cluster. It is, however, not clear whether the mistaken inclusion of non-members will increase or decrease the measured velocity dispersion, and the apparent increase in the velocity dispersions at large radii may be statistical fluctuations, or due to some other cause.

Fig. 5.1 and Table 5.3 show that the velocity dispersions are indeed low in the central areas of the clusters in the sample, but there is

too little information to distinguish any possible fall-off at large radii. Two-body relaxation in clusters would give the lighter galaxies a wider distribution and higher velocity dispersion than the more massive ones. This is illustrated by Fig. 5.2 which shows the dependence of redshift on magnitude for three clusters. There is some indication that the fainter galaxies have a larger velocity dispersion.

Velocities in the individual clusters are discussed below:-

K44 This cluster has the largest body of available data. It is remarkable for the extremely low velocity dispersion of the galaxies in the central group. Most of the redshifts of the galaxies are the mean of determinations by more than one observer so there can be little doubt that the velocity dispersion is accurate. Outside this central region the cluster shows a normal velocity dispersion. Galaxies 4, 10 and 22 have redshifts more than 10^3km/s greater than the other galaxies. Since these three galaxies have similar redshifts and are close to each other on the sky they are probably a group of galaxies in the same supercluster as K44. They have been eliminated when calculating the velocity dispersion (Table 5.3).

Fig. 5.3 shows the redshifts of galaxies near to K44 ($R < 5$Mpc). Of these 7 galaxies, 5 have redshifts appropriate to members of the cluster, and the other two have redshifts similar to those of galaxies 4, 10 and 22. Thus despite their distance from the cluster centre these galaxies show a similar redshift distribution to galaxies much nearer the centre.

Calculation of the velocity dispersions for sets of the faint galaxies and the bright galaxies shows that in the centre the velocity

dispersions are similar (223km/s(4galaxies) and 203km/s(4galaxies)), whereas in the outer region (0.2Mpc$<$R$\leq$0.92Mpc) the faint galaxies have the larger dispersion (366km/s(4galaxies) and 473km/s(3galaxies). The number of galaxies is far too small for this result to be significant.

S40/6 This cluster has a very large velocity dispersion (Table 5.3) with redshifts distributed evenly over a range of ~6000km/s. The elimination of non-members is therefore difficult. It is probable, although not certain, that galaxies 12 and 13 should not be included in the calculation of the velocity dispersion. They have redshifts more than 1000km/s lower than those of the other galaxies and they lie close to each other on the sky and have similar magnitudes. Without these galaxies the velocity dispersion is still very high, although less than the value for A426 (Chincarini & Rood 1971). The central cD of S40/6 has a redshift rather higher than that of the other 6 supposed cluster members, but this may be a sampling problem; two of the galaxies have greater redshifts and four lower. The redshift of the cD, rather than the mean of the 7 galaxies, has been used as the adopted cluster redshift.

2354-35 The spiral galaxy, g2, which is the galaxy in the cluster next in brightness to the giant cD, has been discussed in Chap. 2 where it was suggested that this galaxy is probably a foreground object. Galaxy 6 has a redshift little closer to that of the cD than has galaxy 2. Since its redshift is more than 2.5 times the velocity dispersion (calculated without it) away from the cluster mean, g6 is eliminated in the calculation of the cluster velocity dispersion. The brightest four galaxies in the cluster have a velocity dispersion no greater than the measuring errors expected. This is unlikely to

have resulted from relaxation since these bright galaxies are not concentrated to the centre (Table 5.1). The velocity dispersion of all the galaxies in the cluster (excluding g2 and g6) is similar to that of K44 (Table 5.3).

The redshifts of some of the bright galaxies near to 2354-35 have been measured (App. I) and are shown in Fig. 5.3. The galaxy 2355-35, which is the brightest member of a group, is probably associated with 2354-35. The galaxy 0001-36 may also be a member of the same supercluster; it is the brightest member of a group listed as 0000.6-3609 by Braid & MacGillivray (1978). The other galaxies with measured redshifts are apparently unrelated to the supercluster.

A496 There is little that can be definitely said about this cluster due to the small number of redshifts and the lack of photometry. Four of the galaxies (1,7,8,3), which include the central cD galaxy g1, have a velocity dispersion no greater than the measuring errors expected. The other two galaxies (4,5) have velocities 650km/s less and 1143km/s greater than these galaxies. Galaxy 5 = PKS0431-13.5 has been omitted in the calculation of the velocity dispersion.

Pavo The velocity dispersion found for the Pavo Group (Table 5.3) is typical for rich groups. The central velocity dispersion is similar to that of K44; the group is so compact that no value can be computed for the velocity dispersion outside 0.46Mpc. The pair of galaxies N6872/I4970 have similar redshifts and form a sub-system of the main group. They are unlikely to be entirely unrelated to it since they lie so close to its centre. Their redshifts are ~800km/s greater than the group mean, but a galaxy, I4985, is intermediate in redshift between them and the rest of the group. In view of this doubt about their dynamic status in the group, a velocity dispersion has been calculated without them.

Table 5.1: Adopted Redshifts of Cluster Galaxies

S40/6

Galaxy	B_{27}	cz km/s	R kpc
1	15.07	18081	6
2	15.45	15757	270
3	15.58	16681	721
7	16.25	19703	484
8	16.27	17631	956
9	16.34	16363	921
12	16.50	14258	282
13	16.55	14556	568
25	17.06	18599	546

Pavo

Galaxy	B_{27}	cz km/s	R kpc
I4960		3464	464
I4967		3939	380
I4970		4742	114
N6872		4743	97
X		3778	0
I4972		3635	141
N6876		3884	117
N6877		4103	142
N6880		3963	276
I4985		4442	441

2354-35

Galaxy	B_{27}	cz km/s	R kpc	
1	13.90	14596	0	
2	14.75	12568	363	
3	15.34	14475	933	
4	15.61	14609	1539	
5	15.95	14827	1296	
6	16.05	16370	1429	
8	16.21	14751	277	
10	16.44	14912	213	
12	16.58	14070	370	
13	16.58	15509	786	
X	16.1:	13886	1242:	≠

A496

Galaxy	B_{27}	cz km/s	R kpc	
1		9822	0	
7		9619	819	
8		9733	666	
3		9826	296	*
4		9079	296	*
5		10933	530	+

R is projected distance from the adopted cluster centre.

cz is the heliocentric redshift calculated as the mean of the values found here and those by other workers. (App. I)

B_{27} is the isophotal B_{27} magnitude. (App. IV)

* Redshift from Melnick & Sargent (1977).

\+ Redshift from Whiteoak (1972).

≠ Values of B_{27} and R estimated.

Table 5.1 (cont.)

K44

Galaxy	C ref.	M ref.	B_{27}	R kpc	cz km/s	Vel. refs.
1 = I5353	1	B	13.98	85	8080	G,C,M
2 = I5358	3	A	14.06	104	8483	G,C,M
3	4	F	14.38	93	8021	G,C,M
4	75		14.70	501	10097	G,C
5 = I5354	2	C	14.79	80	8228	G,C,M
6 = I5350	111		14.81	508	8416	G,C
7	41		14.94	817	8306	G,C
8	65		14.95	540	7965	G *
9	42		15.32	809	7551	C
10	44		15.34	577	10038	G,C
11	74		15.52	462	8941	G,C
13	5	L	15.64	63	8403	M,C
17	8/26	Q	15.92	152	8364	M
18	9	D	15.93	242	7315	M
20	64		15.97	663	8117	C
22			16.07	465	10396	G
24			16.12	539	9013	G
25		P	16.20	189	8814	M
28	14		16.28	2	8301	C
	VV19			1539	8750	C

G: This work

C: Chincarini et al (1978)

M: Maccacaro at al (1977)

* The value from C (8660km/s) has been ignored.

Table 5.2: Predicted Non-members in Redshift Samples

Cluster	Scan area squ. deg.	B_{lim}	N_r	N_b	N_f
(1)	(2)	(3)	(4)	(5)	(6)
K44	0.87	16.28	19	28	1.2
S40/6	0.31	17.06	9	25	0.6
2354-35	0.35	16.58	10	13	0.8
A496	0.10	15.3	6	12	0.0
Pavo	0.13	14.0	10	12	0.0

Explanation of columns:

(2) C, the scan area, or, in the case of A496 and Pavo, the approximate area from which the redshifts are drawn.

(3) B_{lim}, the B_{27} of the faintest galaxy for which a redshift is available. The values for A496 and Pavo are estimates.

(4) N_r, the number of galaxies in the cluster with known redshifts; VV19 in K44 is not included.

(5) N_b, the number of galaxies in the scan area at least as bright as B_{lim}. Values for A496 and Pavo are estimates.

(6) N_f, the predicted number of galaxies among those with known redshifts that are non-members. The number of field galaxies per degree, N, is assumed to be:-

$$\log_{10} N = -9.47 + 0.6m \qquad \text{(Chap. 8)}$$

with $m = B_{lim} - A_B$ A_B is the Galactic absorption.

Then:

$$N_f = C\ N\ N_r / N_b$$

Table 5.3: Velocity dispersions

Cluster	e	All			$0.0 \leq R < 0.2$			$0.0 \leq R \leq 0.46$			$0.46 < R \leq 0.92$		
	km/s	$\bar{v}$ km/s	n	S km/s	$\bar{v}$ km/s	n	S km/s	$\bar{v}$ km/s	n	S km/s	$\bar{v}$ km/s	n	S km/s
K44	100	8456	20	775	8221	8	220	8110	9	388	8751	10	958
K44 el.	100	8183	17	427	8221	8	220	8110	9	388	8214	7	497
S40/6	150	16370	9	1720	17537	1		15600	3	1817	16875	4	2128
S40/6 el.	150	17030	7	1289	17537	1		16440	2		17766	3	1429
2354-35	150	14241	11	894	14241	1		13843	5	899	15108	1	
2354-35 el.	150	14269	9	425	14241	1		14228	4	314	15108	1	
A496	120	9673	6	573	9661	1		9423	3	399	9925	3	693
A496 el.	120	9462	5	277	9661	1		9423	3	399	9520	2	
Pavo	80	4041	10	428	4119	6	478	4108	9	396	3444	1	
Pavo el.	80	3876	8	282	3825	4	178	3937	7	241	3444	1	

Cluster: The values for clusters without and with (el.) elimination of possible non-members. These omitted galaxies are:-

In K44; g4, g10, g22 In S40/6; g12, g13
In 2354-35; g2,g6 In A496; g5 In Pavo; N6872, I4970

e: The estimated mean measuring error in the velocities of galaxies of the cluster.

$\bar{v}$: The mean relativistic (not v=cz) velocity of the galaxies.

n: The number of galaxies used in the calculations.

S: The velocity dispersion, corrected for measuring error (Chap. 5.2).

$\bar{v}$, n and S are given for different projected distances from the cluster centre as shown by R (in Mpc).

Fig 5.1: Distribution of Redshifts

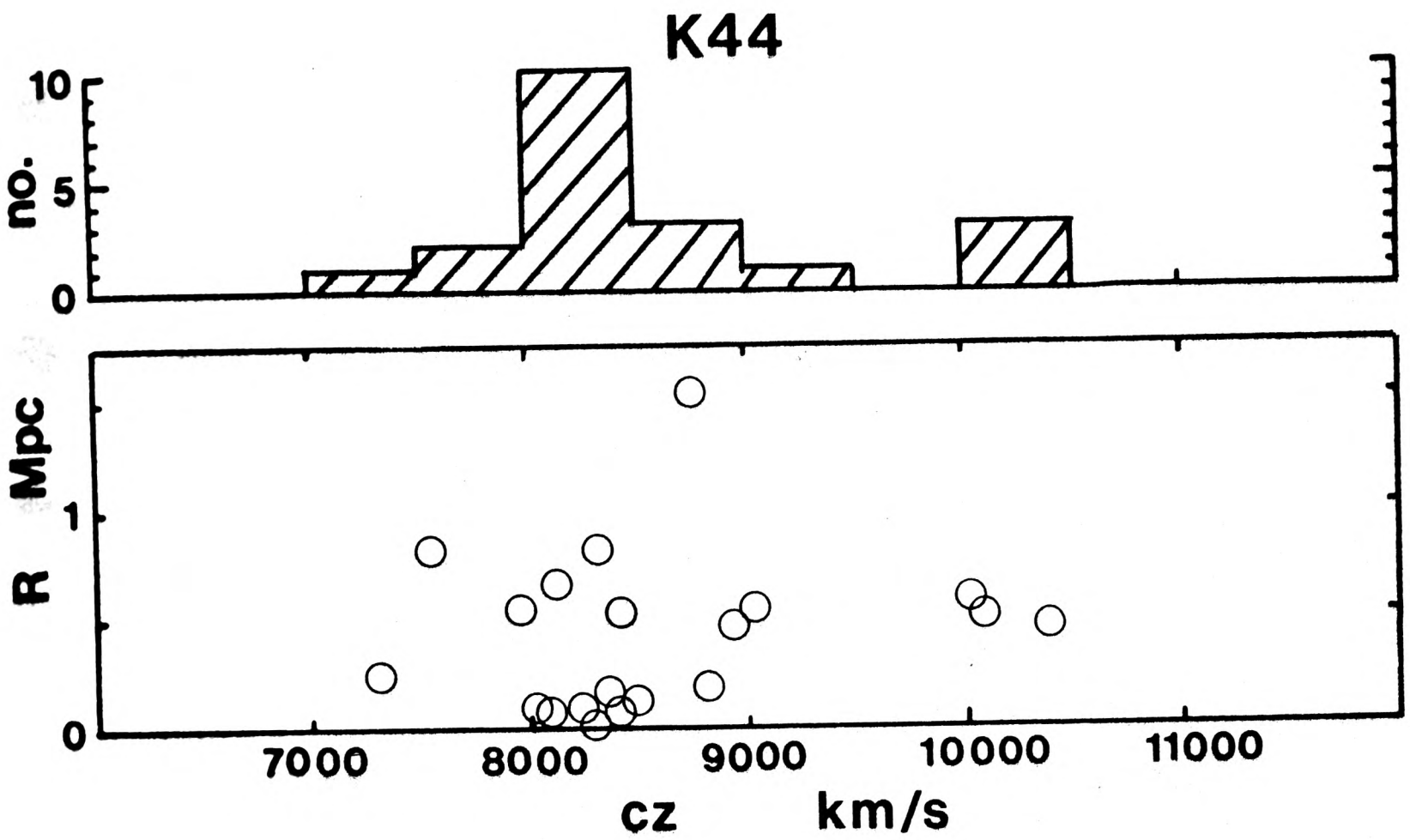

This, and the four diagrams on the next two pages, show the distribution of redshifts in the five clusters: K44, S40/6, 2354-35, A496 and the Pavo Group.

The lower part shows the space distribution of the redshifts, plotted in terms of the projected distance of the galaxies from the adopted cluster centre.

Data are taken from Table 5.1.

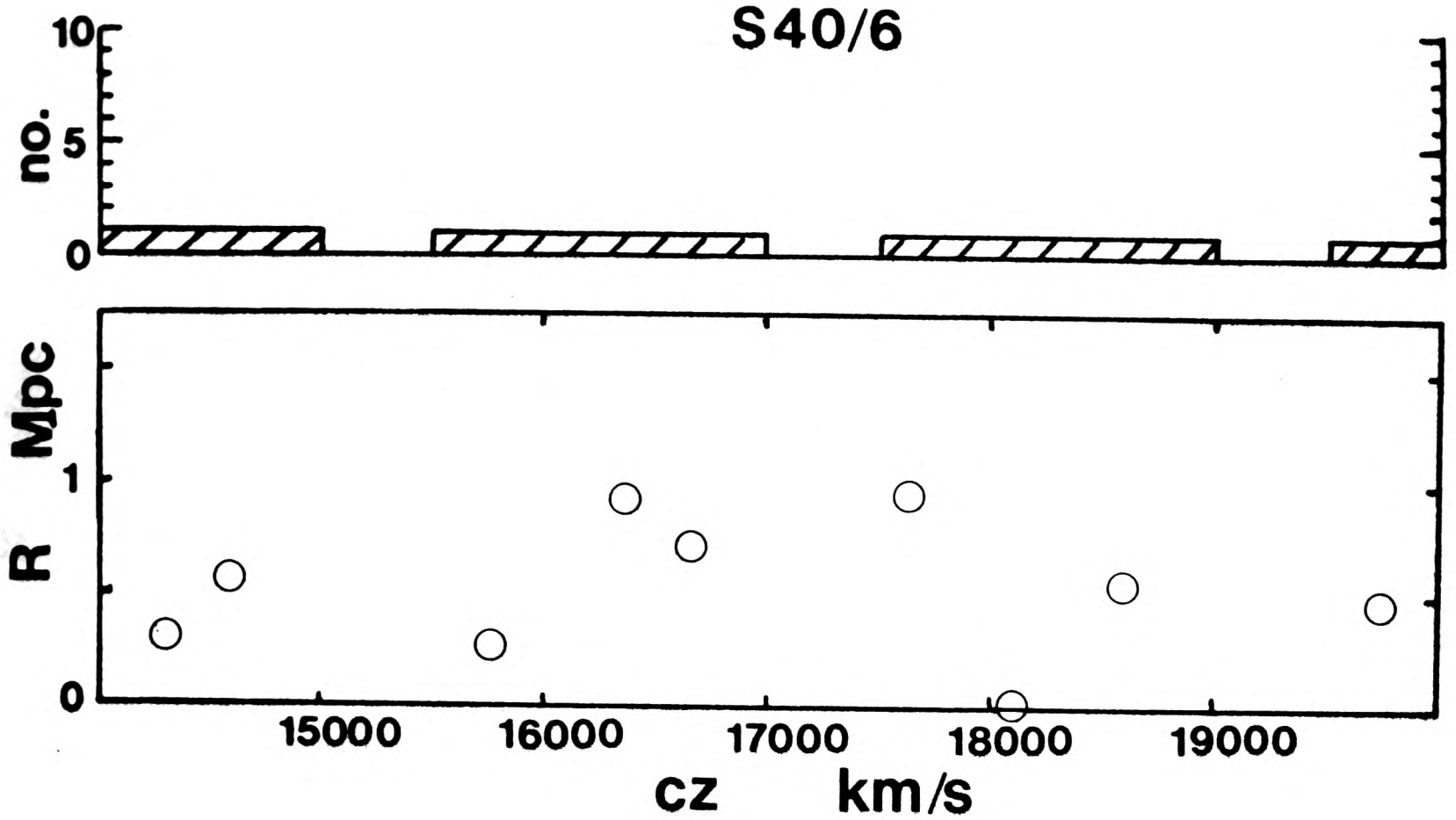
S40/6
10
5
0
no.
R Mpc
1
0
15000
16000
17000
18000
19000
cz km/s

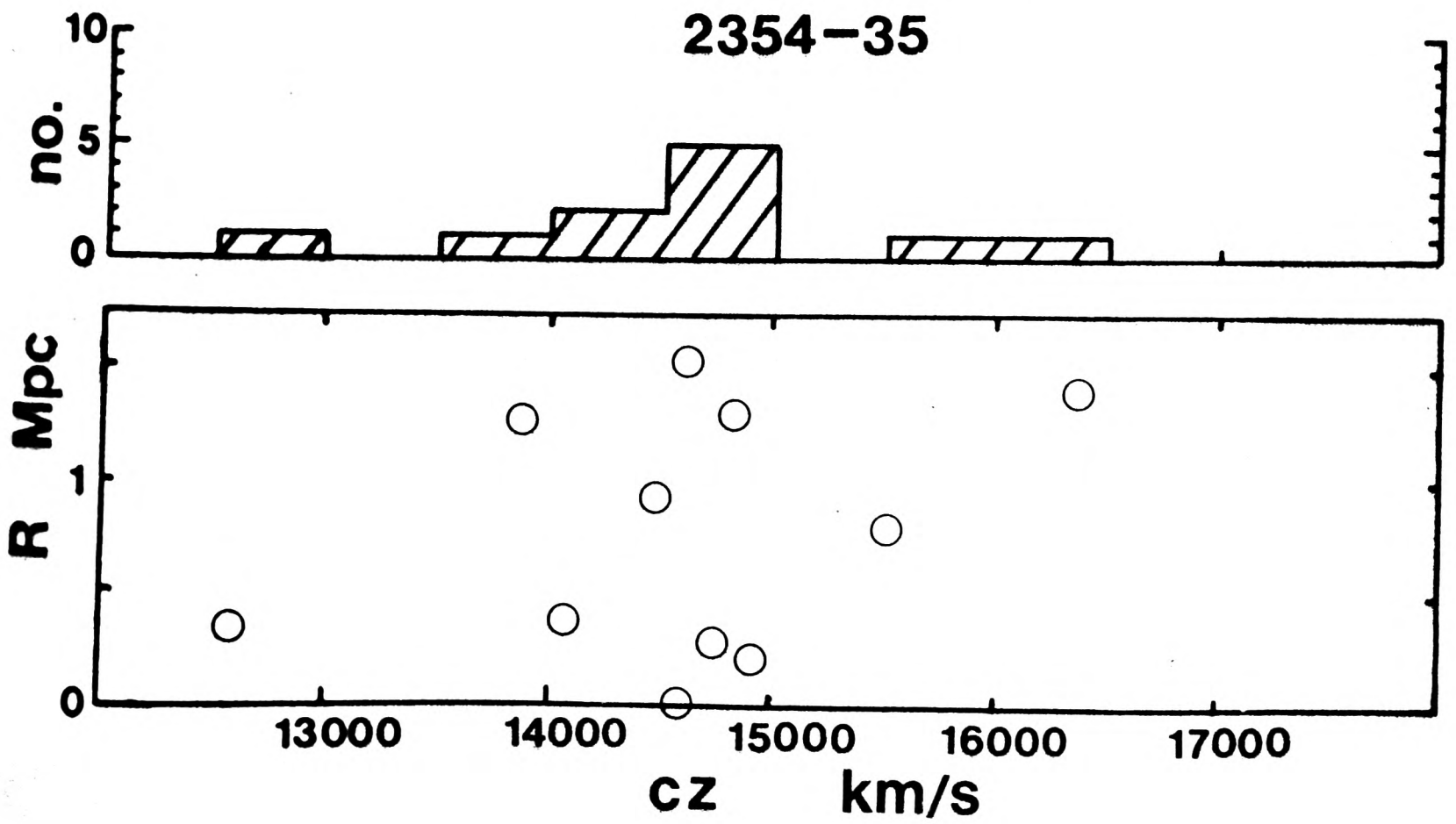
2354−35
10
5
0
no.
R Mpc
1
0
13000
14000
15000
16000
17000
cz km/s

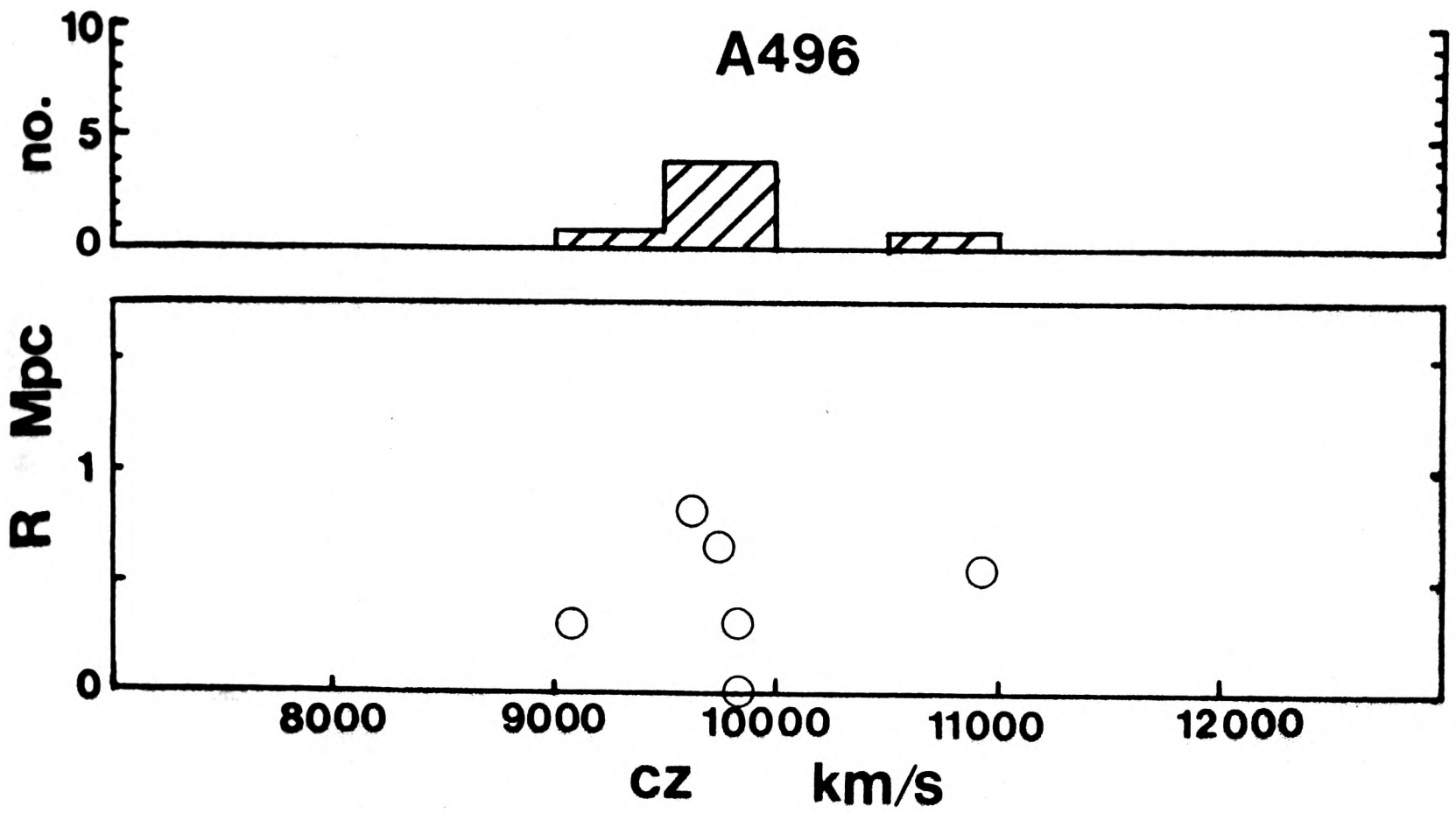
A496
10
5
0
no.
R Mpc
1
0
8000
9000
10000
11000
12000
cz km/s

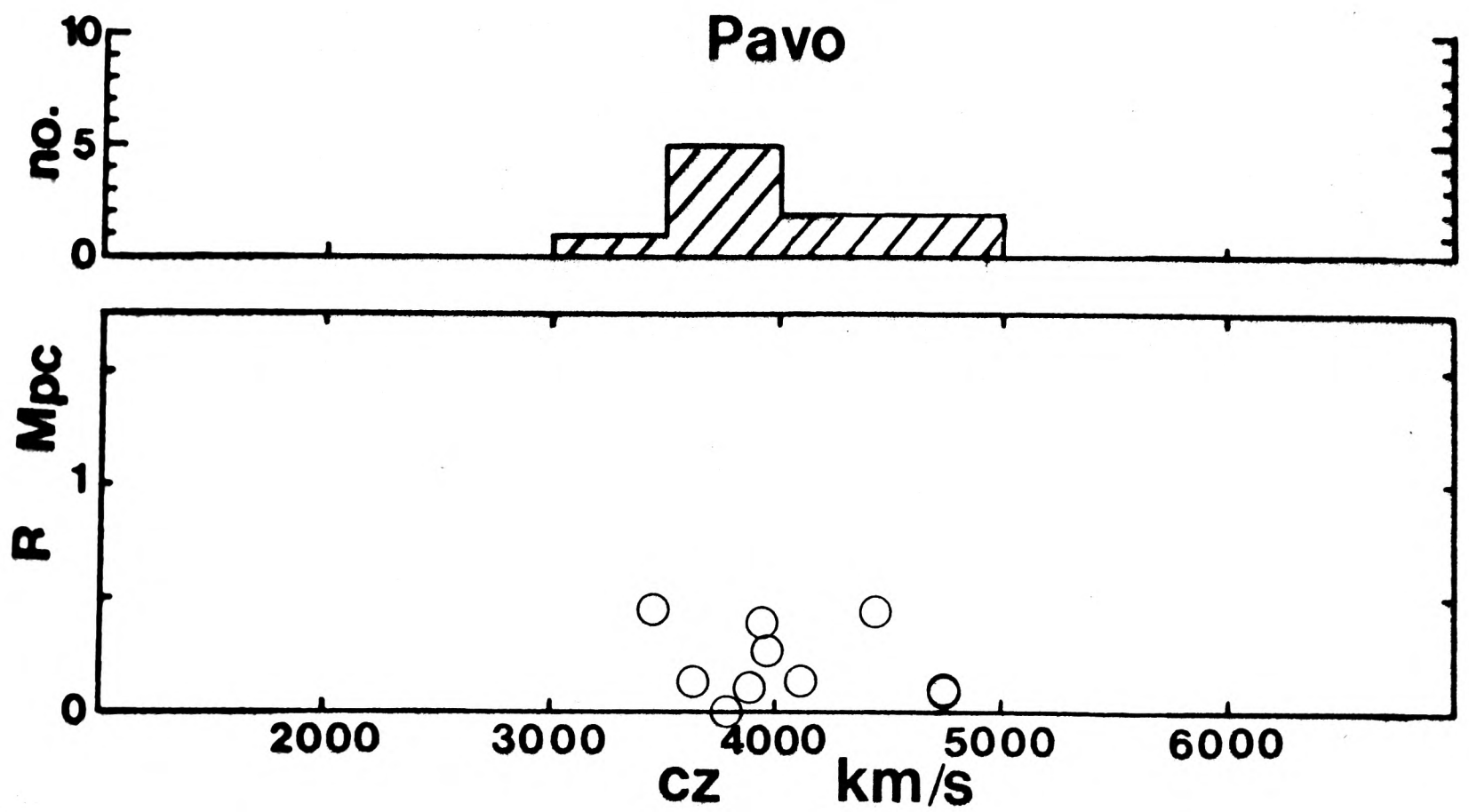
Pavo
10
5
0
no.
R Mpc
1
0
2000
3000
4000
5000
6000
cz km/s

Fig. 5.2: Variation of redshifts with magnitude

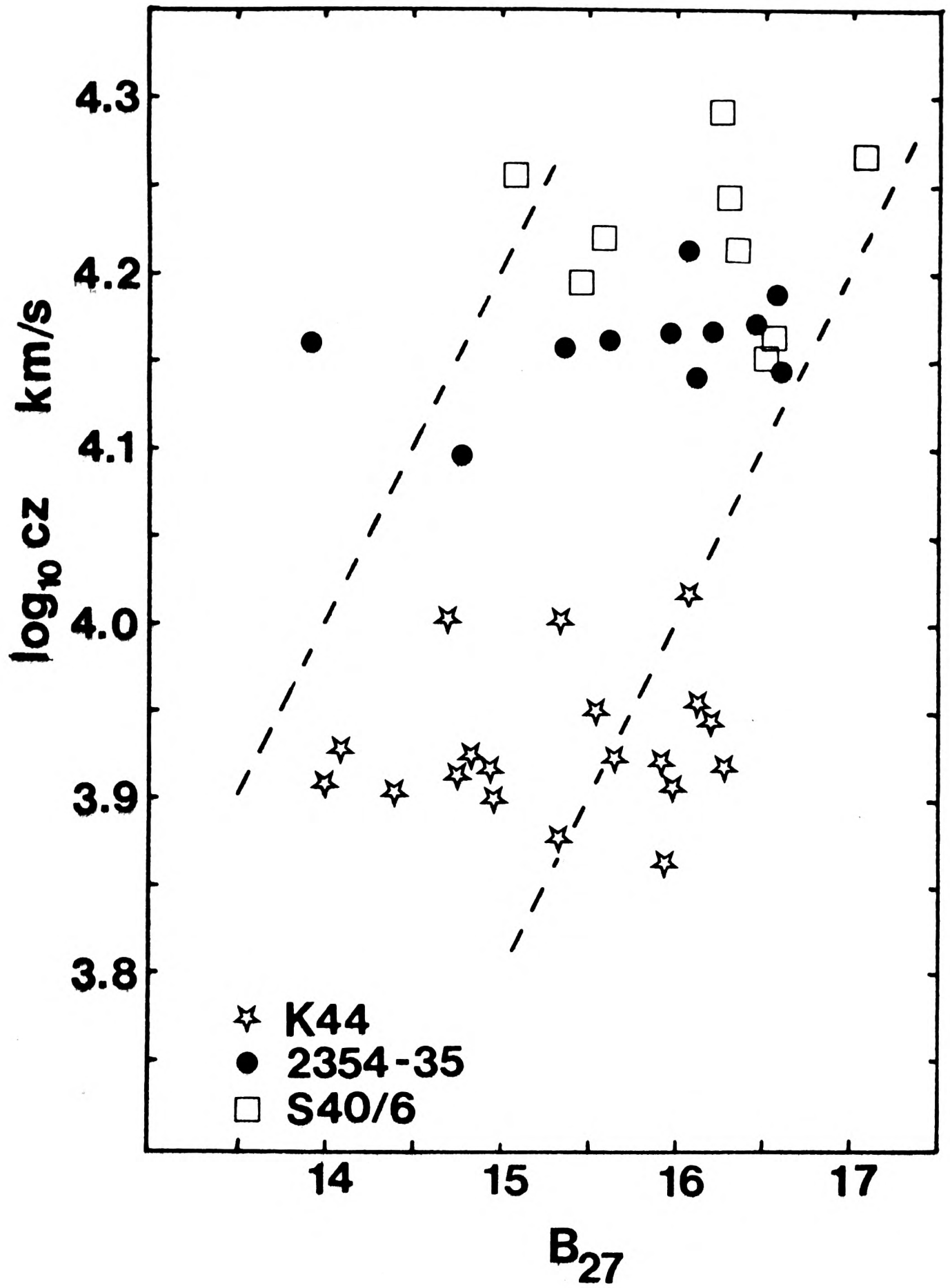

Data from Table 5.1

Dashed lines have gradient of 0.2

Fig 5.3: Velocities of galaxies near K44 and 2354-35

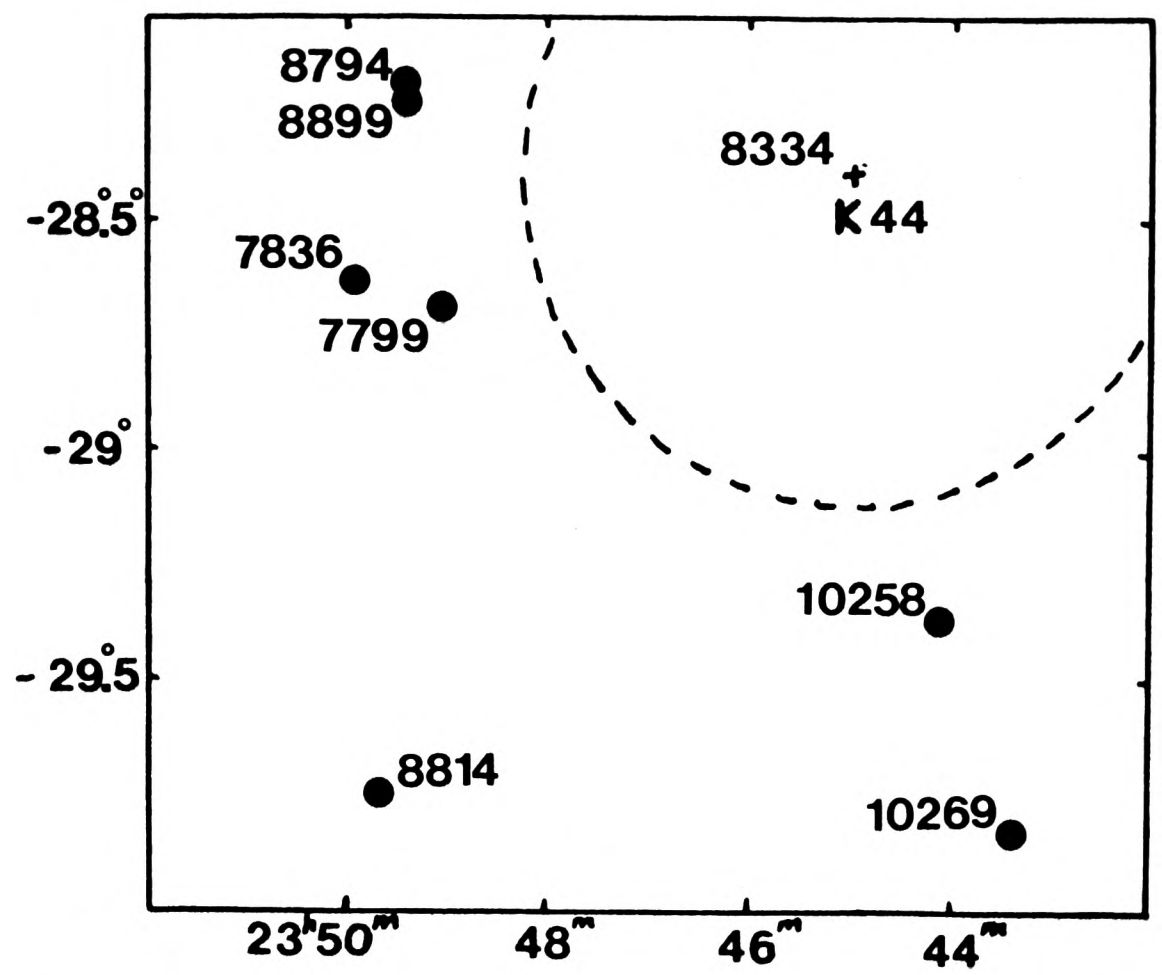

i) K44

Data from Chincarini et al (1978)

Values are of v=cz in km/s. Circle is 2Mpc radius.

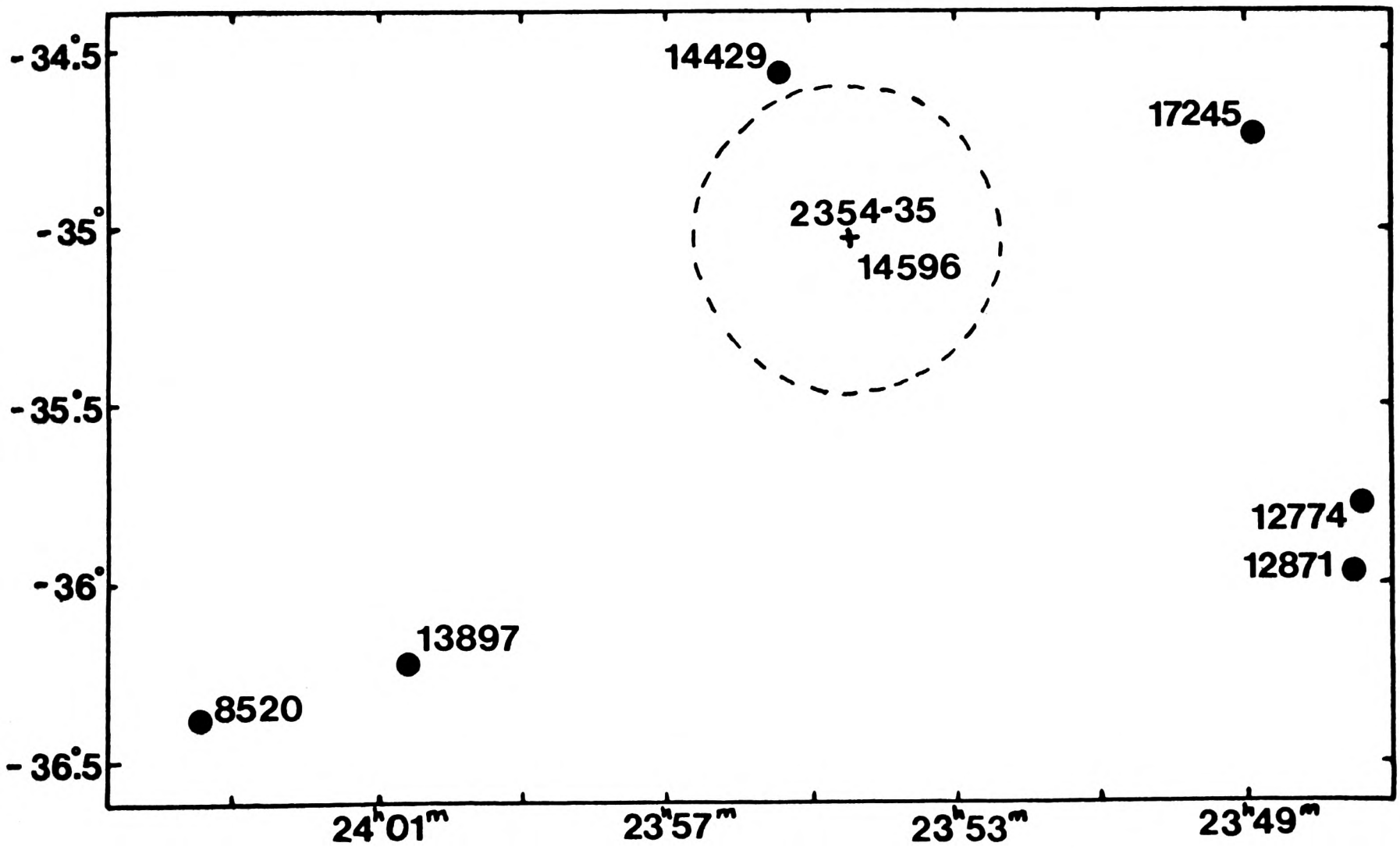

ii) 2354-35

Data from this work (App. I)

Values are of v=cz in km/s. Circle is 2Mpc radius.

Chapter 6: Photoelectric Photometry

6.1 Equipment and Observations

This chapter describes multi-aperture photelectric photometry of galaxies carried out using the 74" and 40" telescopes of the SAAO at Sutherland. The results incidentally help to complete the photometry of NGC and IC galaxies, but their primary aim was to provide standards for the photographic photometry of clusters. Data from this chapter were used in this manner in the study of southern clusters; Chapter 7 describes the way in which this was done.

In April 1976 the People's Photometer was used at the Cassegrain focus of the 74" Radcliffe Reflector at Sutherland. Comments about this telescope may be found in Chapter 3. Due to very bad weather only 4 galaxies were observed. The People's Photometer, described in the SAAO Facilities Handbook, is similar to the photometer on the 20" telescope at Sutherland, and to the RGO Travelling Photometer. It is a single channel instrument; the sky cannot be monitored at the same time as the galaxy, but must be observed separately. Apertures are mounted on slides and can be selected as required. Filters can also be moved into the beam.

Two photomultipliers are fitted, either one of which can be used as detector. Both are fitted with cold boxes, and their photocathodes are S-11 and Extended S-20. To simplify and speed up operation, only the S-20 photomultiplier was used, even for B-band measurements.

The signal, after DC amplification, was displayed on a chart recorder. This showed both a rate of counting and a mean rate for each integration period. The former acts as a check that the transparency of the atmosphere does not change excessively in the course of an integration. Measurements were carried out in 4 colour bands and through 6 apertures for each galaxy.

The observations in October 1977 used the 40" Elizabeth Reflector at Sutherland. The St. Andrew's Photometer, like the People's, is a single channel instrument with similar photomultipliers and cold boxes. Apertures must be selected manually, but the filters are controlled by programmable logic circuits which carry out a previously specified sequence of filter and photomultiplier changes automatically. The signal from the photomultiplier is processed by a pulse-counting system, and the integrated count is printed on a teletype and punched on to paper-tape. A chart recorder monitors the count rate at each instant.

Readings were taken in the B,V,R and I bands and through several apertures. Five were available in the wheel used during all of the nights except for the first. All of these apertures were used except in the event of shortage of time, and on one night when the seeing was bad (~12") so that use of the smallest aperture was thought inadvisable.

The observing and reduction procedures were similar for the two instruments.

Sky readings were taken corresponding to each galaxy reading; repeat measurements on galaxies were made, but not generally on the sky. Some galaxies were observed on more than one night,

especially if there was any reason to doubt the accuracy of the readings.

Both photometers are fitted with Varo image tubes which can be used to look through the aperture. The galaxies and standard stars were centered using the Varos; the brightest part of the image being put into the middle of the aperture. Used on diffuse galaxies without bright nuclei this method would be unsatisfactory, but the nuclei could in all cases be unambiguously identified.

A summary of the photometric equipment is given in Table 6.1. This includes details of the filters used. As noted in the Table, the standard stars used are all in the Harvard E regions which are conveniently spaced around the sky at $\delta \approx -45^{\circ}$. Standard photometry of these stars has been carried out by Cousins using the 18" telescope at the Cape. His BVRI photometry (Cousins 1973,1974) has been extensively used and no serious errors have been found by other workers. The standards were observed at regular intervals through the night using a large aperture (40"); using a smaller one would have resulted in significant light (>1%) being lost by seeing and a consequent overestimation of the brightness of the galaxies.

6.2 Reduction of the Results

The output from the People's photometer was in the form of chart recordings and notes of the amplifier gain settings. The gain calibration of the amplifier ranges was checked to ensure the

compatability of readings on different ranges. The photomultiplier was assumed to be linear; this assumption is unlikely to be significantly incorrect as the light intensities were well within the normal working range, and no anomalies were found between standards of different magnitudes.

The St. Andrews Photometer produced both teletype and punched tape output. The teletype listing was amended to remove the rather frequent errors produced by the character generating system, and corrected for the dead time after a photon detection. This correction is a few percent in the case of bright standard stars (V~8), but much smaller for the galaxy readings since it is proportional to the rate of counting.

The reduction procedure for the data from both instruments used the SAAO computer at the Cape. The sky readings were subtracted from the galaxy and star readings, and corrections made for the extinction which was calculated separately for each night. Colour equations were adopted from previous work by other observers using the same equipment recently enough for there to have been no major change (e.g. due to the mirror coating ageing).

The results, after the combination of data from different nights, are given in App. 5. The colour system is that normally used at the SAAO: B and V are the standard bands as revised in the South by Cousins (1973) and R and I are in the Cape-Kron system, as described by Cousins (1974). The latter bands are approximations to the Kron bands with an adjusted zero-point; R has an effective wavelength of ~6700Å and I of ~8100Å.

No attempt has been made to correct the results for the presence of stars in the aperture when taking the galaxy readings. None in

fact were noticed through the rear-of-aperture viewer, nor were any bright nearby stars apparent on Schmidt plates of the galaxies. When the photoelectric data are used as standards for photographic work, the magnitudes including any stars must be used.

Errors in the magnitudes and colours depend to some extent on the brightness of the galaxy; purely on the basis of photon statistics there will be an error of ~0.02 in V for the faintest galaxies. Most of the error, however, for the brighter galaxies is due to other causes: extinction and sky brightness variations, inaccurate colour equations, and bad centering in the aperture. Galaxy photometry is particularly susceptible to errors caused by sky brightness variations since, through large apertures, even fairly bright galaxies (V~12) are no more than twice the sky brightness. For the fainter galaxies in the sample, the sky contributes most of the light detected. Large aperture readings are also prone to errors if the photocathode is not uniform and is unevenly illuminated by the Fabry lens. Colours that use two photomultipliers are particularly susceptible to this type of error. Drifting stars across the aperture of the People's Photometer showed some variations in count rate with position, enough to cause up to 0.01 magnitudes error, according to galaxy type and profile. No aperture larger than 80" was used since this type of error is greater for large apertures.

The errors in the magnitudes and colours can be estimated by several methods:

a) Comparison between readings in the same night suggest an error of 0.02 mags. in V, B-V and V-R, and of 0.05 mags. in V-I. This error estimate is certainly over-optimistic since it takes no

account of errors in the extinction for the night, or of systematic errors in the photometer.

b) Comparison between readings on different nights for the same galaxies suggests errors of 0.03 in V, 0.02 in B-V, and 0.04 in V-R and V-I.

c) The residuals of standard stars give some idea of how self-consistent the photometry of the night is. Errors judged by this method are very small as stars, measured with short integrations, are not separated by as great a time as galaxies from their sky readings. The photon counts are larger, also leading to greater accuracy.

d) An upper limit to the errors in a colour can be found by assuming the colour varies smoothly across the galaxies, and then finding the amount by which the data are in disagreement. Again this takes no account of the systematic errors in the photometer. Errors estimated in this way are 0.03 for B-V, and 0.02 for V-R and V-I.

e) By far the best test of accuracy is the comparison with previous photometry by other workers. Systematic errors are very unlikely to remain undetected since different telescopes, photometers, standards and reduction methods are used. There is also very little risk of misidentification of galaxies. Other photometry is usually in V and B-V; there are no suitable comparisons for V-R and V-I. Some difficulty arises due to the different aperture sets used by other photometrists, and in only a few cases do the apertures span the whole range of those used here. Plotting the magnitudes against radius and interpolating by hand for all the galaxies in common with previous work suggests an error of ~0.03 in V, assuming all other

work to be equally good and the errors in them random. A similar treatment of B-V gives an estimated error of 0.02. No systematic differences can be seen between the data from different sources, except for a tendency for Alcaino (1974,1976) to find small aperture magnitudes that are too large.

The adopted estimates of the errors in the photoelectric photometry, based on the estimates given above, are:

in V 0.04 in B-V 0.02 in V-R 0.03 and in V-I 0.04

The fainter galaxies will have rather larger errors, particularly in V-I which is adversely affected by the very low count rates in I.

A hidden source of systematic error is the accuracy of the adopted image scale of the 40" telescope. It is possible that the hitherto assumed image scale is too small by ~6% (Corwin 1978, priv. comm.). If this is the case, then the aperture sizes quoted in the present work should be increased by this factor. The effect on the accuracy of the calibration of photographic photometry by these readings is less since, although the galaxies are being sampled at greater radii than assumed, the areas sampled will also be greater. Hence the fainter surface brightness is compensated by larger areas, and the mean derived surface brightness for a particular annulus of the galaxy is not affected by as much as 6%. For the particular example of a galaxy with a profile $B \propto r^{-2}$ (B is surface brightness), a systematic scale error in the aperture sizes has no effect at all on the mean surface brightnesses calculated for annuli.

The results for the photoelectric photometry are given in App. V. Previous photometry by other observers is noted.

Table 6.1: Summary of photoelectric methods

Dates	18-24April 1977	4-10 Oct 1977
Telescope	40", Sutherland	74", Sutherland
Photometer	People's	St. Andrews'
System	DC Amplifier and chart recorder	Pulse-counter and teletype
No. Galaxies Observed	4	17
Filters & Photocathodes:		
B	1mmBG12+2mmBG23 +2mmGG13, Extended S20	1mmBG12+4mmGG385, S11
V	3mmGG495+4mmBG38, Extended S20	2mmOG515, S11
R	2mmOG570, Extended S20	2mmOG570, Extended S20
I	3mmRG9, Extended S20	3mmRG9, Extended S20
Standard Stars	Harvard E region Cousins (1973,1974)	Harvard E region Cousins (1973,1974)

Chapter 7: Photographic Photometry

This chapter describes the methods used for the photographic photometry of the clusters K44 and S40/6. The data for 2354-35 in Bucknell (1977) were obtained by similar techniques, but the automatic star-galaxy sorting was not used. Carter & Godwin (1979) also used similar methods in their study of A1146 from an AAT prime focus plate. The results for these 4 clusters are given in App. IV.

7.1 Plate Material and Colour Systems

The plates of K44, S40/6 and 2354-35 were taken by the U.K. Schmidt Telescope Unit with the 48" Schmidt telescope at Siding Spring, Australia. This has a plate scale of 67.1 arcsecs/mm, similar to that of the Palomar 48" Schmidt.

Hypersensitised IIIaJ, 14"x14", plates were used; they have a high contrast, small grain size and good uniformity, making them ideal for the study of faint galaxies. The plates were treated in the same way as Southern Survey plates; the hypersensitising procedure is discussed by Cannon et al (1978).

A summary of the plate material is shown in Table 7.1.

The photoelectric readings used for the magnitude zero-points of the photographic photometry were in the standard B band, based on the wavelength response of a photocathode behind a filter. To mimic the B band photographically, a 2mm GG395 filter was used with the IIIaJ plates. The redward cut-off is defined by the plate response,

the blueward by the filter. Fig 7.1 shows the resulting band plotted using manufacturers' specifications. The photoelectric B band is included for comparison (Johnson & Morgan 1951, Matthews & Sandage 1963). The match between the bands is not exact, the photographic band being wider than the photoelectric. This may lead to magnitude errors, especially when the galaxy being measured has a spectrum that differs markedly from that of the photoelectric standard. It is encouraging that values for the magnitude zero-point of a plate are not systematically different when galaxies of different colours are used in their determination.

A variety of colour bands have been used for the photographic photometry of galaxies. Oemler (1973,1974) used a red band and one between B and V, whereas Godwin (1976) reduced his data to the standard V band. The red colour of galaxies with redshift $z < 0.5$ make it advantageous to use long wavelength bands, rather than one based on B, especially if the 5577Å night sky emission line can be avoided.

7.2 Plate Scanning

The plates were measured on the Herstmonceux PDS 1010A micro-densitometer. This is a single-beam flat-bed machine, capable of scanning in two dimensions. A PDP minicomputer controls its operation. A beam from the lamp is thrown on to the plate as a spot; the light passes through the plate and is collected by an objective lens. The limiting aperture of the system is in the objective image plane. A photomultiplier detects the signal and feeds it to a logarithmic amplifier. The output is thus values of semi-diffuse density, D = -log (transmission), for points on

the plate. The readings are digitised into 4096 levels (1024 in the case of the 2354-35 data) and recorded on magnetic tape, each tape holding about 4.2×10^6 readings.

A small density-dependent time constant is present in the system, resulting in the apparent "trailing" of high density regions as seen on isophotal maps. Only bright images are affected, and even then only the central contours are distorted; no correction was needed to the isophotal magnitudes.

The position of the PDS table is monitored by Moiré fringe units on the x and y axes; they give a positional accuracy of ~2μm. The area of interest is scanned boustrophedonically and the data converted to a raster scan in the computer reduction. The carriage for the plate is designed for a maximum plate size of 10", so the plates, being 14" square, had to be repositioned on it for scans in different areas. A heavy glass plate was placed on top of the plates during scanning to keep them flat, otherwise they tended to bow due to the edges drooping over the sides of the carriage and because of the "memory" of their bending in the telescope. Use of this cover plate greatly reduced the number of occasions on which it was necessary to refocus the objective between scans on a plate.

A square aperture was used, generally of side 24μm, and the sampling points were separated by 25μm. Rather more information would have been gained by sampling the plate with a smaller aperture and separation, but at the penalty of making the data-reduction more laborious. S40/6 was scanned with 15μm aperture and separation because it is distant and so a smaller area needed to be examined.

Its distance and hence faintness would also make star-galaxy sorting difficult with the larger aperture and separation.

7.3 Calibration of the Plates

Plate calibration was by the rather unsatisfactory temporary system fitted when the telescope was commissioned. This consists of two step wedges, one evaporated metal on glass and the other a photographic copy of the first. Each has seven approximately square steps of progressively increasing density arranged side by side in a line. Beams from separate lamps pass through the wedges and expose areas of emulsion near opposite corners of the plate. The wedges are not identical and many of the steps have large gradients across them. The densest of the steps is so bad as to be unusable, leaving the high density end of the calibration curve ill-defined as a consequence.

The wedge exposures were scanned in 150 lines running along their length so that they passed through all of the steps in turn. Each line contained 1000 points; the line separation was 50μm and the sample separation 25μm, thus covering the complete area of the wedge exposure in the scan. The same aperture was used as for scans of the cluster and standard galaxies.

Any lines that fell outside the area of the wedge exposure were removed from the scan and then representative values for the density of each step were found by two separate procedures:

In the first, a moving window of 5x5 points was passed over the scan. If in any position none of the 25 density values deviated by

more than a defined amount from their mean, then that mean was noted. In this way a list of smoothed density values for flat parts of the steps was formed. Plotted as a frequency histogram, the density of each step of the exposure appeared as a sharp peak. The centroid of each peak was taken as the representative value of the density of a wedge exposure step.

The second method was the averaging together of the lines of the scan to form a single smoothed profile along the length of the wedge exposure. A straight line was fitted to this profile along each step and the middles of the lines were taken as the densities of the steps. Fig. 7.2 shows a typical wedge plotted in this way.

The second method, although crude, was the more satisfactory since, like the calibration of the light intensities exposing the wedge steps, an average over the whole step was used. The first method tended to give density values representative of only the occasional flat portions of the steps and not of the step as a whole.

Some error will be caused by averaging in light intensity over the step during the calibration of the wedges, and then averaging over the density that it causes in the exposure. For IIIaJ emulsion, density and light intensity are linearly related over small ranges and the error is minor compared with errors caused by doubts in the extent of each step and the uncertainties in the wedge intensity calibration.

Values for the intensities were taken from the calibration by Tritton (1977). The log intensity vs. density curve for the IIIaJ

showed the typical form with a low density , under-exposed "toe" and a high intensity saturation. The curves found separately for the two wedges were combined by adding a constant to the log intensity values used for one of them. The intensity units are arbitrary until linked to a photometric system.

Traditionally, plate calibration curves are fitted analytically by a Baker function (Baker 1957, de Vaucouleurs 1968):

$$I = A(10^{D/B} - 1)^n$$

with A, B and n constants; I is intensity and D density.

Or, to allow for the high intensity saturation, the Kaiser function (Honeycutt & Chaldu 1970) which has a gradient that reaches a maximum and then decreases:

$$I = A\ 10^{n(\log(10^{D/B} - 1) + k\ 10^{D/B})}$$

Here k is an extra constant that determines the saturation; if k=0 then the Kaiser form is identical to the Baker function.

The curve for the plate of 2354-35 was fitted by a Kaiser function succesfully. It was not possible to find a stable fit for the other plates since the saturation was not defined well enough, leaving k undetermined. Both Baker functions and cubic polynomials were satisfactory; the latter were used since they show, by chance, the expected form of saturation at high intensities. In general such a low order polynomial cannot be expected to fit calibration curves, but in these cases higher order polynomials fitted less accurately and often showed instabilities due to the small number of data points and their irregular distribution.

The calibration curve for the K44 plate is shown in Fig. 7.3. The form of the curve below the sky density (D~980 PDS units) is

unimportant. The points have a dispersion of ~2% in intensity about this fit.

7.4 Transformation of the scan to intensities

The computer programs used for the reduction of the cluster scans are slightly adapted versions of those given by Godwin (1976, 1977). The method is based on the work of Jones et al (1967).

The first stage is the transformation from the raw scan of density values to a grid of relative intensities, using the plate calibration and correcting for variations of background across the plate. All the clusters are at high galactic latitude, but even so there may be faint luminosity spread across the fields. Such emission has been shown to exist in at least some areas by Sandage (1976a); it may be as bright as μ_v=25mag/□". When only one plate is used there is no way of being sure to what extent the background variations are due to this emission or to changes in the plate characteristics. Vignetting is negligible in the central parts of U.K. Schmidt plates, but the reduction method used corrects for it if present.

The assumption was made that the calibration curve of the plate did not vary in shape from place to place, but that the background variations were caused by a change in the log intensity zero-point. Previous work (Godwin 1976) has shown that this assumption is reasonable, providing the variations are small, and this is supported by the ease with which the data from the two wedge exposures in opposite corners of the plate can be combined in a single curve.

The scans of the wedge exposures, cluster and standard galaxies were all carried out in the same session and the wedge scans were repeated before and after the cluster scans. This makes it possible to detect any drift in the PDS density zero-point and correct for it, on the assumption that it is linear with time, by subtraction.

The density of the sky background in each part of the scan was found by dividing the scan area into a grid of 32x32 squares. The value of the background in each of these 1024 squares was found by eliminating all points with densities deviating from the mean by more than 1 s.d., recalculating the mean and repeating the rejection, and finally recalculating the mean and rejecting those beyond 2.5 s.d.. The mean of all those values remaining was taken as the background value for that square. The simpler method of using the most common value of density in the square as the background could not be used because of the preference in the digitiser for certain values.

Orthogonal polynomials were then fitted to the resulting 32x32 grid of background values. Points deviating more than 1 s.d. from the polynomial were rejected. This process of fitting and rejection was repeated 4 times with rejection limits of 2,2,2 and 3 s.d.s to give a final polynomial representation of the background across the plate. The fitting is not affected by objects much smaller than one of the squares since density values in the image are eliminated when calculating the background for that square. Images a similar size to the squares are also removed since they only affect the background values in at most a few squares and these values are

eliminated in the fitting of the polynomials. Low order polynomials (normally third order) were used so that only images larger than ~200x200 points are likely to alter the background determination, unless they have very low surface brightness and avoid rejection. Ultimately, there is no way of distinguishing between large objects and variations in plate sensitivity that have small spatial wavelengths.

The background polynomial was used to determine at each point the density, D_s, of the sky background; to be contrasted with D_m, the actual density measured at that point. The difference between D_s and D_m is the result of noise and images on the plate. The calibration curve I(D) is used to convert these densities to brightnesses, so that the brightness due to images (and noise), I_i, at that point can be calculated:

$$I_i = \frac{I(D_m)}{I(D_s)} - 1$$

where I_i is in units of the sky brightness.

Any gross mistakes in the background determination produce either spurious low surface brightness objects if the background is too faint, or "shelves" in images if it is too bright. The profiles of the stars in different parts of the plate will also differ if the background is incorrect.

7.5 Absolute Calibration by Photoelectric Readings

Absolute calibration of surface photometry on photographic plates cannot be easily achieved from photoelectric stellar sequences. Images of bright stars are so saturated that most of the light from them is wasted, whereas faint stars only give very inaccurate results unless many are used, and their photoelectric photometry is very time

consuming. Research is at present being carried out in several centres to perfect methods of using stellar photoelectric data, despite the difficulties mentioned above, and in the future it may well become the best technique.

Another method sometimes adopted is the use of a photometer to monitor the sky at the same time as the exposure is taken; the brightness due to stars in the photometer field is then removed to give a value for the sky brightness on the plate. Unfortunately the sky photometer used on the U.K. Schmidt was faultily calibrated at the time the plates were taken, and only tentative guesses at the true sky brightness can be obtained from the readings given (Tritton 1978, priv. comm.).

In this work, a simpler and, at present, more reliable method can be used which depends on the comparison of photoelectric surface photometry of galaxies with the sky brightness. Obviously the method cannot be used for all Schmidt fields since, for example in the plane of the Galaxy, there may be no bright galaxies or similar objects.

The photoelectric photometry of galaxies in the fields of interest is described in Chap. 6 and the results are given in App. V. Additional data have been used from other authors where available, but in the South there has been little photometry carried out on galaxies through more than one aperture.

The photoelectric readings are made through circular apertures and may be subtracted to give the mean surface brightness of annuli of the galaxy. A similar process is carried out in the computer on

the scanned image of the galaxy from the photographic plate, which has been converted to relative intensities as described in the last section, giving the mean surface brightness of each annulus in units relative to the sky brightness. By comparing the values found for an annulus by the photoelectric and photographic methods, the sky brightness may be found. The brightness scale of the photographic scan of the cluster can then be expressed in photometric units instead of relative to the sky. If the calibration curve is accurate for the plate, then the sky brightnesses found using different annuli should agree; this method thus provides a useful check. The zero-points found are shown in Table 7.2. for each plate.

The sky brightness value derived is not that actually seen; it has been altered by the atmospheric extinction since it is found from galaxy photoelectric readings which have themselves already been corrected for the extinction.

Typically the sky brightnesses found from the annuli of both the same and different galaxies have a dispersion of ~0.15mags. Part of this is due to the uncertainty in the calibration curve of the plate and background fitting, but errors in the photoelectric photometry are also significant since the brightness for each annulus is the difference between two photoelectric readings. The area inside the smallest aperture cannot be used for the determination of sky brightness since the calibration curve is unreliable for the over-exposed nucleus of the galaxy.

7.6 Determination of Galaxy Magnitudes

The aim is to derive isophotal magnitudes for each object in the scan area. The data for the photometry were the 2000x2000 point arrays

of brightness readings produced by the transformation of the PDS densitometer scan. For processing, these arrays were divided into squares of 250x250 points, the maximum size that can be held conveniently in the computer core. The squares overlapped so that most of the images were completely contained within at least one square. Squares were specially centered on the remaining images that were still split. Occasionally a rectangle larger than the 250x250 point squares was needed to contain an image; this necessitated holding the data in disk storage and reading parts of it into and out of the computer core as needed, resulting in a large increase in the computer time for the processing.

Each square was smoothed by replacing each value by the centre-weighted mean of the 3x3 square of values around it. The array of brightness values was then contoured at 0.25mag intervals, starting from the brightest isophote, and all the brightness of an image inside the limiting isophote added to give the magnitude. Any object with a central isophote fainter than μ_B=26mag/□" was ignored, so too were any objects with an isophotal magnitude fainter than B_{27}=21.0. Contour maps and listings of the image details were produced by the computer for each of the squares.

Overlaps, when close images share some of their isophotes, are normal rather than the exception in crowded fields; some rule-of-thumb must be used to apportion the light between the overlapping images. All luminosity in the image from areas fainter than the last individual isophotes was divided between the overlapping images in the ratio of the areas of their last individual isophotes. Hence the image that is largest at the merging surface brightness will be allocated most of the light from the combined image fainter

than the isophote level at which they merged. Multiple overlaps are dealt with by the same principle, starting at the brightest overlaps and dealing with successively fainter ones.

Too much of the luminosity tends to be allocated to stars in the event of overlaps with galaxies since the steep stellar profile causes them to have comparatively large inner isophotes. Conversely the haloes of giant galaxies may be partially given to overlapping companions which have steep profiles; in such cases, where the objects truly overlap in space, the division of luminosity between them is to some extent arbitrary.

The limiting isophote used was μ_B=27mag/□". Even with the dark skies found, the parts of the galaxies near this isophote are affected by significant noise. In general, however, only ~0.2mags of the light from a galaxy comes from between the μ_B=26mag/□" and μ_B=27mag/□" isophotes. Using a faint limiting isophote gives more morphological information about the galaxies and avoids the need for large seeing corrections. The magnitudes derived are also more representative of the total luminosity of the galaxies and cluster. Photographic photometry to levels fainter than μ_B=27mag/□" would have needed extreme care, and there would have been problems with excessive noise and microdensitometer quantisation (Clark 1973, Carter & Dixon 1978).

The isophotal magnitudes must be corrected for several effects before the results for different clusters can be compared. The corrections are outlined in Chap. 8, where the luminosity functions of clusters are discussed. The results of the photographic photometry given in App. IV do not include these corrections.

7.7 Star-Galaxy Sorting

The sorting of stars from galaxies has traditionally been carried out by eye from the plate, since the pattern recognition necessary is difficult to carry out infallibly by computation. In view of the new generation of fast measuring machines coming into use (e.g. COSMOS and the Cambridge APM), there has recently been an increase of interest in sorting images automatically. Enormous human labour would be needed to classify the huge numbers of images that these machines can study: they are capable of examining the millions of images on a single Schmidt plate in a day.

For this study a hybrid approach was used. Images were sorted by eye using both the isophotal maps and direct inspection of the plate. In addition, though not for 2354-35, an automatic procedure was used to produce supplementary information in the form of parameters that correlate well with the class of objects. The method used has been developed in Oxford (Carter & Godwin 1979), but similar methods have been investigated elsewhere (e.g. Hooley 1978, MacGillivray et al 1976).

A sample of 30 probable stars is selected by eye from isophotal maps. The profiles of these images are then scaled in intensity to fit together and yield a standard star profile. The saturated inner regions, $\mu_B < 22$mag/□", and noisy outer regions, $\mu_B > 26.25$mag/□", of the stars are omitted in this process. The stars are chosen to cover the same range of magnitudes as the galaxies of interest to ensure that the standard profile derived is suitable for the magnitude range in which it is to be used. If a galaxy is included in the sample of 30

stars, it is apparent by its lack of fit to the standard profile derived, and it may be eliminated.

The star profiles fit together accurately in the range B_{27}=17 to B_{27}=20.5. The profile shape is not due simply to "seeing"; internal reflections and diffraction in the telescope are also present as can be seen from the complex form of the images of bright stars. Fortunately these processes do not differ greatly over small areas of the plate. Obviously, a single standard profile could not be used over the entire field of a Schmidt plate.

The standard profile is approximated by an eighth order polynomial; satisfactory fits cannot be found using a gaussian. Fig. 7.4 shows the standard star profile for the scan of S40/6 with its polynomial approximation. The profile of each object that is to be sorted is trimmed to remove parts that are overlapping with other images, or are saturated ($\mu_B < 22$mag/□") or too faint ($\mu_B > 26.25$mag/□"). The part of the profile remaining is compared with the standard profile and 3 parameters derived:

α) The standard and image profiles, both expressed in mag/□" are subtracted at each radius to give their magnitude difference in brightness. α is the slope of the linear regression of these differences against radius. Because their profiles differ from the standard only by a scaling factor in intensity, the magnitude difference is roughly constant for stars and $\alpha \sim 0$. Galaxies, with flatter profiles, have $\alpha < 0$.

β) This is the value of the magnitude shift needed to fit the standard profile to the image profile. It is thus a measure of the magnitude of the object if it has a star-like profile.

γ) In finding the best fit between the image and the standard profiles, a good fit will be achieved only if the image is of a star. If its profile is flat, like a galaxy's, then the standard profile will be too bright at the centre and too faint in the outer regions. γ is the amount by which the image profile falls fainter than the standard profile at the centre when they are fitted.

The most useful parameter is κ; this is a measure of the overall "flatness" of the image compared to a star. The distribution of objects in the field of K44 is shown plotted in Fig. 7.5 in the κ-magnitude plane. The separation apparent between the stars in the upper part of the plane and the galaxies at the bottom is better than can be achieved by plotting mean surface brightness, rather than κ, as has been used in some previous studies (Godwin & Peach 1977). Additional information is provided by γ. This is able to distinguish between stars and galaxies with stellar profiles except for a flat centre. κ is incapable of distinguishing these types of object since all available isophote levels of the galaxy suggest that it is stellar in profile.

The final decision as to whether an object should be classified as star or galaxy was taken on the basis of both visual evidence and the parameters κ and γ of the object. If there was serious doubt about the nature of an object then it was not included in the list of galaxies; totally reliable separation of the types of object is impossible to achieve. Any extremely compact galaxies will be classed as stars and without spectroscopic data it is impossible to assess how common such objects are. A few objects lie between the star and galaxy sequences in Fig 7.5 brightwards of where they merge. These

may be true compact galaxies, the result of stars superimposed on faint galaxies, the effect of noise on the plate, or even due to the abnormality of the stellar profile if a star has an abnormal colour. Allen et al (1978) examined a selection of very compact galaxies found on plates similar to those used here; they found that only 3 out of 31 were galactic stars and the rest were almost certainly galaxies. The enlargements of the plates that they reproduce suggest that their sample is morphologically similar, though in general brighter than, the dubious galaxies found in the present study. More recent work (Carter 1978, priv. comm.) comparing the sorting of stars and galaxies on a field of a Schmidt plate with a deeper AAT prime focus plate, shows that the automatic sorting method is rather better than the experienced eye in reliability, except in the case of very crowded areas where the multiple overlaps and distortions produce spurious classifications. It therefore seems that the combination of human and machine sorting used will probably have been rather better than the unaided eye, although possibly not as perfect as if the automatic method had been relied on to a greater extent.

Some images are entirely omitted from the analysis since they fail to reach the minimum surface brightness of 26mag/□" imposed in the reduction. The sequence of galaxies in Fig 7.5 shows considerable thinning towards the edges, and unless very compact and very diffuse galaxies form isolated populations in the diagram, they are probably quite rare. As a check, the distribution of images identified as stars was examined; no concentration is found to the centre of the clusters as would be the case if many were cluster galaxies that had been misidentified.

Table 7.I: Schmidt Plate Material

Cluster	Date Taken	Plate No.	Field No.	Field Centre (1950)	Exposure mins.	Sky μ_B mags/□"	Seeing	Zenith Distance
2354-35	1974 July 21/22	J0738	349	$00^h00^m-35^o$	40	22.84	Good	5^o
S40/6	1977 Nov. 16/17	J3762	118	$04^h26^m-60^o$	75	23.42	Good	35^o
K44	1977 Aug. 8/9	J3466	471	$23^h46^m-30^o$	20	¼ moon	Mod.	0^o
	1977 Nov. 6/7	J3730	471	$23^h46^m-30^o$	80	23.10	Mod.	0^o

All exposures are hypersensitised IIIaJ 14" plates with a GG395 filter.

Table 7.2: Photoelectric Zero-points for Plates

Cluster	Galaxy	Galaxy zero-point B mag/□"	Adopted plate zero-point B mag/□"	References & no. of apertures
A1146	A1146cD	22.80	22.80	S76: 2
2354-35	2354-35cD	22.85	22.84	WW69: 1 G: 5*
	N7793	22.84		A74: 1 BP76: 2 V72: 3
S40/6	I2056	23.54	23.42	G: 3 SV78: 1*
	N1543	23.36		G: 3 S75: 1 Sh66: 1
	N1672	23.46		A76: 3
K44	N7755	23.22	23.10	G: 5 BP76: 1 V72: 1
	I5353 = K44g1	23.04		G: 5

* indicates photoelectric data available too late to be used, but confirming the readings included.

References:

G: This work (App. V & Chap. 6)
S76: Sandage et al 1976
SV78: Sandage & Visvanathan 1978a
BP76: Bucknell & Peach 1976
S75: Sandage 1975b
A74: Alcaino 1974
A76: Alcaino 1976
WW69: Westerlund & Wall 1969
Sh66: Shobbrook 1966
V72: de Vaucouleurs & de Vaucouleurs 1972

The number of apertures is shown after each reference, This is the number used in the calibration; readings through apertures that were too small to be of use may be given by these or other references.

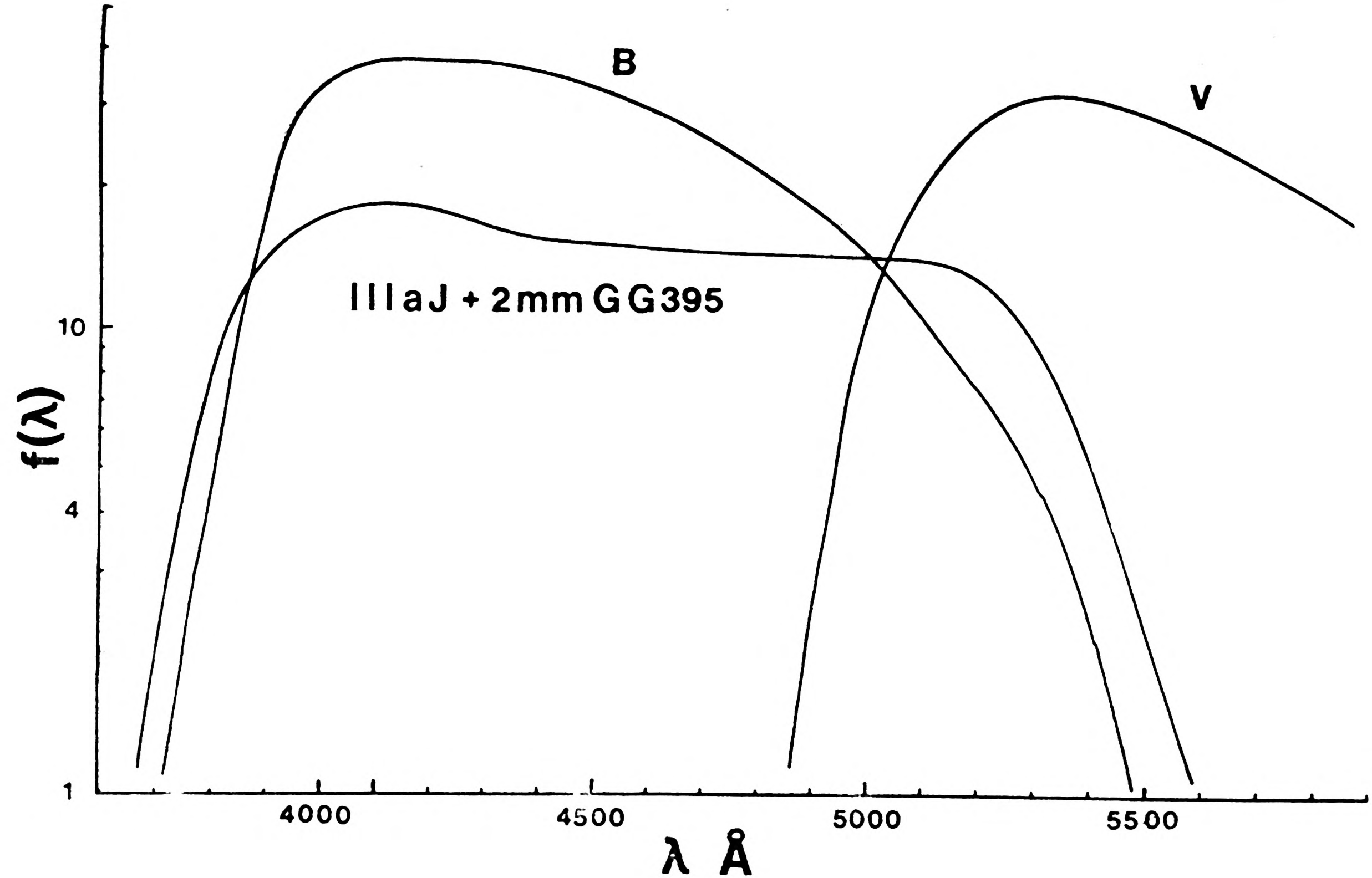

Fig. 7.1 Photoelectric and photographic colour bands

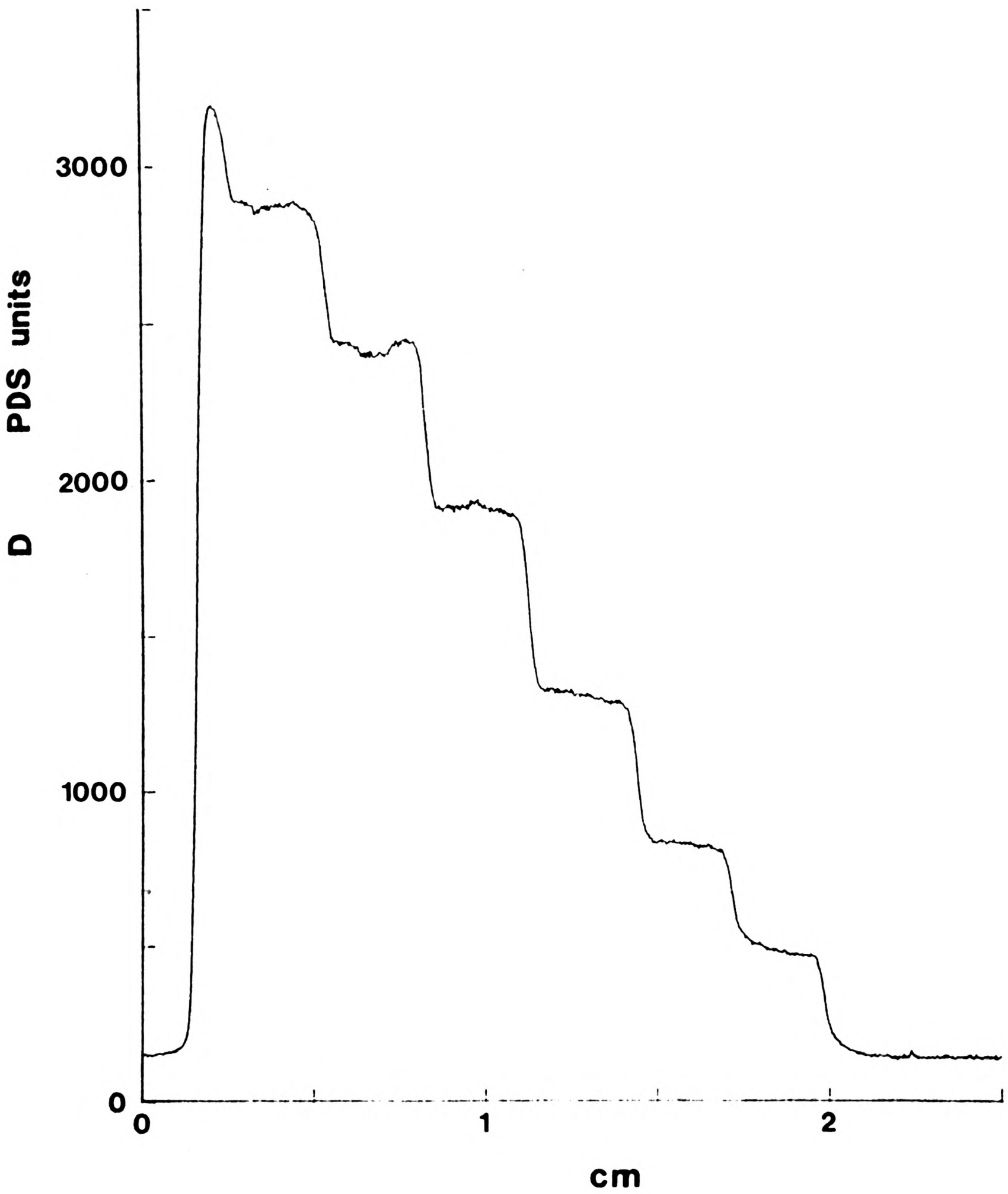

Fig. 7.2: Profile of upper wedge exposure, K44 plate

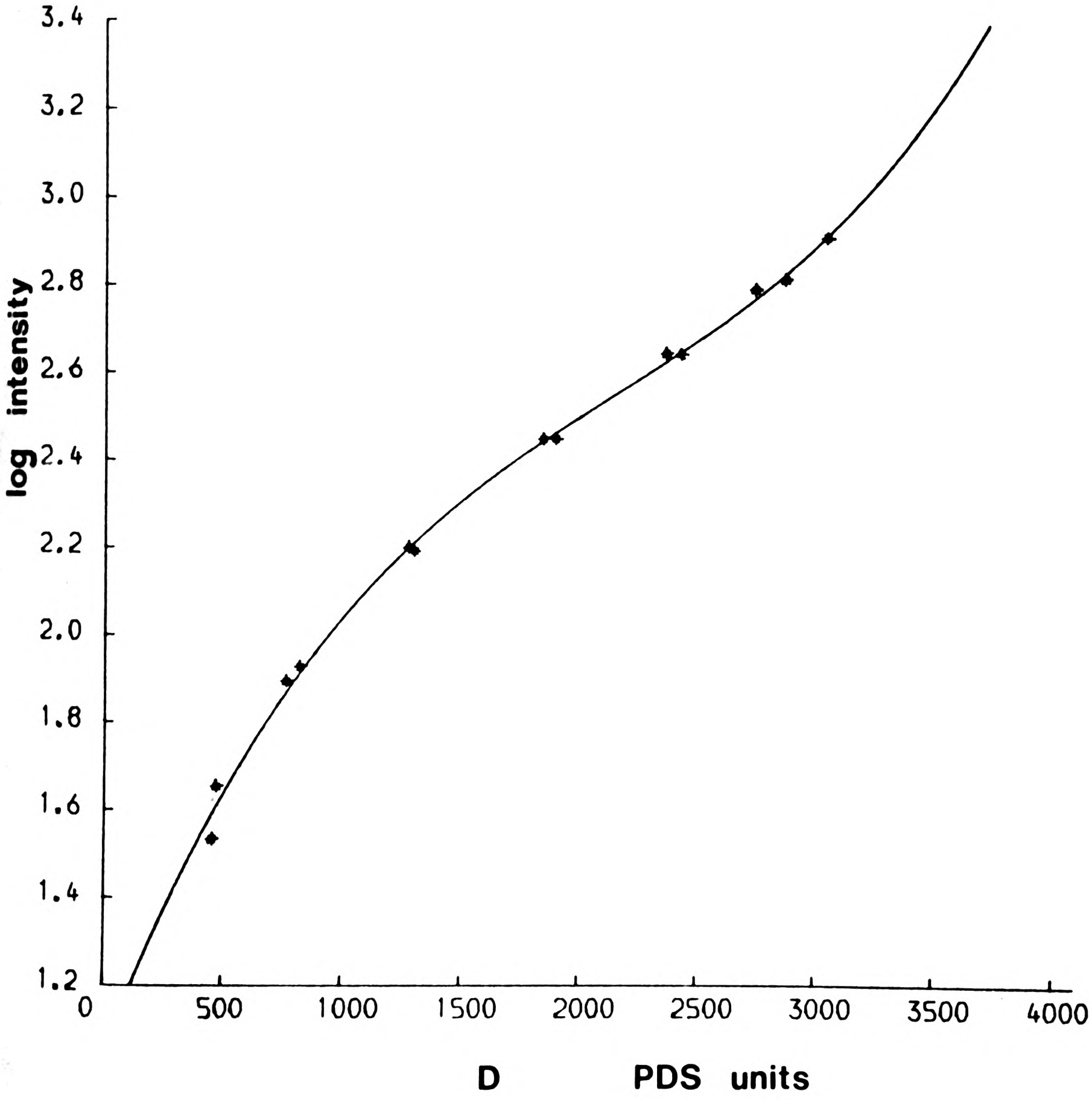

Fig 7.3: Log intensity vs. density calibration curve for K44 plate

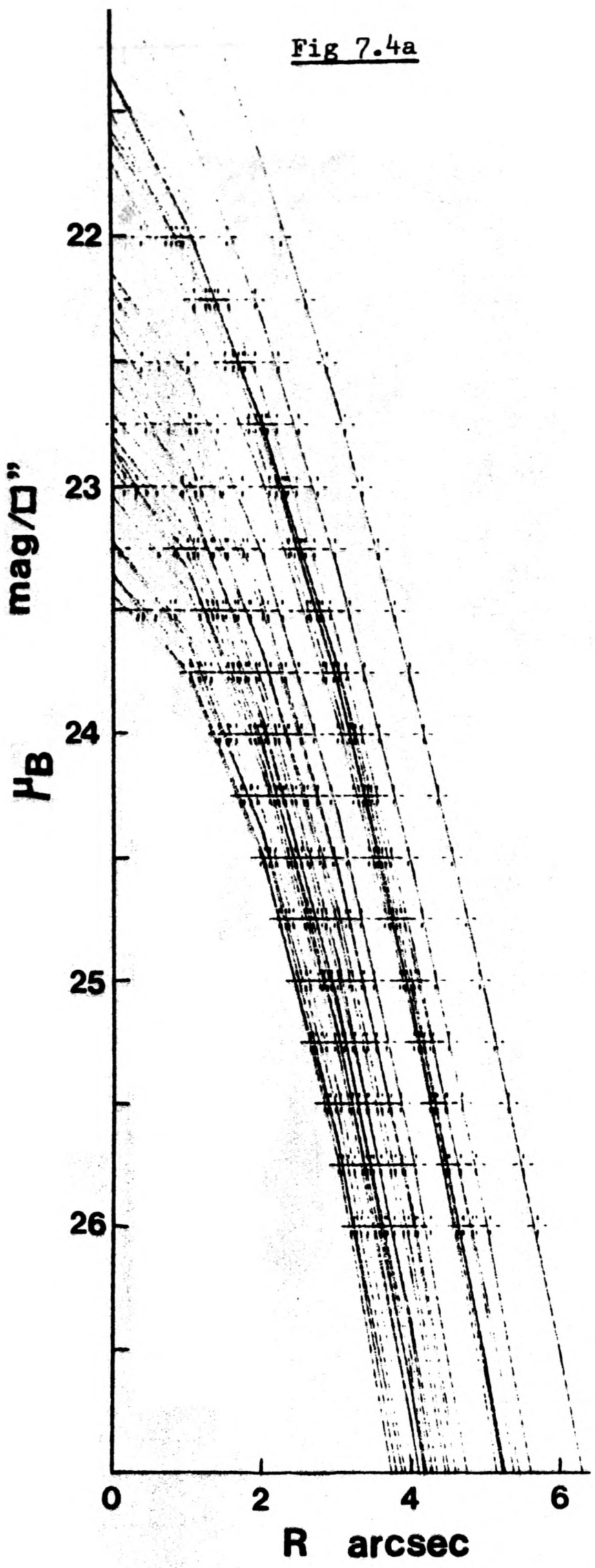

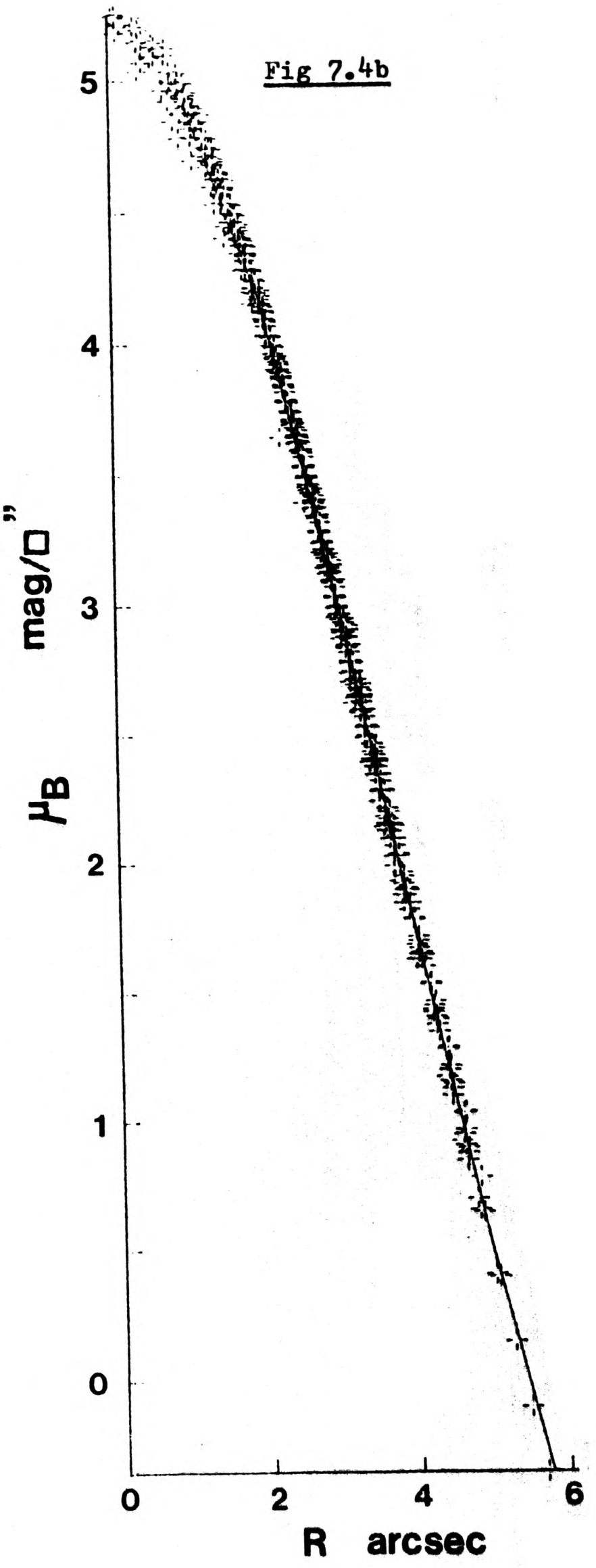

Fig 7.4: Sample of stars from S40/6 scan

a) Before scaling in brightness

b) After scaling in brightness (zero-point arbitrary)

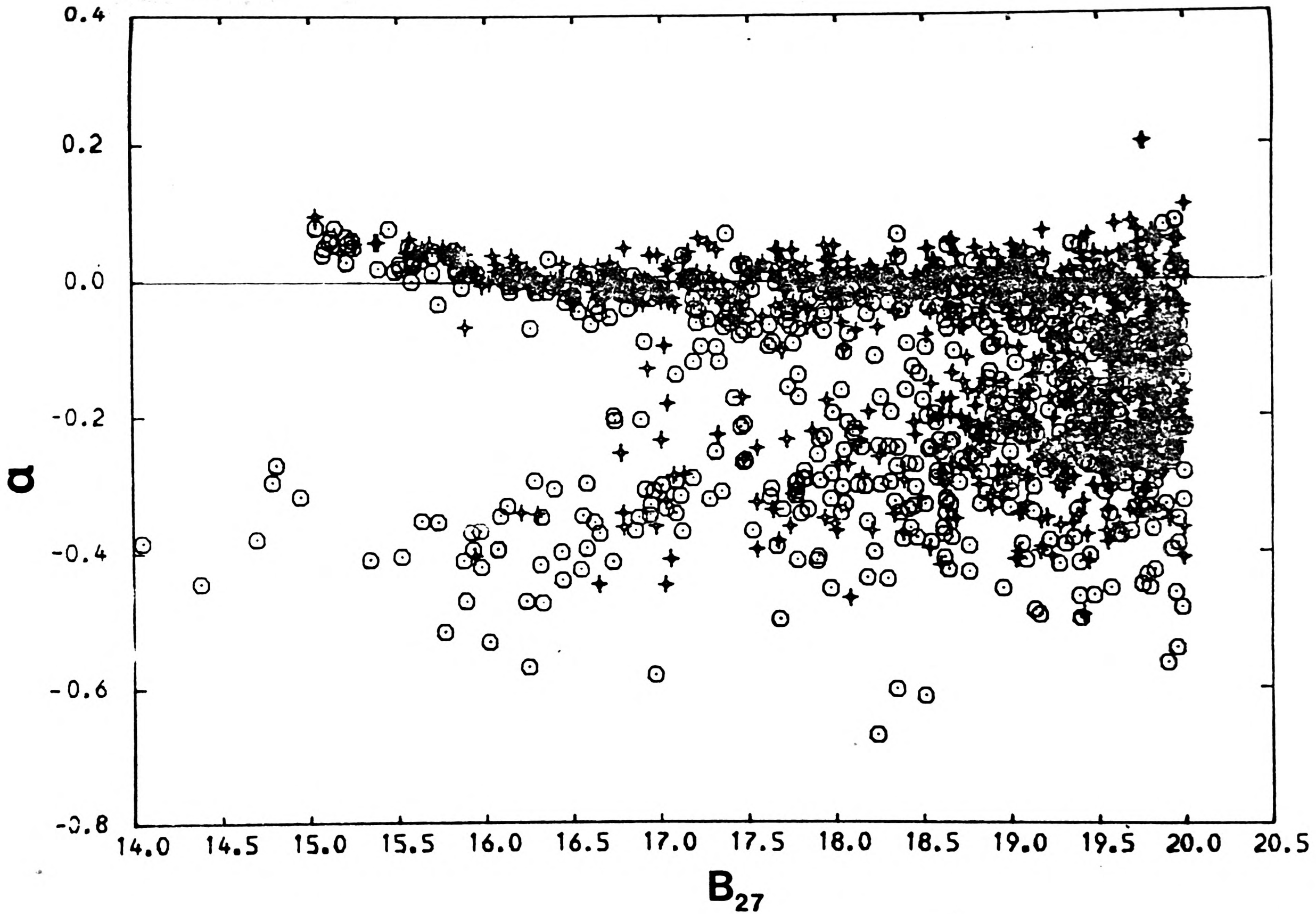

Fig. 7.5: α vs. magnitude plot of objects in K44 scan

Circles are overlapped images

Chapter 8 Discussion of the Cluster Photometry

8.1: Corrections to the Magnitudes

B_{27} magnitudes of galaxies in four clusters are available: S40/6, K44, 2354-35 and A1146. The methods of reduction used are discussed in Chapter 7 and the magnitudes are listed in App. IV. These magnitudes are those actually measured; to make the data for the clusters inter-comparable, certain corrections must be made. These are discussed below and summarised in Table 8.1:

i) Relative distance: The relative distances of the clusters are known from the redshifts, and the magnitudes of the cluster members can therefore be converted to absolute values by subtraction of the normal distance modulus:

$$DM = 25 + 5\log_{10}(cz/H_o) \qquad H_o = 50 \text{km s}^{-1} \text{Mpc}^{-1}$$

ii) Seeing: A result of "seeing" is that light is spilt inwards and outwards across the limiting isophote. The nett transfer is outwards and a correction is necessary to compensate for this. Large seeing corrections are not needed in the present work since the limiting isophote is faint; the loss of light from images in isophotal photometry is, in any case, partially compensated by an increase in isophotal radius. The corrections are greatest for the smaller galaxies which lose a greater proportion of their light by seeing. Numerical experiments (Hoffman & Crane 1977) indicate that despite poor seeing for the K44 plate, even the faintest galaxies in K44, S40/6 and 2354-35 are rarely altered in magnitude by more than 0.04. No seeing corrections have therefore been made. Corrections are needed, however, for the magnitudes of galaxies in A1146. The method of Carter & Godwin (1979) has been used. M87-type profiles of a range

of isophotal radii are convolved computationally with the profile of the seeing disk found from the star profiles on the plate. This yields a set of seeing-degraded M87-type profiles and the seeing correction to the isophotal magnitudes to allow for the degrading can be found by comparing the isophotal magnitudes of the undegraded and degraded profiles. Each of the observed galaxy images is assumed to have a M87-type profile, degraded by the seeing, and the correction calculated for a degraded profile of that radius is used to find the true magnitude. The correction is 0.1mag for 3.3" radius galaxy images, 0.2mag for 2.7" and 0.3mag for 2.4".

iii) Galactic Absorption: The absorption due to the Galaxy is assumed to follow Sandage's (1973) expression:

$$A_B = 0 \qquad |b^{II}| > 50^o$$

$$A_B = 0.132\ (\text{cosec}\ b^{II} - 1) \qquad |b^{II}| < 50^o$$

A_B is the B-band absorption in magnitudes. Other authors (Holmberg 1975, de Vaucouleurs & Malik 1969) have suggested the presence of $\sim$ 0.2mag absorption even at the galactic poles.

iv) Extragalactic absorption: The extent of extragalactic and intra-cluster absorption is unknown and no correction can be made.

v) Atmospheric Absorption: No correction is needed since the magnitude zero-points are derived from photoelectric readings reduced to outside the atmosphere.

vi) K-corrections: The relative motions of the galaxy and the observer "stretch" and redshift the emitted light by the Doppler shift. Thus light from a narrow band of the galaxy's spectrum is received in a wider, redder band. The K-correction to allow for this depends not only on the galaxy redshift, but also on the spectrum of the light when emitted. In the case of the cluster A1146, the

B-band K-corrections differ by ~0.3 mags between E and Sb galaxies. The K-corrections adopted in the present work are those by Pence (1976) for E galaxies, assuming no absorption by the Galaxy at its South pole. Obviously, the corrections are incorrect for any spiral galaxies in the sample, which will have corrected magnitudes that are too bright.

vii) Isophotal contraction: The observed surface brightness of an object is fainter than the rest value by $2.5 \log_{10}(1+z)^4$ magnitudes, assuming a standard cosmology (Stock & Schuecking 1957). Galactic absorption and the K-effect also reduce the observed surface brightness. A consequence is that the observed μ = 27 mag/□" limiting isophote corresponds to a brighter isophote at the galaxy, and the luminosity between the apparent and rest limiting isophotes is lost from the isophotal magnitude. In the present work it is assumed that a change in limiting isophote of m magnitudes will result in a loss of m/5 magnitudes from the isophotal magnitude and a correction is made accordingly.

viii) Extrapolation to total magnitudes: Beyond μ_B = 27mag/□" the tracing of a galaxy profile becomes difficult due to background variations, detector quantisation, merging with nearby galaxies, and noise. Extrapolation of galaxy magnitudes to an infinitely faint isophote is impossible and the size of the contribution to the total magnitude from beyond the limiting μ_B = 27mag/□" isophote is unknown. The galaxies that have been examined in detail are mostly giants, and the form of the profiles of fainter cluster members has not been investigated at faint brightness levels. No extrapolation to a "total" magnitude is attempted in the present work; corrections calculated on the basis of de Vaucouleurs' (1959) empirical

formula would be less than 0.5 mag.

The corrections for distance modulus, galactic absorption, the K-effect, isophotal contraction and, for A1146, seeing, have been applied to the galaxy magnitudes before the construction of the absolute luminosity functions of the clusters (Fig. 8.2). The uncertainties in the corrections are significant, reaching up to 0.2mag for the fainter galaxies with the possibility of a further 0.2mag zero-point error depending on the true galactic absorption at the pole.

8.2: Correction of Samples for Field Galaxies

It has been pointed out (Chap. 5) that the "field" galaxies that contaminate the bright end of the luminosity functions are predominantly members of the supercluster around the cluster. At fainter magnitudes, where the contamination is greater, the "field" galaxies will be in general the brightest members of clusters and groups at much greater redshifts. It is therefore possible to apply a correction for these "field" galaxies that is reasonable since they will be spread evenly across the field of the cluster. The correction that has been used here was derived by fitting two straight lines to the data of Karachentsev & Kopylov (1977) in the B-band:

$$\log_{10}(N \geqslant m) = -a + b.m$$

$N \geqslant m$ is the number of galaxies per square degree brighter than m. Fainter than m=17.6: a=6.1154, b=0.42724 gave the best fit. Brighter than this, the expected 0.6m form was used: a=9.47, b=0.6. This may be extrapolated to give 1024 galaxies per square degree at m_B=20.8. Austin & Peach (1974) found this density of "field" galaxies at m_v=20.0, the difference in magnitudes occurring because of the different limiting

magnitude and the colour difference.

The field corrections have themselves been corrected for galactic absorption before being applied to the observed galaxy counts. The reliability of the field corrections is poor at faint magnitudes, and could be in error by as much as 50% at B_{27}= 22mag; this will have little effect on any conclusions drawn from the form of the luminosity functions.

The galaxy counts remaining after the subtraction of the field corrections refer to a cylindrical volume through the supercluster around the cluster. Standard radii of 0.92Mpc and 0.46 Mpc have been used to define this cylinder, the angular extent of 0.92Mpc is noted in App. VI. Any likely change in q_o would have a negligible effect on these radii.

8.3: Analytic Representations of the Luminosity Function

Most known members of the Local Group are low luminosity dwarfs; it seems probable that most galaxies in all clusters are of this type. However, a magnitude limited sample of galaxies (e.g. RCBG2) contains a preponderance of giant galaxies, leading to the early belief that galaxies have a preferred, bright magnitude (e.g. Hubble 1936, Holmberg 1950). More recently attempts have been made to find a suitable, normally monotonic, analytic representation of the luminosity function for galaxies in groups, clusters and the "field".

Abell (1962,1965) used two straight lines to fit the logarithmic cumulative luminosity function; the corner between the lines corresponds to a "knee" seen in the observed function of many clusters at $M_V^* \approx -21.5$. This magnitude is sufficiently constant for there to be the possibility of using it as a standard candle. As with the

magnitude of the brightest galaxy, evolutionary effects confuse any simple interpretation.

Other analytic forms have been suggested by Kiang (1961), Zwicky (1957), Holmberg (1969) and Schechter (1976). The latter has gained some popularity; it has the form (for the differential luminosity function):

$$P(L)dL = (L/L^*)^a \exp(-L/L^*)\, d(L/L^*)$$

where L^* is a standard luminosity, similar to Abell's M^*, and a is a constant. P(L) is the frequency distribution of galaxy luminosities.

Godwin & Peach (1979b) suggest that no analytic form may be entirely satisfactory, and that the parameters in the expressions do not have any obvious physical significance. Instead they derive a parameter f for each cluster, calculated as the ratio of the numbers of galaxies in the ranges $M_{v_{25}} = -19.8$ to -20.8 and $M_{v_{25}} = -21.8$ to -22.8; a large value of f corresponds to a "steep" luminosity function.

8.4: Discussion of the Luminosity Functions

Fig. 8.1 shows the luminosity functions of the clusters K44, S40/6, 2354-35 and A1146. The magnitudes used are uncorrected, taken from App. IV. The function is plotted for all galaxies within the scan area. The data for A1146 are plotted with and without the correction for seeing degradation, there is no significant difference brighter than $B_{27} = 21.8$mag. Arrows on the diagrams show the limits of completeness for the samples.

The absolute luminosity functions are plotted in Fig. 8.2. The magnitudes used in these have been corrected for distance modulus,

galactic absorption, the K-effect, isophotal contraction and, in the case of A1146, seeing. The functions for galaxies within 0.92Mpc projected radius and 0.46Mpc projected radius of the centre are given.

Comparison of these luminosity functions with those of other clusters (Oemler 1974, Dressler 1976, Godwin 1976, Godwin & Peach 1977, Bucknell et al 1979) shows that the luminosity functions for the four clusters have the expected, almost monotonic shape. There are peaks in the functions at $B_{27} \approx -19.5$ (corresponding to Abell's "knee") with dips faintward. These features are strongest in central ($R \sim 0.46$Mpc) zones of the clusters. Similar dips occur in the functions of some other clusters (Godwin & Peach 1979b), but it is difficult to judge how significant they are. No explanation has been advanced to explain them.

Values of F have been calculated for inner and outer zones of the clusters and are shown in Table 8.2; the magnitude bands have been shifted 0.8 magnitudes faintwards from those used for $M_{v_{25}}$ by Godwin & Peach (1979b). The errors on F are always large (>30%) owing to the paucity of galaxies in the brighter band. The values of F are therefore not significantly different and would not be expected to be. The greatest difference apparent is that between the inner and outer zones of K44 in the sense that the inner zone has a steeper luminosity function. The other clusters have similar values for F in the inner and outer zones. The values found, $F \sim 5$, are typical for spiral-poor and cD clusters, whereas spiral-rich clusters have $F \sim 2.5$.

Mass segregation of the galaxies in a cluster may result from two-body relaxation; the more massive galaxies would form a more centrally concentrated distribution with a smaller velocity dispersion. To test segregation in the clusters, the magnitude of a galaxy was used as an indicator of its mass. F would provide a measurement

of the segregation, but instead ratios of the number of galaxies have been constructed using wider bands, resulting in smaller error margins on the results. The values found are shown in Table 8.3.

In A1146 the ratios are similar in the inner and outer zones. The other clusters exhibit reverse segregation in that there are proportionately more bright galaxies in the outer zones. If mass segregation does occur, therefore, it is masked by a stronger effect in the opposite sense. Godwin & Peach(1979b) and Dressler (1978b) have also found a reverse segregation in cD clusters. When the data for the four clusters in the present sample are combined, they show reverse segregation significant at the 95% confidence level.

8.5: Radial Profiles of the Clusters

The radial density profiles of the clusters may be conveniently expressed in terms of the mean surface density of galaxies on the sky at each radius: $\sigma(r)$. This parameter is plotted for each of the clusters in Fig. 8.3. Galaxies brighter than $M_{B_{27}} = -19$ are included and the appropriate correction for field galaxies has been made. The data have been binned into 0.2Mpc annuli. There are too few galaxies for the profiles to be plotted using galaxies of different ranges of $M_{B_{27}}$.

The profiles of S40/6 and A1146 hardly differ, except that S40/6 has a higher density in the central region. Similarly the profiles of 2354-35 and K44 are alike except that K44 is denser in the centre. The profile of K44 is rather irregular; the maximum at $\log R \approx -0.3$ is probably due to the presence of a group of non-members to the East of the cluster centre (Chap.2). The combined data from all the clusters is consistent with a power law, $\sigma \propto R^{-a}$, where a is slightly greater

than 1. Other workers (e.g. Yahil 1974, Zwicky 1957) have found that cluster profiles often have this form.

Zwicky (1957) has proposed that the profiles should be fitted by the theoretical profile of a gravitating isothermal sphere; other workers have followed this practice (Austin & Peach 1974, Avni & Bahcall 1976). The theoretical profile is a power law with a density enhancement in the centre. There is little physical significance in the fit since clusters are not isothermal nor symmetric. The expressions used to fit the profiles of elliptical galaxies (King 1966, de Vaucouleurs 1959) have also been used for clusters, again with little physical significance. The small number of galaxies and the confusion by the irregular "field" make it possible to fit this variety of functions to the same data. This is in contrast to the fitting of functions to the profiles of elliptical galaxies and globular clusters where a greater range of density values is available (10^4 not 10^2).

The present study does not follow the profiles out far enough to reach the region where maxima have been found in the profiles of several clusters (reviewed in Bahcall 1977a). The reality of these features is still in doubt; they would have to be very large space density perturbations to appear as significant projected maxima.

Table 8.1: Corrections to the Magnitudes

	K44	S40/6	2354 -35	A1146	Notes
1) Distance	36.11	37.79	37.33	39.57	$25 + 5 \log_{10}(cz/H_o)$
2) Seeing	.00	.00	.00	depends on radius	Assuming M87 profiles, scaled to radius.
3) Galactic A_B Absorption	.00	.07	.00	.11	Sandage (1973)
4) K_B	.13	.29	.23	.68	Pence (1976)
5) $(1+z)^4$ Dimming	.12	.25	.21	.56	Acts on surface brightnesses only
6) Isophotal Contraction	.05	.12	.09	.27	((3)+(4)+(5))/5
Total magnitude correction	36.28	38.27	37.65	40.63 + seeing correction	(1)+(2)+(3)+(4)+(6)

The individual corrections are described in detail in the text.

All quantities are in magnitudes in the B-band.

Table 8.2: Values of $\mathcal{F}$

Cluster	$R \leq 0.92$Mpc			$R \leq 0.46$Mpc			$0.46\text{Mpc} < R \leq 0.92\text{Mpc}$		
	N_F	N_B	$\mathcal{F}$	N_F	N_B	$\mathcal{F}$	N_F	N_B	$\mathcal{F}$
K44	26.6	6.3	4.2	17.5	2.0	8.9	8.2	4.3	1.9
S40/6	56.9	10.6	5.4	32.2	5.9	5.5	24.7	4.7	5.2
2354-35	31.1	5.7	5.5	14.8	2.9	5.0	16.4	2.8	5.9
A1146	40.8	9.3	4.4	15.9	4.3	3.7	24.8	5.0	5.0

N_B: No. of galaxies with $-22\text{mag} < M_{B_{27}} \leq -21\text{mag}$, field removed.

N_F: " " " " $-20\text{mag} < M_{B_{27}} \leq -19\text{mag}$, " "

$\mathcal{F}$: N_F / N_B

Table 8.3: Luminosity segregation

Cluster	$N_{I,F}$	$N_{O,F}$	$N_{I,B}$	$N_{O,B}$	R_I	R_O
K44	18.5	8.6	7.9	12.6	2.4 ± 1.0	0.7 ± 0.3
S40/6	36.4	27.2	15.6	21.7	2.3 ± 0.7	1.3 ± 0.4
2354-35	14.9	14.7	6.7	9.1	2.2 ± 1.1	1.6 ± 0.7
A1146	18.1	29.4	16.0	27.0	1.1 ± 0.4	1.1 ± 0.3
Total	87.9	79.8	46.1	70.4	1.9 ± 0.4	1.1 ± 0.2

R: The ratio N_F / N_B

N: The number of galaxies in the radius and magnitude class after field corrections have been made

I: Class of galaxies with $R \leq 0.46$Mpc

O: Class of galaxies with $0.46\text{Mpc} < R \leq 0.92\text{Mpc}$

B: Class of galaxies with $M_{B_{27}} \leq -20.2$

F: Class of galaxies with $-20.2 < M_{B_{27}} \leq -19.1$

Fig 8.1: Luminosity functions of the clusters

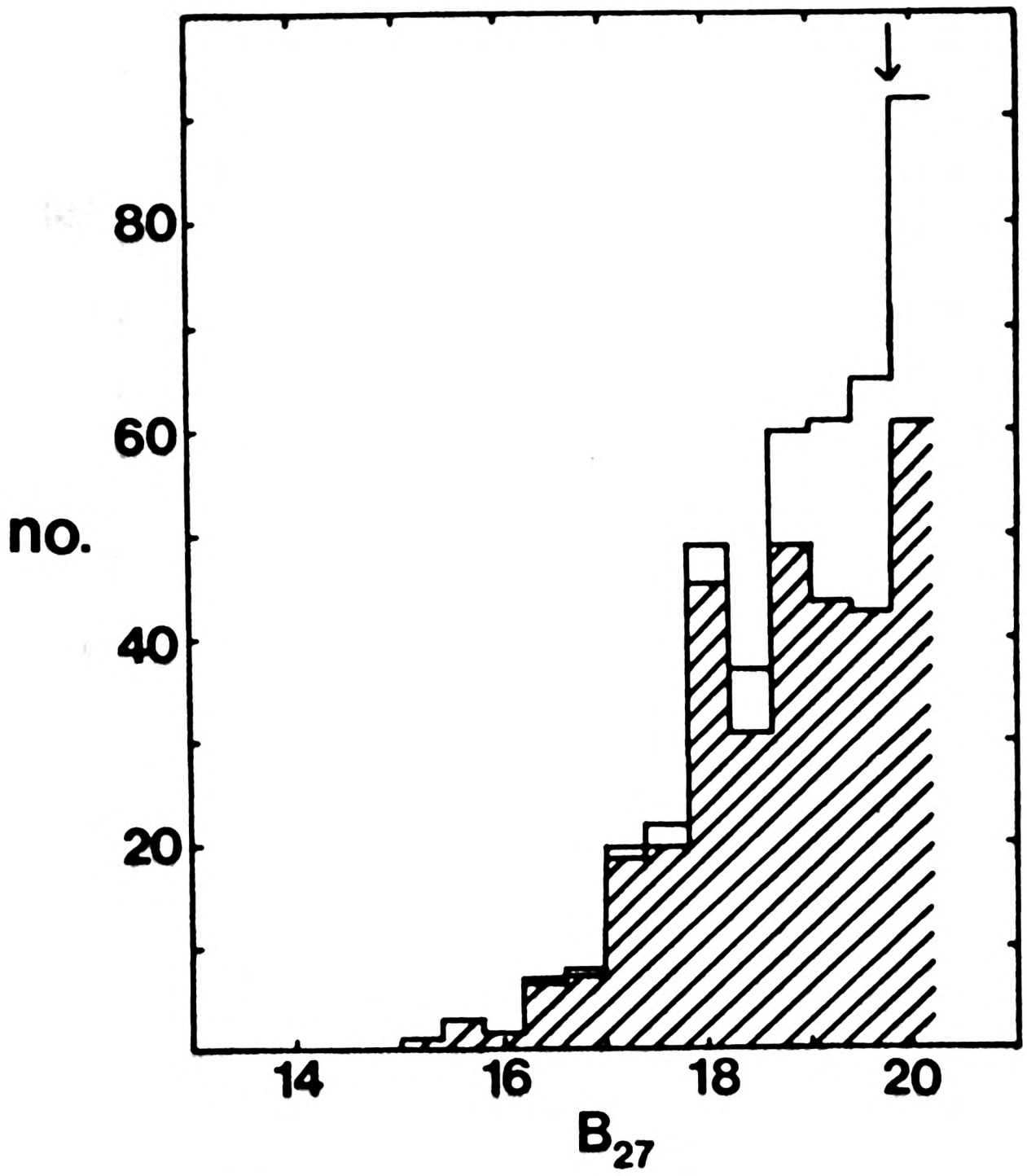

a) S40/6

These luminosity functions are constructed from the observed galaxy magnitudes as given in App. IV. All galaxies inside the scan area are included. The functions after correction for "field" galaxies are shown hashed.

Galaxies have been placed in 0.4mag bins; all bins faintward of the arrow may suffer significantly from incompleteness and contamination by stars that have been mis-identified as galaxies.

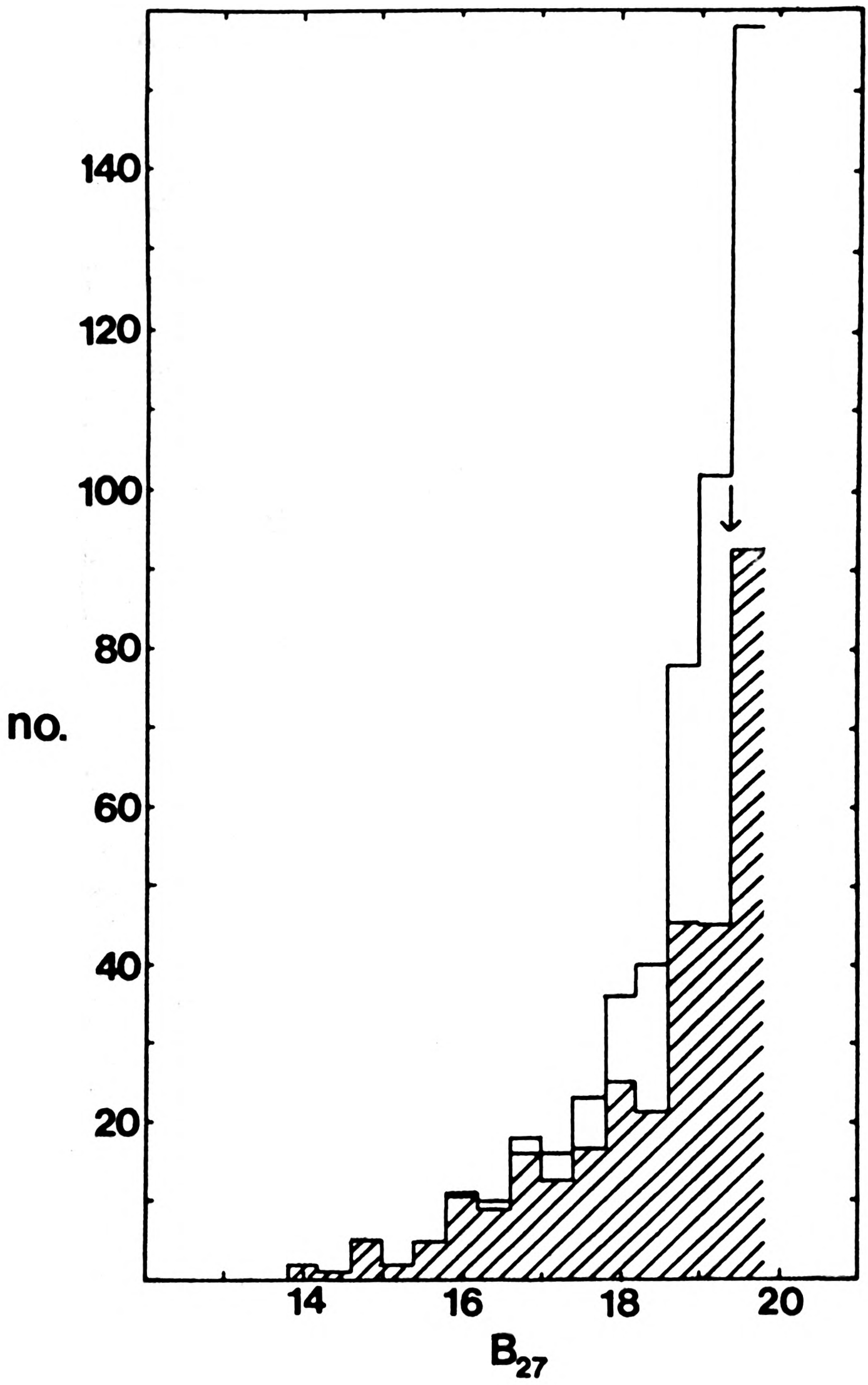

b) K44

A correction has been made for the omitted area around the star.

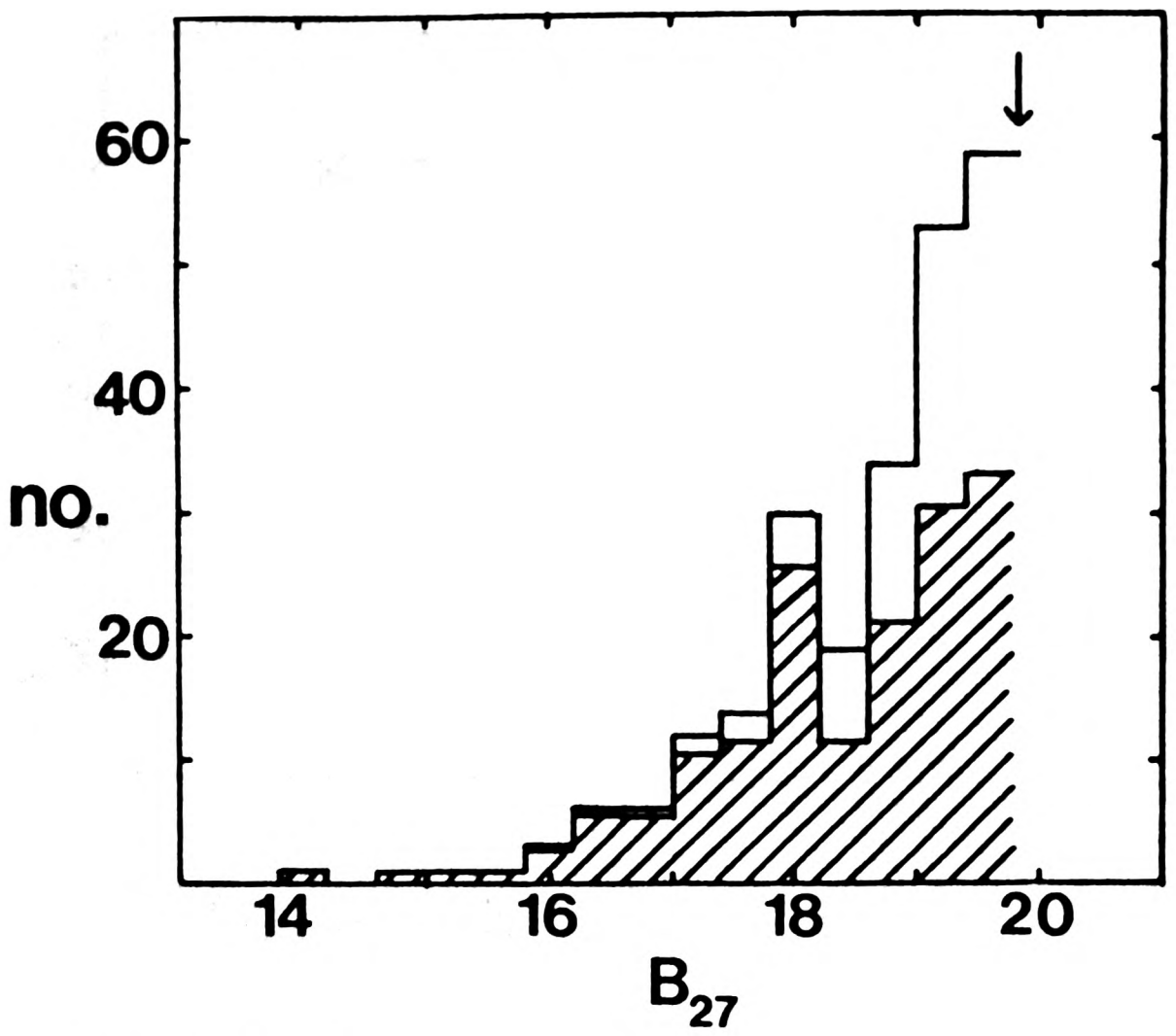

c) 2354-35

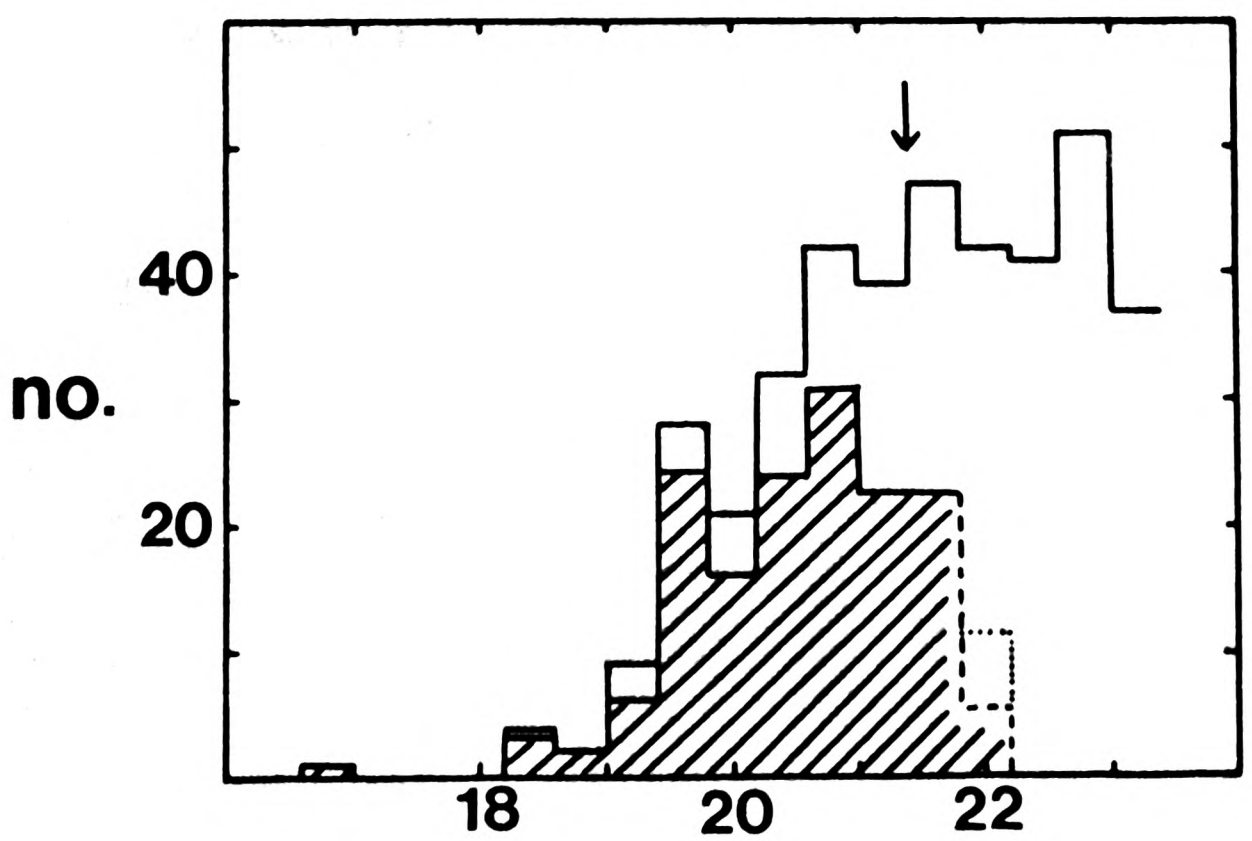

d) A1146

Function before seeing correction is shown dotted and after is shown dashed.

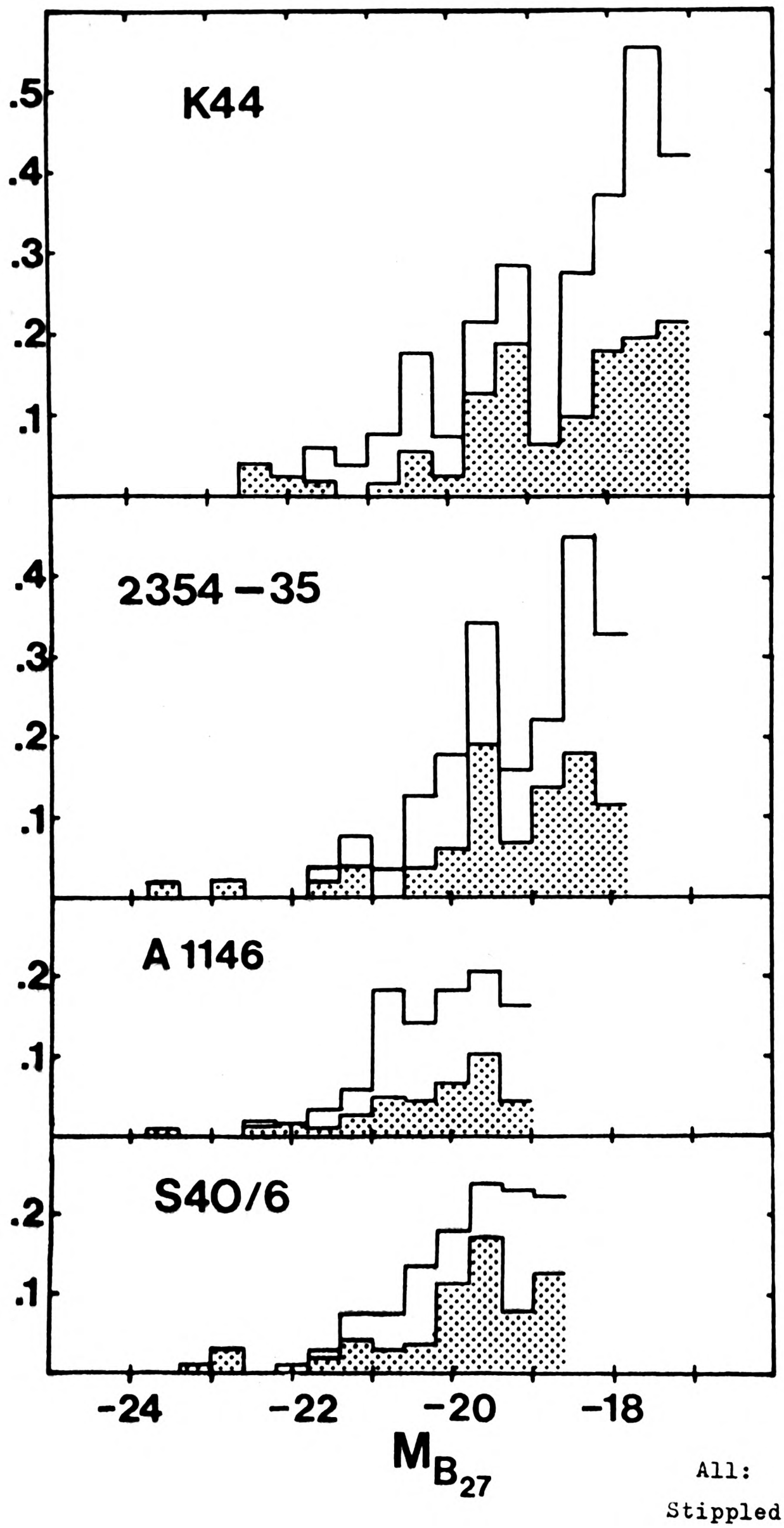

Normalised to no. of galaxies with R≤ 0.92Mpc, $M_{B_{27}} \leq -19$
Galaxies down to the completeness limit are included, and field corrections applied. The data for A1146 are seeing corrected.

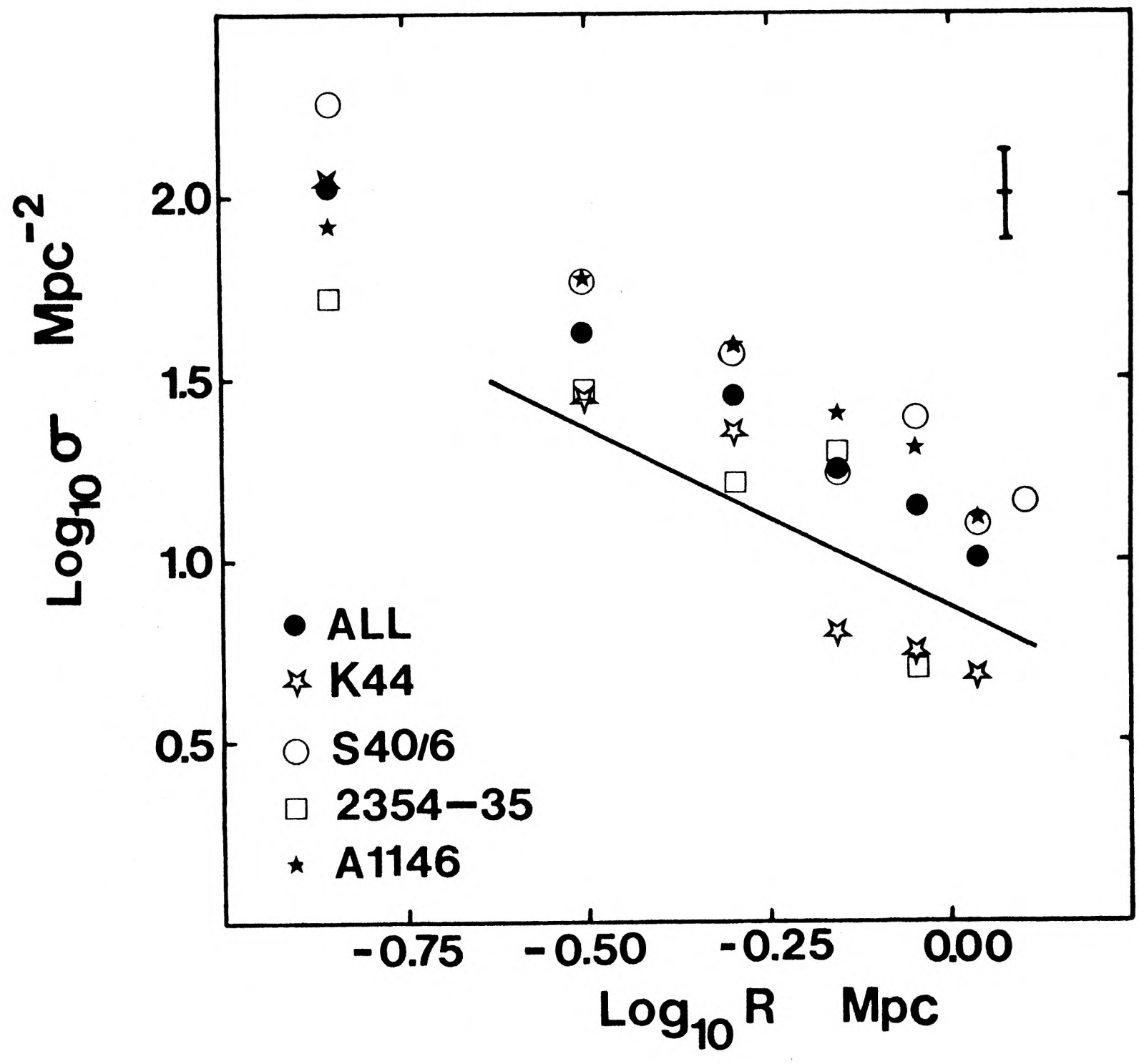

Fig. 8.3: Radial profiles of the clusters

Galaxies brighter than $M_{B_{27}} = -19$ are included in the data. Field corrections have been applied. Counts are binned into 0.2Mpc annuli; the radius shown is the effective radius: $R^2_{eff} = \frac{1}{2}(R^2_{inner} + R^2_{outer})$. Corrections have been made to the K44 data for the area around the star for which no magnitudes are available.

A typical error bar is shown in the top right hand corner. The straight line has slope $\sigma(R) \propto R^{-1}$.

Chapter 9 General Discussion and Conclusions

9.1 X-ray Emission from Clusters

The resolution of X-ray telescopes is as yet very poor and for most X-ray sources identified with clusters the only information available is a position and an estimate of the luminosity. Few clusters more distant than $z \approx 0.06$ are strong enough emitters to be detected at all, and of the less distant clusters only a minority have been detected. Papers by Gursky & Schwartz (1977), McHardy (1978) and Jones & Forman (1978) review the present state of knowledge about the X-ray properties of clusters.

The source structure has been investigated in a few nearby clusters. Coma, Perseus and Virgo all show diffuse emission, with enhancements around N1275 and M87 in the latter two clusters. There is no reason to doubt that all rich clusters produce at least some diffuse X-ray emission; McHardy (1978) suggests that Abell clusters have a lower limit of 10^{36} Watts for their 2-10keV luminosity.

Three mechanisms have been proposed for the X-ray production:

i) Inverse Compton scattering of microwave background photons on relativistic electrons, which produces X-ray photons (Felten & Morrison 1966, Brecher & Burbidge 1972). The electrons are emitted by active radio galaxies and are also the source of synchrotron radio emission.

ii) Bremsstrahlung from hot gas in the cluster, giving a thermal spectrum of X-rays. The intensity depends on the square of the gas density; the gas distribution inferred from the observations is similar to that of the galaxies, although there are large uncertainties.

iii) The integrated emission from all sources in the galaxies of a cluster will produce significant X-ray luminosity. This would appear diffuse in the low resolution detectors employed (Katz 1976).

The mechanism most favoured at present is the second: emission from hot intracluster gas. All three mechanisms must occur to at least some extent, but inverse Compton emission will only be important near to active galaxies. Key evidence in favour of the gas theory is the presence of iron emission lines in the spectra of some clusters (Mitchell et al 1976, Serlemitsos et al 1977). The abundance of iron is between 30% and 100% solar, according to model (Malina et al 1978). The presence of gas is also suggested by observations of tailed radio galaxies in clusters; these appear to be galaxies with double radio sources that leave a trail of radio-emitting plasma behind as the galaxy moves through the intracluster gas. The tails are orientated at no preferred angle to the cluster centre; consistent with the gas being at equilibrium in the clusters. Calculations of the gas density and temperature necessary to confine the tails give values in agreement with the $\sim 10^{-3}$ particles/cm^3 and $\sim 10^8$ ^oK needed for the X-ray emission. The gas confines other radio sources in the cluster, allowing them to last long enough for a noticeable steepening of their spectra to occur (McHardy 1978). The gas may also be detectable by causing an observable diminution of the microwave background, but the data must be treated with extreme care and are not yet conclusive (Tarter 1978).

If the gas is primordial and has fallen into the gravitational well of the cluster (Gunn & Gott 1972), then it must have been mixed at some stage with gas super-rich in iron. Alternatively the gas may

originate from the galaxies themselves (Yahil & Ostriker 1973), a result of stellar winds, supernovae and, once gas is present in the cluster, ram-pressure stripping of gas from spiral galaxies. The present expected rate of gas loss from elliptical galaxies is low, but may have been greater at earlier stages in their evolution, especially if there was an initial generation of very massive stars that produced the enriched gas and whose burnt out remains perhaps constitute the missing mass (Malina et al 1978, De Young 1978).

Infalling gas is heated as it loses its potential energy; this applies to gas shed by cluster galaxies in the outer regions of the cluster as well as to primordial gas (Cowie & Binney 1977). The gas can also be heated by the motion of galaxies through the clusters; the gas temperature (10^8 ^oK) is that expected if there is equipartition of energy between the gas and galaxy motion. Relativistic electrons responsible for the radio emission in clusters may in certain circumstances also give significant heating (Lea & Holdman 1978).

Both isothermal and adiabatic steady-state models of the gas distribution have been used. Isothermal models need a gas mass of approximately 10% of the cluster virial mass (Lea 1977), but in an adiabatic distribution there may be more gas, much of it existing at a lower temperature on the fringes of the cluster and contributing little to the X-ray luminosity (Gull & Northover 1975). Such large quantities of gas could not easily be enriched to the observed iron abundance. Silk (1976) suggests that the gas may accrete on to the central galaxy in the cluster, forming a cD galaxy, or it may form new elliptical galaxies in the core. No evidence of star formation is seen in the centre of clusters, however, and it is difficult to produce convincing models in which it is hidden (Cowie & Binney 1977).

The cooling time for gas in a cluster is of the same order as the Hubble time so rapid accretion is not expected, even if the gas receives no energy input.

The X-ray luminosity is greatest for rich, Coma-type clusters, but it is not clear which of the optical properties determines the X-ray luminosity since the optical properties are themselves correlated. Solinger & Tucker (1972) claimed that the X-ray luminosity will depend on the velocity dispersion, S, of the cluster, since a large velocity dispersion increases the gas temperature, and also because clusters with large velocity dispersions have large virial masses and therefore (possibly) large masses of gas. Their arguments were refined by Silk (1976), but recent work has suggested that there is no strong dependence of the X-ray luminosity L_x on S (Vidal 1977, McHardy 1978). The data now available, including those derived in the present work, show that there <u>is</u> a correlation of L_x with S (Fig. 9.1); the best fit straight line gives the relationship $L_x \propto S^t$ where $t = 2.03 \pm 0.80$.

The temperature of the gas, inferred from the spectrum, is strongly correlated with the velocity dispersion (Mitchell et al 1977); this is to be expected if there is some degree of equipartition between gas and galaxy motions.

Several workers have found a correlation between the richness of a cluster and its L_x (McHardy 1978, Bahcall 1977a, Jones & Forman 1978). This is predicted by almost any model of gas origin and distribution. There may also be a correlation with the occurrence of a cD galaxy in the centre of the cluster (Bahcall 1974, 1977b, McHardy 1978, Jones & Forman 1978), but it is difficult to disentangle this from the correlation between cluster richness and the occurrence of cD galaxies. The cD does not necessarily cause the extra X-ray emission

itself; an alternative explanation is that the mass of cD clusters may be underestimated relative to the mass of spiral-rich, non-cD clusters. This tends to occur since:

i) Non-cD, spiral-rich clusters emit much of their light from bright, massive stars, and their M/L values may be lower than other clusters.

ii) Assessing the richness and mass of a cluster by counting galaxies takes no account of the significant fraction of luminosity and probably mass of the cluster in the cD galaxy.

If the gas mass is a fixed fraction of the virial mass, then the gas mass and hence L_x will be greater in cD clusters than in non-cD clusters assessed as the same richness.

This correlation between richness and L_x is found in the present data; Fig 9.2 shows the relationship between L_x and optical luminosity L_o, a measure of the richness. The best fit straight line gives: $L_x \propto L_o^w$ where $w = 1.87 \pm 0.71$. L_o is defined in Table 9.1.

The galaxy types in the cluster population may also give some clue as to the presence of intracluster gas. Rich clusters tend to contain small proportions of spiral galaxies. If this is due simply to initial conditions at the formation of the cluster, then the X-ray luminosity may be correlated, via richness, with the absence of spiral galaxies. Even so, it is interesting that the populations of clusters with large X-ray luminosities are deficient in spiral as compared to SO galaxies (Melnick & Sargent 1977, Bahcall 1977c, McHardy 1978, Tytler & Vidal 1978). A possible explanation is that the gas responsible for the X-ray emission transmutes spiral into SO galaxies by ram-pressure stripping.

We may simplify our consideration of the X-ray emission by using L_o as an indicator of the galaxy density in the cluster core and assuming that the gas density is proportional to it. Since the X-ray flux depends on the square of the gas density we have $L_x \propto L_o^2$. L_x will also depend on the gas temperature. We assume that $L_x \propto T$. If there is equiparition between the galaxy and gas motions, then $T \propto S^2$. Thus, in this naïve model we expect:

$$L_x \propto S^2 \, L_o^2$$

The data are consistent with this expression; in Fig. 9.3 the best fit is $L_x \propto (L_o \, S)^p$ where $p = 1.56 \pm 0.30$. S and L_o are not independent of each other, but are empirically found to covary. Fig. 9.4 shows their dependence in the present data set; the best fit to the points gives $S \propto L_o^m$ where $m = 0.57 \pm 0.20$.

A more sophisticated approach uses the full thermal bremsstrahlung expression for L_x (Bahcall 1977c):

$$L_x = \rho_x^2 \, R_x^3 \, T^{0.8} \, e^{-E/kT_x} (1 - e^{-\Delta E/kT_x})$$

where L_x is measured in the energy band E to ΔE, and ρ_x, R_x and T_x are the gas density, radius, and temperature. This expression includes the Gaunt factor, which is approximated by $g \propto T^{0.3}$.

R_x, T_x and ρ_x are not known in most clusters, so the assumptions $T \propto S^2$, $\rho_x \propto L_o$, and R_x constant must be made. For the band 2-10keV, and measuring S in units of 10^3km/s, the expression reduces to:

$$L_x \propto X \quad \text{where } X = L_o^2 \, S^{1.6} \, e^{-0.193/S^2} (1 - e^{-0.771/S^2})$$

In this expression, the gas thermal velocity is assumed to be S.

Fig. 9.5 shows the observed relationship between L_x and X; as might be expected it is very similar to Fig. 9.3. The best fit to the data is $L_x \propto X^q$ where $q = 0.92 \pm 0.18$. This is consistent with the direct proportionality predicted above.

We have shown that the X-ray and optical observations are in agreement with predictions derived using a hot-gas emission model for the observed X-ray flux. The data, however, are very limited in both quality and quantity, hindering any detailed evaluation of predictions. A further difficulty is that most well-studied clusters are rather similar, having high X-ray luminosities, few spiral galaxies, large populations and are centered on cD galaxies. A more varied sample is needed for a full evaluation of the model.

9.2: Formation and Evolution of Clusters

In this section the processes of formation and evolution that may have occurred or still be occurring in clusters are discussed. There is little chance, using present techniques, of observing the predicted evolution directly by comparing distant with nearby clusters. However, observations by Butcher & Oemler (1978) of two very high redshift clusters ($z > 0.4$) suggest that they may contain abnormally high proportions of blue galaxies, but selection effects may have influenced the choice of these clusters. If all rich clusters at similar redshifts show the same property, it will be difficult to account for it on the basis of evolution processes at present known.

i) Cluster formation and infall: The classic description of cluster collapse is given by Gunn & Gott (1972). They outline how, in the early Universe after recombination, a density perturbation slows its

expansion and breaks away from the surrounding Universe, eventually collapsing gravitationally. The material in the perturbation may have already formed galaxies when it collapses. Galaxies and gas in the surrounding region continue to fall into the cluster; the gas is heated by shocking and viscous dissipation and provides at least some of the observed X-ray emission. The galaxies falling in are not yet stripped by the intracluster gas and include a large proportion of spiral galaxies. The large velocity dispersion observed for the spiral population in some clusters may be because many of these galaxies have not yet reached the core of the cluster and when seen near the cluster centre have large line-of-sight infall velocities (Moss 1976).

Not all clusters have necessarily completed their collapse yet; ragged spiral-rich clusters may still be undergoing this process. Even for the rich Coma Cluster, the collapse time is ~40% of the Hubble time if the virial mass is the true cluster mass.

An alternative theory of cluster formation, reviewed in Doroshkevich et al (1978), describes the evolution of "pancakes" of gas into stars, galaxies and clusters of galaxies. Galaxies are formed comparatively late in this process and the early evolution of clusters is dominated by the dynamics of the gas in the "pancakes".

ii) <u>Relaxation and dynamical evolution</u>: The galaxies in the collapsing cluster will sub-cluster by gravitational attraction (White 1977). These groups merge in subsequent evolution, but some trace of their existence may be left as an asymmetry in the cluster. Violent relaxation (Lynden-Bell 1967) acts in less than twice the collapse time; this is the randomisation of galaxy orbits by the rapidly varying gravitational fields that they experience. No equipartition of energy between the galaxies is produced.

If the cluster forms from a "pancake", the protogalaxy distribution may be relaxed by "pre-virialisation" due to the turbulent conditions (Davis & Peebles 1977).

The timescale for relaxation by two-body interactions is rather longer than for violent relaxation. If the time in years for a large alteration in the velocity distribution to be produced is T_r then (Bahcall 1977a):

$$T_r = \frac{2.10^{10}\ v^3}{M^2\ N\ \ln\Lambda}$$

v is the galaxy radial velocity (in 10^3km/s), M is a galaxy mass (in $10^{12}M_\odot$), N is the density of galaxies (in 10^3/Mpc^3) and Λ is the ratio of maximum to minimum impact parameters ($\ln\Lambda \approx 5$).

Using values for these parameters appropriate to rich clusters, we find that only the most massive ($10^{12}M_\odot$) galaxies can have attained any degree of two-body relaxation and that the lighter galaxies are virtually unaffected. Two-body relaxation produces equipartition of energy between the galaxies so that the massive galaxies lose velocity and sink to the centre of clusters. If the virial mass of clusters is concentrated in the galaxies, it is difficult to explain the lack of observed segregation of bright galaxies (Rood 1965, White 1977); in some rich clusters the segregation observed is in the opposite sense (Chap. 8).

A particular case of two-body relaxation occurs when a massive galaxy moves through a homogeneous sea of much lighter bodies. This may be a useful approximation in clusters if, for instance, most of the virial mass of the cluster were distributed evenly in intracluster space so that the dynamical evolution of the cluster was dominated by this sea. It may also apply when galaxies move through the diffuse haloes of other galaxies, such as a central cD. In these cases the

moving galaxy experiences a resistive force, "dynamical friction", as it loses energy to the sea (Chandrasekhar 1943). The timescale for this process is the same as for normal two-body relaxation, except that a factor of MN in the denominator is replaced by the density of the sea, ρ. Thus if T_d is the timescale in years:

$$T_d = \frac{2.10^{10}\ v^3}{\rho\ M \ln \Lambda}$$

v is the galaxy radial velocity (in 10^3km/s), M is its mass (in $10^{12}M_\odot$), ρ is the sea density (in $10^{15}M_\odot/\mathrm{Mpc}^3$) and Λ is the ratio of maximum to minimum impact parameters again. In this and the previous expression the galaxy radial velocity (i.e. the velocity in the line of sight) is assumed to be $3^{-\frac{1}{2}}$ of the true three-dimensional velocity.

iii) Interactions between galaxies: Slow moving galaxies can merge very rapidly if they pass close to each other. If the relative velocities are similar to the velocity dispersion of the stars in the galaxies, and the galaxies pass within their half-mass radii, then the merging may be accomplished in approximately one orbit (White & Sharp 1977). All the translational energy is converted into kinetic energy of the stars in the merged galaxies.

Mergings will take place mostly in the dense central regions of clusters where the collision probability is highest and there is a supply of massive, slow moving galaxies sinking to the centre. The "cannibalism" of massive galaxies by a galaxy at rest in the centre is one possible mechanism for the formation of cD galaxies. (Ostriker & Hausman 1977, Hausman & Ostriker 1978, White 1976). Multiple nuclei are often present in cD galaxies; these may be the half-digested remains of galaxies that have recently merged with the cD. These

accreted galaxies bring in extra energy to the cD galaxy and this may result in the characteristic inflated haloes of cD galaxies (but see the next section for a fuller discussion of the origin of cD's)

The probability of direct collision is high for galaxies always in the core of clusters ($\approx 10^9$ years between collisions of 10kpc radius galaxies), but is much smaller in the outer regions and the average cluster galaxy has probably not experienced one. Collisions between spiral galaxies result in stripping of their gas content since it cannot interpenetrate (Spitzer & Baade 1951). Other than in the early stages of galaxy evolution the disk population of spirals is too numerous for these stripped galaxies to appear as ellipticals; instead they may appear to be S0 galaxies (i.e. galaxies with disks but no young star population). A similar gas stripping process occurs when spiral galaxies move through the intracluster gas (Gunn & Gott 1972). Evidence for gas stripping is shown by spiral galaxies in rich clusters; such galaxies have been found to be deficient in HI (Sullivan & Johnson 1978), lacking well developed arms (van den Bergh 1976) and anomalously red (Holmberg 1958). These are all symptoms of gas loss. The low proportion of spiral galaxies in rich clusters may also be due to gas stripping.

A recent study (Sandage & Visvanathan 1978b) compared the properties of S0 galaxies both inside and outside clusters. They found that all S0 galaxies form a homogeneous class, with no evidence for clusters having a population of recently stripped (within 10^9yrs), and hence very blue, S0 galaxies. Any stripping must have been largely completed at an earlier stage in cluster evolution. Many of the S0's they studied were too far from clusters to have been made by stripping in clusters.

Although direct collisions are not common, less violent encounters between galaxies are not so unusual. Outer layers of galaxies may be

removed tidally in such interactions; if galaxies are initially embedded in large (>100kpc) haloes, then much of the mass of a cluster could be left as debris in intracluster space by the present epoch (Zwicky 1937, Gallagher & Ostriker 1972, Richstone 1976). The haloes of cD galaxies may be the luminous part of this debris. The probable distribution of the material is not clear; interactions leading to the tidal stripping will be commonest near the centre of a cluster since their frequency depends roughly on the square of the galaxy density, but the ultimate distribution of the shed material depends on the energy with which it is liberated. Measurements of the intergalactic luminosity in the Coma Cluster (Melnick et al 1977, Mattila 1977) show that it contains no more than 25% of the cluster luminosity and has a colour B-V = 0.54 $\pm$ 0.19. It cannot therefore contain the missing binding mass unless its mass-to-light ratio is at least ~700 solar.

Observations of elliptical galaxies in several clusters by Strom & Strom (1978) show that in cD and spiral-poor clusters these galaxies have smaller characteristic sizes than elsewhere. This suggests that tidal stripping has removed their outer visible layers, and presumably, if they exist, their dark heavy haloes. This loss of heavy haloes from the cluster galaxies will slow the evolution rate of clusters as the galaxies become lighter, and their two-body evolution times become in consequence longer.

9.3 The cD Phenomenon and Brightest Members

The classification of a galaxy as being a "cD" is to some extent a matter of personal opinion; no definitive definition has yet been adopted. However, observers would agree that there exist, at the centres

of some rich clusters, galaxies which are abnormally bright, have elliptical cores, are surrounded by diffuse haloes when seen on Schmidt plates, and which are often radio sources. These "cD" galaxies were noted by Matthews et al (1964) and Morgan & Lesh (1965). Statistical studies show that the dominant galaxy in a cluster tends to be located at or near the cluster centre, and that such central, dominant galaxies are often associated with strong radio sources (Leir & van den Bergh 1977).

Galaxies having cD characteristics are generally found in the centres of rich clusters, possibly in part because that is where they are generally looked for and because isolated cD galaxies may be mistaken for SO galaxies not so far away (e.g. the cD galaxy in S40/6: see Chap. 2). N4839 in the Coma Cluster, despite being far from the cluster centre, has the typical elliptical core and diffuse halo of a cD. Morgan et al (1975) and Albert et al (1977) have published lists of galaxies in poor groups which appear to be in the cD class. Observations of a sample of these galaxies showed that their haloes were either faint or possibly caused by interactions with a nearby galaxy (van den Bergh 1977b). Redshifts and photometry indicate that several of these possible cD galaxies are as bright as the brightest members of some clusters, although fainter than the "classic" cD galaxies such as that in A1413 (Thomas & Batchelor 1978).

Out of 104 clusters in Abell Distance Classes 1 to 4 classified by Leir & van den Bergh (1977), the distribution into Bautz- Morgan classes was: Class I:11clusters, I-II:9, II:22, II-III:20, III:42. Although, as they point out, there are severe difficulties in the consistent application of the Bautz-Morgan classification system, it is apparent

that the classic cD cluster, normally B-M class I, is comparatively rare and that most clusters have no dominant galaxy.

Fig. 9.6 shows the profiles of the cD galaxies in the 4 clusters for which photographic photometry was described in Chap. 7. The profiles were found by measurement of isophotal contour maps of the galaxies. They are plotted as the geometric mean of the major and minor radii of the galaxy at each surface brightness; the data from the two sides of the galaxy have been averaged. Hence, at a given surface brightness, the radius is calculated by:

$$R = (\tfrac{1}{2}(b_1 + b_2) \times \tfrac{1}{2}(a_1 + a_2))^{\frac{1}{2}}$$

where a_1 and a_2 are the radii on the minor axis and b_1 and b_2 are the radii on the major axis. The surface brightnesses are corrected for galactic absorption, the K-effect, and cosmological $(1+z)^4$ dimming; the calculation of the radii includes the $(1+z)^{-2}$ cosmological term.

The figure shows that cD galaxies have profiles that exhibit approximately power law dependence on radius, with an index of less than two. They hence must show a cut-off at a radius beyond the range shown in the plot if they are to extrapolate to a finite total galaxy luminosity. The profile of M87, one of the two brightest galaxies in the Virgo Cluster is included for comparison; the data for this galaxy have been taken from Carter & Dixon's (1978) compilation of measurements by several observers. Although not usually classified as a cD galaxy, M87 has the characteristic profile.

No discontinuity is apparent in the profiles between a "core" and a "halo". The impression of two-component structure is given by visual comparison of these galaxies with normal elliptical galaxies which have profiles that follow steeper power laws in their outer regions

(e.g. Oemler 1976). Thus although "halo" is a convenient term for the diffuse outer regions of cD galaxies, it should not be thought to imply that haloes are necessarily physically distinct from the rest of the galaxy.

The V-band photometric data of Oemler (1976) for 3 cD galaxies are compared in Fig. 9.7 with the photoelectric measurements (App. V) on the cD galaxy in 2354-35. Oemler's observations were carried out in a band intermediate between B and V and then transformed into the V-band; there may therefore be a zero-point error between the photographic and photoelectric measurements. It is also not clear which corrections Oemler applied to his data to transform them into the galaxy rest frame. With these reservations, Figs. 9.6 and 9.7 indicate that the cD galaxies in 2354-35, S40/6 and A1146 are very similar both to each other and to the "classic" cD's investigated by Oemler. The cD galaxy in K44 is rather fainter, but not as faint as M87.

The profiles have not been followed to extremely large radii because:

i) The outer regions of the galaxies are very irregular and much affected by other images.

ii) There must remain doubts about the accuracy of the photographic photometry at very faint surface brightness levels owing to the difficulty of setting the background level accurately. This problem is made particularly acute in K44 by the nearby bright star.

iii) the corrections from observed surface brightness into the galaxy frame are large; for the A1146 cD, the observed surface brightness μ_B = 26.5mag/□" corresponds to μ_B = 25.15mag/□" at the galaxy.

The nature of the formation and evolution of cD galaxies is uncertain. It may not be necessary to postulate any evolution if the formation of a

supergiant galaxy is favoured at the centre of a cluster or if there is some mechanism by which supergiant galaxies tend to reach the centre of the cluster. If, for instance, cD galaxies were very massive ($\sim 10^{14} M_{\odot}$) then two-body relaxation would bring them to the centre within a Hubble time. Since the dynamics of normal elliptical galaxies is not fully understood (e.g. Binney 1978), it is possible that the haloes of cD galaxies are a necessary consequence of their mass; no normal, halo-less, elliptical galaxies have yet been examined that have luminosities as great as cD galaxies such as those in K44, 2354-35 and A1146.

The evolution of clusters was discussed in the last section, where it was pointed out that cD galaxies may owe their brightness and extended profiles to the accretion of either debris left in intracluster space by galaxy interactions, or of galaxies brought to the cluster centre by dynamical friction or other two-body interactions. Massive galaxies are especially susceptible to this "cannibalism" since they have the shortest timescales for dynamical evolution. The asymmetrical shape and multiple nuclei of many cD galaxies may be explained as the symptoms of a recent capture of another galaxy; the capture disturbs the cD and the nucleus of the victim galaxy remains undisrupted inside the cD. The steady input of energy to the cD from cannibalised galaxies may inflate it, and as it becomes more diffuse the nuclei are able to survive disruption for longer periods (Hausman & Ostriker 1978). Eventually the cD may not increase in brightness in its central regions after further accretion, but become more extended instead.

A tendency for cD galaxies to be aligned with their clusters was found by Sastry (1968) and has also been noted in more recent work by Dressler (1978b) and Carter & Metcalfe (1979). The alignment of the cD galaxies with the cluster galaxy distribution in the present sample

of four clusters is shown in Fig. 9.8. S40/6, K44 and 2354-35 all show alignment, but in A1146 the cluster does not have a strong orientation. This is reflected in the cD galaxy in A1146 which has a much lower ellipticity than those in the other three clusters. A possible reason for the observed alignments is that the cD galaxy is constructed out of material accreted from the cluster, as galaxies or debris, and which retains its anisotropy. The galaxies having the most relaxed distribution in the cluster, and which are the most likely to be accreted, may have a more anisotropic distribution than the other galaxies (Binney 1977); this would enhance the anisotropy of the accreting cD galaxy. However, it is not impossible that the alignment originates from conditions at the formation of the cluster and galaxies, and is nothing to do with evolution of the cD.

The variation in ellipticity with radius for the four cD galaxies is shown in Fig. 9.9; the data used are the same as for the derivation of the cD profiles (Fig. 9.6). All four galaxies have ellipticities that increase with radius. This is as would be expected if accreted material, which determined the orientation of the cD, formed a major part of the cD galaxy. Such material would probably have a high velocity dispersion and be seen mainly in the outer regions of the galaxy where its elliptical distribution would therefore be most apparent. However, although the explanation of this phenomenon by an accretion process is attractive, an increase in ellipticity with radius has been seen in several normal elliptical galaxies (e.g. by Carter 1978), and may be due to another cause.

The colours of cD galaxies are generally similar to those of bright elliptical galaxies. The photoelectric data of App. V show the cD galaxy in 2354-35 to have a colour of $B-V \approx 0.97$ after correction for

the K-effect (Pence 1976) and assuming zero galactic absorption. This a typical colour for the bright ellipticals in the sample. The cD also shows the same colour gradient as that found in normal ellipticals, i.e. becoming slightly bluer towards the outside. If the cD is composed mainly of bright elliptical galaxies that have been accreted then one might expect its colour to be constant across its face, unless the red cores of accreted galaxies were not disrupted but sank to the centre of the cD. If the cD were formed from tidally stripped debris then the resulting galaxy would probably be bluer than bright ellipticals since the faint galaxies that form much of the cluster population are bluer than bright ones, and their outer regions which are the most liable to stripping are bluer than the inner regions. The formation of the cD wholly from debris thus seems improbable, but formation from accreted galaxies is possible providing that either the original galaxy is not entirely overwhelmed or the accreted galaxies are not completely disrupted so that their nuclei give the cD the observed central redness.

An investigation of the velocity dispersion of the stars in the halo of the cD galaxy in A401 (Faber et al 1977) showed that the dispersion, determined by measuring the widths of optical absorption lines, is not abnormally large. The observations were made at the centre of the cD and at a point in the halo, 43kpc from the galaxy centre, with a surface brightness of $\mu_B = 24.5$mag/□". The central velocity dispersion was measured as 480 ± 120km/s and the halo dispersion as 470 ± 250km/s ; the large error limits are a consequence of the extreme faintness of the halo compared with the night sky. These data suggest that the halo of the A401 cD cannot be formed entirely out of stars having the velocity dispersion of the cluster as might be the case if they were accreted as debris from the cluster. However, up to 50% of the halo stars could have a very high velocity dispersion without the bread wings on the absorption lines having been detectable.

In summary, then, although there is no evidence to prove that cD galaxies were not initially formed just as they are now, observations point towards there being something special about them; they have a tendency to be sited in the centre of a cluster, they are often the source of strong radio emission, they have diffuse haloes, they are very bright, they tend to be aligned with the distribution of galaxies in their cluster, they often have multiple nuclei, and their ellipticities normally increase with radius. None of these characteristics is necessarily the product of evolution, but the observations of cDs are consistent with their formation by accretion, most probably of other galaxies. The "seed" galaxy would normally be a large galaxy in the centre of a cluster and have a low velocity, thus increasing the chance of capturing other galaxies. The colour gradient across a cD would be either from the stellar population of the "seed" or due to the redness of accreted undisrupted galaxy nuclei. Multiple nuclei in cDs may be the remains of succesive accreted galaxies. The formation of cD galaxies from debris tidally stripped in encounters between cluster members is less likely than cannibalism since the galaxy produced would be too blue and have a large velocity dispersion. The colour data almost certainly rule out the formation of cD galaxies by continuing gas accretion since the resulting cD would be very blue.

No single mechanism is necessarily responsible for the observed nature of cD galaxies, and the problem for the future is to determine, both theoretically and observationally, which of the possible processes are significant and which are not. Even if evolution by accretion can be shown to have been important in the history of some cD's, it does not follow that all cD galaxies were formed in this way. Just as there is no evidence that cD galaxies have not always been as they are now, there is also no reason to doubt that bright central galaxies in

clusters will occasionally accrete other galaxies, debris, or gas. A further problem to be faced in any comprehensive theory of cD galaxy formation and evolution is the absence of cD galaxies in most clusters; there is a danger that accretion theories, if made capable of explaining cD galaxies in some clusters, will also predict cD galaxies in many clusters in which they are in fact absent.

The evolution of cD galaxies is of special interest in view of their use as cosmological standard candles. If the magnitudes of brightest cluster members are measured photoelectrically within a standard metric radius, then the dispersion is indeed very small, suggesting that the magnitudes are almost independent of the cluster in which the galaxy is located (Sandage 1976b, Tremaine & Richstone 1977). Isophotal magnitudes, which are presumably more representative of the true luminosity of the galaxies, show a considerably larger dispersion: 0.57mag instead of 0.38mag for a set of 12 clusters (Godwin & Peach 1979a). Similar dispersions have been found in isophotal magnitudes of brightest members by Dressler (1978a).

The larger dispersion of isophotal magnitudes is consistent with the predictions of a statistical model in which all galaxy magnitudes in the cluster, including the brightest member's, are taken statistically from a universal luminosity function and in no way depend on the magnitudes of other galaxies in the cluster (e.g. Geller & Peebles 1976). The statistical model also predicts the magnitude intervals between successively fainter members of the cluster. Table 9.2 lists the difference between the magnitudes of the three brightest members M_1, M_2 and M_3 in 24 clusters; these values have been derived from the isophotal photometry in the present work, in Dressler (1976) and in Godwin & Peach (1979a). The mean differences between these

magnitudes predicted by the statistical theory are in Table 9.3. It is apparent that the observations show significantly larger differences than the theory predicts for the richer clusters. This is at least in part the result of a strong selection bias towards rich clusters with dominant cD galaxies in the sample from Dressler and the present work. In effect, many clusters have been included largely because of their big M_2-M_1 value. However, Geller & Peebles (1976), using a less biassed sample taken from Sandage's photoelectric work, found that there is a class of clusters that may have anomalously large M_2-M_1 values.

If we split the sample of 24 clusters into those that contain galaxies claimed to be cD's, and those that do not, we find that as expected the cD clusters have the larger value of $\langle M_2-M_1 \rangle$: 1.4 ± 0.5 against 0.4 ± 0.3. The cD clusters have M_2-M_1 values ranging from 2.3 to 0.5. If we assume that all clusters, including the cD clusters, originally obeyed the statistical theory and the brightest members of some clusters evolved to cDs, then we might expect evolution of ~1mag to have occurred giving the observed $\langle M_2-M_1 \rangle$. In practice this figure will be an upper limit since:

i) Clusters with very bright brightest members ab initio, although not necessarily cD galaxies, would probably have the highest probability of turning their brightest member into one by evolution. In this case a large M_2-M_1 would be, at least in part, primeval.

ii) If cannibalism is the dominant form of evolution, then it may increase M_2-M_1 not only by the gain in luminosity of the brightest member, but also by the removal of the second brightest which, as a massive galaxy, stands a high chance of being one of the victims.

If we take the view that cD galaxies are the result of cannibalism, and assume that the most likely accretion occurs first, i.e. of the

second brightest by the first brightest, then starting with the statistical model values of $M_2-M_1=0.3$ and $M_3-M_2=0.2$ leads to a value after the accretion of $M_2-M_1=0.8$. It is thus possible to make a quite typical, regarding galaxy magnitudes, cD cluster from a normal cluster by a single accretion. Obviously to produce $M_2-M_1=2.3$ rather more galaxies must be accreted, but starting from the standard statistical model cluster and assuming 0.3mag spacing between successive galaxies the accretion of only the second, third and fourth brightest galaxies is needed.

Thus, although it is impossible with the extremely biassed sample of isophotal photometry available to show that cD clusters form a separate class from other clusters and are not just the extreme of a range of clusters which all obey the statistical model, the data are sufficient to put limits on possible evolution. We have found that even if cannibalism by the brightest member accounts for all the difference between cD clusters and the other clusters, it does not necessarily imply a continual holocaust at the centre of the cluster. The sporadic accretion of a few bright galaxies is quite sufficient to produce the brightest of the observed cD galaxies.

9.4 Core Evolution

We have seen that there is good, but not overwhelming, evidence that evolution plays a part in determining the present properties of clusters. A problem that still remains is whether all clusters are at different points on essentially the same evolutionary track, or whether the evolution that occurs in a particular cluster is determined by its initial state (if it is realistic to separate evolution from initial conditions). The role of chance must also not be ignored. It was shown

in the last section that the differences between clusters with and without cD galaxies may possibly be caused by the accretion of very few, sometimes only one, bright galaxies by the brightest members. The first chance accretion of a galaxy may inflate the accreting galaxy, increasing the chance of further cannibalism. Hence a single chance accretion may trigger a phase of rapid core evolution. Simulations by Hausman & Ostriker (1978) examined the accretion of galaxies in a model cluster, and found that until the supply of victims in the cluster core becomes depleted the central galaxy increases in luminosity roughly exponentially with time.

The observations on K44 and 2354-35 are relevant to this discussion since they may form a before-and-after pair in this process of rapid core evolution. In most respects the two clusters are very similar: e.g. in velocity dispersion (Table 5.3), in profile (Fig. 8.3), and in optical luminosity (Table 9.1). Their cores are, however, very different. That of K44 shows a very low velocity dispersion (Table 5.3), high density of galaxies (Fig. 8.3), has a core depleted (although not significantly) of bright galaxies (Tables 8.2,8.3), and has a disturbed, comparatively faint cD galaxy with a double nucleus. 2354-35 shows none of these properties.

Calculation of the timescale for the accretion of the bright galaxies in the core of K44 may be made using the expression given in Hausman & Ostriker (1978) for the rate of cannibalism of galaxies with masses in the range M to M+dM:

$$\frac{d^2N}{dMdt} = 24\ (2\pi)^{\frac{1}{2}}\ \frac{G\ M\ \ln\Lambda\ R^3\ n(M)}{S\ r_c^2}$$

where G is the gravitational constant ($=1.3\ 10^{11} km^3 s^{-2} M_\odot^{-1}$), Λ is the ratio of maximum to minimum impact parameters ($\ln\Lambda \sim 4$), S is the line-of

sight velocity dispersion (220km/s for the core of K44: see Table 5.3), R is the radius from the cD centre inside which an orbiting galaxy can be considered captured since it rapidly and continually loses energy to the dense sea of stars of the cD (Ostriker & Tremaine 1975), r_c is the isothermal radius of the cluster core, and n(M) is the number density of galaxies in the core.

Inversion of this formula gives the timescale for the accretion of a particular galaxy in the core:

$$a = \frac{\frac{4}{3}\pi S r_c^5}{24 (2\pi)^{\frac{1}{2}} G M \ln\Lambda R^3}$$

The mass of the accreted galaxy will be taken as $10^{12} M_\odot$. Fig. 2.1 indicates that r_c is very roughly $3\frac{1}{2}$arcmin $\approx$ 160kpc. R is not easy to estimate so a conservative guess is made that it is the separation of the two cD nuclei $\approx$ 31kpc (using a $\frac{1}{2}\pi$ deprojection factor). This is almost certainly an underestimate; no galaxy is likely to be able to survive intact that close to the cD centre. Using these estimates, the derived timescale is $3\ 10^9$ years; an increase in R would decrease this value.

The mass of the galaxy has been set as 10^{12} since this is slightly less than the mass of g5, a typical bright core galaxy, derived using the mass-to-light ratio of 20 solar found by the virial theorem for the core (see next section).

The calculated timescale for the accretion of $\sim 3\ 10^9$ years suggests that the present state of K44 is a transition phase. In another $6\ 10^9$ years the bright galaxies in the centre will probably have been cannibalised by the cD galaxy and the core of the cluster will resemble that in 2354-35. The off-centre double nucleus of the cD in K44 may show that it is already starting the accretion the surrounding galaxies.

The final magnitude of the cD galaxy after it has accreted the bright galaxies in the cluster core may be estimated by adding the present B_{27} luminosities of galaxies 1,5,13,17,23,25 and 28 to that of the cD (galaxies 2 and 3). The resulting magnitude is 12.51, equivalent to a corrected absolute magnitude of -23.77, just 0.02 mag brighter than the absolute magnitude of the cD in 2354-35: $M_{B_{27}} = -23.75$.

The correspondence is fortuitously close in view of the arbitrary magnitude limit set on the accreted galaxies and the unknown part of the luminosity lost or gained across the limiting isophotes. Even so, it shows that the present state of 2354-35 is consistent with it having passed through an intermediate stage similar to K44.

Tightly-knit cores, such as that in K44, are not usual in clusters, nor is the low velocity dispersion in the core; few other clusters can have cores with such short timescales for dynamical evolution. The formation of such a core by evolution seemes unlikely; two-body relaxation is too slow to strip a population of galaxies of $\frac{3}{4}$ of their translational energy. In any case, two body processes could only give a low velocity core of very massive galaxies, whereas the observations show that the low core velocity dispersion is shared by bright and faint galaxies alike. It thus seems probable that the core of K44 is an original sub-cluster of the main cluster, and has avoided disruption since. It is tempting to speculate that the core may have its present form and therefore be able to evolve rapidly only because the rest of the cluster is dynamically unevolved and has not yet subjected it to the rigours of violent relaxation. Clusters such as Coma which have much less pronounced minima in their velocity dispersions at their centres may originally have had a core similar

to that in K44 but have partially disrupted it in the course of dynamical evolution.

This theory of cD formation may give a clue to the possible similarity of very bright cD galaxies. If there were an upper limit on the amount of material with which a low velocity dispersion core could be formed, then this upper limit would be reflected in the present cD galaxies; once a cD has depleted its core, then it can evolve only slowly. Fast moving galaxies from the rest of the cluster that it may be able to capture will inflate it and possibly not result in any brightness increase in its observable regions. If the cD galaxies in S40/6 and A1146 are postulated to have reached this stage of quiescent middle-age, it is, however, unclear why S40/6 is surrounded by a very high density of faint galaxies, whereas the cD in A1146 is not (Fig. 8.3).

There is no evidence to suggest that all cD galaxies were formed from low velocity dispersion cores, and the apparent evolutionary track between K44 and 2354-35 may be a mirage. The model gives, however, a possible solution to the problem stated in the last section: the difficulty of constructing an evolutionary theory of cD formation which does not predict cD's in more clusters than the small fraction in which they are actually seen. By postulating an undisrupted low dispersion core as the necessary precursor of a cD galaxy, the presence or absence of a cD galaxy in a cluster is determined by the initial conditions of cluster formation, just as it is if cD galaxies are born as cD's.

9.5 The Missing Mass Problem

Calculations of the mass in clusters, using the virial theorem in a simple-minded fashion, produce values for the mass-to-light ratios for the component galaxies that are far in excess of the values found by other methods. This has been known since the researches of Zwicky (1933) and Smith (1936).

The virial mass of a cluster, M, can be found by equating its kinetic energy with half its negative potential energy due to gravity:

$$2\left\langle \tfrac{1}{2} \sum_i m_i v_i^2 \right\rangle = G\left\langle \tfrac{1}{2} \sum_i \sum_{j \neq i} \frac{m_i m_j}{r_{ij}} \right\rangle$$

where m_i is the mass of the i-th galaxy, v_i its velocity and r_{ij} its distance from the j-th galaxy. Taking averages over states of the cluster gives an expression in observables:

$$M = \frac{3 R S^2}{G} \qquad R = 2R'$$

where R' is the mean harmonic mass-weighted separation of the galaxies in the cluster. S, the line-of-sight velocity dispersion has been assumed to be $3^{-\frac{1}{2}}\sigma$. (σ is the 3-dimensional velocity dispersion); the actual conversion factor between them depends on the dynamics of the cluster. In the extreme case of a cluster in which all galaxy orbits are radial and the redshift sample is near the cluster centre in projection, then $\sigma \approx S$.

R has usually been calculated by fitting a theoretical function to the 2-D radial galaxy distribution and adopting a value of R appropriate to that fit, or by using strip counts or direct measurements of the galaxy distribution (reviewed by Rood et al 1972 and Bahcall 1977a). These methods are insensitive to the outer regions of the cluster.

R is strongly affected by outlying galaxies unless the profile of the galaxy distribution falls off faster than an inverse square dependence on radius. Since the inner regions of clusters, out to 1Mpc, have much flatter profiles than this (Chap. 8) and the profiles of the outer regions of clusters cannot be measured easily owing to contamination by non-members, it is possible that R is largely determined by large populations of galaxies far from the cluster centres. Evidence from redshift surveys (Chap. 5) shows that clusters probably have large haloes of galaxies extending many Mpc in radius. R will then be of comparable size to these haloes if they contain a major proportion of the cluster membership.

In view of this doubt about the correct value of R to use, the virial properties of the 3 clusters in the present sample with both redhsifts and photometry are presented in Table 9.4 in terms of a parameter χ where $\chi = \frac{M}{L}\frac{1}{R}$. The mass-to-light ratio of the cluster is M/L. The virial theorem becomes:

$$\chi = \frac{3\,s^2}{G\,L}$$

where L is the optical luminosity of the cluster. A line of constant χ is marked on Fig. 9.4 which shows velocity dispersion plotted against optical luminosity for a large set of clusters (Table 9.1). The best fit relation found for these parameters is $S \propto L^{0.57\pm0.20}$ (Chap. 9.1), consistent with a universal value of χ, although suggesting that there may be an increase in χ for luminous clusters. This may be due to the same cause as the greater mass-to-light ratios found for rich clusters than poor clusters and groups by many workers. The constancy of χ could also be produced by an anti-correlation of R with M/L, but there is no observational evidence to support this (Godwin & Peach 1979b).

The M/L value appropriate to galaxies is still a matter of heated debate. Although M/L found for elliptical galaxies by measurement of their stellar velocity dispersions is in the range 3 - 30 solar units (e.g. Faber & Jackson 1976), calculations using the dynamics of binary galaxies and groups of galaxies yield values in the range 20 - 100 (e.g. Turner 1976, Gott & Turner 1977). The mass-to-light (M/L) ratios of spiral galaxies, found by measuring their rotation curves, are typically in the range 1 - 10 (e.g. Balkowski et al 1972).

A typical value of R that has been used for clusters is 1Mpc; in this case χ is the mass-to-light ratio for the cluster. Table 9.4 shows that the 3 clusters then have very high mass-to-light ratios. Several factors tend to reduce this anomaly:

i) The extrapolation of the galaxy magnitudes to infinitely faint limiting isophotes will add perhaps ~10% to the cluster luminosity, and hence reduce M/L by a similar amount.

ii) Inclusion of galaxies fainter than $M_{B_{27}}$ will also increase the cluster luminosity. The faint end of the galaxy luminosity function is unknown in clusters; the best data currently available are those in the present work for K44. We find that inclusion of galaxies within 0.92Mpc of the centre and $-18 \geqslant M_{B_{27}} > -19$ adds only ~ 8% to the cluster luminosity and those with $-17 \geqslant M_{B_{27}} > -18$ a further ~6%. Galaxies in this magnitude range are considerably fainter than the LMC (M_B=-18.2 Allen 1973), and it seems unlikely that much of the cluster luminosity can lie in galaxies fainter than $M_{B_{27}} = -17$. A reasonable correction for faint galaxies would be 25% extra luminosity and hence a comparable reduction in M/L.

iii) Intergalactic luminosity cannot be estimated easily from the present data since the background fitting techniques used in the

photographic photometry hide it. For an indication of how much might remain undetected, a rough calculation shows that an area of radius 200kpc in 2354-35 that had a surface brightness due to intergalactic luminosity of μ_B = 26mag/□" would have same total magnitude as the central cD galaxy approximately. Such an area of luminosity would probably be detected by the methods used. A reasonable proportion of the total luminosity in intergalactic regions would be ~25% at most; this is similar to the value found by Melnick et al (1977) for the Coma Cluster.

iv) The cluster extends far beyond the 0.92Mpc radius used; if the profile has an inverse square dependence on radius, then succeeding annuli of equal width will have equal populations of cluster galaxies. Since clusters are known to extend to at least ~5Mpc, and the profiles may be flatter than inverse square, the majority of the population may be outside 0.92 Mpc. Although only the centre of the cluster need be used in some methods of determining the M/L, such as fitting a King profile, the number of galaxies is too small for accurate fits (Avni & Bahcall 1976) and the applicability of the methods suspect. However, as the outer regions of clusters are unexplored, we cannot make corrections to M/L for the effect on R and L of the outer parts of the cluster.

v) This discussion has assumed that the virial mass of a cluster is truly representative of the actual mass, implying that the cluster has reached a steady state. Although this is probably true in the inner regions of clusters such as S40/6, there is no possibility of the outer regions of clusters having reached equilibrium. The crossing time of a galaxy 4Mpc out from the centre of K44 is 10^{10} years. It is thus possible that we see a mixed system, parts of which are in virial equilibrium but embedded in a non-virialised halo. The higher

velocities of the non-virialised galaxies will predominate in the calculated velocity dispersion. If the cluster is gravitationally bound, then its mass cannot be less than $\frac{1}{2}$ of its calculated virial mass. Thus, depending on the degree of virialisation, the cluster M/L ratio may be up to a factor of two less than the virial value.

vi) The 3-dimensional velocity dispersion is calculated by assuming a $3^{\frac{1}{2}}$ conversion factor. The true factor is between 1 and $3^{\frac{1}{2}}$ depending on the form of the galaxy orbits in the cluster. This can reduce the derived M/L value by up to a factor of 3.

It seems not unlikely, then, that the true mass-to-light ratios of the clusters may be as little as $\frac{1}{4}\chi$. The mass-to-light ratios for K44 and 2354-35 are then not in serious disagreement with the mass-to-light ratios calculated for elliptical galaxies by other means. Other clusters (e.g. A194: Chincarini & Rood 1977) have been found to have similar M/L ratios and also present no severe missing mass problem. The problem is only acute in some very rich clusters, such as Coma, S40/6 and Perseus, which have high velocity dispersions. No answer to the problem is offered here; the various possibilities are reviewed in Bahcall (1977a), Abell (1975) and elsewhere. The solutions proposed include sub-clustering, black holes, intergalactic M dwarfs, bricks, cold gas, heavy neutrinos and various more exotic adjustments to the laws of physics. It seems not unlikely that some of the missing mass may be in the form of dark haloes of dim stars or black holes around galaxies, probably at the present epoch tidally stripped from the galaxies in clusters to form a dark intracluster sea (Chap. 9.2). Despondency about the missing mass problem is unjustified in view of our ignorance of the structure and dynamics of the outer parts of clusters and the uncertainty in the mass-to-light ratios of galaxies found by other methods.

To conclude this section we note that the centre of K44 provides a dynamical system largely independent of the rest of the cluster; this is indicated by their very different velocity dispersions. The virial theorem may be applied to this core. As usual, estimating an appropriate value for a characteristic length, R, is not straightforward. The method adopted here is to calculate R', the mean harmonic separation by evaluating it for the four most luminous galaxies in the core: g1, g2/g3 (the cD), g5 and g13. These give R' = 112 arcsec = 135kpc (using the usual $\frac{1}{2}\pi$ deprojection factor). Hence, with R = 2R' = 270kpc and S = 220km/s, the virial mass of the core is 9.1 $10^{12} M_{\odot}$. Using the value calculated in the last section, M_B = -23.77 as the core magnitude, we find M/L = 18. On this rough calculation, therefore, the core of K44 appears to have a similar mass-to-light ratio to that found for elliptical galaxies; there is no missing mass to explain here at least.

9.6: So where has all this got us.....

These discussions and conclusions may give the impression that in the study of the structure and evolution of clusters of galaxies there is a rather high ratio of speculation to hard fact. This is undoubtedly the case, and although the work presented here represents some progress in evaluating the many interrelated possibilities and theories, it is still difficult to write much about cluster formation with confidence, and almost nothing with certainty. The study of clusters is still in its infancy, and much fundamental work has still to be carried out.

Listed below are some of the main points of this thesis.

i) Observations have been carried out to increase the number of well-studied clusters. Galaxy velocities, positions and magnitudes have

been derived in a sample of southern clusters.

ii) As part of this work, photoelectric photometry has been carried out on a set of bright galaxies, helping to bring the standard catalogue data on southern galaxies up to the same detail as on northern.

iii) X-ray emission from clusters has been discussed; the data are compatible with the standard theory of bremsstrahlung emission from hot intracluster gas. A set of rich, X-ray bright, cD clusters have been found to be very similar to each other.

iv) The membership by clusters of large-scale density enhancements has been emphasised. Cluster cores as we see them at the present epoch are in general at very early stages in their evolution, only partly relaxed at most and still probably subject to continual infall of material.

vi) The cD galaxies in the cluster sample are found to be of the "classic form". They are aligned with their clusters, have ellipticities which increase with radius, and are centrally placed. These properties are compatible with evolution of the cDs by accretion of galaxies, but other causes cannot be eliminated.

vi) K44 and 2354-35 are used as examples of evolutionary stages in a possible process of rapid core evolution in which a probably primeval low velocity dispersion cluster core undergoes transmutation by dynamical friction into a cD galaxy.

vii) The missing mass problem is found to be not severe in K44 and 2354-35. The core of K44, in particular, has a similar mass-to-light ratio to that found by other methods for elliptical galaxies.

9.7: ....And where do we go from here?

The rate of progress in cluster research may be expected to increase in the near future. The advent of automatic plate measuring machines will make the collection of photometric and positional data on clusters a routine and comparatively foolproof matter, allowing the collection of data samples far larger than are possible by present methods. The quality and quantity of X-ray data will also improve in the near future. HEAO-B has already been succesfully launched and will soon start to provide the first high-resolution X-ray images of clusters.

There is much important work on clusters that remains to be done. Observations on the shapes, profiles and colour distributions of cD galaxies are particularly important since they play key rôles in the theories of cluster evolution. Basic photometric data on clusters, including galaxy colours, are still needed; the present surveys, including the work described here, cover only small areas and examine only the brighter galaxies. In view of the great variations between clusters, a large set may have to be studied in detail before general conclusions can be reached. More work is also necessary on regions of space which do not contain clusters, otherwise the true nature of the sparse outer regions of clusters cannot be assessed. Redshifts are needed, both in these outer regions to recognise non-members, and over all parts of clusters to explore their dynamics. Only the Coma Cluster has yet been investigated in detail, and full redshift surveys of other types of clusters would be very interesting.

X-ray observations from HEAO-B will provide much additional information about the gas composition, distribution and temperature in clusters; no doubt the discussion of X-ray emission given in the

present work will appear in less than a year to be naïve, if not misguided. Theoretical studies are also becoming more sophisticated as improvements in the speed of computers make simulations of complex dynamical processes increasingly realistic; this trend will certainly continue.

Perhaps it has not been emphasized enough in the preceding pages that the study of clusters cannot be divorced from work in other parts of astronomy and natural philosophy. Stellar evolution, computer design, galaxy dynamics, television technology: all these and many other subjects influence research on clusters. In turn, the results of cluster research may affect profoundly our understanding, both of the stellar systems and super-systems that lie scattered across the Universe, and of the large scale nature of space and time themselves.

Table 9.1 Properties of Clusters

Cluster	L_x log Watts	L_o log $10^{11} L_\odot$	S log km/s	X log	Sources
A98		1.26	2.88		S: FD77 L_o: D76
A154	< 37.70	1.12	2.93	1.83	S: McH78 L_o: D76
A168	< 37.26	0.93	2.76	1.17	S: McH78 L_o: D76
A194	< 36.52	1.13	2.59	1.07	S: McH78 L_o: O74
A262	< 36.46		2.63		S: McH78
A401	38.26	1.29	3.11	2.28	S: H77
A426	38.14	1.53	3.14	2.77	S: YV77 L_o: BGP79
A496	37.37		2.63		S: G78
A576	37.14		3.03		S: McH78
A754	38.02		2.96		S: YV77
A1060	36.29		2.89		S: YV77
A1146	38.35	1.18			L_o: CG79
A1314	< 37.12	1.13	2.81	1.69	S: C76 L_o: O74
A1367	36.78	1.11	2.78	1.61	S: YV77 L_o: Gd79
A1377		1.01	2.51		S: HMS56
A1656	37.89	1.39	2.98	2.42	S: YV77 L_o: GP77
A1940	37.94		2.73		S: YV77
A2029	38.29	1.21	3.18	2.13	S: YV77 L_o: D76
A2065	37.66	1.45	3.07	2.59	S: S77 L_o: BGP79
A2147	37.40	1.16	3.03	1.98	S: YV77 L_o: BGP79
A2151	< 37.27	1.27	2.78	1.89	S: HMS56 BB59 L_o: BGP79
A2199	37.41	1.21	2.93	2.02	S: YV77 L_o: BGP79

Table 9.1 (cont.)

Cluster	L_x log Watts	L_o log $10^{11} L_\odot$	S log km/s	X log	Sources
A2256	37.96	1.47	3.11	2.63	S: YV77 L_o: D76
A2319A	38.22		2.93		S: YV77
A2670		1.26	2.99		S: S73, O73 L_o: BGP79
Virgo	36.40	0.80	2.82	1.03	S: YV77 L_o: BGP79
Cen.	36.80		2.97		S: YV77
K44	37.06	1.10	2.63	1.15	S: G78 L_o: G78
S40/6	38.21	1.42	3.11	2.53	S: G78 L_o: G78
2354-35	< 37.59	1.16	2.63	1.26	S: G78 L_o: B77
Pavo	< 36.43		2.55		S: G78
0152+3337		1.39	2.84		S: S72 L_o: M75

Notes:

L_x values have been taken from McHardy (1978), except for the upper limit for flux from 2354-35 which was estimated from maps shown in the 2A catalogue (Pounds et al 1978) and the value for S40/6 which was calculated from the flux given in the 2A catalogue by the relation: $\log L_x = 40.35 + \log S_x + 2\log z$ where S is the flux in Ariel counts.

L_o values are the sum of the V_{25} luminosities of galaxies within 0.92Mpc of the cluster centre brighter than $M_{V_{25}} = -20.8$. Data in other bands have been normalised to the V-band.

S_o values are calculated as described in Chapter 5.

X values are derived from L_o and S using the formula given in Sec. 9.1

References to sources:

FD77: Faber & Dressler 1977
D76: Dressler 1976
McH78: McHardy 1978
O74: Oemler 1974
CG79: Carter & Godwin 1979
Gd79: Godwin 1979 (unpub.)
GP77: Godwin & Peach 1977
O73: Oemler 1973
S73: Sargent 1973
H77: Hintzen et al 1977
YV77: Yahil & Vidal 1977
BGP79: Bucknell et al 1979
G78: This work
C76: Coleman et al 1976
HMS56: Humason et al 1956
BB59: Burbidge & Burbidge 1959
S72: Sargent 1972
M75: Massey 1975
S77: Spinrad 1977
B77: Bucknell1977

Table 9.2: Bright Members

Cluster	Richness	Type	M_2-M_1	M_3-M_2	M_3-M_1	Source
S40/6 ^{o}	(3)	cD	0.9	0.1	1.0	G
K44 $^{+}$	(1)	III/cD	0.5	0.7	1.2	G
A1146	4	cD	1.3	0.2	1.5	G
2354-35 *	(1)	cD	1.4	0.3	1.7	G
A2256	2	II-III	0.3	0.3	0.6	D
A2029	2	cD	2.3	0.4	2.7	D
A168	2	II	1.0	0.0	1.0	D
A154	1	I-II	0.1	1.4	1.5	D
A2670	3	cD	1.2	0.2	1.4	D,O
A98	3	II-III	0.7	0.5	1.2	D
A1413	3	cD	1.7	0.4	2.1	D,O
A665	5	III	0.6	0.0	0.6	D
A2218	4	cD	1.5	0.0	1.5	D
A401	2	cD	1.9	0.0	1.9	D
Virgo	0	III	0.5	0.0	0.5	O
A426	2	I-II	0.6	0.2	0.8	O
A1377	1	II-III	0.1	0.6	0.7	O
A1553	2	II-III	0.1	0.3	0.4	O
A1656	2	II	0.4	0.2	0.6	O
A1930	1	III	0.8	0.4	1.2	O
A2065	2	III	0.1	0.2	0.3	O
A2147	1	II	0.3	0.3	0.6	O
A2151	2	III	0.1	0.1	0.2	O
A2199	2	cD	1.2	0.1	1.3	O

M_1, M_2 and M_3 are magnitudes of three brightest cluster members.

o: M_1 is sum of cD nuclei (g_1 and g_4).

+: M_1 is sum of cD nuclei (g_2 and g_3).

*: g2, the bright spiral has been omitted.

Sources: G: This work D: Dressler 1976 O: Godwin & Peach 1979a

Table 9.3: Observed and Predicted Magnitude Differences

a) Observed

Data from Table 9.2

Richness	No. of Clusters	% of Clusters	$\langle M_2-M_1 \rangle$	$\langle M_3-M_2 \rangle$	$\langle M_3-M_1 \rangle$
1	6	26	.5 ±.5	.6 ±.4	1.2 ±.4
2	10	43	.8 ±.8	.2 ±.1	1.0 ±.8
3	4	17	1.1 ±.4	.3 ±.2	1.4 ±.4
4	2	9	1.4	.1	1.5
5	1	4	.6	.0	.6

Error bars are standard deviations

b) Predicted

Richness	$\langle M_2-M_1 \rangle$	$\langle M_3-M_2 \rangle$	$\langle M_3-M_1 \rangle$
1	.4	.2	.6
2	.4	.2	.6
3	.3	.2	.5
4	.3	.2	.5

Table 9.4: Virial Properties of Clusters

Cluster	L $10^{12} L_\odot$	S km/s	χ $M_\odot\ L_\odot^{-1} Mpc^{-1}$
K44	1.22	427	104
2354-35	1.53	425	82
S40/6	2.78	1289	417

L: The total luminosity, in solar units, of the B_{27} values for all galaxies brighter than $M_{B_{27}} = -19$ and within 0.92Mpc of the cluster centre.

S: The corrected line-of-sight velocity dispersion (Table 5.3)

χ: Calculated as $\frac{3\ S^2}{G\ L}$ where G is the gravitational constant.

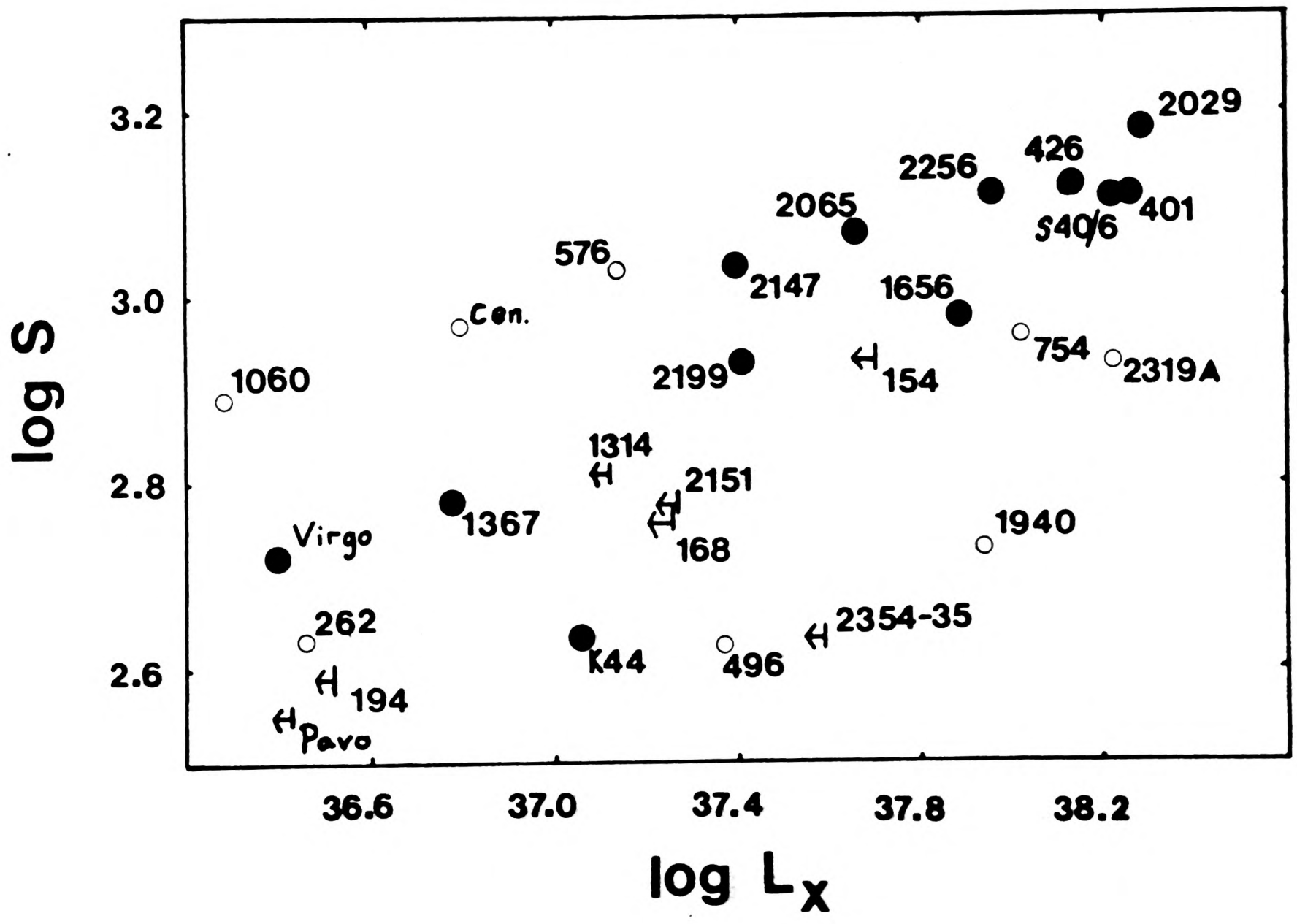

Fig. 9.1: Relation between velocity dispersion and X-ray luminosity

Data from Table 9.1

L_X is in Watts, S in km/s. In this and succeeding graphs, the clusters for which L_X, L_O and S are all available are shown with filled circles.

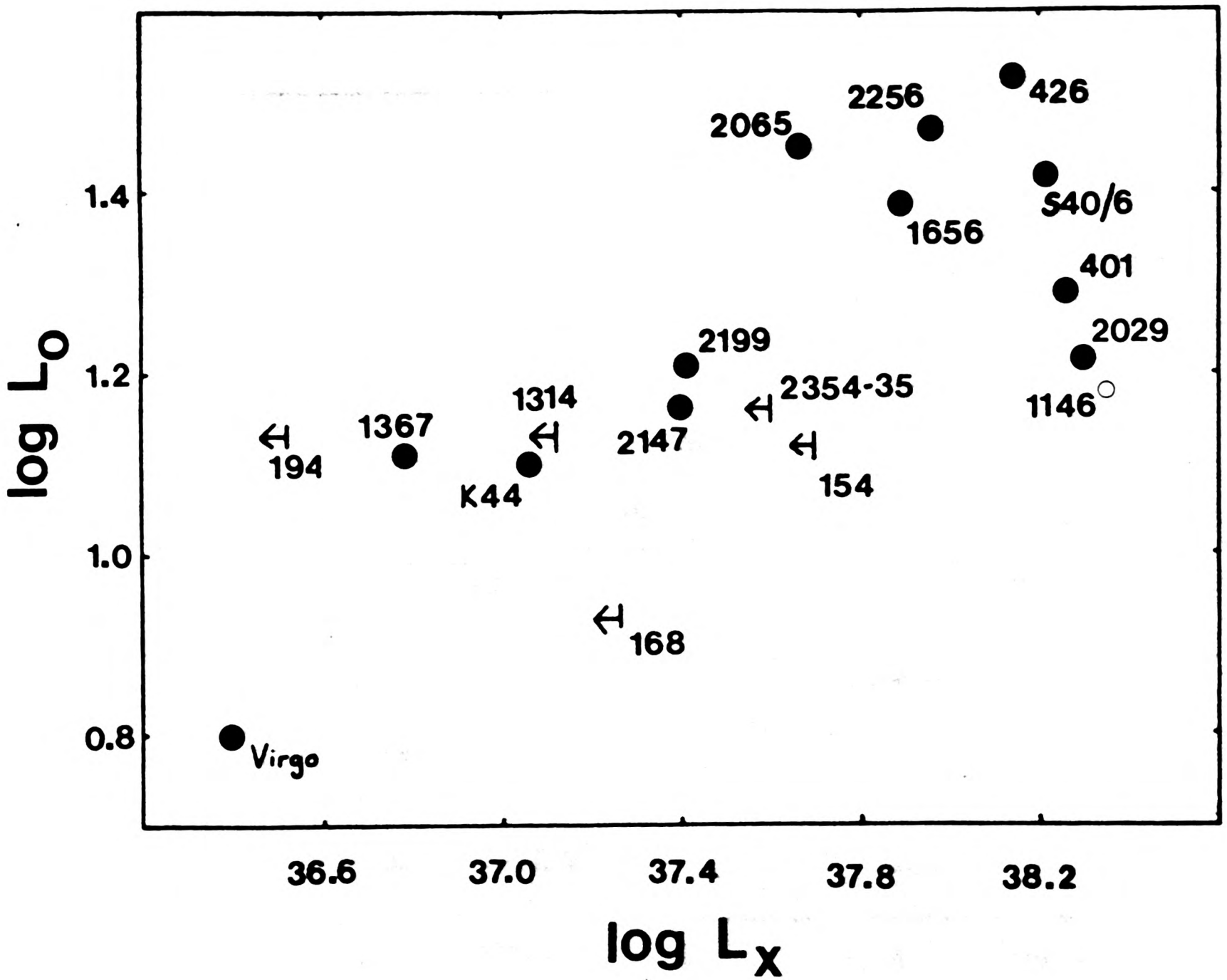

Fig. 9.2: Relation between optical and X-ray luminosities of clusters

L_o in $10^{11} L_\odot$ Data from Table 9.1

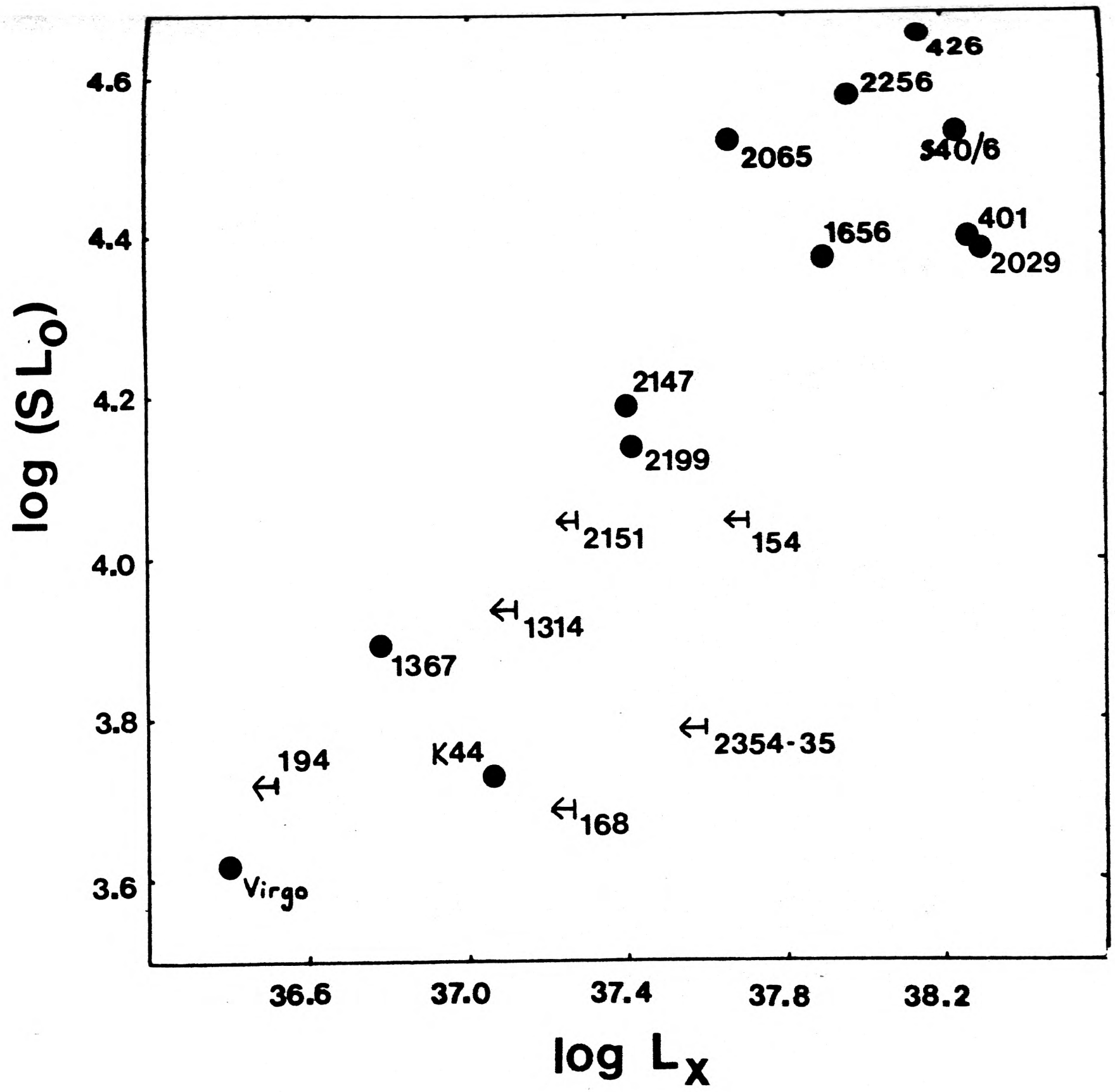

Fig. 9.3 Relation between product of velocity dispersion and optical luminosity, and X-ray luminosity

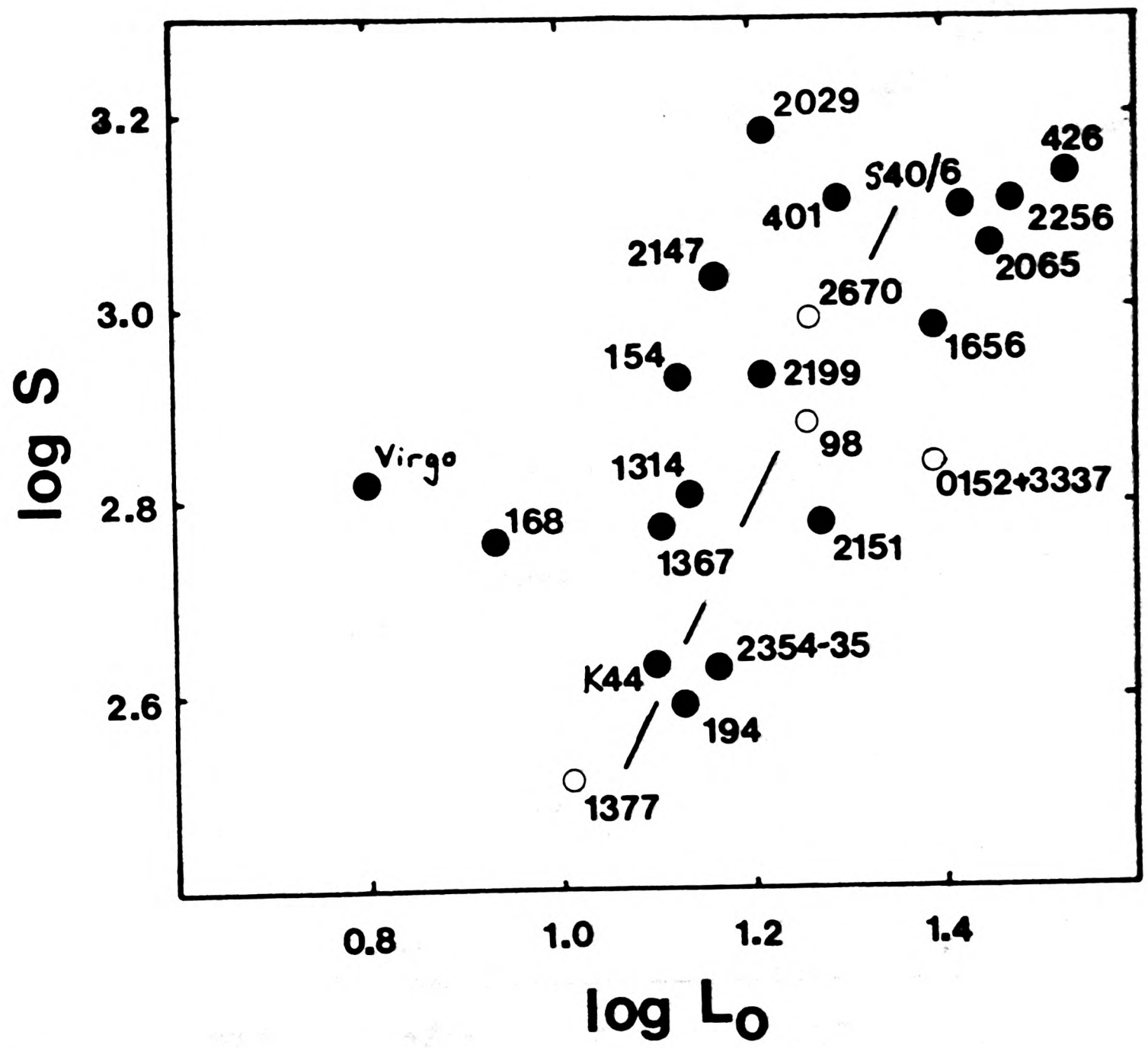

Fig. 9.4 Relation between velocity dispersion and optical luminosity

The straight line shows $S^2 \propto L$ Data from Table 9.1

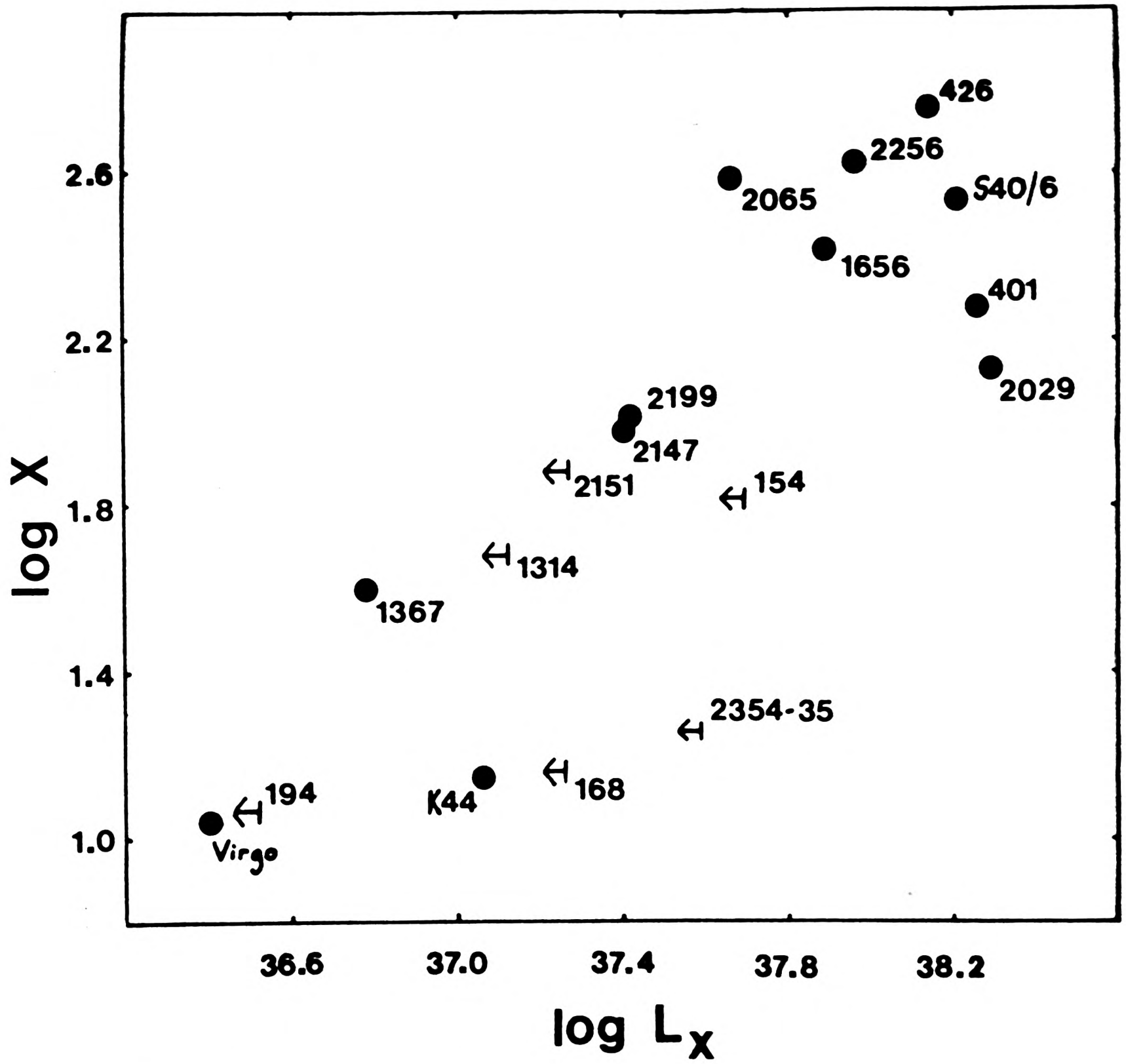

Fig 9.5 Relation between X and X-ray luminosity

X is defined in text

Data from Table 9.1

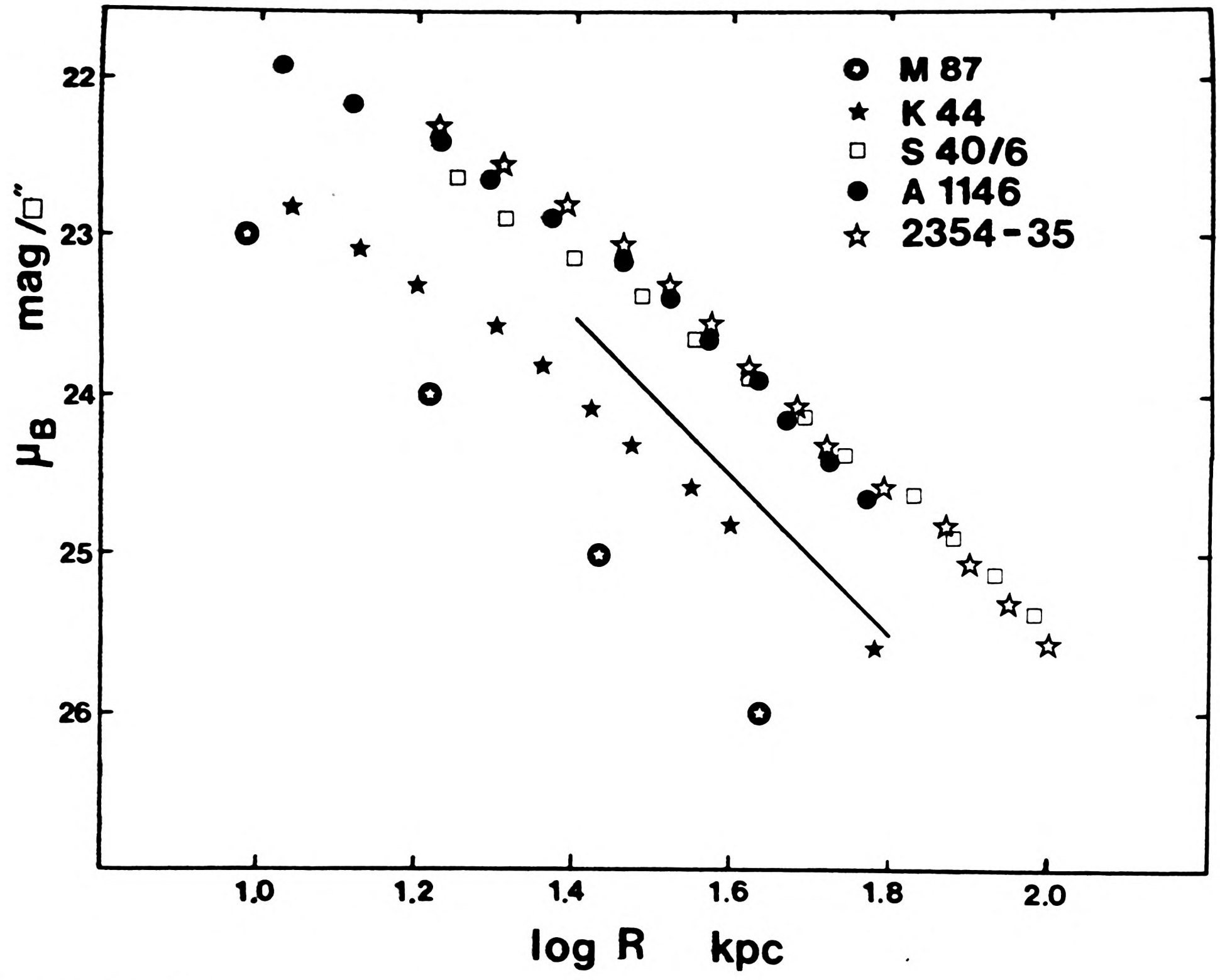

Fig. 9.6: Profiles of cD Galaxies

Data for M87 from Carter & Dixon (1978).

μ_B is rest frame surface brightness. Line shows $10^{-0.4\mu_B} \propto R^{-2}$

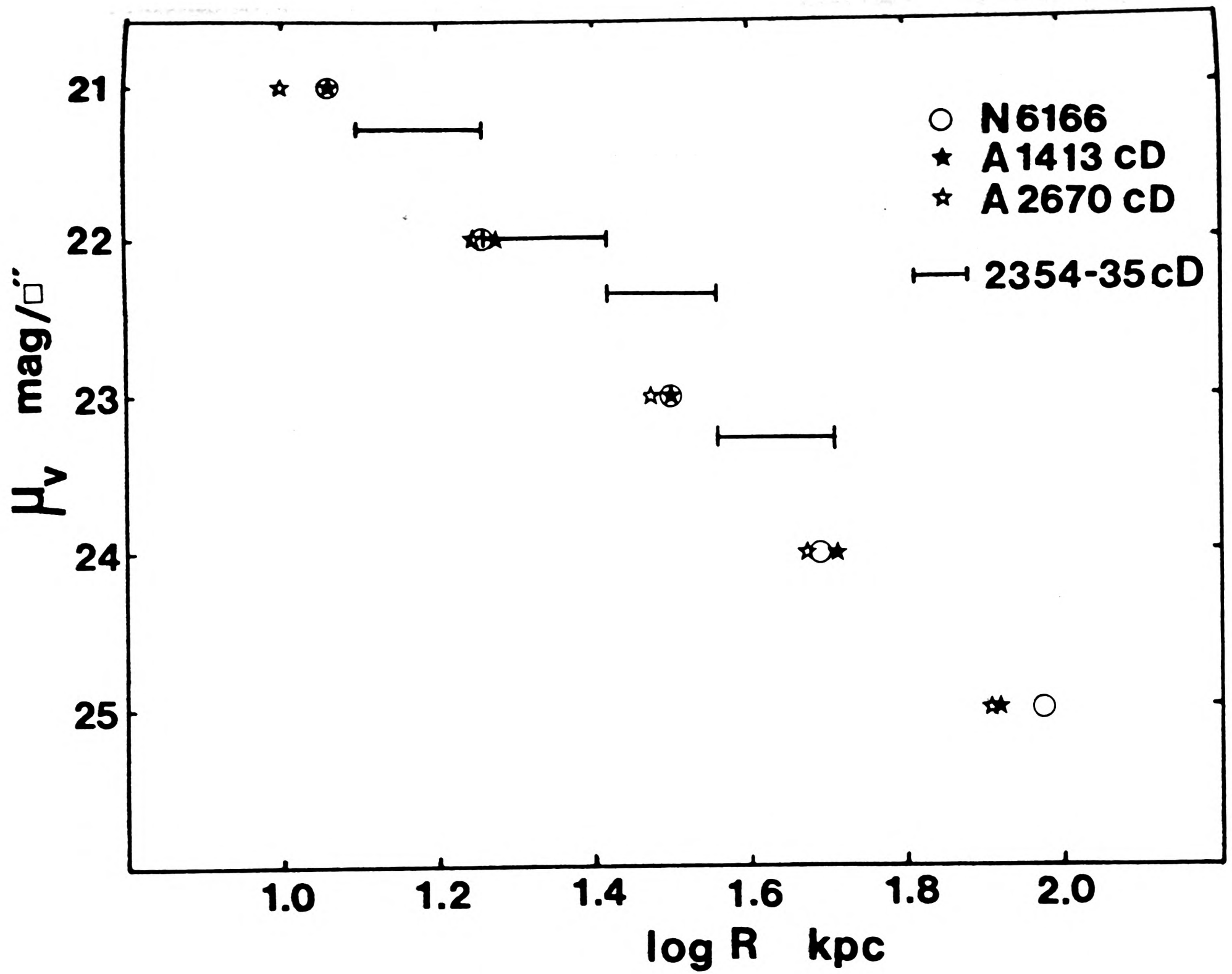

Fig. 9.7: Comparison with Oemler's Measurements

Data for N6166, A1413cD and A2670cD from Oemler (1976).
Data for 2354-35cD from App. V, shown as mean surface brightness in annuli.
μ_v is rest frame surface brightness.

Fig 9.8: Alignment of cD Galaxies with their Clusters

a) S40/6

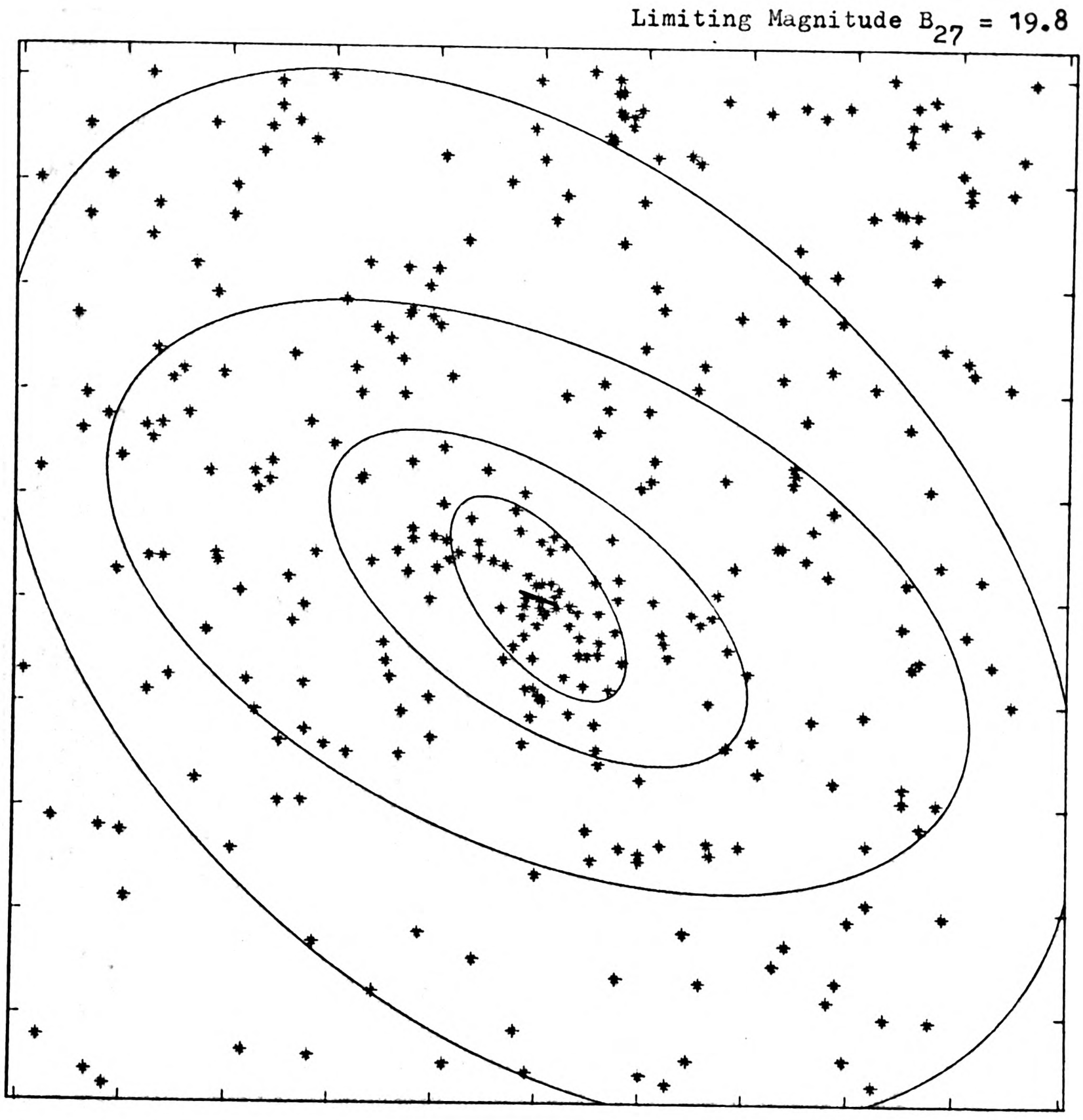

In this set of four diagrams the distribution of galaxies in the field of the clusters is shown and the orientation of the cD galaxy is indicated by a straight line at its position. Each ellipse has been constructed by iteration from a circle centred at the brightest galaxy. In each iteration the ellipticity of the distribution of galaxies within the ellipse is calculated (Trumpler & Weaver 1953) and a new ellipse constructed with that ellipticity, and the same area as the original circle. Eventually a stable solution is found in which the ellipse is consistent with the distribution of the galaxies which it contains.

b) <u>K44</u>

Limiting Magnitude B_{27} = 19.4

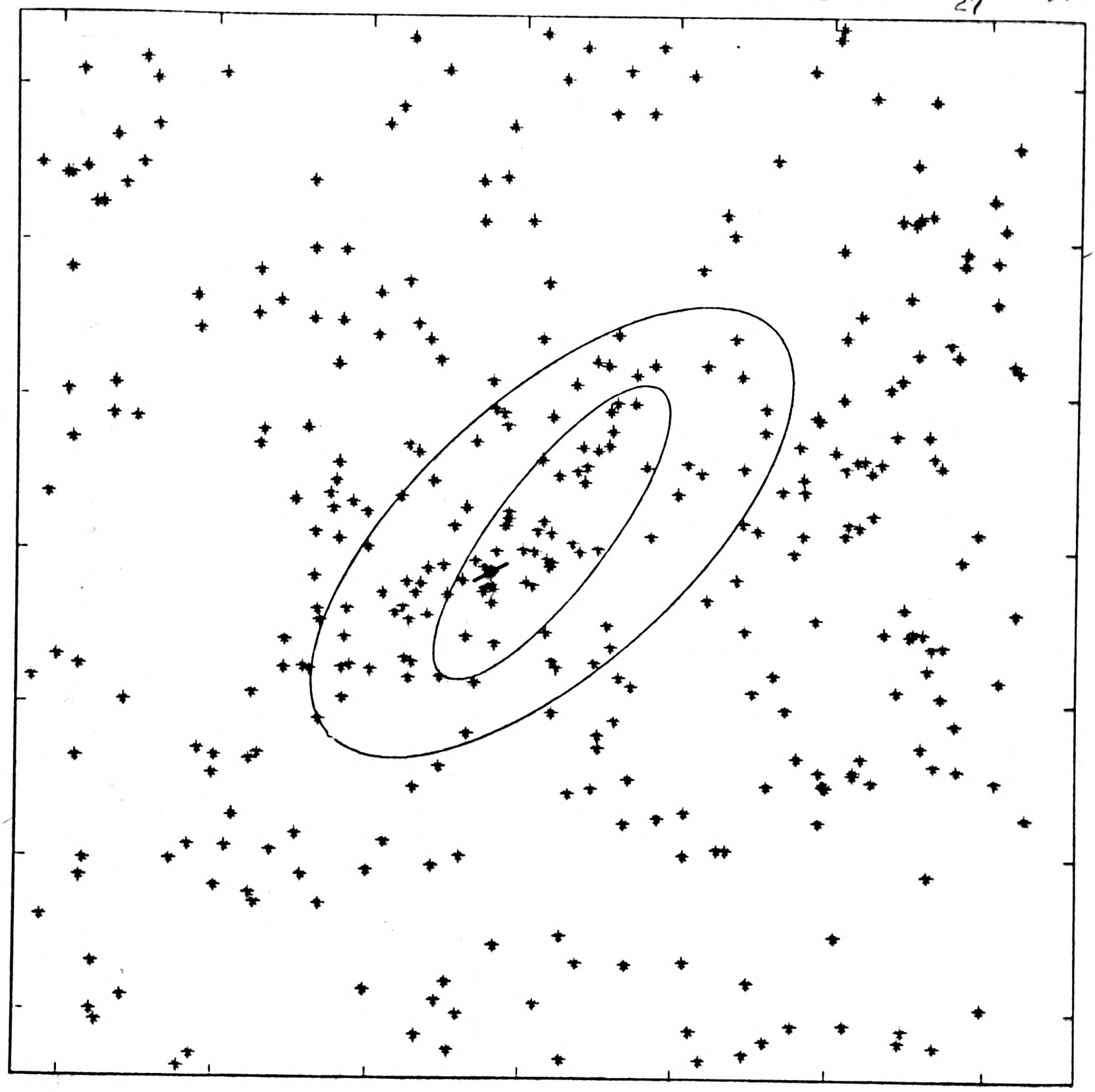

c) <u>2354-35</u>

Limiting Magnitude B_{27} = 20.0

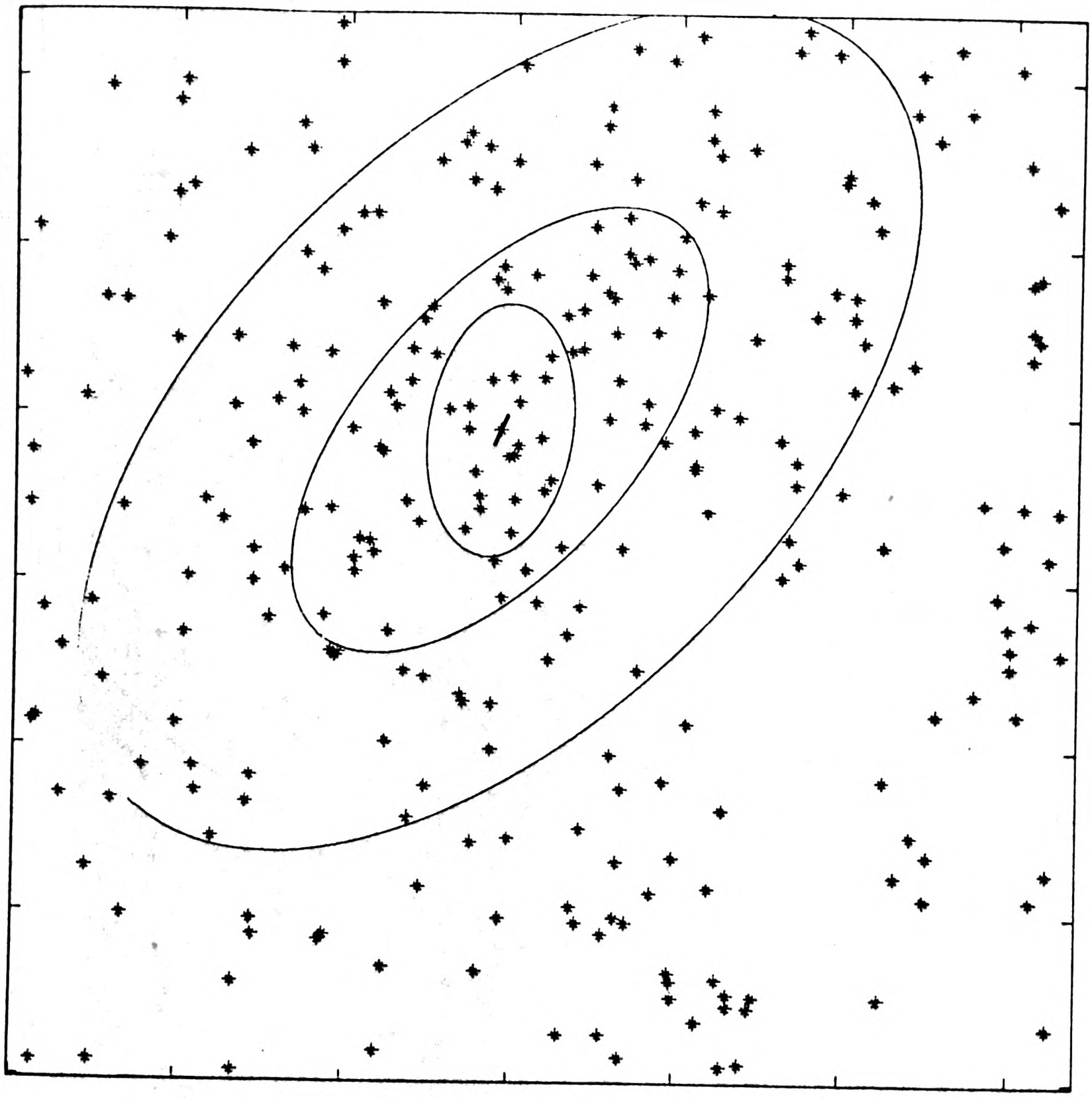

d) A1146

Limiting magnitude B_{27} = 22.0

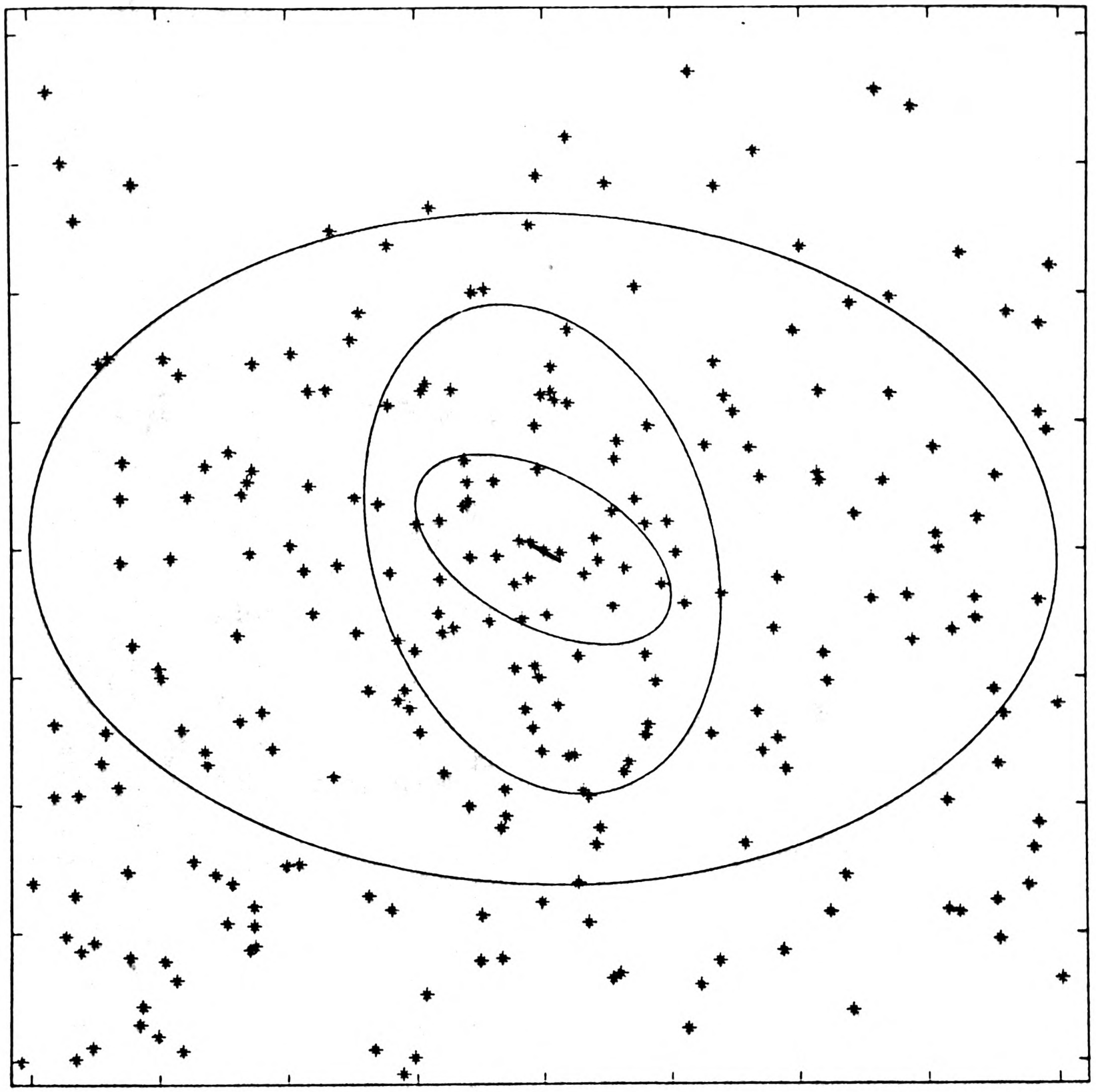

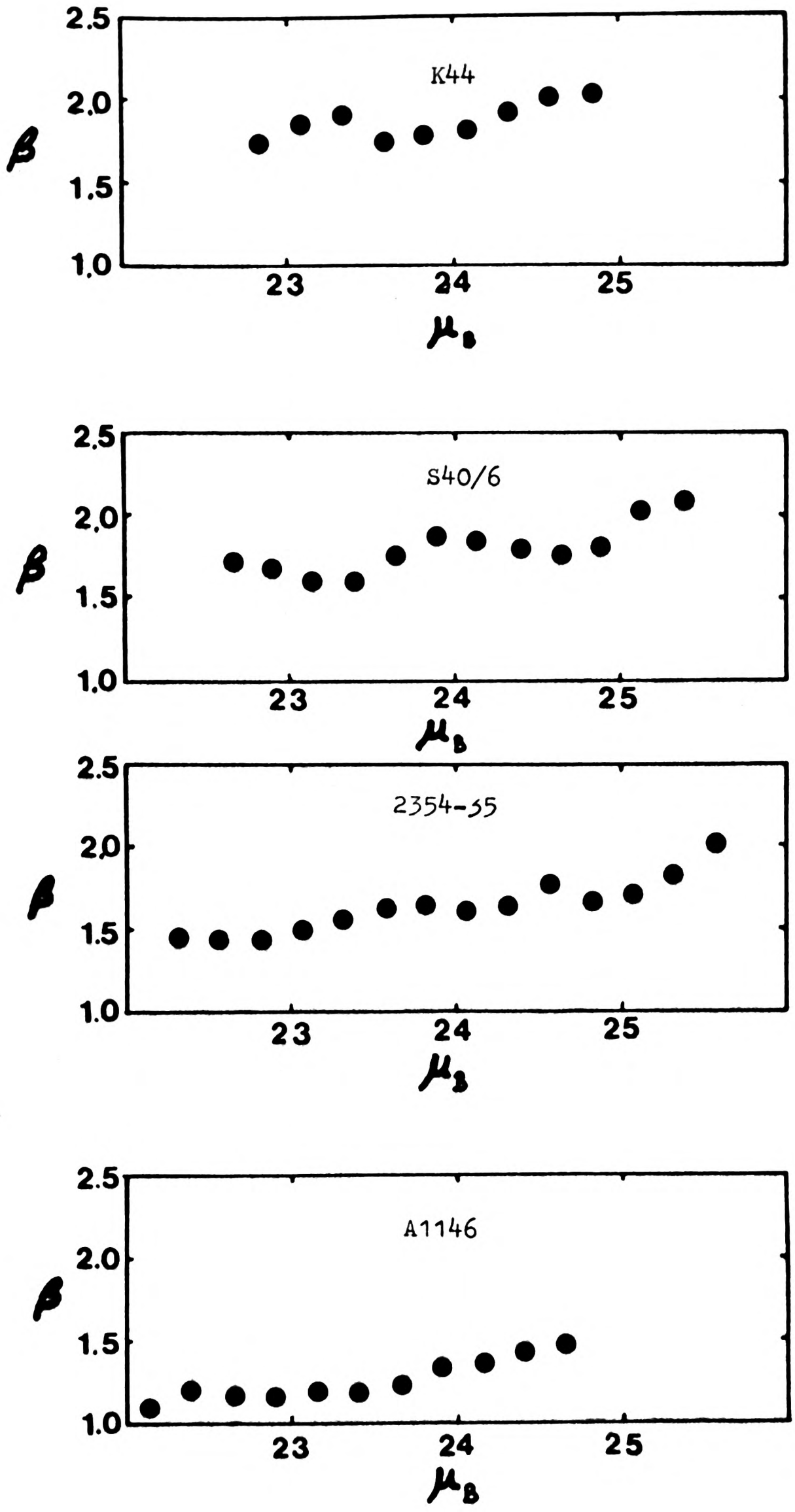

Fig. 9.9: Ellipticities of cD galaxies

β is the ratio of major to minor radii.

μ_B is the rest frame surface brightness (in mag/□").

Appendix I: Redshift Results

These tables show the results of the redshift observations. The columns are as follows:

Name: The numbering systems for clusters K44, A1146, S40/6 and 2354-35 are the same as used for the photographic photometry. IC and NGC numbers are shown where appropriate. Finding charts charts for the galaxies are in App. III.

Spectrum: The spectra, with details of their exposure times etc., are shown in App. II. Those taken in 1976 have a designation starting with a letter, and those in 1977 with a number.

cz: The velocities shown are v=cz, corrected to the heliocentric frame.

s.e.: The standard error is the "internal error" calculated from the disagreement between the individual velocities of the galaxy lines.

Error Class: The classes of external error are described in Chap. 4:

a=60-120km/s b=120-180km/s
c=180-240km/s d= possibility of gross error

Lines: The lines used in the redshift calculation are shown. Those visible, but not used, are omitted. OII = OII 3727Å (em.)

Other Sources: Results are reduced to heliocentric and do not include Sandage's (1978) 30km/s correction into the 21cm system.

The references are as follows:

S78: Sandage 1978
V75: Vidal 1975
M76: Martin 1976
W77: West 1977
CT78: Chincarini et al 1978
MS77: Melnick & Sargent 1977
WW69: Westerlund & Wall 1969
PK67: Perek & Kohoutek 1967

T72: Tritton 1972 W72: Whiteoak 1972

W53: Wilson 1953 M77: Maccacaro et al 1977

The results are arranged in the following tables:

a) S40/6 Velocities
b) A496 Velocities
c) 2354-35 Velocities
d) Velocities of objects near 2354-35
e) K44 Velocities
f) K2 Velocities
g) Pavo Group Velocities
h) Velocities of other galaxies
i) Velocities of Standards

S40/6 Velocities

Name	Spectrum	cz km/s	s.e. km/s	error class	Lines	Other Sources
1	6a	17907	53	b	H,K,G,Na,Hδ	V75: 18255
2	9b	15757	76	b	H,K,CaI,G,Mg, Ca+Fe,NaD,Hβ	
3	10b	16681	134	c	H,K,FeI,NaD	
7	10a	19703	79	b	H,K,G,MgI,NaD	
8	21a	17631	32	b	H,K,G,MgI	
9	15a	16363	113	c	H,K,CaI,G, MgI,NaD	
12	18a	14258	62	b	H,K,G,MgI	
13	15b	14426	82	c	H,K,Hδ,Hσ,OII	
	21c	14686	10	c	H,OII	
15	6b	12825	64	d	Hα (em)	
16	24b	17407	234	d	H,K	
25	21b	18599	112	c	H,K,G,MgI,NaD	

A496 Velocities

Name	Spectrum	cz km/s	s.e. km/s	error class	Lines	Other Sources
1	αc	9743	37	b	H,K,FeI,NaD	MS77: 9900
7	23b	9619	63	b	H,K,G,FeI, Hδ,Hβ,NaD	
8	24a	9733	124	c	H,K,G,FeI,Mg, Ca+Fe,Hβ	

2354-35 Velocities

Name	Spectrum	cz km/s	s.e. km/s	error class	Lines	Other Sources
1	Va	14596	70	b	H,K,G,OII	W72: 14594
2	Vb	12568	75	b	H,K,G,FeI,NaD	
3	Vc	14475	102	b	H,K,CaI	
4	Za	14609	32	b	H,K,G	
5	9a	14827	32	b	H,K,G,FeI,MgI	
6	Zb	16498	152	c	H,K,CaI,NaD	
	17b	16241	90	b	H,K,G	
8	γb	14751	167	c	H,K,G,NaD	
10	γc	14953	104	b	H,K,CaI,G	
	22a	14870	71	b	H,K,G,NaD	
12	δa	14056	41	b	H,K,Hδ	
	8b	14084	123	b	H,K,G,FeI,NaD	
13	17a	15509	39	b	H,K,G,MgI,NaD	
X	Wa	13886	43	b	H,K,G,NaD	

Velocities of objects near 2354-35

Name	Spectrum	cz km/s	s.e. km/s	error class	Lines	Other Sources
2355-35	Na	14429	63	b	H,K	
0001-36	Nb	13897	134	c	H,K,G,NaD	
2349-35	Rc	17245	117	c	H,K	
2347-36g1	αb	12774	78	b	H,K,NaD	
2347-36g2	δb	12871	64	b	H,K,NaD	
0007-36	αa	36757	97	d	H,K,FeI,NaD,Hβ	
	22b	33991	173	c/d	H,K,Hδ,Hβ	
0003-35	14b	34152	69	d	H,K,G	
0003-36g1	20a/b	8422	67	b	H,K,G,NaD,OII	
0003-36g2	23a	8619	49	b	H,K,CaI,FeI,NaD,Hδ	

K44 Velocities

Name	Spectrum	cz km/s	s.e. km/s	error class	Lines	Other Sources
1=I5353	Ja	7945	150	c	H,K	CT78: 7990 M77: 8304
2=I5358	Jc	8561	57	b	H,K	CT78: 8554 M77: 8334
3	Jb	8147	90	b	H,K	CT78: 7972 M77: 7945
4	Mb/Mc	10102	41	a	H,K,G	CT78: 10091
5=I5354	Eb	8355	76	b	H,K,MgI,NaD	CT78: 8116 M77: 8214
6=I5350	4a	8407	111	c	H,K,CaI,G, FeI,MgI	CT78: 8424
7	Ra	8259	37	b	H,K	CT78: 8353
8	Ma 14a	8050 7880	77 42	b b	H,K H,K,NaD	CT78: 8660
10	Rb	9981	93	b	H,K,G	CT78: 10095
11	Ya	8958	21	b	H,K	CT78: 8923
19	5a	8626	217	d	H,K,Ca+Fe	
22	13b	10396	70	b	H,K,G	
24	13a	9013	66	b	H,K,G,NaD,Hβ	

K2 Velocities

Name	Spectrum	cz km/s	s.e km/s	error class	Lines	Other Sources
9	Oc	5941	63	b	H,K,G	
10	Ob	5721	56	b	H,K,G,NaD	
14	Oa	6729	41	b	H,K,G,MgI,NaD	
19	δc	7083	83	b	H,K,NaD	
20	ϵa	6805	89	b	H,K,NaD	
21	ϵb	6994	41	b	H,K,Mg	

Pavo Group Velocities

Name	Spectrum	cz km/s	s.e km/s	error class	Lines	Other Sources
I4960	Ub	3439	103	b	H,K,G	S78: 3489
I4967	Ua	3755	26	a	H,K,G	S78: 4123
I4970	Xc	4759	49	a	H,K,CaI	S78: 4725
N6872	Tb	4626	56	a	H,K,G,FeI, MgI,NaD	V75: 4850 S78: 4707 WW69: 4690 M76: 4840
X	Xb	3778	24	a	H,K,G,NaD, Hδ	
I4972	δa	3635	20	b	H,NaD	
N6876	Da	3928	36	a	H,K	V75: 3920 S78: 3969 WW69: 3720
N6877	Lb	4158	35	a	H,K	V75: 4010 S78: 4142
N6880	Lc	3987	36	a	H,K,G,MgI, NaD,OII	S78: 3939
I4985	Xa	4442	35	a	H,K,G,MgI, NaD,OII	

Other Velocities of Galaxies

Name	Spectrum	cz km/s	s.e. km/s	error class	Lines	Other Sources
N6769	Ca	3686	48	a	H,K,G	M76: 3820 RCBG1: 3530 W77: 3920 S78: 3913
N6770	Ha	3826	54	a	H,K,G,OII	M76: 3910
	Hb	3883	43	a	H,K,OII	RCBG1: 3630 W77: 3950 S78: 3833
N6810	Ta	2066	68	b	H,K,OII	M76: 2025 RCBG1: 1823
2040-26	Qa	12222	92	b	H,K,NaD	T72: 12090
S149/5	7a	22342	77	b	H,K,G	
S149/10	8a	23090	80	b	H,K,G,NaD	

Velocities of Standards

Name	Spectrum	cz km/s	s.e. km/s	error class	Lines	Other Sources
N6818 (plan.)	La	7	36		emission spectrum	PK67: 17
HD 157457	Ba	4	27		H,K,G	W53: 18
	Gd	-42	167		H,K,G	M76: 5
HD 16815	Fb	-195	14		H,K,G	W53: -9 M76: -99

Appendix II: Spectroscopic Plates

1976 Plates

Date 1976	SAAO Plate	Spectrum Ref.	Object	Exposure mins.	Comments
Aug. 23/24	1315	Ba	HD157457	0.25	Best
		b	"	0.50	
		c	"	1	
		d	"	2	
	1316	Ca	N6769	40	Overexposed
	1317	Da	N6876 (Pavo)	40	"
	1318	Ea	K44g1 = I5353	60	Unmeasurable
		b	K44g5 = I5354	55	Overexposed
	1319	Fa	HD16815	0.25	
		b	"	0.50	Best
		c	"	1	
		d	"	2	
		e	"	3	
Aug. 24/25	1320	Ga	~~HD~~157457	0.25	
		b	"	0.50	
		c	"	1	
		d	"	2	Best
	1321	Ha	N6770	20	Interrupted: telescope failure
		b	"	20	
	1322	Ia	N6818 (plan.)	1	
		b	"	2	
		c	"	4	
		d	"	6	

App II (cont)

Date 1976	SAAO Plate	Spectrum Ref.	Object	Exposure mins.	Comments
	1323	Ja	K44g1 = I5353	45	Unusable: ITS fault
		b	K44g3	45	
		c	K44g2 = I5358	45	
	1324	Ka	2354-35g10	45	Unusable
		b	A496g1	27	Dekker fault
Aug. 25/26	1325	La	N6818 (plan.)	5	
		b	N6877 (Pavo)	15	
		c	N6880 (Pavo)	20	
	1326	Ma	K44g8	25	
		b	K44g4	10	Curtailed, but usable
		c	"	30	
	1327	Na	2355-35	40	
		b	0001-36	45	
	1328	Oa	K2g14	25	
		b	K2g10	35	
		c	K2g9	15	
Aug. 26/27	1329	Pa	HD157457	0.50	cirrus
		b	"	1	"
	1330	Qa	2040-26	40	"
		b	K44g6 = I5350	35	"

App II (cont)

Date 1976	SAAO Plate	Spectrum Ref.	Object	Exposure mins.	Comments
	1331	Ra	K44g7	27	cirrus
		b	K44g10	25	"
		c	2349-35	30	"
	1332	Sa	K2g4	35	poor seeing
Aug. 27/28	1333	Ta	N6810	15	
		b	N4872 (Pavo)	15	
	1334	Ua	I4967 (Pavo)	25	
		b	I4960 (Pavo)	20	
		c	K44g11	23	) double exposure:
		d	K44g15	40	) both unmeasurable
	1335	Va	2354-35g1	40	
		b	2354-35g2	40	
		c	2354-35g3	40	
	1336	Wa	2354-35gX	40	
		b	HD16815	0.75	
Aug. 28/29	1337	Xa	I4985 (Pavo)	25	bright moon
		b	Pavo gX	20	
		c	I4970 (Pavo)	15	
	1338	Ya	K44g11	20	
	1339	Za	2354-35g4	35	
		b	2354-35g6	40	

App II (cont)

Date 1976	SAAO Plate	Spectrum Ref.	Object	Exposure mins.	Comments
	1340	κa	0007-36	45	
		b	2347-36g1	25	
		c	A496g1	25	
Aug. 29/30	1341	βa	N6818 (plan.)	20	
	1342	γa	I4972 (Pavo)	25	
		b	2354-35g8	35	
		c	2354-35g10	35	
	1343	δa	2354-35g12	35	
		b	2347-36g2	30	
		c	K2g19	30	
	1344	εa	K2g20	30	
		b	K2g21	30	

App II (cont)

1977 Plates

Date 1977	SAAO Plate	Spectrum Ref.	Object	Exposure mins.	Comments
Oct. 11/12	1558	3a	N6876 (Pavo)	20	Fault: unusable
	1559	4a	K44g6 = I5350	40	
	1560	5a	K44g19	60	
	1561	6a	S40/6g1	60	
		b	S40/6g15	70	
Oct. 12/13	1562	7a	S149/5	70	
Oct. 13/14	1563	8a	S149/10	80	
		b	2354-35g12	80	
	1564	9a	2354-35g5	70	
		b	S40/6g2	50	
	1565	10a	S40/6g7	55	
		b	S40/6g3	45	
Oct. 14/15	1566	13a	K44g24	50	
		b	K44g22	50	
	1577	14a	K44g8	35	
		b	0003-35	100	
	1578	15a	S40/6g9	50	
		b	S40/6g13	80	

App II (cont)

Date 1977	SAAO Plate	Spectrum Ref.	Object	Exposure mins.	Comments
	1579	16a	HD16815	0.5	
		b	"	1	
		c	"	2	
Oct. 15/16	1580	17a	2354-35g13	55	
		b	2354-35g6	65	
	1581	18a	S40/6g12	15	
Oct. 16/17	1582	19a	2354-35g21	5	terminated by cloud
		b	"	75	
	1583	20a	0003-36g1	25	moon & terminated by cloud
			"	40	
	1584	21a	S40/6g8	45	
		b	S40/6g25	60	
		c	S40/6g13	20	terminated by dawn
Oct. 17/18	1585	22a	2354-35g9	35	
		b	0007-36	75	
	1586	23a	0003-36g2	30	interrupted by cloud
		b	A496g7	35	
	1587	24a	A496g8	35	
		b	S40/6g16	35	terminated by dawn

Appendix III: Finding Charts

Maps of the clusters K44, S40/6, A1146 and 2354-35 are given in App.IV. Finding charts of the other clusters mentioned in the text are given below; descriptions of these clusters may be found in Chap.8.

The positions of stars are marked by crosses and of galaxies by circles. Coordinates on the charts are the 1950.0 RA and dec. of SAO stars. The orientation is normal, i.e. North up and East left, but may not be exact.

The charts are as follows:

Fig.	Cluster	Fig.	Cluster
AIII.1	2349-35	AIII.7	2143-58
AIII.2	2355-35	AIII.8	2151-58
AIII.3	2347-36	AIII.9	K2
AIII.4	0001-36	AIII.10	A496
AIII.5	0003-35	AIII.11	Pavo
AIII.6	0007-36		

Where only one galaxy is shown, it is this galaxy of which the redshift has been measured.

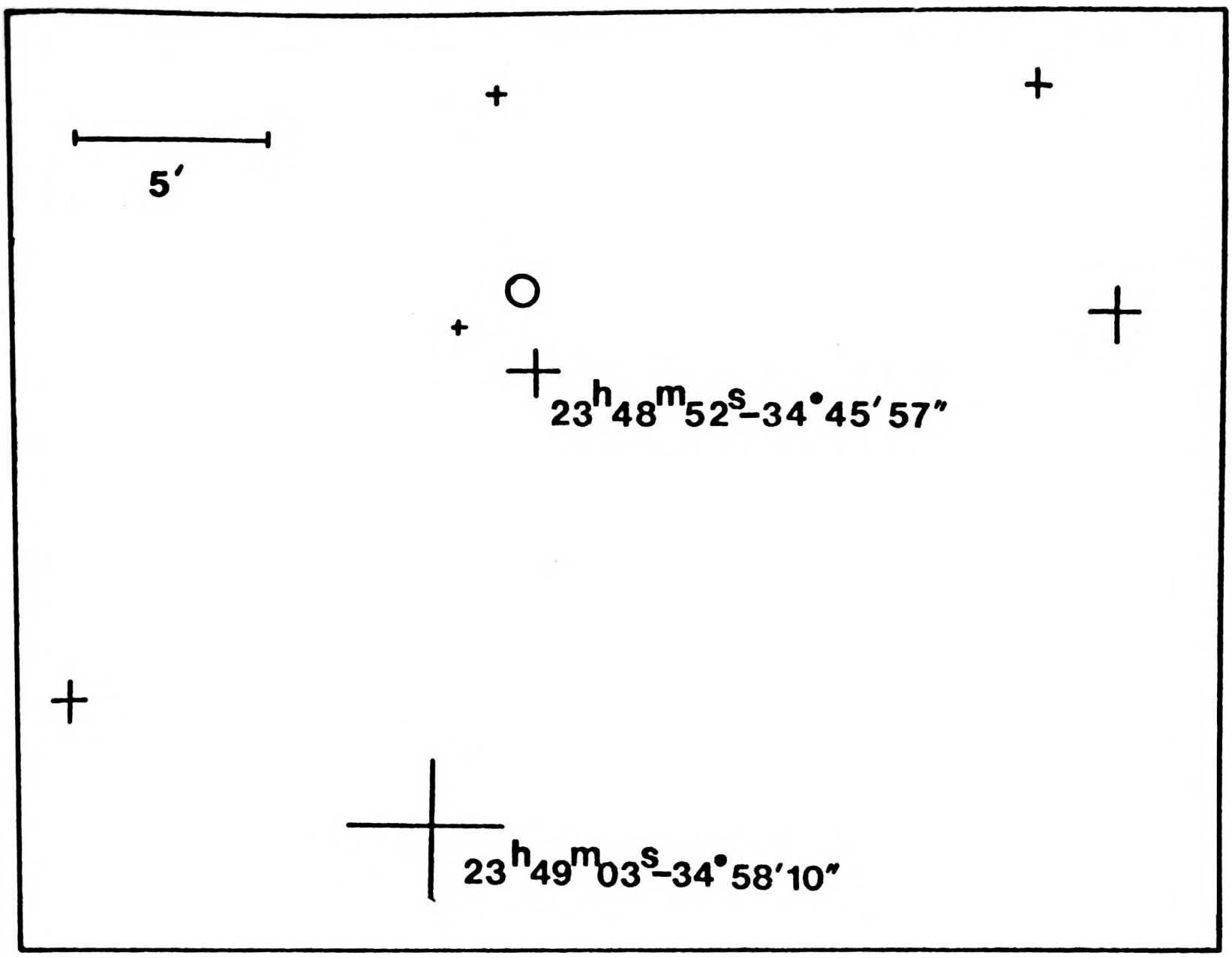

Fig. AIII.1: 2349-35

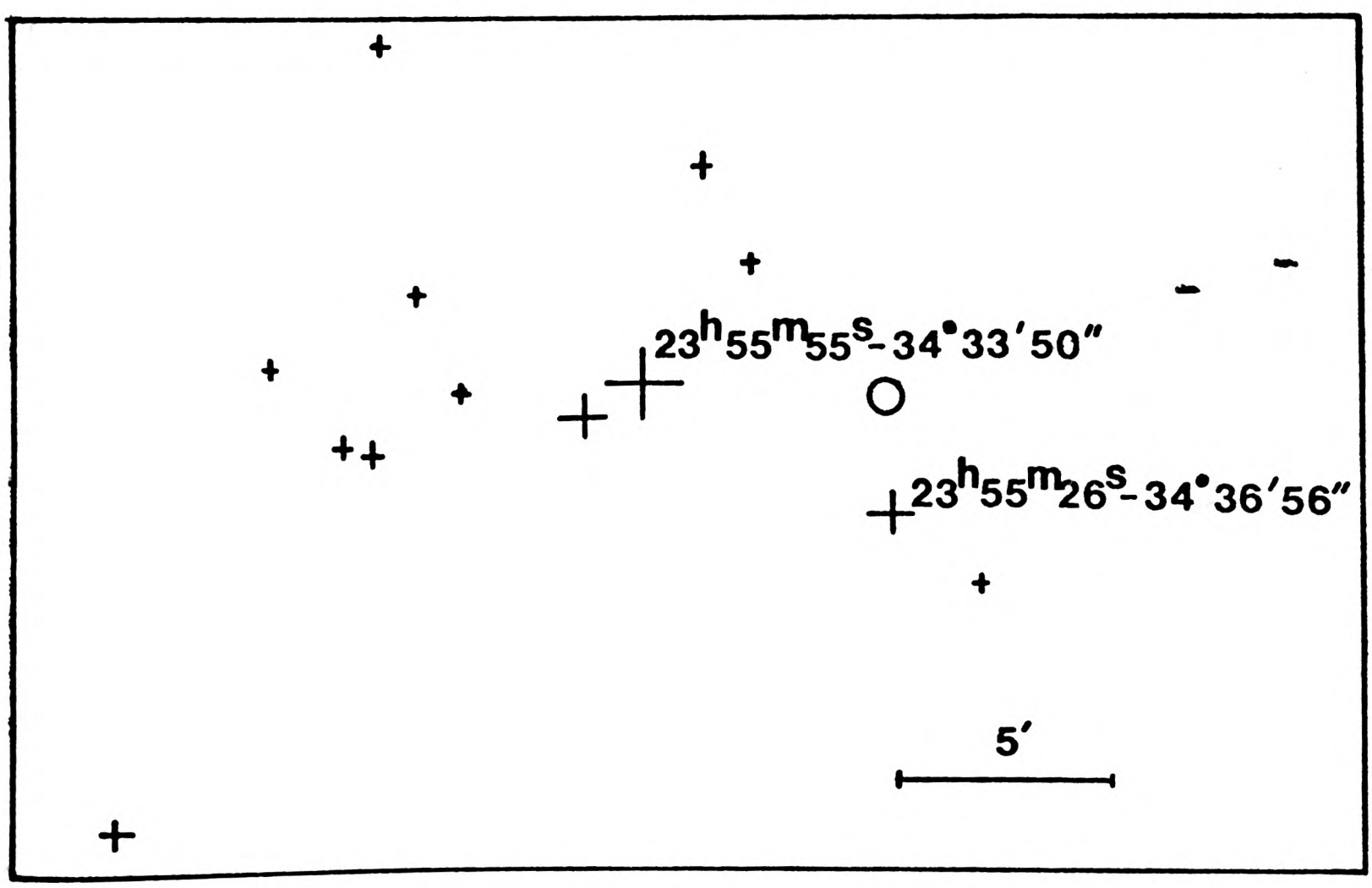

Fig. AIII.2: 2355-35

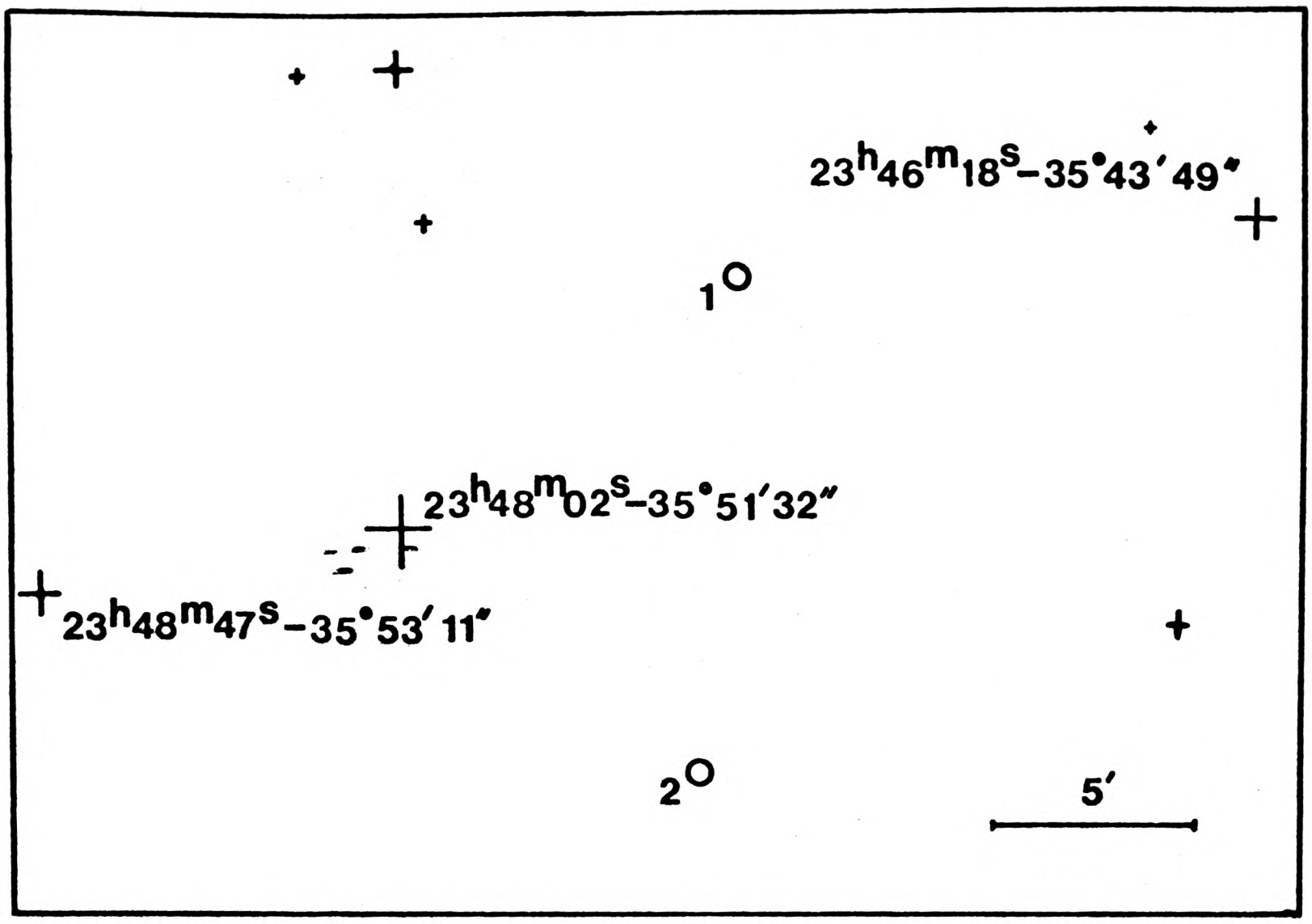

Fig. AIII.3: 2347-36

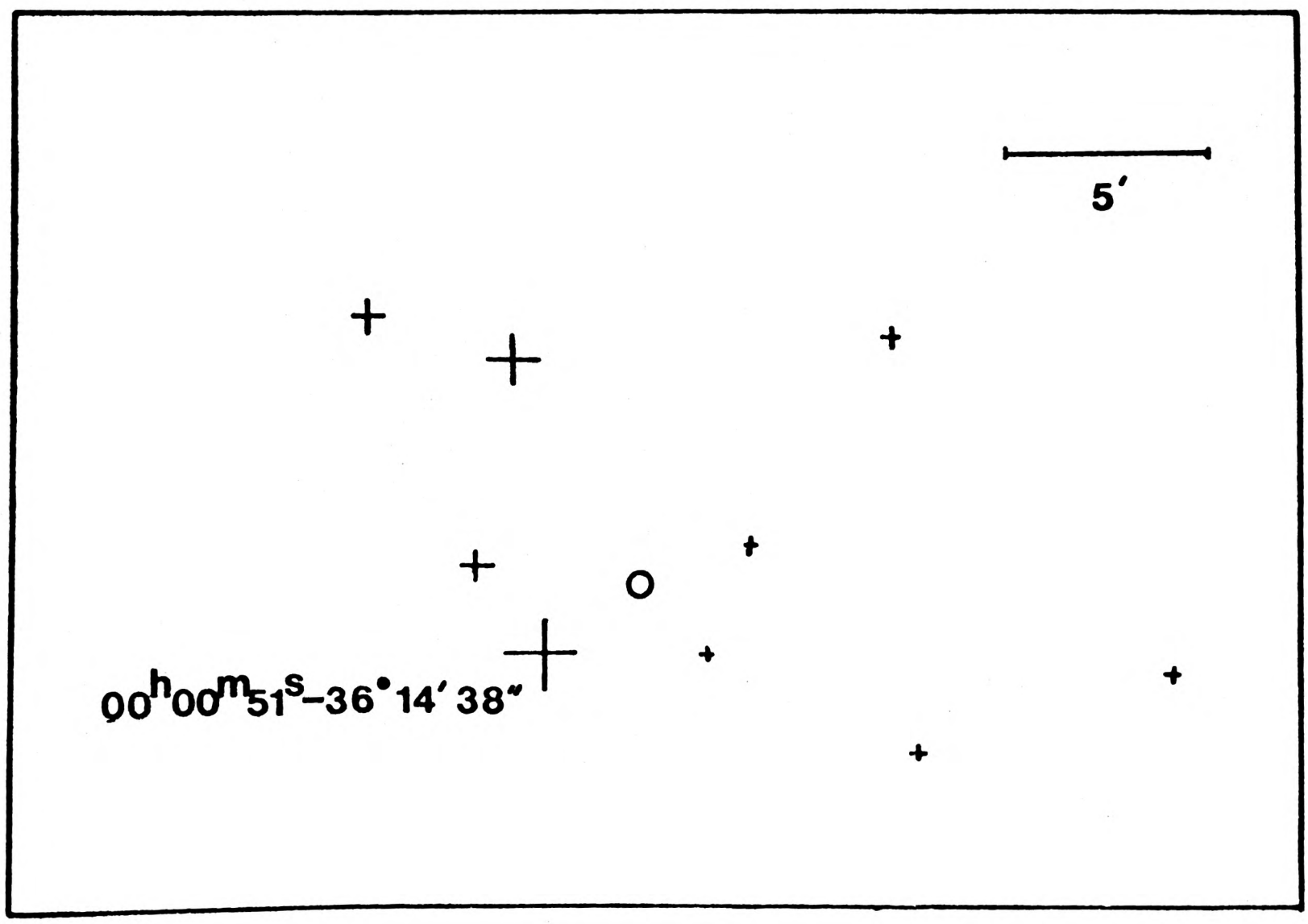

Fig. AIII.4 0001-36

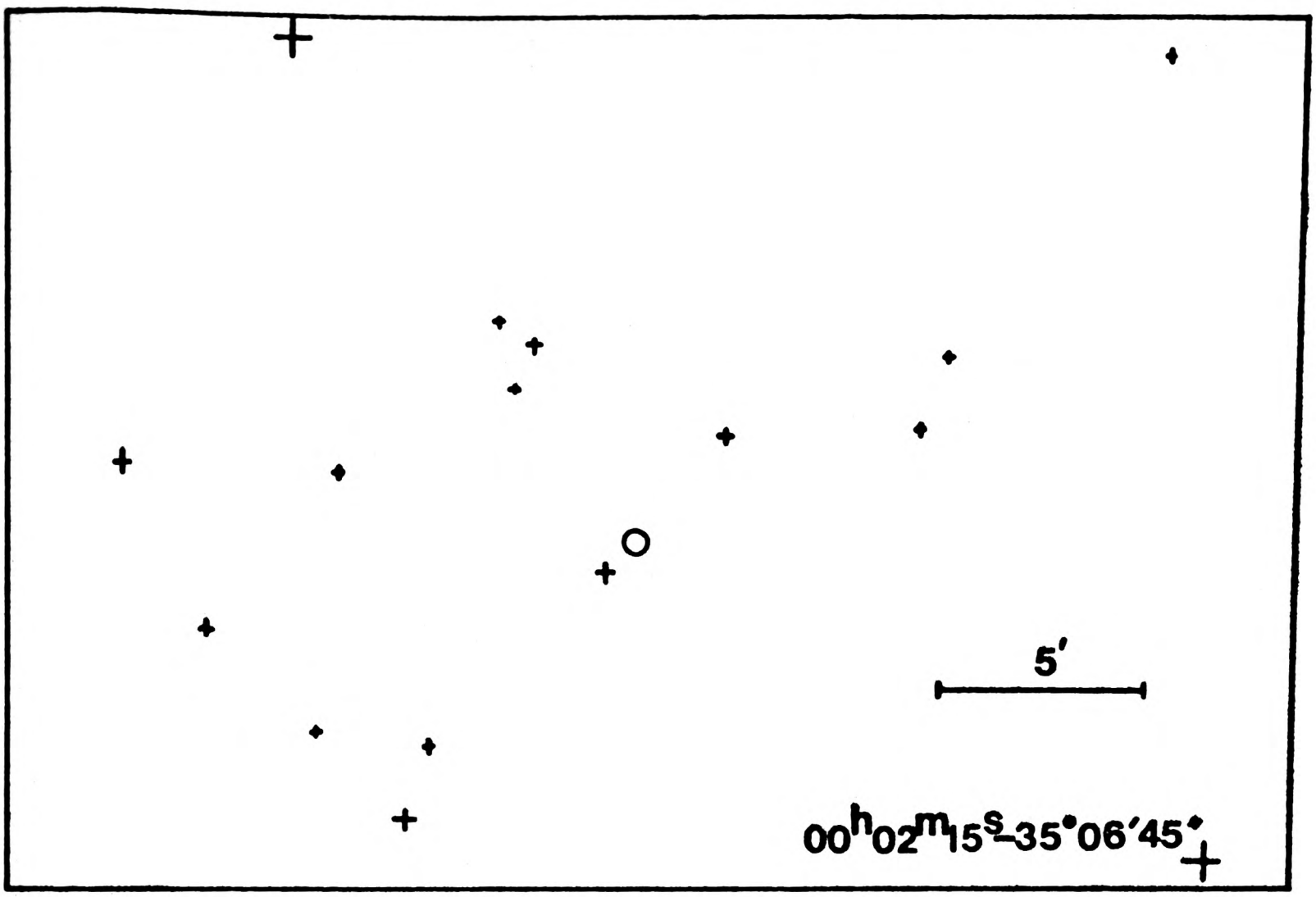

Fig. AIII.5: 0003-35

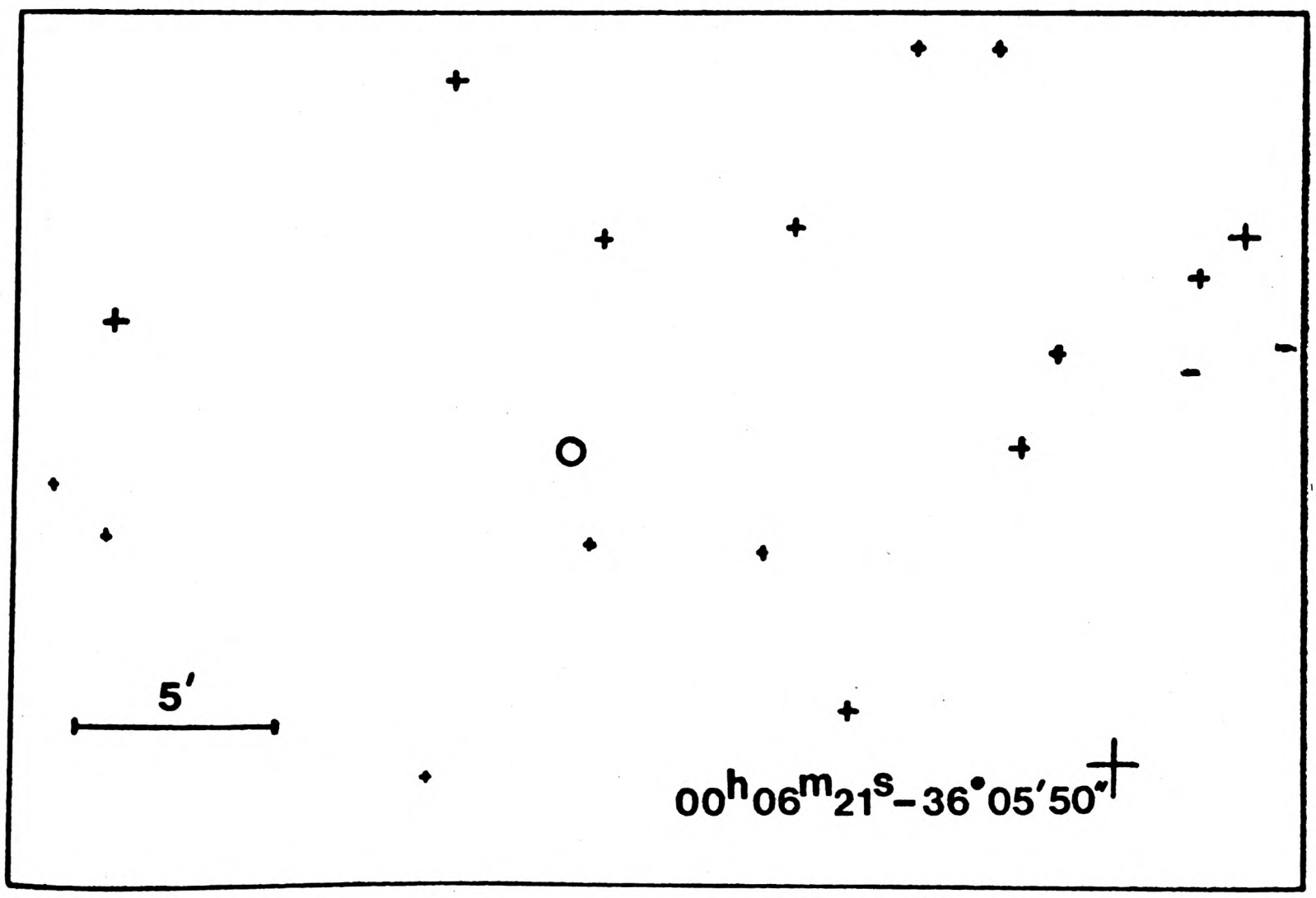

Fig. AIII.6: 0007-36

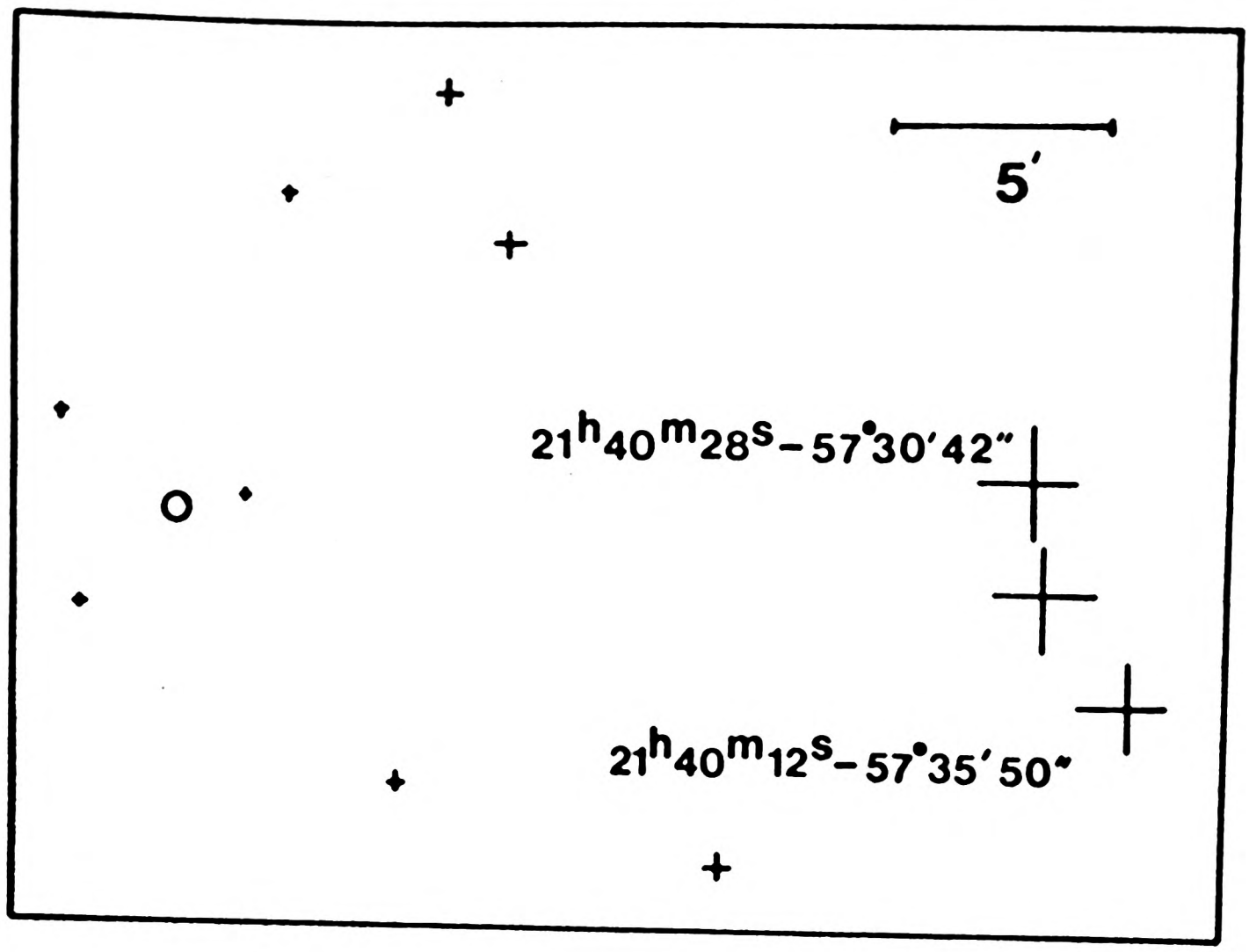

Fig. AIII.7: S149/5

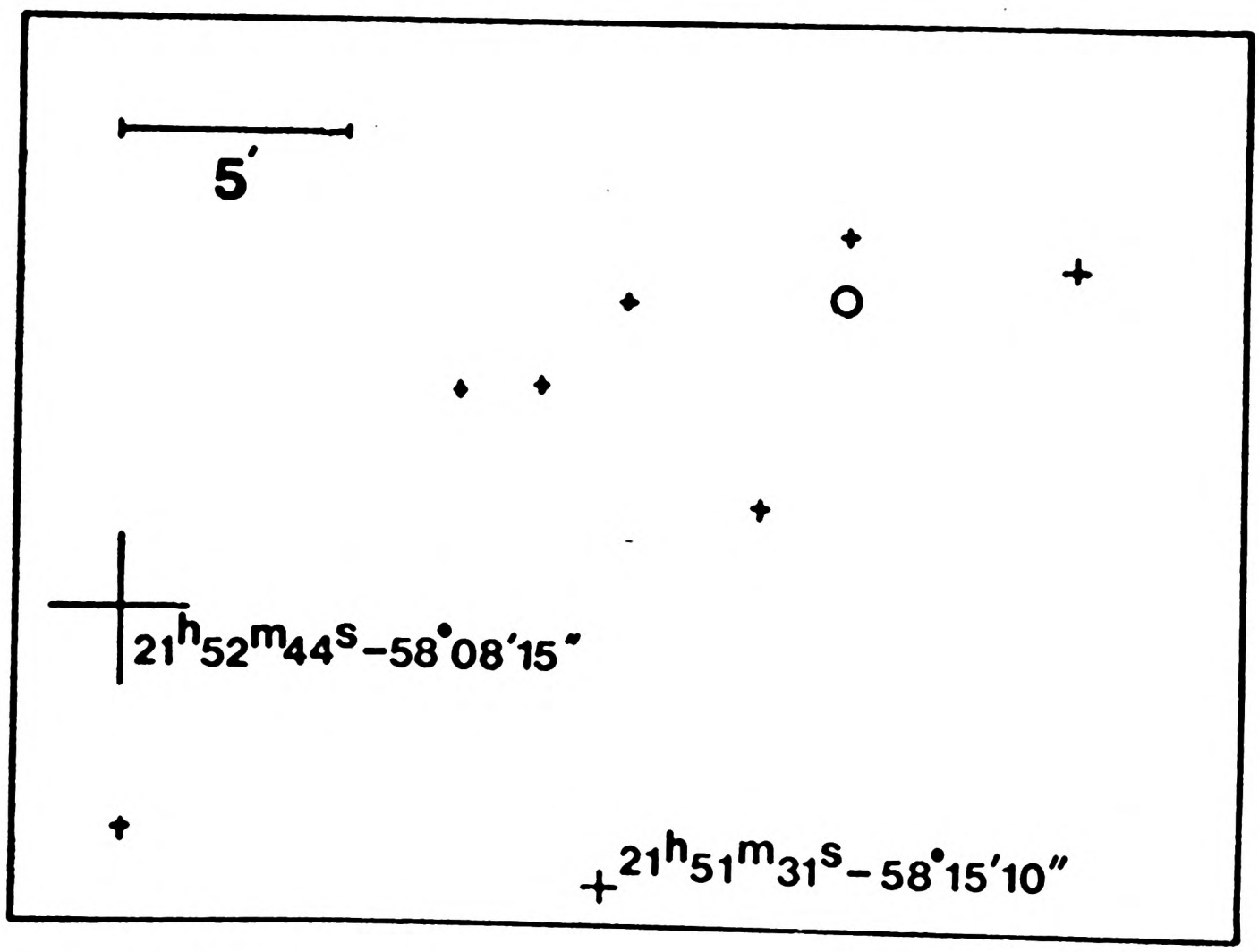

Fig. AIII.8: S149/10

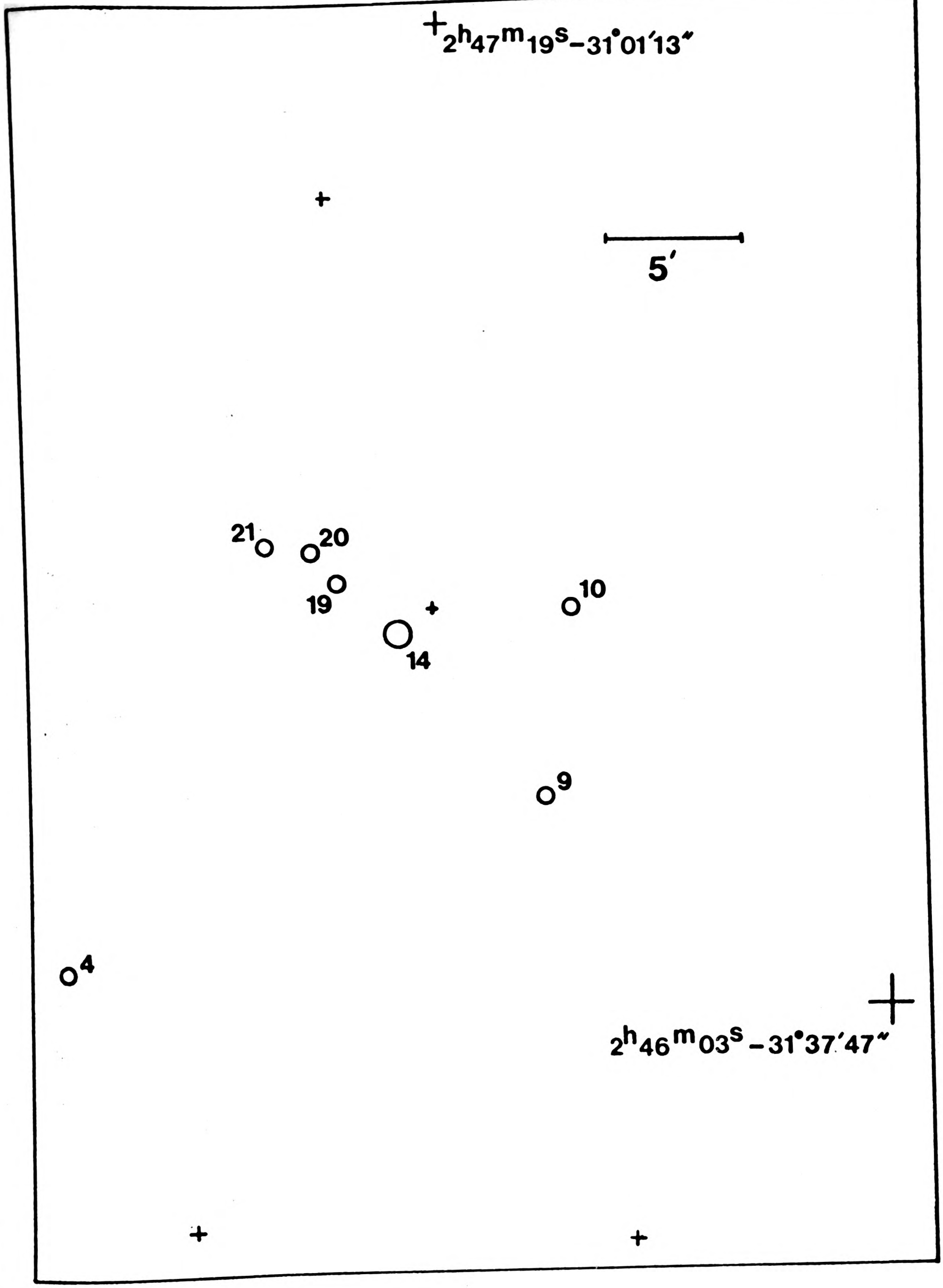

Fig. AIII.9: K2

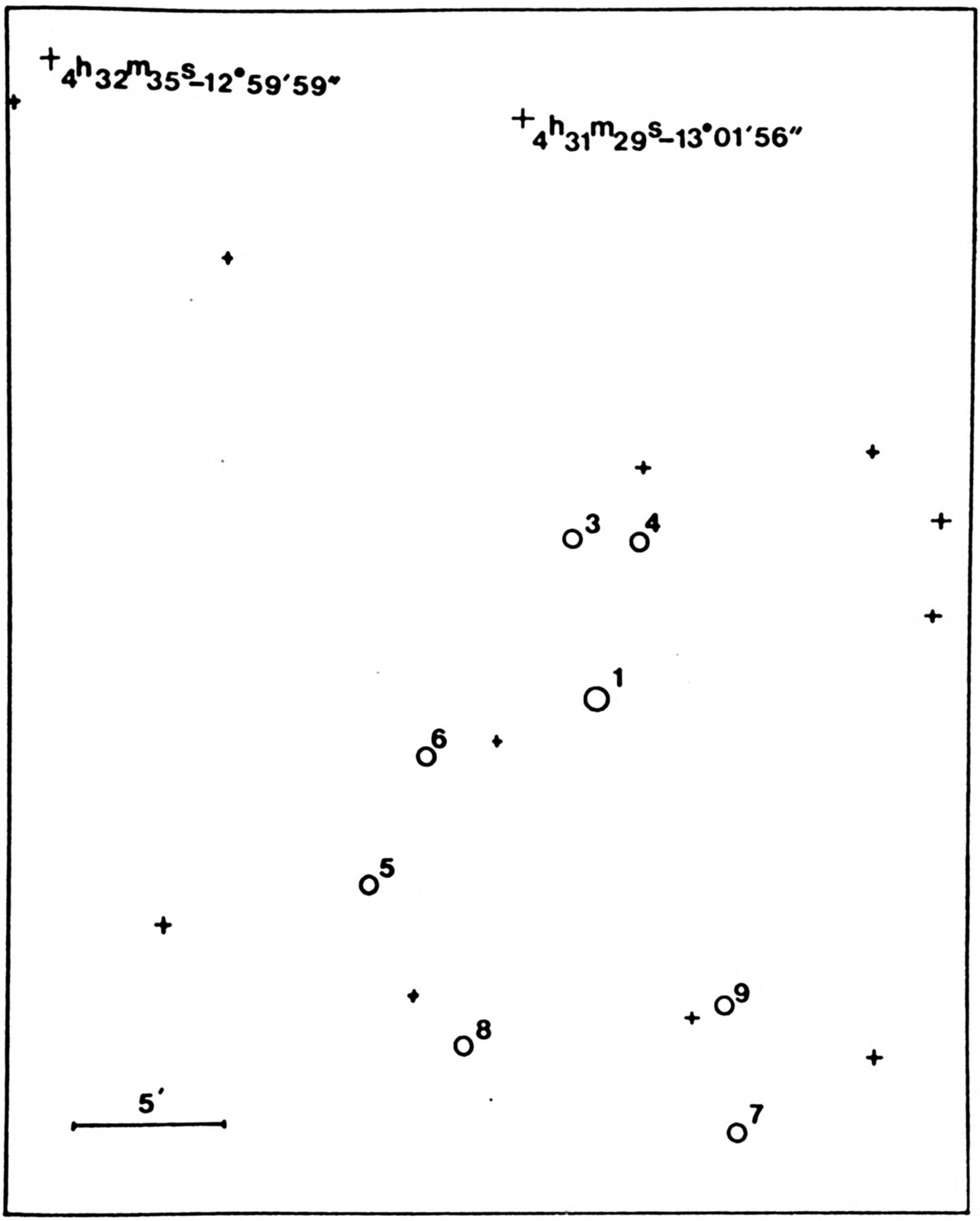

Fig. AIII.10: A496

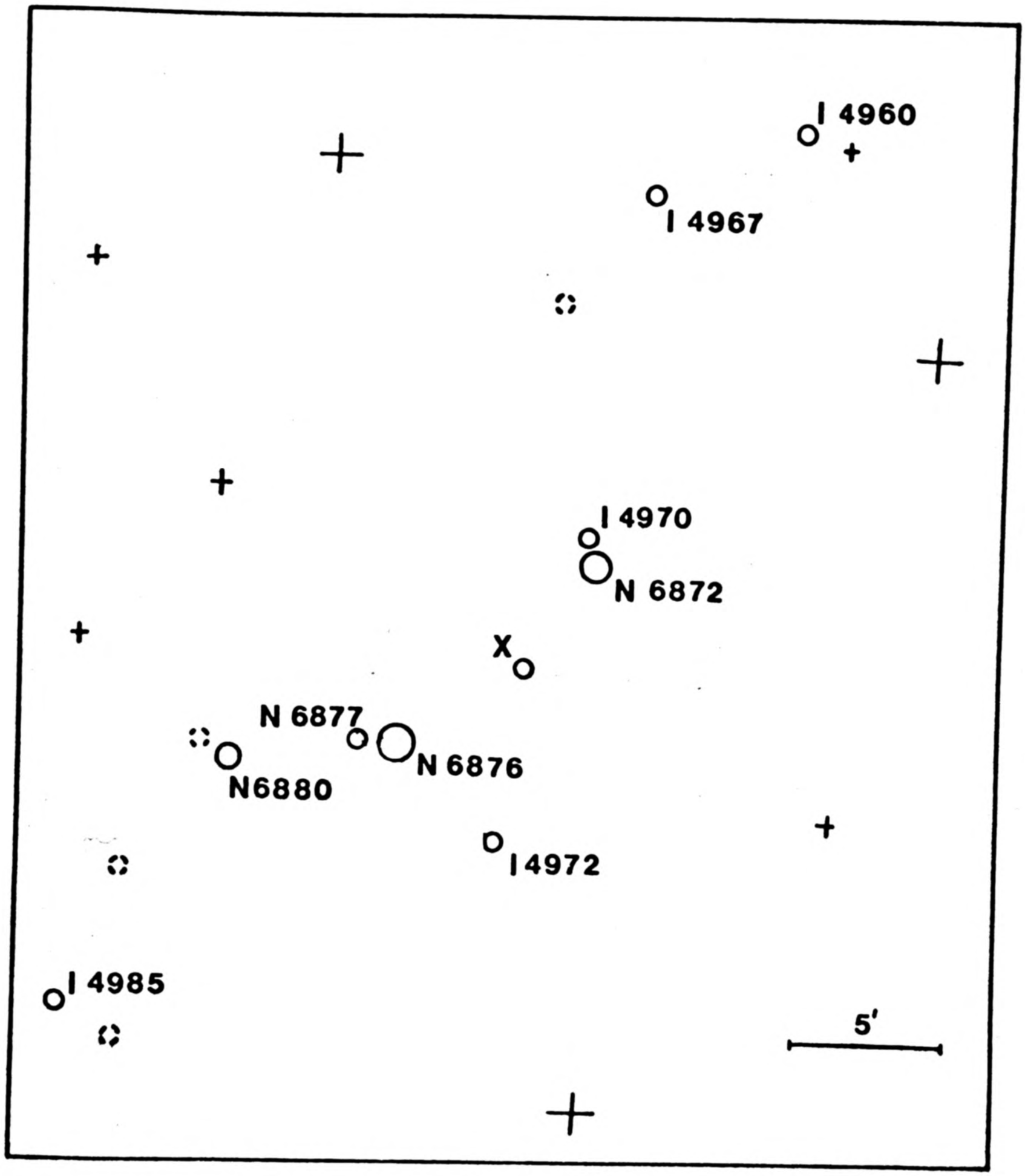

Fig AIII.11: Pavo

Appendix IV: Results of Photographic Photometry

This appendix presents the results of the photographic photometry of 4 clusters: K44, S40/6, A1146 and 2354-35. The magnitudes in A1146 are from Carter & Godwin (1979), and in 2354-35 from Bucknell (1977). For each cluster, a table of magnitudes and a map is given.

The galaxies are listed in the tables in order of magnitude, with the coordinates in arcsecs; x increases westwards, y northwards. The magnitudes are the observed B_{27} isophotal magnitudes, uncorrected for seeing, isophotal contraction, obscuration etc.. A radius, R_{27}, is given for each galaxy; this is calculated by $R_{27} = (\frac{A}{\pi})^{\frac{1}{2}}$ where A is the area within the μ_B = 27mags/□" isophote. Symbols used in the notes column are:

- ● (for K44) The galaxy lies nearer than 636" to the bright star and its magnitude may be affected by this.
- ** (for K44 and S40/6) The galaxy overlaps another object at an isophote brighter than μ_B = 24mags/□".
- * (for K44 and S40/6) The galaxy overlaps another object at an isophote between μ_B = 27mags/□" and μ_B = 24mags/□" inclusive.
- × The galaxy is cD in nature.

The maps of the clusters show the galaxies listed in the tables. The radii are plotted to scale, except in the large scale maps of the centres of K44 and S40/6 where the radii are reduced by a factor of 3.5 to lessen confusion. Crosses on the maps indicate galaxies for which no radius is available

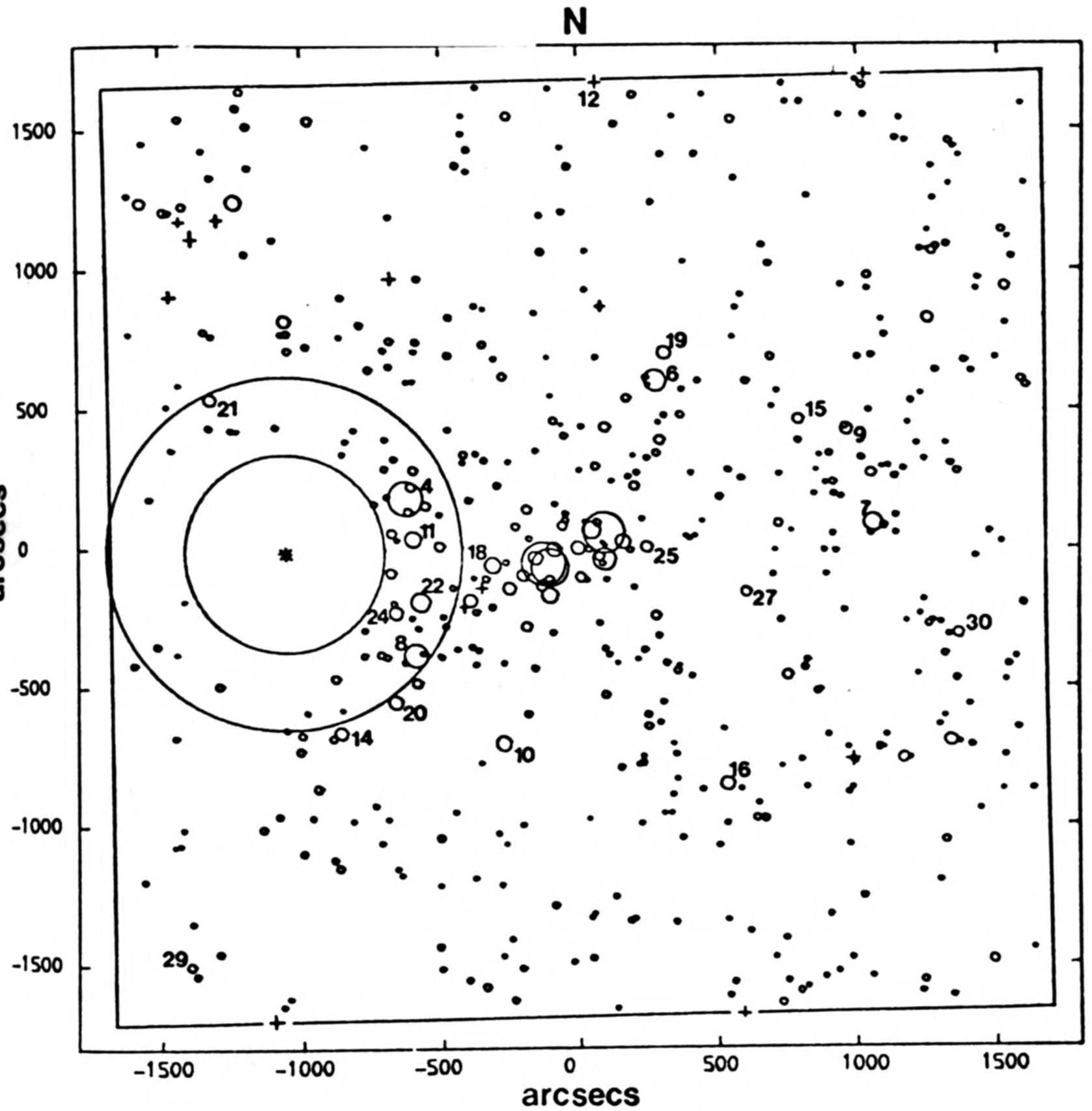

K44

The inner rectangle is the scan area, rotated 0.77°.
Star position is (-1059,-16), with circles radii 356" and 636".
Galaxy VV19 has approximate coordinates (-1900,660)

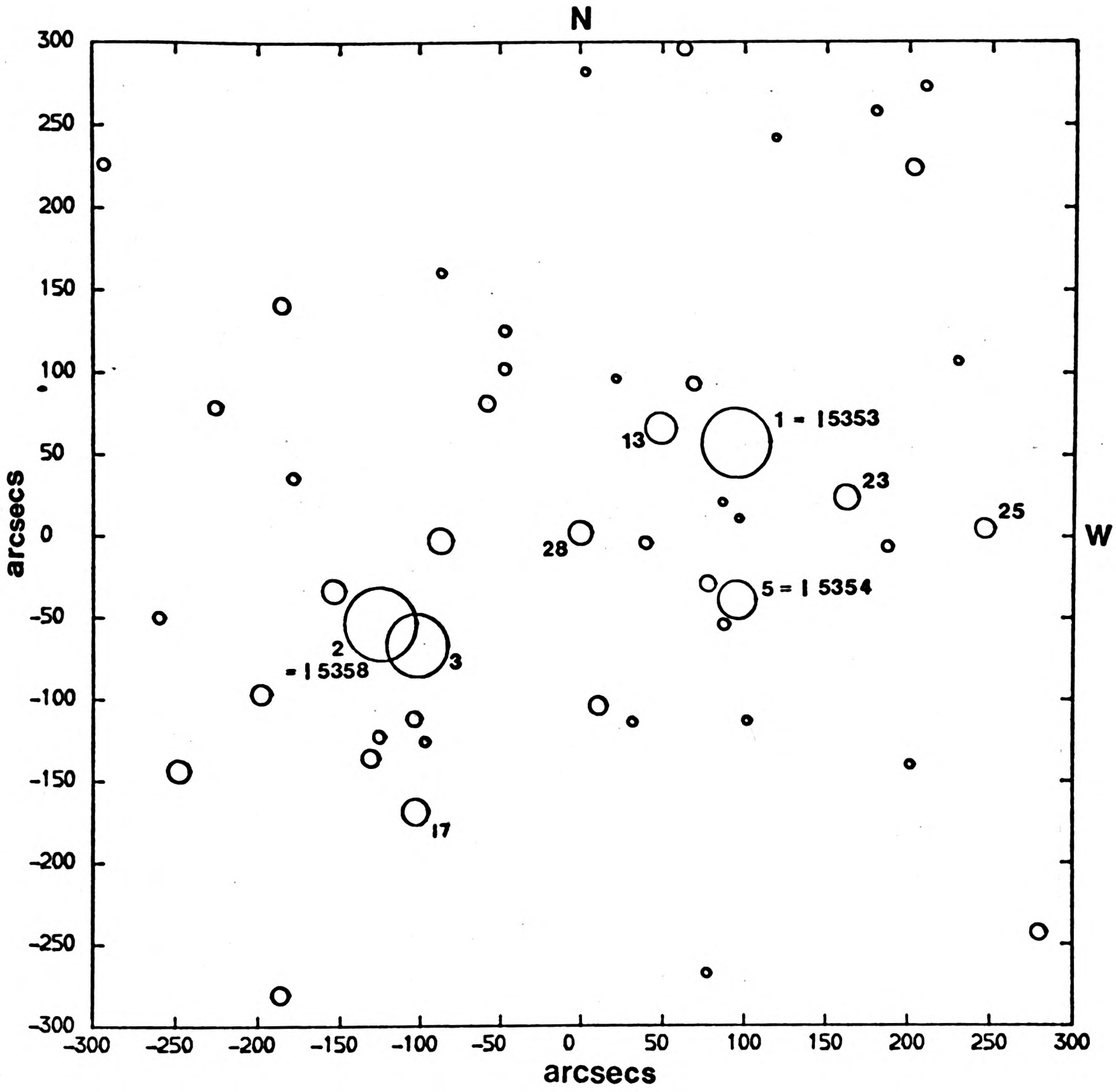

K44 (centre)

Galaxy radii not to scale

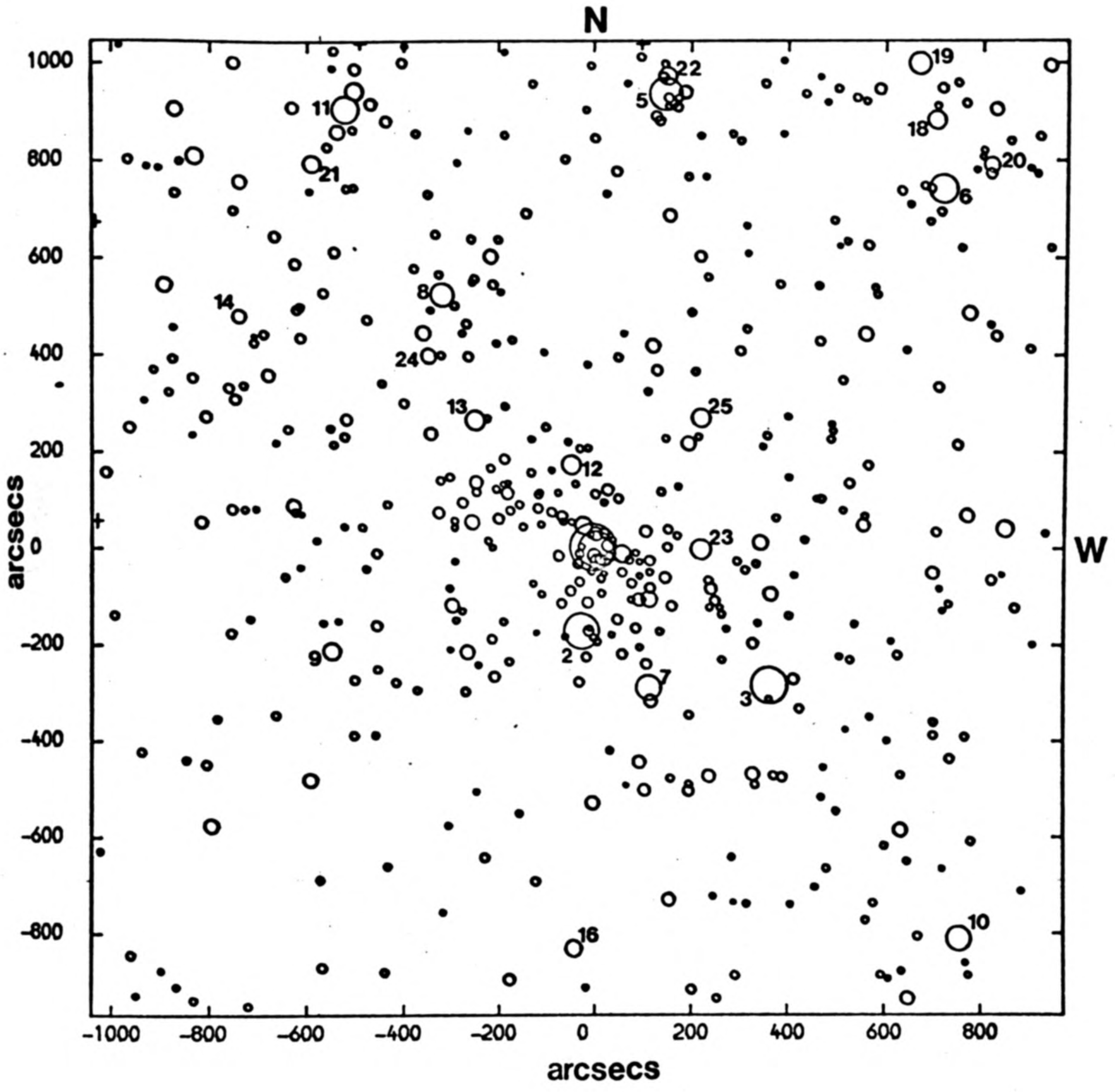
N
W
arcsecs
arcsecs
1000
800
600
400
200
0
-200
-400
-600
-800
-1000
-800
-600
-400
-200
0
200
400
600
800
1
2
3
5
6
7
8
9
10
11
12
13
14
16
18
19
20
21
22
23
24
25

S40/6

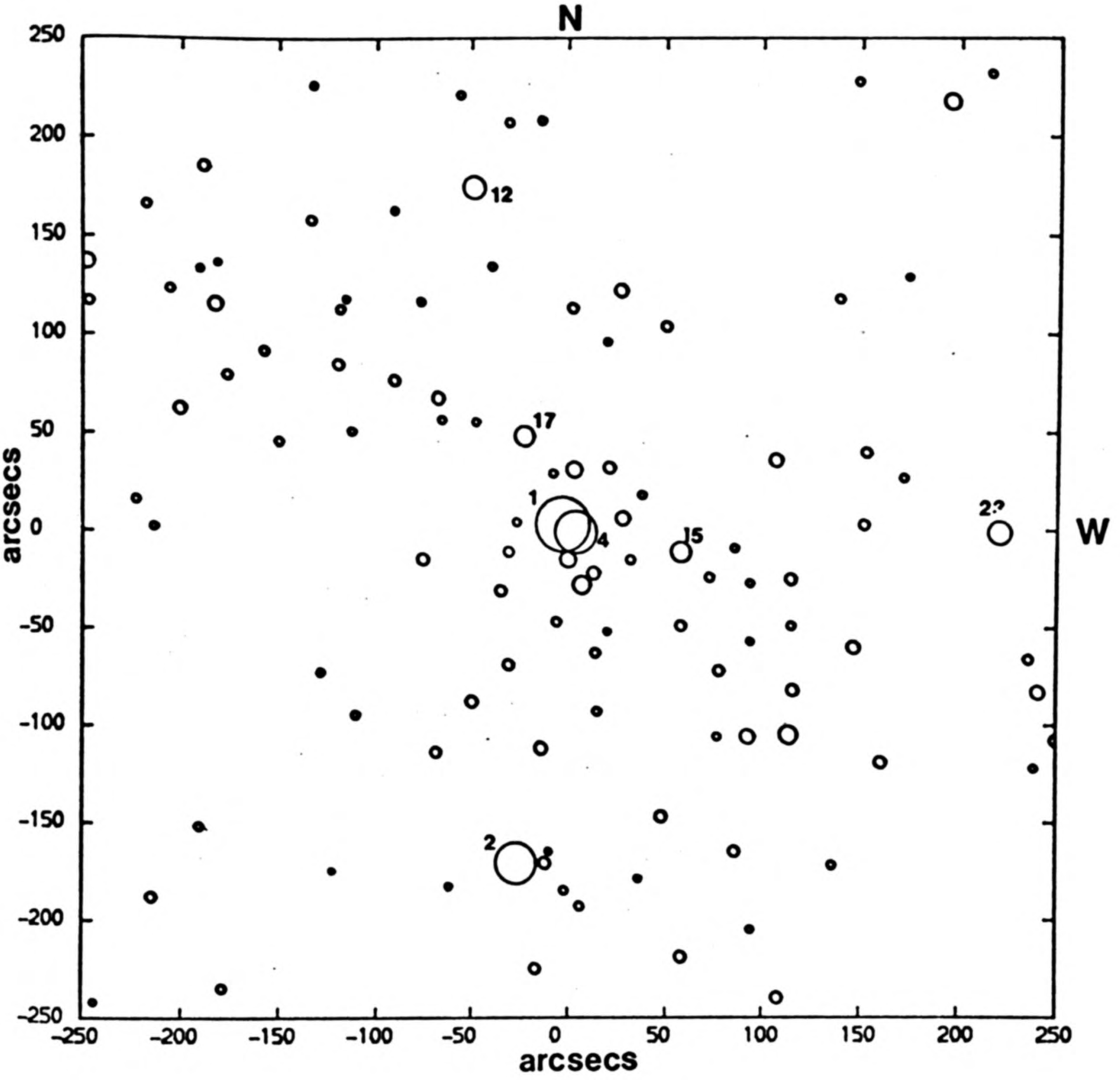

S40/6 (centre)

Galaxy radii not to scale.

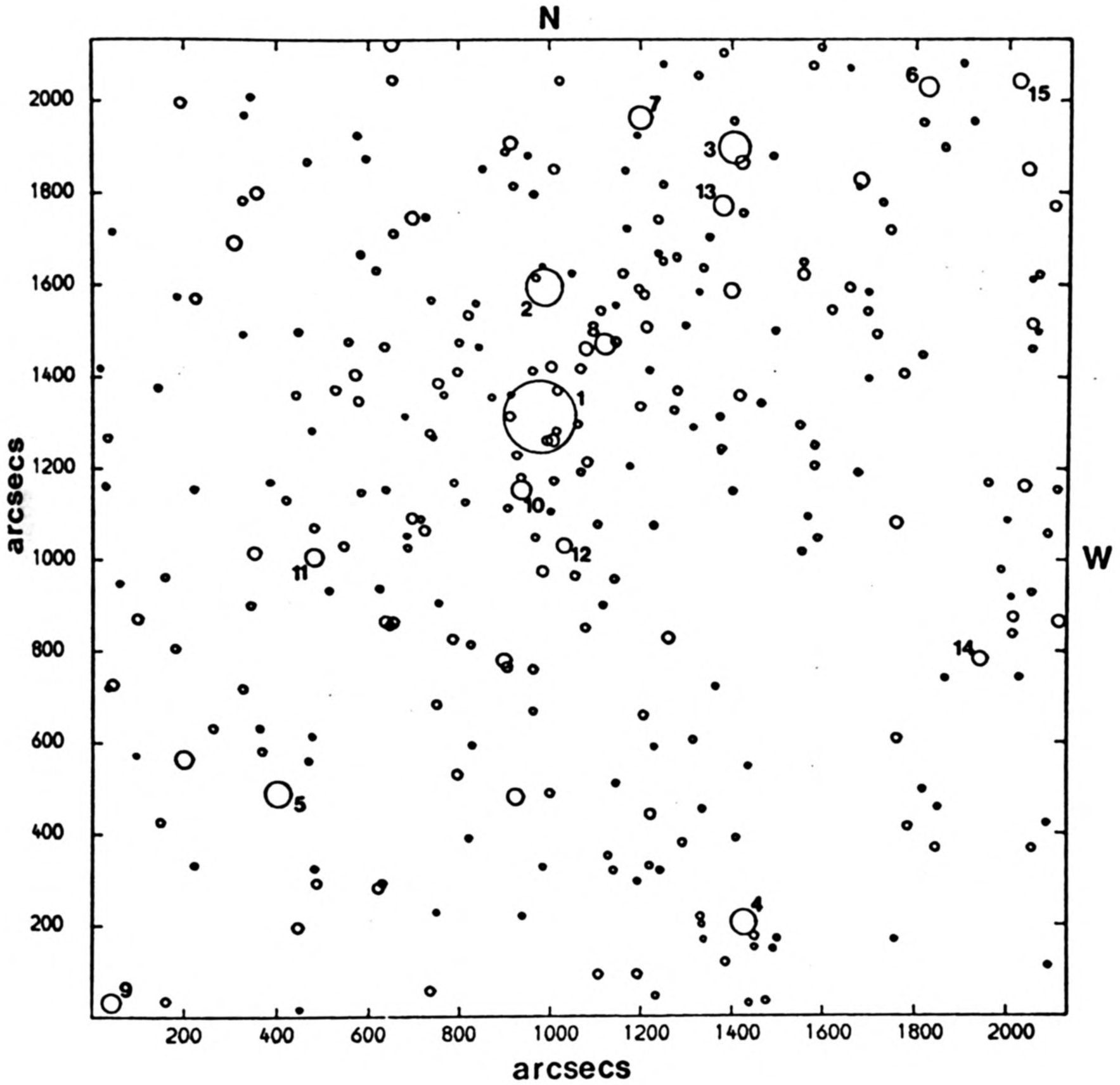

2354−35

Galaxy X has approximate coordinates (1469,2143)

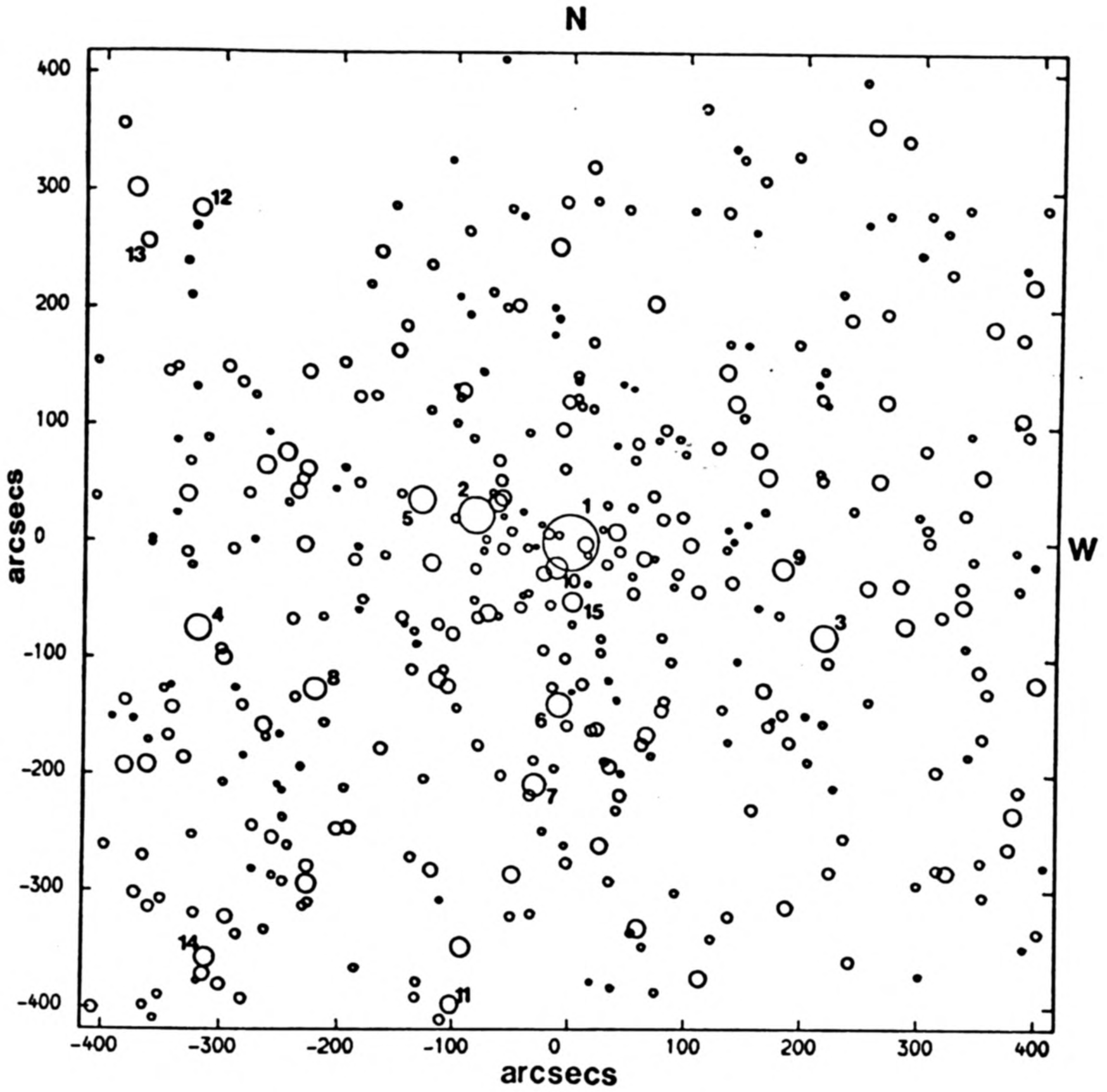
N
W
arcsecs
arcsecs
400
300
200
100
0
-100
-200
-300
-400
-400
-300
-200
-100
0
100
200
300
400
1
2
3
4
5
6
7
8
9
10
11
12
13
14
15

A1146

GALAXY	X ARCSECS	Y	B_{27}	R_{27}	NOTES
1	95	57	13.98	74.04	
2	-125	-54	14.06	78.46	
3	-102	-67	14.38	67.49	
4	-630	181	14.70	61.75	
5	96	-39	14.79	40.71	
6	279	603	14.81	39.21	
7	1063	91	14.94	32.57	
8	-593	-384	14.95	42.37	
9	966	428	15.32	21.60	
10	-271	-704	15.34	23.20	
11	-603	34	15.52	28.51	
12	70	1668	15.60		
13	49	66	15.64	32.58	
14	-862	-663	15.73	22.79	
15	793	464	15.76	19.30	
16	535	-852	15.89	24.37	
17	-103	-169	15.92	28.50	
18	-310	-60	15.93	30.34	
19	311	703	15.94	23.98	
20	-667	-553	15.97	24.91	
21	-1327	536	16.02	21.44	
22	-577	-192	16.07	33.80	
23	163	24	16.07	26.70	
24	-665	-231	16.12	24.14	
25	247	5	16.20	20.77	
26	-1111	-1685	16.20		
27	605	-158	16.23	17.87	
28	0	2	16.28	24.80	
29	-1397	-1501	16.29	15.35	
30	1369	-309	16.32	19.14	
31	-251	1543	16.32	15.76	
32	-1239	1243	16.44	26.86	
33	-87	-3	16.54	26.96	
34	-1554	-34	16.55	24.72	
35	755	-460	16.58	17.92	
36	1342	-697	16.58	22.34	
37	174	540	16.62	14.99	
38	722	90	16.65	15.23	
39	959	439	16.65	11.92	
40	280	-243	16.65	16.44	
41	294	390	16.72	17.48	
42	98	-528	16.77	13.48	
43	1019	1656	16.78	12.97	
44	-506	-1043	16.78	13.01	
45	-248	-144	16.85	23.12	
46	-682	-88	16.88	17.93	
47	-131	-136	16.89	18.62	
48	991	-756	16.90		
49	-679	55	16.91	16.98	
50	-394	-187	16.94	24.03	
51	76	-29	16.94	17.12	
52	97	436	16.97	18.09	
53	-1009	-730	16.97	15.19	
54	-1296	-494	17.00	13.06	
55	-52	406	17.01	12.15	
56	1529	940	17.02	17.40	
57	-186	-281	17.03	18.21	
58	203	224	17.03	16.82	
59	-347	732	17.04	12.91	
60	-272	618	17.05	14.25	
61	1143	-750	17.09	19.03	
62	1255	826	17.09	19.06	
63	-351	-139	17.10		
64	-868	-1150	17.11	15.06	
65	-198	-97	17.12	20.99	
66	63	296	17.13	14.68	
67	351	-744	17.27	19.67	
68	-185	140	17.28	16.06	
69	-1002	-672	17.31	13.44	
70	-999	-1096	17.35	11.52	
71	282	1343	17.46	13.08	
72	1263	-275	17.47	12.50	
73	1363	-474	17.48	11.52	
74	-341	-1579	17.48	13.09	
75	11	-104	17.52	13.04	
76	368	480	17.54	13.20	
77	1601	-200	17.55	11.65	
78	-1515	-349	17.55	12.36	
79	-887	-1120	17.62	11.88	
80	508	1885	17.64	11.66	
81	-891	-693	17.66	13.02	
82	-1297	-1456	17.67	11.56	
83	-945	-1486	17.67	11.67	
84	-89	-1287	17.74	11.45	
85	1516	1405	17.75	11.25	
86	1205	1065	17.77	11.37	
87	1054	271	17.77	11.27	
88	-1104	-1123	17.78	11.37	
89	-611	2233	17.78	11.96	
90	-90	459	17.78	11.67	
91	1114	2497	17.80	11.50	
92	590	-1661	17.80	12.11	
93	1243	-1561	17.81	11.75	
94	549	-1535	17.82	11.44	
95	-511	-1434	17.82	11.44	
96	918	1237	17.84	11.53	
97	1327	1457	17.89	11.74	
98	-507	478	17.90	11.72	
99	309	-3862	17.91	11.68	
100	-779	-1372	17.93	11.50	
101	-443	-1640	17.93	11.34	
102	730	-968	17.94	11.56	
103	-966	81	17.97	11.45	
104	-58	1531	17.97	11.56	
105	-972	604	17.97	11.30	
106	601	-517	17.98		
107	863				

GALAXY	X ARCSECS	Y	H 27	R 27	NOTES
108	1361	277	17.99	12.94	
109	-1598	-418	18.001	11.49	
110	683	1021	18.001	10.52	
111	1492	-1489	18.003	14.59	
112	-717	-382	18.004	14.42	
113	83	-54	18.005	11.61	
114	-182	-597	18.005	12.40	
115	242	614	18.007	10.93	
116	-133	1063	18.007	11.58	
117	-882	-4466	18.008	14.81	
118	77	-2688	18.11	9.08	
119	730	-259	18.12	10.89	
120	-1434	1539	18.12	12.04	
121	-585	968	18.14	9.75	
122	691	669	18.14	13.40	
123	319	-414	18.15	11.48	
124	1569	207	18.17	13.44	
125	-1143	-1009	18.18	12.15	
126	69	93	18.19	13.94	
127	291	-315	18.19	9.76	
128	-1297	1175	18.20		
129	1322	-1057	18.20	13.10	
130	1038	978	18.22	13.94	
131	233	-366	18.24	9.96	
132	1548	-422	18.24	10.26	
133	184	-1344	18.26	10.53	
134	-592	742	18.26	11.92	
135	-620	133	18.30	15.32	
136	-1335	4327	18.30	11.78	
137	-2335	-1627	18.31	11.66	
138	2247	3226	18.32	10.87	
139	1281	3480	18.33	10.32	
140	1096	823	18.34	12.60	
141	-1326	-1533	18.35	12.66	
142	1054	533	18.35	11.68	
143	47	-1477	18.36	9.87	
144	1092	767	18.38	11.62	
145	792	386	18.38	11.29	
146	2500	-601	18.38	11.41	
147	1020	526	18.39	11.41	
148	-4002	173	18.40	21.71	
149	-1062	817	18.41	14.24	
150	-2268	78	18.41	17.16	
151	-5580	154	18.43	19.26	
152	-1570	1240	18.44	9.59	
153	-3766	870	18.44	10.30	
154	1305	-2680	18.45	11.44	
155	1282	1080	18.45	11.82	
156	-47	1002	18.46	10.86	
157	586	253	18.47	12.15	
158	-37	1368	18.48		
159	-633	970	18.50	12.76	
160	671	-976	18.51	9.62	
161	1084	-717	18.52		
162	1138	259	18.53	11.85	
163	540	283	18.54	10.65	
164	1163	118	18.54	9.64	
165	252	-643	18.55	12.70	
166	-364	-366	18.57	10.66	
167	372	571	18.58	8.80	
168	63	687	18.59	9.00	
169	1334	-515	18.59	10.17	
170	1044	497	18.60	9.47	
171	1028	1688	18.60		
172	-1378	-1530	18.60	10.37	
173	446	-672	18.61	9.53	
174	1320	-384	18.61	11.59	
175	1271	1253	18.62	11.69	
176	-697	-390	18.62	12.99	
177	-1428	1207	18.62	15.71	
178	153	-792	18.62	11.51	
179	-336	-110	18.62	13.34	
180	904	541	18.63	12.26	
181	1604	580	18.63	13.64	
182	232	-776	18.63	11.94	
183	200	1623	18.65	13.45	
184	-476	694	18.64	12.13	
185	-569	-485	18.64	11.11	
186	433	603	18.65	9.31	
187	-1562	-1106	18.65	10.31	
188	-740	-927	18.66	8.20	
189	352	-443	18.66	12.51	
190	927	-361	18.66	11.50	
191	641	-997	18.66	10.43	
192	1137	1466	18.66	9.52	
193	803	-766	18.66	11.46	
194	1432	969	18.66	11.52	
195	-374	341	18.66	11.55	
196	-825	-403	18.66	11.75	
197	1414	63	18.66	11.75	
198	887	-454	18.66	11.76	
199	-1546	1546	18.66	11.77	
200	-293	2287	18.66	11.77	
201	666	107	18.66	11.78	
202	1887	-65	18.66	11.78	
203	-1370	913	18.66	11.78	
204	-228	-413	18.66	11.78	
205	2287	1545	18.66	11.78	
206	1337	305	18.66	11.78	
207	-956	-1305	18.66	11.78	
208	997	771	18.66	11.78	
209	-1465	355	18.66	11.78	
210	-563	-377	18.66	11.78	
211	-1343	518	18.66	11.78	
212	1536	-750	18.66	11.78	
213	1320	1089	18.66	11.78	
214	-1392	-1347	18.66	11.78	
215	1478	58	18.66	11.78	

GALAXY	X ARCSECS	Y ARCSECS	B_{27}	R_{27}	NOTES
216	-373	-228	18.87	11.70	*
217	1091	295	18.87	8.11	*
218	-1436	-1067	18.86	7.78	
219	210	273	18.88	10.00	
220	-860	900	18.88	10.36	*
221	986	-765	18.88	7.80	**
222	1552	1045	18.89	7.52	
223	-510	122	18.89	9.80	●
224	1276	-262	18.90	9.92	*
225	1063	-728	18.91	8.92	
226	347	-1550	18.92	8.13	
227	406	272	18.92	8.74	
228	180	258	18.93	8.59	
229	421	46	18.93	7.10	**
230	-381	-106	18.94	8.90	*
231	-154	352	18.94	9.70	
232	-47	125	18.94	11.06	*
233	-1035	-963	18.96	10.80	*
234	1530	808	18.96	9.93	
235	305	-555	18.96	8.66	
236	-293	-1028	18.97	8.26	
237	-1324	1330	18.97	9.72	*
238	1400	-565	18.98	9.32	
239	1225	1072	18.98	9.62	
240	1110	-675	18.99	8.53	
241	-453	-1422	18.99	9.50	●
242	-603	282	18.99	9.01	●
243	-260	-50	19.00	9.26	**
244	1416	-713	19.00	9.92	*
245	-365	1650	19.00	9.87	
246	298	1411	19.00	9.51	*
247	-633	1446	19.00	9.91	**
248	-557	1206	19.00	9.22	
249	1057	-1545	19.00	8.86	●
250	-777	-294	19.00	8.65	●
251	-1544	179	19.00	8.55	
252	-1384	675	19.00	8.37	
253	1195	530	19.00	8.44	
254	-1400	1428	19.00	8.45	
255	342	1547	19.00	8.78	
256	-277	-1466	19.00	8.31	
257	902	-675	19.00	8.92	
258	-718	-1061	19.00	8.78	
259	-97	-1260	19.00	8.67	*
260	-672	-1970	19.00	8.65	*
261	338	-890	19.00	8.79	
262	-686	1188	19.00	8.89	
263	-1120	1366	19.00	8.99	
264	974	-883	19.00	8.99	*
265	1301	-639	19.00	9.10	
266	1635	-870	19.00	9.10	
267	1182	-266	19.00	9.32	**
268	32	-1140	19.00	9.42	*
269	-1392	1113	19.00	9.10	**+
270	-1471	904	19.00	9.10	**+
271	-1371	1115	19.00	9.00	
272	701	-95	19.00	9.11	
273	-1424	-1010	19.00	9.23	
274	1215	377	19.00	8.68	
275	1426	931	19.00	8.50	
276	1026	-1257	19.00	8.61	
277	1320	377	19.00	10.82	*
278	744	-1400	19.00	7.75	
279	714	567	19.00	9.24	
280	-1451	-679	19.00	8.47	
281	26	1066	19.00	10.10	*
282	119	242	19.00	7.17	
283	-452	-950	19.00	7.15	
284	888	-7	19.00	7.82	
285	-1230	1578	19.00	9.16	*
286	1345	-1615	19.00	12.36	
287	197	335	19.00	9.64	
288	134	1519	19.00	9.97	
289	-202	-997	19.00	9.77	
290	-685	745	19.00	11.17	
291	-101	549	19.00	9.33	
292	-206	-1512	19.00	12.84	
293	-704	303	19.00	9.81	
294	-846	385	19.00	10.57	*
295	-793	802	19.00	9.80	*●
296	1234	-1600	19.00	9.20	*●
297	-1444	-579	19.00	12.97	
298	722	-2668	19.00	9.27	●
299	135	-1653	19.00	9.85	
300	-471	8832	19.00	9.44	
301	-1255	4225	19.00	9.58	
302	-820	-9	19.00	9.51	●
303	768	649	19.00	9.74	
304	797	-1599	19.00	9.16	
305	1245	-1186	19.00	8.56	*
306	-500	-3901	19.00	9.76	
307	-600	6011	19.00	9.29	
308	-1005	7111	19.00	9.68	
309	-245	-1408	19.00	9.31	*
310	-1422	1228	19.00	9.15	*
311	-1194	1512	19.00	9.18	
312	911	51	19.00	9.27	
313	1230	557	19.00	9.22	
314	1052	694	19.00	8.88	
315	-1473	1206	19.00	9.22	
316	973	-721	19.00	8.89	*
317	-661	-1155	19.00	9.90	*
318	-306	681	19.00	9.23	
319	1429	-30	19.00	9.30	
320	938	1550	19.00	9.31	
321	-1481	511	19.00	9.31	
322	1223	-457	19.00	9.49	
323	-388	-554	19.00	9.83	*

K44 (cont)

GALAXY	X ARCSECS	Y ARCSECS	B 27	R 27	NOTES
324	-585	-287	19.31	10.44	
325	557	-1566	19.31	11.07	
326	-1071	-1640	19.32		
327	822	1263	19.32		
328	419	1411	19.32		
329	582	911	19.32		
330	-356	-774	19.33		
331	-1057	-652	19.34		
332	960	-224	19.34		
333	111	-383	19.35		
334	1164	286	19.35		
335	921	194	19.36		
336	-375	-618	19.36		
337	-313	-212	19.36		
338	1594	1307	19.36		
339	448	1624	19.37		
340	-857	339	19.37		
341	534	-993	19.38		
342	535	-1541	19.38		
343	-157	-452	19.39		
344	-866	759	19.39		
345	850	196	19.39		
346	131	-1257	19.39		
347	-743	161	19.39	11.75	
348	82	866	19.40		
349	-420	-205	19.40		
350	202	-140	19.41	8.91	
351	1522	25	19.41	8.94	
352	-421	1425	19.41	9.22	
353	-1056	772	19.41	12.19	
354	142	-413	19.42	8.87	
355	-281	-1213	19.42	9.71	
356	695	511	19.43	9.13	
357	1025	1550	19.43	8.76	
358	447	98	19.44		
359	401	37	19.44	8.51	
360	1243	321	19.44	8.67	
361	-403	1351	19.44	9.71	
362	-419	339	19.44	13.45	
363	647	-920	19.45	9.47	
364	355	-833	19.45	8.46	
365	233	-752	19.45	9.16	
366	896	235	19.45	8.46	
367	1373	-705	19.46	8.32	
368	3	282	19.46	8.36	
369	-762	643	19.46	12.78	
370	11	440	19.47	9.69	
371	-1104	1107	19.47	8.95	
372	1575	-395	19.47	8.46	
373	-1216	1636	19.47	14.16	
374	1145	54	19.47	8.75	
375	1171	1458	19.47	8.59	
376	225	-995	19.48	7.69	
377	-1348	779	19.48	11.99	

GALAXY	X ARCSECS	Y ARCSECS	B 27	R 27	NOTES
378	584	-870	19.49	7.55	
379	-2643	-1066	19.49	8.56	
380	-6227	598	19.49	7.36	
381	1361	1405	19.50	8.56	
382	-985	725	19.50	11.48	
383	1037	932	19.50	8.04	
384	264	1241	19.51	8.06	
385	-858	-582	19.52	8.09	
386	-86	1600	19.52	8.09	
387	8049	-94	19.52	8.34	
388	4069	-4613	19.52	8.83	
389	-7066	2888	19.52	10.75	
390	43	-1331	19.53	8.52	
391	24	929	19.53	8.27	
392	1582	1588	19.54	8.28	
393	1046	1486	19.54	9.20	
394	751	-1561	19.54	8.66	
395	930	-11	19.54	8.26	
396	-813	429	19.54	8.82	
397	-647	-1179	19.54	8.61	
398	1230	-2339	19.54	8.62	
399	-1486	-2800	19.55	10.35	
400	-1033	6588	19.55	8.67	
401	-2543	512	19.55	9.13	
402	-4937	-3626	19.55	8.27	
403	733	1675	19.56	8.55	
404	-422	1662	19.56	8.61	
405	5644	3109	19.56	8.41	
406	873	869	19.56	8.85	
407	-461	-5126	19.56	8.93	
408	-1135	1436	19.56	8.54	
409	522	6588	19.57	8.87	
410	1327	-653	19.57	8.93	
411	1006	-1350	19.57	8.54	
412	-3880	-1324	19.57	8.36	
413	-1236	-1189	19.57	8.75	
414	1796	422	19.57	8.52	
415	-884	1597	19.57	8.27	
416	935	-591	19.57	8.20	
417	-477	-1522	19.58	8.66	
418	857	4228	19.58	8.26	
419	1300	283	19.58	8.22	
420	37	-1201	19.58	8.66	
421	746	-975	19.58	8.66	
422	87	1598	19.58	8.00	
423	-695	21	19.58	8.00	
424	-1048	-975	19.58	8.00	
425	848	-1617	19.58	8.66	
426	-1561	336	19.58	8.66	
427	-672	1453	19.58	8.66	
428	554	3220	19.59	8.66	
429	204	7600	19.59	8.66	
430	-504	-629	19.59	8.66	
431		-1515	19.62	8.28	

GALAXY	X ARCSECS	Y	H 27	R 27	NOTES
432	377	1029	19.62	6.84	
433	943	946	19.62	8.91	
434	-507	-346	19.62	8.51	•
435	540	-1614	19.63	10.00	•
436	-765	1437	19.63	7.15	
437	-1005	437	19.63	9.08	●
438	1009	-721	19.63	6.73	•
439	307	-956	19.64	7.65	
440	709	-6	19.64	6.68	
441	-1614	771	19.64	7.15	
442	987	-446	19.65	7.21	
443	217	-781	19.65	8.55	•
444	-698	1187	19.65	10.58	:●
445	-509	707	19.65	8.11	•
446	230	1107	19.66	8.35	
447	-1440	588	19.66	7.20	
448	1184	452	19.66	7.81	
449	-404	-1555	19.67	9.69	
450	978	-1071	19.67	8.76	•
451	-689	654	19.67	11.06	
452	732	-788	19.67	6.66	
453	-1419	-1900	19.67	6.42	●
454	614	-1382	19.67	8.95	
455	1528	-873	19.67	6.16	
456	97	11	19.68	7.45	•
457	1087	822	19.68	7.96	•
458	199	-1337	19.68	8.04	•
459	-178	35	19.69	11.30	•
460	-103	1646	19.69	9.29	
461	-662	30	19.70	8.78	•●
462	-1431	1174	19.70		:•+
463	-1076	770	19.70	9.25	•
464	252	582	19.71	6.63	•
465	1151	1534	19.71	7.71	
466	-495	-245	19.71	9.73	• ●
467	-708	712	19.71	10.26	
468	102	-113	19.71	8.54	•
469	706	-1478	19.71	7.92	•
470	53	-1317	19.72	7.40	•
471	985	-1476	19.72	9.07	
472	-25	-1491	19.72	8.83	
473	560	1325	19.72	6.33	
474	-1352	1424	19.72	7.50	
475	-344	850	19.72	6.86	
476	1536	1115	19.73	6.72	
477	1539	-478	19.73	7.21	
478	822	-864	19.73	7.34	•
479	1342	1438	19.74	8.30	•
480	387	45	19.74	7.09	
481	1100	-745	19.75	7.02	
482	-508	-1214	19.75	6.95	•
483	-608	-250	19.76	9.39	●
484	817	-431	19.76	12.15	
485	214	-400	19.76	6.19	•

GALAXY	X ARCSECS	Y	H 27	R 27	NOTES
486	1264	1367	19.76	7.46	
487	342	-706	19.76	7.14	
488	1495	685	19.76	7.84	
489	332	-956	19.76	7.17	
490	1446	-943	19.77	8.23	
491	363	-425	19.77	7.74	*
492	1319	-807	19.77	7.38	
493	-1323	763	19.77	9.52	
494	-1456	-1072	19.77	6.69	
495	372	-1040	19.78	8.83	*
496	1252	1138	19.78	6.68	
497	-1615	1200	19.78	9.61	
498	822	-1582	19.78	7.84	*
499	-157	846	19.78	8.16	
500	-1203	1057	19.78	9.78	*
501	1582	-650	19.79	8.92	
502	505	-1074	19.79	8.34	
503	1636	-1447	19.79	6.76	
504	22	96	19.80	7.84	*
505	-419	1549	19.80	7.50	
506	-634	-411	19.80	9.77	*
507	1248	1071	19.80	7.13	*

GALAXY	X ARCSECS	Y ARCSECS	B 27	R 27	NOTES
1	-3	3	15.07	48.80	** X
2	-27	-171	15.45	36.89	
3	364	-284	15.58	37.65	*
4	4	-1	15.65	37.58	** X
5	147	936	16.06	33.43	**
6	718	742	16.18	29.12	*
7	113	-289	16.25	25.80	
8	-320	523	16.27	23.71	
9	-550	-214	16.34	17.49	*
10	756	-811	16.36	25.09	*
11	-523	903	16.42	27.79	*
12	-49	174	16.50	19.64	*
13	-250	265	16.55	20.01	*
14	-740	478	16.78	13.67	*
15	58	-11	16.80	17.75	**
16	-44	-831	16.90	16.85	*
17	-23	48	16.91	17.65	**
18	704	883	16.94	18.53	*
19	669	999	16.94	22.25	*
20	818	791	16.95	16.04	*
21	-590	790	16.98	17.06	*
22	151	973	17.03	17.93	**
23	221	-1	17.05	20.73	*
24	-344	397	17.05	15.17	*
25	221	271	17.06	18.78	*
26	156	687	17.12	16.41	*
27	851	42	17.12	16.98	*
28	-257	55	17.20	16.78	*
29	366	-94	17.22	15.80	**
30	114	-1056	17.22	16.18	**
31	-627	86	17.22	14.16	**
32	-871	859	17.24	14.66	**
33	-4	-529	17.26	13.61	**
34	-360	444	17.27	14.63	**
35	701	-500	17.29	12.30	**
36	-963	250	17.31	10.58	**
37	-832	808	17.31	16.50	*
38	-525	265	17.34	14.90	*
39	195	218	17.34	14.08	*
40	-218	602	17.38	13.82	*
41	774	487	17.40	14.37	*
42	-267	-215	17.42	14.22	*
43	-893	544	17.45	14.84	
44	-179	-895	17.48	11.37	
45	94	-444	17.49	12.41	**
46	937	994	17.55	12.70	*
47	-539	856	17.57	14.96	*
48	-560	443	17.59	14.06	*
49	-816	53	17.61	11.52	*
50	345	13	17.62	15.16	*
51	649	-285	17.64	15.42	**
52	-739	-935	17.64	13.35	*
53		754	17.	13.	*
54	23	-106	17.64	12.78	*
55	-438	878	17.65	10.74	
56	-593	-432	17.67	13.90	*
57	557	49	17.69	12.86	*
58	-1030	58	17.70		** +
59	-299	-118	17.76	14.08	*
60	827	905	17.77	13.02	*
61	-754	80	17.78	9.62	*
62	121	419	17.78	13.73	*
63	-834	551	17.79	9.16	
64	-613	432	17.81	9.66	**
65	219	603	17.81	10.81	**
66	-1012	157	17.83	10.18	
67	-761	330	17.83	10.42	
68	-327	74	17.85	11.29	**
69	567	173	17.84	8.90	
70	117	-317	17.85	12.66	*
71	772	69	17.85	13.79	*
72	187	940	17.86	12.95	*
73	-210	-266	17.86	10.41	
74	-183	115	17.87	12.41	*
75	635	-585	17.88	13.79	*
76	98	1038	17.90		** +
77	-1035	674	17.90		** +
78	3	31	17.91	13.76	*
79	0	-15	17.94	14.19	**
80	104	-502	17.96	11.88	*
81	-344	237	17.96	12.66	*
82	817	773	17.97	10.37	*
83	1	645	17.97	10.26	
84	-457	-161	17.97	10.30	
85	-576	-689	17.99	10.63	*
86	-753	1001	18.00	11.94	*
87	-795	-576	18.00	14.10	*
88	751	215	18.01	9.53	
89	329	-197	18.02	10.46	*
90	238	-473	18.04	10.86	*
91	-667	641	18.05	10.84	*
92	-249	137	18.05	11.21	
93	629	-244	18.06	11.13	
94	830	-123	18.06	11.25	*
95	872	-177	18.07	11.39	*
96	-756	356	18.08	12.14	*
97	-680	509	18.08	11.30	*
98	-742	302	18.09	11.97	*
99	27	1226	18.11	11.31	*
100	-871	733	18.11	12.72	
101	587	946	18.12	11.70	*
102	147	-660	18.12	11.92	*
103	414	-2721	18.13	11.99	*
104	565	626	18.13	10.99	*
105	-607	271	18.15	10.09	*
106	-504	941	18.	10.	*
107			18.		

GALAXY	X ARCSECS	Y	B_{27}	R_{27}	NOTES
108	716	948	18.18	12.61	*
109	154	-730	18.19	12.75	*
110	523	156	18.19	12.88	
111	917	849	18.20	12.98	
112	161	-119	18.20	12.98	**
113	130	369	18.21	13.02	
114	105	-504	18.21	13.00	*
115	250	-108	18.22	13.04	*
116	48	-147	18.23	13.06	*
117	241	-83	18.26	13.06	*
118	49	395	18.27	13.09	*
119	313	-44	18.28	13.08	**
120	-875	321	18.30	13.17	
121	28	6	18.30	13.26	*
122	-124	-692	18.31	13.29	
123	58	-219	18.33	13.31	*
124	-752	695	18.35	13.36	
125	737	-437	18.36	13.36	*
126	107	36	18.36	13.63	
127	-76	-15	18.37	13.59	*
128	633	738	18.39	13.56	
129	329	-469	18.39	13.60	*
130	466	429	18.42	13.23	
131	-61	76	18.44	13.30	*
132	711	335	18.44	13.30	
133	116	-82	18.44	13.58	*
134	520	-475	18.45	13.64	
135	223	-65	18.47	13.11	*
136	-277	95	18.48	13.17	
137	-213	544	18.50	13.22	*
138	-477	470	18.50	13.22	
139	-50	-83	18.51	13.69	*
140	13	-22	18.52	13.71	**
141	142	971	18.53	13.71	
142	-32	-277	18.54	13.72	**
143	115	-25	18.55	13.74	
144	-69	-114	18.56	13.76	**
145	-215	-186	18.56	13.77	
146	201	-916	18.56	13.79	*
147	-228	79	18.58	13.80	
148	-470	914	18.58	13.80	*
149	-967	802	18.60	13.80	
150	470	104	18.60	13.81	*
151	-504	987	18.62	13.82	
152	-175	430	18.63	13.86	*
153	-103	251	18.63	13.86	
154	-440	-880	18.64	13.87	*
155	-12	-171	18.65	13.89	
156	513	349	18.66	13.90	*
157	21	32	18.67	13.90	
158	-230	-642	18.67	13.90	*
159	-1220	84	18.67	13.91	
160	-189	185	18.68	13.92	*
161	46	777	18.68	13.92	
162	135	881	18.68	13.92	*
163	152	3	18.69	13.93	
164	-271	-298	18.69	13.93	*
165	128	890	18.70	13.94	
166	-35	-31	18.71	13.94	*
167	-805	-449	18.71	13.95	
168	-373	-295	18.72	13.95	*
169	-639	244	18.72	13.96	
170	714	695	18.74	13.96	*
171	58	-49	18.76	13.97	
172	1088	-240	18.77	13.97	*
173	-688	67	18.79	13.98	
174	-457	-11	18.80	13.98	*
175	52	113	18.80	13.98	
176	530	-231	18.80	13.98	*
177	-177	79	18.81	13.98	
178	708	35	18.82	13.98	
179	353	957	18.85	13.98	
180	209	366	18.86	13.98	
181	-189	851	18.86	13.98	
182	-202	636	18.87	13.98	
183	-553	246	18.89	13.98	
184	-153	40	18.89	13.98	*
185	-631	907	18.90	13.98	*
186	197	-346	18.90	13.98	*
187	136	-172	18.90	13.98	
188	489	-227	18.90	13.98	
189	-938	-423	18.90	13.98	
190	693	743	18.91	13.98	
191	900	413	18.91	13.98	
192	315	-739	18.91	13.98	
193	-14	-1112	18.93	13.98	
194	781	-609	18.93	13.98	
195	-17	-2258	18.94	13.98	
196	153	9282	18.94	13.98	
197	706	912	18.95	13.98	
198	-690	440	18.96	13.98	
199	194	766	18.96	13.98	
200	-504	-389	18.97	13.98	
201	-883	323	18.97	13.98	
202	-503	-274	18.97	13.98	
203	426	-333	18.97	13.98	
204	-1388	2946	18.98	13.98	
205	-1334	6460	18.98	13.98	
206	-405	10073	18.98	13.98	
207	-624	-361	18.98	13.98	
208	703	-737	18.98	13.98	
209	578	422	18.98	13.98	
210	-710	2999	18.98	13.98	
211	-400	3225	19.00	13.98	
212	111	9586	19.00	13.98	
213	540	5643	19.00	13.98	
214	-252	2402	19.00	13.98	
215	-487	1400	19.05	13.98	

S40/6 (cont)

GALAXY	X ARCSECS	Y	B_{27}	R_{27}	NOTES
219	-664	-347	19.05	7.79	
217	196	-490	19.06	7.22	*
218	680	748	19.06	7.68	*
219	818	463	19.07	7.24	
220	515	80	19.08	6.46	
221	-626	585	19.09	10.72	*
222	-417	-279	19.09	7.00	*
223	635	-471	19.11	7.42	*
224	206	-26	19.11	7.42	*
225	384	540	19.11	7.64	
226	-331	-69	19.11	7.26	*
227	-524	229	19.12	8.52	*
228	-265	396	19.12	8.45	
229	302	640	19.13	7.06	*
230	253	-934	19.13	7.80	
231	765	-917	19.13	7.14	
232	235	561	19.13	8.14	*
233	292	-887	19.13	8.05	*
234	-455	-252	19.13	7.60	*
235	-31	207	19.13	7.31	*
236	-31	-11	19.13	7.72	*
237	463	543	19.13	9.55	
238	215	232	19.13	7.79	
239	562	-775	19.13	7.55	
240	285	-642	19.13	8.82	
241	-19	-912	19.13	8.22	*
242	644	411	19.13	6.25	
243	-435	90	19.13	7.55	
244	171	909	19.13	7.36	
245	-201	62	19.13	9.66	*
246	-460	-588	19.13	8.95	
247	705	-580	19.13	7.50	*
248	-206	125	19.13	7.59	*
249	-264	403	19.13	7.67	*
250	768	-391	19.13	8.67	*
251	-568	-870	19.13	8.88	*
252	404	-139	19.13	8.89	*
253	-259	637	19.13	8.53	*
254	236	-66	19.13	8.30	*
255	-144	690	19.13	8.08	*
256	-994	-139	19.13	7.79	*
257	-645	-61	19.13	7.96	*
258	-119	112	19.13	7.62	*
259	86	-165	19.13	9.55	
260	734	-115	19.13	8.96	*
261	-716	-148	19.13	8.35	*
262	315	454	19.13	7.26	*
263	334	-491	19.13	7.71	*
264	-546	213	19.13	7.89	*
265	601	-618	19.13	8.60	*
266	-294	501	19.13	7.77	*
267	-960	-844	19.13	8.19	
268	502	947	19.13	7.76	*
269	898	784	19.13	5.89	*

GALAXY	X ARCSECS	Y	B_{27}	R_{27}	NOTES
270	-490	1041	19.40		*+
271	-448	540	19.41	6.72	
272	139	118	19.41	6.65	
273	-68	-477	19.41	7.97	*
274	78	-72	19.41	9.13	
275	335	-31	19.42	9.12	*
276	32	-15	19.42	7.20	*
277	493	244	19.43	7.40	
278	-379	576	19.43	8.85	*
279	-134	157	19.44	7.45	*
280	-304	-85	19.44	6.46	
281	-18	905	19.44	6.63	
282	757	621	19.44	6.63	
283	-158	91	19.45	7.32	
284	358	234	19.45	8.86	*
285	404	677	19.45	7.66	
286	748	959	19.47	9.65	*
287	-434	-661	19.48	6.64	*
288	721	-12	19.48	8.62	
289	-214	62	19.48	7.49	
290	96	1012	19.51	8.62	*
291	435	936	19.53	7.17	*
292	-277	4	19.53	7.26	
293	377	64	19.54	7.76	
294	-222	802	19.54	9.91	
295	-666	-911	19.54	7.87	
296	571	-350	19.55	8.54	*
297	-201	-149	19.55	7.41	
298	-731	535	19.56	7.41	*
299	-247	117	19.57	7.13	
300	201	488	19.57	9.57	
301	490	250	19.57	7.58	
302	457	-704	19.58	7.59	
303	73	-24	19.59	8.14	
304	25	731	19.60	7.45	
305	670	-800	19.61	7.41	
306	-479	-45	19.62	7.45	
307	6	-193	19.62	8.51	*
308	460	104	19.64	8.69	*
309	-88	994	19.65	9.00	*
310	-580	15	19.66	7.77	*
311	200	90	19.66	8.18	*
312	-400	134	19.68	7.26	*
313	145	998	19.69	7.71	*
314	173	927	19.69	8.25	*
315	802	821	19.69	7.35	
316	-505	735	19.70	7.59	
317	-197	529	19.70	7.46	
318	285	654	19.70	7.41	
319	579	539	19.71	8.60	*
320	503	-836	19.71	7.77	*
321	50	104	19.71	8.19	
322	158	-478	19.72	7.69	*
323	-846	-440			*

GALAXY	X ARCSECS	Y ARCSECS	B_{27}	R_{27}	NOTES
324	-831	-938	19.72	7.06	
325	-319	-756	19.72	5.56	
326	-8	29	19.73	6.96	*
327	38	18	19.73	6.60	*
328	505	625	19.74	6.40	
329	-567	-156	19.74	4.94	*
330	-2	-135	19.75	7.06	*
331	-257	549	19.76	6.53	*
332	481	-665	19.78	7.20	
333	219	850	19.78	5.90	
334	909	-199	19.78	5.08	
335	77	-106	19.79	6.82	*
336	265	-231	19.81	7.04	
337	775	-887	19.81	6.46	
338	-131	956	19.83	7.12	
339	-223	16	19.85	7.06	*
340	-77	116	19.85	6.61	*
341	-191	-152	19.86	7.12	
342	-721	-950	19.86	7.50	
343	-191	133	19.87	6.06	*
344	-705	800	19.87	6.70	
345	94	-57	19.88	6.20	*
346	-10	-165	19.88	5.88	**
347	636	-878	19.89	6.44	*
348	32	-420	19.89	6.40	
349	648	-650	19.89	6.26	*
350	436	19	19.89	6.55	*
351	-111	-95	19.90	6.82	
352	-248	-506	19.90	5.27	*
353	-116	117	19.90	5.80	*
354	583	525	19.90	7.07	
355	560	68	19.90	6.68	*
356	-784	-355	19.91	6.78	
357	-545	609	19.91	1 1.11	*
358	886	-712	19.91	5.59	
359	-289	794	19.91	5.29	
360	390	1004	19.91	5.36	
361	-294	45	19.92	6.50	
362	799	807	19.93	5.84	*
363	-985	1037	19.95	5.37	
364	-898	-876	19.95	5.30	*
365	-307	-576	19.95	5.71	
366	314	666	19.95	5.74	
367	-506	741	19.96	7.12	
368	-349	728	19.97	7.70	
369	274	-168	19.98	6.15	*
370	-568	525	19.99	9.00	*
371	480	919	19.99	5.37	
372	174	129	20.00	5.94	*
373	-929	783	20.00	5.73	*
374	-56	221	20.00	6.58	
375	36	-179	20.00	5.78	*
376	-874	456	20.00	5.92	*
377	68	957	20.01	5.70	

GALAXY	X ARCSECS	Y ARCSECS	B_{27}	R_{27}	NOTES
378	521	634	20.02	6.21	*
379	-862	798	20.02	6.53	*
380	-179	-235	20.02	7.80	
381	-14	208	20.02	6.79	
382	769	-861	20.02	6.59	
383	115	-49	20.03	7.37	
384	-48	55	20.03	6.61	*
385	-107	405	20.03	6.67	*
386	-303	-210	20.05	5.07	
387	94	-27	20.05	6.54	
388	246	-723	20.05	6.76	*
389	-375	853	20.06	7.40	*
390	-400	1035	20.06	5.94	
391	475	-455	20.06	5.15	
392	-158	-551	20.06	6.27	
393	-225	269	20.07	6.70	*
394	608	-894	20.07	6.80	**
395	-66	56	20.07	7.09	*
396	-265	860	20.07	6.99	
397	941	621	20.09	6.90	
398	317	609	20.09	5.10	
399	651	710	20.09	6.51	
400	-521	739	20.10	7.23	*
401	260	-122	20.10	6.36	*
402	-1024	-629	20.10	6.11	*
403	-344	491	20.10	5.97	
404	-62	-183	20.11	6.19	*
405	-611	69	20.12	5.16	*
406	721	-666	20.12	6.67	
407	172	27	20.13	6.29	
408	-244	-242	20.13	5.92	
409	-230	766	20.14	5.37	
410	-323	1405	20.14	5.94	*
411	-150	45	20.15	5.50	**
412	349	212	20.16	5.71	*
413	539	-1508	20.16	5.94	
414	-322	398	20.16	5.31	*
415	-123	-1754	20.17	5.73	
416	-206	423	20.17	5.42	*
417	-622	490	20.18	6.03	
418	61	449	20.18	6.36	*
419	-914	369	20.18	6.04	*
420	508	-224	20.18	5.05	
421	239	-1222	20.18	5.41	
422	148	228	20.18	5.44	*
423	521	-376	20.19	6.88	
424	15	-93	20.20	6.60	*
425	86	-9	20.20	6.80	
426	-950	-926	20.20	6.60	*
427	-548	1026	20.21	6.81	**
428	20	-52	20.21	5.86	*
429	401	274	20.21	6.54	
430	501	-546	20.21	6.43	
431	-278	444	20.22	6.47	

GALAXY	X ARCSECS	Y	H_{27}	R_{27}	NOTES
432	615	-192	20.22	4.86	
433	-294	57	20.22	7.11	
434	857	840	20.22	7.57	
435	415	-55	20.23	5.81	*
436	-537	-152	20.23	5.53	
437	912	773	20.23	6.16	*
438	560	921	20.23	6.77	
439	14	-63	20.24	7.87	*
440	787	781	20.24	6.30	*
441	-91	162	20.24	5.82	*
442	-710	436	20.24	4.77	*
443	403	148	20.24	5.86	
444	264	-136	20.24	7.17	*
445	289	-735	20.25	4.61	
446	363	-313	20.25	6.17	*
447	94	-205	20.25	6.27	
448	465	971	20.25	5.20	
449	-615	496	20.26	7.59	*
450	607	-399	20.26	5.60	
451	-133	226	20.26	6.00	
452	-218	166	20.27	7.64	*
453	-327	564	20.27	7.48	
454	-524	44	20.27	5.97	
455	300	854	20.28	4.97	
456	-835	234	20.28	4.80	
457	-560	824	20.29	8.46	*
458	-15	380	20.29	6.06	*
459	372	-472	20.29	8.37	*
460	692	675	20.31	6.82	*
461	934	32	20.31	6.03	
462	-129	-73	20.32	6.45	
463	-613	-41	20.33	5.15	
464	-304	147	20.33	8.21	*
465	-508	860	20.33	7.66	
466	152	911	20.35	5.81	*
467	-551	989	20.36	5.69	*
468	-189	1022	20.36	5.45	
469	-293	-27	20.36	5.70	
470	-664	216	20.36	5.63	*
471	-905	785	20.37	5.49	*
472	-182	136	20.37	5.25	*
473	66	-492	20.37	4.87	*
474	-113	50	20.37	6.78	*
475	-278	-130	20.38	6.78	
476	470	-517	20.38	5.95	*
477	844	-54	20.38	4.58	
478	339	-154	20.38	6.21	
479	715	-83	20.40	5.45	
480	-934	306	20.40	5.44	
481	407	-740	20.40	5.61	

GALAXY	X (ARCSECS)	Y (ARCSECS)	B 27	R 27	NOTES
1	979	1313	13.90	78.96	X
2	989	1595	14.75	40.13	
3	1405	1898	15.34	34.00	
4	1427	205	15.61	27.63	
5	403	488	15.95	27.89	
6	1826	2029	16.05	20.30	
7	1200	1962	16.19	24.29	
8	1123	1472	16.21	22.15	
9	44	32	16.34	20.02	
10	938	1153	16.44	20.39	
11	482	1005	16.49	18.77	
12	1032	1031	16.58	15.83	
13	1381	1772	16.58	21.35	
14	1944	784	16.69	15.68	
15	2024	2041	16.79	15.68	
16	1400	1588	16.80	15.97	
17	2115	866	16.87	13.53	
18	1682	1828	16.97	15.40	
19	200	564	17.00	18.77	
20	915	1907	17.02	13.47	
21	2044	1851	17.02	13.66	
22	925	480	17.04	17.52	
23	1761	1083	17.05	12.69	
24	1214	1509	17.15	11.21	
25	309	1690	17.19	14.70	
26	1081	1462	17.19	14.17	
27	352	1014	17.31	13.35	
28	651	2123	17.32	14.30	
29	653	863	17.33	11.79	
30	1422	1866	17.33	14.24	
31	906	779	17.37	15.33	
32	638	864	17.43	12.69	
33	621	282	17.44	11.36	
34	2054	1516	17.47	11.73	
35	2101	1771	17.48	10.60	
36	697	1744	17.56	13.60	
37	1558	1623	17.57	11.79	
38	1083	1214	17.58	10.46	
39	1418	1360	17.59	11.15	
40	1960	1170	17.68	8.27	
41	695	1091	17.69	11.10	
42	446	196	17.71	11.05	
43	1007	1262	17.72	13.53	
44	579	1346	17.79	9.80	
45	1004	1422	17.80	11.26	
46	1262	829	17.82	11.84	
47	1717	1494	17.82	8.82	
48	2014	839	17.83	8.70	
49	646	856	17.84	9.58	
50	193	1994	17.86	10.95	
51	529	1370	17.87	9.32	
52	754	1385	17.87	10.65	
53	1200	1336	17.88	9.15	
54	1222	441	17.90	10.60	
55	984	975	17.90	11.41	
56	225	1569	17.93	10.27	
57	906	765	17.96	10.75	
58	1762	608	17.97	9.80	
59	1338	1637	18.00	7.90	
60	546	1029	18.02	9.36	
61	786	826	18.02	9.99	
62	99	871	18.05	10.31	
63	358	1798	18.06	12.75	
64	822	1534	18.09	9.63	
65	1010	1851	18.09	10.41	
66	2039	1163	18.10	12.57	
67	1056	965	18.12	8.98	
68	797	1410	18.14	8.86	
69	45	727	18.15	11.47	
70	572	1403	18.15	11.41	
71	1068	1418	18.16	9.90	
72	913	1314	18.16	9.85	
73	1146	1477	18.18	10.41	
74	1209	1579	18.20	9.54	
75	903	1888	18.20	7.61	
76	487	292	18.22	9.67	
77	1620	1546	18.24	8.78	
78	653	2044	18.29	9.76	
79	2016	876	18.34	10.90	
80	1250	1652	18.39	7.79	
81	1381	2102	18.39	9.79	
82	1786	1213	18.44	9.74	
83	723	1064	18.44	7.75	
84	1846	369	18.45	9.54	
85	327	718	18.46	9.67	
86	1162	1625	18.47	9.53	
87	1113	1544	18.49	10.78	
88	1197	1591	18.54	9.92	
89	629	292	18.55	10.62	
90	963	760	18.56	10.65	
91	1239	1742	18.56	9.12	
92	1079	1851	18.57	10.82	
93	995	1261	18.58	10.66	
94	1106	92	18.63	8.49	
95	1331	218	18.63	7.80	
96	482	1069	18.64	8.70	
97	750	1683	18.65	9.37	
98	1658	1595	18.66	10.01	
99	1378	1244	18.66	9.34	
100	1022	2043	18.68	9.27	
101	814	1126	18.69	9.19	
102	970	1615	18.69	9.77	
103	1128	351	18.70	9.34	
104	1450	175	18.73	9.44	
105	796	529	18.76	9.27	
106	1746	1720	18.76	10.19	
107	161	35	18.77	9.98	

GALAXY	X ARCSECS	Y	B_{27}	R_{27}	NOTES
108	327	1781	18.78	8.62	
109	1386	119	18.80	8.38	
110	1558	1650	18.81	7.65	
111	965	1796	18.84	7.07	
112	826	814	18.85	7.82	
113	1281	1370	18.86	8.98	
114	636	1465	18.87	8.98	
115	1816	1952	18.87	8.08	
116	1230	1076	18.88	7.50	
117	1279	1660	18.88	7.68	
118	1776	1408	18.89	9.63	
119	801	1474	18.92	7.60	
120	1274	1328	18.93	7.93	
121	2090	1059	18.95	8.08	
122	1326	2054	18.95	7.58	
123	1551	1296	18.96	8.01	
124	1438	29	18.97	7.10	
125	1292	579	18.97	8.19	
126	262	631	18.98	8.34	
127	1989	980	18.99	7.01	
128	368	581	19.00	8.08	
129	921	1814	19.01	7.54	
130	1316	604	19.02	7.14	
131	968	1049	19.02	7.79	
132	789	1168	19.02	7.58	
133	1140	319	19.03	7.58	
134	344	900	19.06	7.80	
135	1143	958	19.06	7.80	
136	443	1358	19.06	8.08	
137	767	1360	19.06	7.54	
138	1167	1848	19.06	7.57	
139	1250	1818	19.06	7.27	
140	1590	1049	19.07	7.04	
141	1638	1153	19.07	7.22	
142	1069	1192	19.08	8.22	
143	181	806	19.08	8.30	
144	557	1475	19.08	8.36	
145	739	1566	19.08	7.36	
146	577	1922	19.09	6.63	
147	735	57	19.10	6.41	
148	680	1315	19.14	7.27	
149	1232	45	19.14	7.04	
150	1465	1543	19.14	7.75	
151	1697	1543	19.15	7.45	
152	1017	1370	19.17	7.90	
153	34	1260	19.18	7.45	
154	1583	1252	19.22	8.16	
155	1851	457	19.23	8.16	
156	421	1130	19.23	7.91	
157	1425	1756	19.23	7.65	
158	468	1665	19.24	7.91	
159	2068	1623	19.24	7.65	
160	1578	2075	19.26	8.66	
161	1334	201	19.26	6.63	
162	735	1276	19.26	8.58	
163	656	1710	19.26	8.27	
164	1556	1019	19.28	7.23	
165	478	1281	19.28	6.16	
166	1677	1192	19.28	6.97	
167	1405	1955	19.28	7.75	
168	2056	930	19.30	7.14	
169	1475	34	19.31	7.82	
170	448	1496	19.31	7.40	
171	1818	497	19.33	6.78	
172	1049	1625	19.33	6.60	
173	624	937	19.36	7.01	
174	1403	1151	19.36	7.04	
175	1596	2115	19.37	8.04	
176	363	651	19.38	6.72	
177	596	1872	19.38	6.59	
178	222	1155	19.39	6.48	
179	715	1088	19.39	6.54	
180	1868	742	19.40	6.51	
181	1009	1173	19.40	6.12	
182	2029	744	19.42	6.91	
183	1193	295	19.43	6.57	
184	962	1413	19.43	8.23	
185	928	1229	19.44	8.58	
186	854	1851	19.44	7.58	
187	1863	1896	19.44	7.20	
188	1375	1314	19.46	7.20	
189	749	228	19.47	6.19	
190	386	1168	19.48	6.19	
191	908	1113	19.48	7.47	
192	2066	1499	19.49	7.13	
193	952	1880	19.49	6.99	
194	478	613	19.50	5.99	
195	963	668	19.50	7.58	
196	159	962	19.50	7.34	
197	685	1026	19.50	7.47	
198	482	324	19.51	7.75	
199	2091	111	19.52	6.85	
200	18	1418	19.52	7.34	
201	1816	1449	19.52	7.36	
202	1220	1415	19.54	8.01	
203	1583	1207	19.54	6.10	
204	754	905	19.55	6.10	
205	1699	1585	19.55	6.04	
206	1015	1282	19.56	8.12	
207	1902	2080	19.57	6.91	
208	514	932	19.58	6.57	
209	1497	1501	19.58	6.27	
210	618	1630	19.60	7.91	
211	1207	658	19.61	7.54	
212	144	1375	19.61	8.94	
213	584	1146	19.61	7.10	
214	984	327	19.63	7.20	
215	1336	452	19.63	6.72	

2354-35 (cont)

GALAXY	X ARCSECS	Y	B_{27}	R_{27}	NOTES
216	1338	198	19.64	6.51	
217	2011	920	19.64	5.51	
218	1062	1297	19.64	8.19	
219	2053	1462	19.64	6.94	
220	1106	1078	19.65	7.72	
221	2088	423	19.66	6.45	
222	60	948	19.66	6.05	
223	683	1052	19.66	6.05	
224	2110	1155	19.66	6.01	
225	937	1180	19.67	8.58	
226	1219	329	19.68	7.30	
227	1699	1398	19.69	6.24	
228	821	969	19.70	6.54	
229	35	720	19.70	6.10	
230	584	1065	19.70	7.10	
231	149	426	19.75	8.27	
232	1242	319	19.77	6.48	
233	1365	722	19.77	5.99	
234	1437	547	19.77	5.91	
235	185	1575	19.77	5.80	
236	1146	1556	19.77	6.07	
237	1402	148	19.78	6.51	
238	1299	1512	19.78	6.27	
239	2056	568	19.79	8.25	
240	1729	1779	19.80	7.54	
241	938	220	19.81	6.30	
242	1329	1585	19.81	5.96	
243	344	2006	19.81	6.55	
244	1178	1205	19.82	6.16	
245	1925	1954	19.83	6.54	
246	1501	170	19.84	7.01	
247	1569	1096	19.84	6.27	
248	45	1715	19.84	5.83	
249	327	1491	19.85	5.69	
250	1002	1106	19.86	6.50	
251	1192	92	19.87	9.54	
252	1450	151	19.87	6.75	
253	874	1355	19.87	7.17	
254	839	1559	19.87	6.69	
255	2053	1613	19.87	6.16	
256	984	1640	19.88	5.69	
257	1410	389	19.89	6.81	
258	1250	2078	19.90	5.77	
259	232	352	19.91	6.60	
260	1146	509	19.91	6.42	
261	1118	901	19.91	6.88	
262	1316	1291	19.91	5.69	
263	727	1748	19.91	7.17	
264	1170	1722	19.92	6.57	
265	450	17	19.93	6.21	
266	96	572	19.93	5.62	
267	470	559	19.93	6.05	
268	1351	1704	19.93	6.09	
269	1000	438	19.94	8.04	

GALAXY	X ARCSECS	Y	B_{27}	R_{27}	NOTES
270	1230	589	19.94	5.46	
271	742	1267	19.94	5.83	
272	915	1361	19.94	6.36	
273	1376	1237	19.94	4.94	
274	846	1464	19.94	6.05	
275	1491	1880	19.94	6.94	
276	2001	1088	19.95	5.44	
277	829	595	19.96	6.51	
278	331	1966	19.96	5.94	
279	1658	2070	19.97	5.91	
280	1193	1924	19.97	6.21	
281	1239	1668	19.98	6.05	
282	1677	1815	19.98	5.75	
283	1756	168	19.99	6.02	
284	30	1160	19.99	6.69	

GALAXY	X ARCSECS	Y	H_{27}	R_{27}	NOTES
1	0	0	16.94	24.07	x
2	-82	23	18.25	15.61	
3	220	-81	18.42	10.90	
4	-321	-75	18.45	10.62	
5	-130	56	18.46	11.52	
6	-9	-140	18.80	10.41	
7	-30	-209	18.97	9.49	
8	-221	-127	19.02	9.19	
9	184	-22	19.02	8.70	
10	-12	-22	19.06	9.14	
11	-102	-397	19.13	7.40	
12	-320	284	19.34	7.10	
13	-365	256	19.36	6.19	
14	-313	-357	19.38	6.12	
15	2	-51	19.39	8.12	
16	-299	-100	19.40	6.80	
17	-227	-294	19.45	6.99	
18	-93	-348	19.45	7.12	
19	60	-332	19.45	7.40	
20	170	57	19.46	7.10	
21	352	-234	19.53	7.01	
22	-375	301	19.54	7.61	
23	-71	-61	19.55	7.10	
24	-121	-18	19.56	7.01	
25	-95	130	19.59	6.19	
26	-11	253	19.59	7.01	
27	-228	62	19.62	6.60	
28	-363	-192	19.63	7.10	
29	-49	-268	19.66	6.01	
30	-265	-158	19.66	6.51	
31	-246	76	19.66	7.30	
32	-382	-195	19.66	6.91	
33	-63	34	19.66	7.61	
34	67	-186	19.66	7.61	
35	-330	40	19.69	6.80	
36	142	120	19.69	6.10	
37	40	9	19.70	7.10	
38	27	-261	19.71	6.51	
39	-230	-3	19.74	6.39	
40	-264	65	19.75	6.51	
41	289	-71	19.75	7.01	
42	113	-375	19.76	6.91	
43	-236	43	19.79	6.51	
44	361	185	19.79	6.39	
45	-115	-118	19.82	6.91	
46	162	80	19.84	6.10	
47	353	58	19.84	6.10	
48	134	147	19.85	6.19	
49	266	54	19.90	6.60	
50	15	-2	19.93	6.69	
51	-227	145	19.98	5.69	
52	-7	97	19.98	5.69	
53	64	-14	19.99	6.10	
54	259	357	20.00	6.10	
55	394	221	20.00	6.39	
56	401	-121	20.00	6.91	
57	-59	38	20.00	6.69	
58	168	-127	20.00	6.91	
59	257	-38	20.00	6.30	
60	271	122	20.00	5.99	
61	72	205	20.00	6.30	
62	24	-161	20.00	5.59	
63	63	-174	20.00	5.19	
64	-408	-400	20.00	5.61	
65	-23	-27	20.00	6.19	
66	-332	-186	20.00	6.10	
67	325	-284	20.00	6.39	
68	188	-314	20.00	5.91	
69	-342	-143	20.00	5.21	
70	-301	-380	20.00	5.10	
71	104	-2	20.00	5.91	
72	35	-193	20.00	5.91	
73	140	-34	20.00	5.19	
74	285	-36	20.00	5.69	
75	-227	-279	20.00	5.39	
76	-102	-79	20.00	5.49	
77	18	321	20.00	5.10	
78	-106	-124	20.00	6.10	
79	338	-54	20.00	6.19	
80	-257	-254	20.00	5.29	
81	-165	-178	20.00	5.10	
82	386	107	20.00	5.99	
83	-46	203	20.00	5.99	
84	-301	-93	20.00	6.30	
85	-296	149	20.00	5.99	
86	-192	-246	20.00	5.99	
87	-315	-371	20.00	5.99	
88	-151	164	20.00	5.99	
89	19	-162	20.00	6.80	
90	127	82	20.00	5.49	
91	-2	121	20.00	5.99	
92	-120	-282	20.00	5.49	
93	-115	-71	20.00	5.99	
94	-202	-247	20.00	5.99	
95	-184	124	20.00	5.99	
96	-60	53	20.00	5.99	
97	44	-218	20.00	5.69	
98	80	-145	20.00	6.60	
99	100	-172	20.00	6.60	
100	-232	53	20.00	6.22	
101	-80	-55	20.00	6.22	
102	158	-230	20.00	6.22	
103	-282	-342	20.00	5.99	
104	111	-42	20.00	6.69	
105	378	-203	20.00	6.69	
106	-296	-322	20.00	6.69	
107	-147	-65	20.00	6.69	

GALAXY	X ARCSECS	Y ARCSECS	B_{27}	R_{27}	NOTES
108	-366	-270	20.68	4.50	
109	-144	185	20.68	4.61	
110	-62	70	20.69	4.69	
111	58	85	20.70	4.50	
112	-166	248	20.73	5.01	
113	-373	-302	20.74	4.80	
114	305	80	20.74	4.50	
115	-283	-141	20.75	4.30	
116	386	176	20.76	5.01	
117	-361	-314	20.77	4.61	
118	-188	-16	20.77	4.89	
119	138	-322	20.77	4.30	
120	223	-103	20.79	4.61	
121	-382	-137	20.80	4.69	
122	-346	145	20.83	4.30	
123	-240	-67	20.85	4.69	
124	-2	-158	20.85	4.50	
125	-345	-167	20.86	4.40	
126	-58	-6	20.86	4.61	
127	-79	-175	20.87	4.40	
128	80	20	20.87	4.80	
129	184	-148	20.87	4.30	
130	-330	-10	20.88	4.30	
131	359	-129	20.92	4.40	
132	134	263	20.96	4.40	
133	271	197	20.97	4.50	
134	386	-214	20.97	4.50	
135	225	-284	20.99	4.69	
136	-386	356	20.99	4.50	
137	-2	-276	20.99	4.50	
138	-5	291	21.00	4.69	
139	216	124	21.00	4.50	
140	43	-88	21.03	4.40	
141	355	-168	21.03	4.30	
142	-82	-23	21.05	4.11	
143	-5	63	21.06	4.30	
144	-291	-7	21.06	4.61	
145	-34	-218	21.06	4.50	
146	82	97	21.08	4.40	
147	-138	-110	21.09	4.61	
148	316	-197	21.10	4.30	
149	-278	41	21.11	4.69	
150	55	-44	21.13	4.69	
151	-19	7	21.14	4.20	
152	32	-19	21.15	4.11	
153	-122	237	21.16	4.50	
154	97	22	21.16	3.49	
155	-96	124	21.17	4.30	
156	-274	-244	21.19	4.30	
157	-284	130	21.20	4.20	
158	82	-137	21.20	5.10	
159	352	-110	21.21	4.40	
160	93	-27	21.21	4.20	
161	392	93			

GALAXY	X ARCSECS	Y ARCSECS	B_{27}	R_{27}	NOTES
162	339	25	21.22	4.61	
163	-170	125	21.23	3.99	
164	337	-38	21.24	5.01	
165	287	344	21.25	4.69	
166	217	54	21.26	4.30	
167	317	-282	21.26	4.40	
168	242	-361	21.27	4.50	
169	-59	-201	21.28	3.99	
170	-181	-50	21.30	3.80	
171	-138	-271	21.33	3.99	
172	35	-292	21.33	3.80	
173	405	-536	21.35	4.50	
174	72	40	21.36	3.99	
175	307	12	21.37	3.99	
176	-111	-410	21.39	4.50	
177	41	-231	21.39	3.99	
178	-226	-310	21.40	3.80	
179	-238	-134	21.42	4.69	
180	11	-122	21.43	3.99	
181	19	172	21.43	3.99	
182	132	-144	21.44	3.99	
183	172	-156	21.44	4.50	
184	-230	-313	21.44	3.69	
185	325	231	21.45	3.99	
186	240	192	21.45	5.19	
187	-351	-307	21.48	3.70	
188	-43	-56	21.48	4.61	
189	-339	149	21.49	3.99	
190	-197	153	21.49	4.11	
191	-89	266	21.49	4.50	
192	-23	-95	21.49	4.50	
193	237	-255	21.49	3.99	
194	356	-300	21.53	3.99	
195	-110	-110	21.53	4.11	
196	-4	-100	21.56	4.11	
197	-37	-5	21.56	4.50	
198	-31	-188	21.56	3.80	
199	309	1	21.57	4.50	
200	-287	-357	21.58	3.99	
201	-323	-519	21.59	3.99	
202	-148	41	21.59	4.50	
203	149	108	21.60	3.99	
204	-328	68	21.60	4.50	
205	114	371	21.60	3.99	
206	196	171	21.60	4.50	
207	320	-63	21.61	3.99	
208	31	-189	21.61	3.99	
209	54	-336	21.61	4.50	
210	54	30	21.63	3.99	
211	6	145	21.64	4.50	
212	165	310	21.66	4.50	
213	6	124	21.67	3.99	
214	-184	50	21.68	4.50	
215	-33	-320	21.70	3.99	

GALAXY	X ARCSECS	Y	B_{27}	R_{27}	NOTES
216	-15	-125	21.73	4.11	
217	-325	-252	21.76	3.31	
218	-248	-292	21.76	3.69	
219	-244	-261	21.76	3.40	
220	181	-62	21.76	3.49	
221	9	117	21.77	3.40	
222	56	71	21.78	3.49	
223	88	-103	21.78	3.59	
224	386	-40	21.79	3.40	
225	-133	-391	21.80	3.80	
226	-17	-54	21.81	3.90	
227	-352	-389	21.82	3.49	
228	-213	-156	21.82	3.40	
229	-399	-261	21.83	3.40	
230	-50	-322	21.84	3.99	
231	-83	-50	21.89	3.31	
232	354	-275	21.89	3.69	
233	49	285	21.90	3.59	
234	-162	-12	21.91	3.49	
235	27	-83	21.92	3.31	
236	-56	201	21.93	3.40	
237	-122	113	21.94	3.40	
238	-10	6	21.94	3.20	
239	123	-341	21.94	3.31	
240	-263	-198	21.95	3.40	
241	244	28	21.97	3.31	
242	80	-82	21.98	3.49	
243	-365	-398	21.99	3.49	
244	215	60	21.99	3.31	
245	-98	-143	22.00	3.40	
246	19	115	22.00	3.40	
247	-100	20	22.00	3.69	
248	104	331	22.01	3.59	
249	-127	-204	22.02	3.59	
250	-248	-237	22.04	3.00	
251	-84	89	22.04	3.31	
252	-51	9	22.09	3.80	
253	-249	-214	22.10	3.19	
254	-349	-127	22.11	3.20	
255	346	-15	22.11	3.40	
256	-408	38	22.12	3.00	
257	-99	102	22.12	3.00	
258	92	-302	22.12	3.00	
259	-23	-249	22.13	3.20	
260	147	328	22.14	3.20	
261	-13	-195	22.16	3.20	
262	27	-95	22.17	3.49	
263	-154	287	22.18	3.00	
264	-67	42	22.18	3.00	
265	-36	94	22.19	3.00	
266	6	139	22.19	3.00	
267	15	-11	22.20	3.00	
268	-196	-212	22.24	3.20	
269	-186	-366	22.24	3.10	
270	-73	2	22.24	3.31	
271	71	-184	22.24	2.89	
272	-326	-21	22.25	3.00	
273	-52	285	22.25	3.20	
274	-407	154	22.27	3.00	
275	75	-387	22.27	3.10	
276	-273	125	22.29	2.89	
277	-356	-409	22.30	3.00	
278	405	286	22.30	3.40	
279	32	32	22.31	3.31	
280	-68	214	22.32	3.31	
281	22	292	22.32	3.20	
282	136	171	22.33	3.00	
283	-214	-65	22.33	3.20	
284	105	284	22.33	2.80	
285	300	23	22.35	2.69	
286	-263	-333	22.37	3.49	
287	307	281	22.37	3.10	
288	-299	-207	22.38	3.00	
289	99	76	22.38	3.00	
290	206	-189	22.38	3.10	
291	258	-137	22.38	3.20	
292	218	148	22.39	3.00	
293	-175	220	22.43	3.00	
294	300	-295	22.45	3.51	
295	-132	-378	22.45	3.49	
296	28	11	22.50	2.80	
297	-62	-64	22.51	2.70	
298	-244	33	22.53	3.10	
299	-362	-171	22.54	2.80	
300	-136	-77	22.54	3.10	
301	73	-14	22.54	2.60	
302	-195	-5	22.55	2.70	
303	-313	88	22.56	3.10	
304	-331	239	22.57	2.89	
305	-30	-4	22.59	2.19	
306	137	-172	22.59	2.60	
307	204	-149	22.59	2.70	
308	233	214	22.59	2.99	
309	64	-348	22.60	2.80	
310	45	136	22.61	2.10	
311	-328	210	22.64	2.70	
312	135	-6	22.64	3.00	
313	343	-184	22.65	2.80	
314	383	-7	22.65	2.89	
315	-324	269	22.66	2.89	
316	78	88	22.66	2.70	
317	15	-36	22.67	2.70	
318	340	-90	22.67	2.79	
319	272	281	22.69	2.89	
320	321	266	22.69	2.89	
321	214	-159	22.70	2.89	
322	209	247	22.71	2.70	
323	-257	-287	22.72	2.80	

GALAXY	X ARCSECS	Y ARCSECS	R_{27}	R_{27}	NOTES
324	339	266	22.72	3.40	
325	90	238	22.73	2.80	
326	-274	-281	22.74	2.60	
327	-253	-209	22.74	2.19	
328	-75	-8	22.74	2.80	
329	388	235	22.75	2.70	
330	163	-56	22.75	2.60	
331	-59	412	22.77	2.60	
332	-11	192	22.77	2.70	
333	37	-383	22.77	2.70	
334	228	-212	22.78	2.70	
335	-36	-44	22.79	3.00	
336	168	27	22.80	2.80	
337	-134	-88	22.81	2.60	
338	-88	195	22.82	2.70	
339	-76	146	22.82	2.70	
340	-320	-377	22.83	2.50	
341	45	-199	22.84	2.60	
342	-100	133	22.86	2.10	
343	34	-119	22.86	2.60	
344	94	89	22.86	3.00	
345	-42	279	22.89	2.40	
346	251	394	22.91	2.80	
347	302	-373	22.91	2.60	
348	-261	93	22.91	2.00	
349	-375	-155	22.93	2.50	
350	-145	-71	22.93	2.50	
351	-25	15	22.93	2.60	
352	54	-29	22.95	3.10	
353	399	-19	22.95	2.70	
354	40	63	22.95	2.50	
355	-4	-261	22.96	2.80	
356	140	337	22.96	2.70	
357	-196	63	22.97	2.60	
358	-233	-194	22.98	2.70	
359	408	-279	22.99	2.50	
360	254	273	23.01	2.50	
361	213	137	23.03	2.40	
362	343	95	23.03	2.70	
363	-323	132	23.03	2.60	
364	-184	-59	23.05	2.50	
365	-343	-124	23.06	2.40	
366	-97	210	23.06	2.50	
367	145	-102	23.07	2.50	
368	382	102	23.07	2.10	
369	-58	22	23.08	2.50	
370	2	-71	23.09	2.89	
371	-393	-151	23.10	2.50	
372	41	-156	23.10	2.70	
373	153	16	23.10	2.40	
374	175	-153	23.10	2.50	
375	54	152	23.11	2.00	
376	-360	-2	23.12	2.70	
377	-273	1	23.12	2.40	
378	-339	24	23.13	2.30	
379	-289	-126	23.13	2.60	
380	-339	86	23.14	2.30	
381	391	-349	23.14	2.60	
382	-251	-166	23.17	2.40	
383	-204	45	23.18	2.40	
384	-282	-184	23.19	2.50	
385	221	119	23.19	2.30	
386	-41	26	23.21	2.60	
387	-112	-308	23.24	2.40	
388	19	-376	23.25	2.50	
389	152	170	23.25	2.40	
390	158	266	23.31	2.50	
391	-360	2	23.33	2.50	
392	-41	-46	23.33	2.50	
393	-104	326	23.37	2.50	
394	-15	201	23.38	2.50	
395	136	11	23.38	2.19	
396	141	1	23.38	2.40	
397	-15	178	23.47	2.19	
398	2	-129	23.47	2.00	

Appendix V: Photoelectric Photometry Results

This Appendix contains the results of photoelectric photometry with the 40" and 74" telescopes at Sutherland. The equipment, observing techniques and reduction procedures are described in Chapter 6.

The columns are:

Type — Taken from RCBG2 where possible; otherwise estimated from Schmidt plates.

cz — The heliocentric velocity in km/s. Values are taken from RCBG2, except I5353 and 2354-35cD which are from App. I.

Tel. — The telescope used in the observations.

Ap. — The aperture diameter in arcsecs.

V, B-V, V-R and R-I — B and V are the standard bands, R and I are in the Cape-Kron system (see Chap. 6). Errors are:
in V 0.04, in B-V 0.02, in V-R 0.03 and in V-I 0.04
Where the results are given in parentheses, the errors may be up to twice these values.

Other Sources — The references are as follows:

A76: Alcaino 1976
WW69: Westerlund & Wall 1969
BP76: Bucknell & Peach 1976
W79: Wegner 1979

	Type	cz km/s	Tel.	Ap. arcsec	V	B-V	V-R	R-I	Other Sources
N1031	L		40"	28.3	13.39	1.01	0.61	1.21	
				40.1	13.13	0.97	0.60	1.24	
				56.2	12.94	0.93	0.59	1.20	
				79.7	12.75	0.92	0.54	1.15	
N1079	L	2252	40"	28.3	12.61	0.95	0.59	1.19	RCBG2
				40.1	12.30	0.94	0.58	1.18	BP76
				56.2	12.03	0.92	0.58	1.14	
				79.7	11.79	0.91	0.55	1.09	
N1097	S	1320	40"	21.7	(11.55)	0.81	0.64	1.23	RCBG2
				30.7	(11.23)	0.81	0.63	1.24	BP76
				43.0	(10.98)	0.84	0.62	1.24	A76, W79
N1387	L	1239	40"	19.6	12.05	1.03	0.63	1.33	
				28.3	11.79	1.01	0.64	1.31	
				40.1	11.58	0.99	0.63	1.30	
				56.2	11.40	1.01	0.63	1.30	
				79.7	11.24	1.03	0.64	1.30	
N1533	L	773	40"	19.6	12.20	1.00	0.62	1.25	RCBG2
				28.3	11.96	1.00	0.62	1.24	W79
				40.1	11.76	0.99	0.61	1.23	
				56.2	11.55	1.00	0.60	1.22	
				79.7	11.30	1.03	0.61	1.22	
N1543	L	1400	40"	28.3	(11.85)	1.00	0.60	1.20	RCBG2
				56.2	(11.32)	0.97	0.60	1.23	
				79.7	(11.14)	0.96	0.57	1.17	
N3268	E	2761	74"	12.0	13.21	0.96	0.71	1.32	RCBG2
				27.0	12.89	1.07	0.71	1.29	
				30.0	12.80	1.04	0.71	1.30	
				36.0	12.69	1.05	0.70	1.31	
				48.0	12.46	1.05	0.70	1.29	
				60.0	12.32	1.05	0.69	1.28	

	Type	cz km/s	Tel.	Ap. arcsec	V	B-V	V-R	R-I	Other Sources
N5968	S		74"	12.0	14.23	1.04	0.70	1.23	W79
				27.0	13.78	1.07	0.62	1.16	
				30.0	13.62	1.05	0.67	1.21	
				36.0	13.48	0.99	0.64	1.14	
				48.0	13.06	0.97	0.61	1.17	
				60.0	12.83	0.95	0.65	1.14	
N6942	L		40"	19.6	13.43	1.01	0.61	1.24	W79
				28.3	13.12	1.00	0.61	1.20	
				40.1	12.79	1.00	0.57	1.14	
				56.2	12.51	0.95	0.55	1.09	
				79.7	12.25	0.92	0.55	1.13	
N7125	S	3012	40"	40.1	13.88	0.54	0.42	(0.86)	W79, BP76
N7126	S		40"	21.7	(13.43)	0.79	0.58	1.18	W79
				28.3	13.26	0.76	0.57	1.15	BP76
				40.1	13.00	0.74	0.58	1.17	
				43.0	(12.92)	0.75	0.58	1.18	
				56.2	12.83	0.73	0.60	1.24	
N7412	S	1705	40"	19.6	14.09	0.78	0.55	(1.15)	RCBG2
				28.3	13.55	0.76	0.53	(1.11)	W79
				40.1	13.10	0.72	0.51	1.04	BP76
				56.2	12.61	0.67	0.50	0.92	
				79.9	12.07	0.61	0.41	0.81	
N7755	S	2923	40"	19.6	13.49	0.89	0.61	1.21	RCBG2
				28.3	13.19	0.90	0.60	1.19	W79
				40.1	12.86	0.84	0.59	1.17	BP76
				56.2	12.51	0.79	0.64	1.31	
				79.7	12.24	0.74	0.70	1.50	
N7793	S	209	40"	21.7	(13.16)	0.61	0.49	0.98	RCBG2
				28.3	12.86	0.62	0.47	0.94	W79
				30.7	(12.67)	0.64	0.49	0.98	BP76
				40.1	12.31	0.64	0.48	0.98	A76
				43.0	(12.13)	0.65	0.49	0.99	
				56.2	11.76	0.63	0.46	0.92	
				79.7	11.24	0.59	0.44	0.88	

	Type	cz km/s	Tel.	Ap. arcsec	V	B-V	V-R	R-I	Other Sources
I1954	S		40"	28.3	13.26	0.58	0.47	0.90	BP76
				40.1	12.77	0.57	0.45	0.89	
				56.2	12.28	0.56	0.45	0.87	
				79.7	11.95	0.54	0.40	0.81	
I2056	S	1089	40"	19.6	12.87	0.57	0.47	0.94	
				40.1	12.20	0.56	0.48	0.95	
				79.7	11.97	0.57	0.49	1.05	
I4296	E	3629	74"	12.0	12.55	1.02	0.66	1.20	RCBG2
				27.0	12.16	1.06	0.59	1.11	W79
				30.0	12.11	1.01	0.65	1.19	
				36.0	11.98	0.93	0.71	1.24	
				48.0	11.76	0.99	0.63	1.14	
				60.0	11.61	0.99	0.59	1.14	
I4329	L/E	4416	74"	12.0	13.38	1.01	0.67	1.19	RCBG2
				27.0	13.03	1.05	0.67	1.19	BP76
				30.0	12.90	1.03	0.66	1.19	
				36.0	12.75	1.03	0.63	1.15	
				48.0	12.47	1.04	0.63	1.13	
				60.0	12.33	1.02	0.66	1.12	
I5020	L?		40"	19.6	13.86	0.94	0.59	(1.23)	
				28.3	13.40	0.90	0.57	1.17	
				40.1	13.01	0.81	0.54	1.10	
				56.2	12.87	0.79	0.52	0.95	
				79.7	12.72	0.79	0.47	0.81	
I5353	E	8080	40"	19.6	14.09	1.03	0.58	(1.20)	
				28.3	13.79	1.02	0.56	(1.16)	
				40.1	13.55	1.00	0.57	(1.16)	
				56.2	13.35	0.99	0.57	(1.22)	
				79.7	13.15	0.96	0.56	(1.21)	
2354-35	cD	14600	40"	19.6	14.58	1.12	0.67	(1.33)	WW69
				28.3	14.14	1.13	0.64	(1.27)	
				40.1	13.83	1.12	0.63	(1.24)	
				56.2	13.50	1.11	0.63	(1.19)	
				79.7	13.26	1.07	0.64	(1.32)	

Appendix VI: Cluster Data

	K44	S40/6	2354-35	A1146	Notes
R.A.) (1950)	$23^h44^m59^s.3$	$4^h30^m32^s.9$	$23^h54^m27^s$		Chap. 2
dec.)	$-28^\circ24'10''$	$-61^\circ33'26''$	$-35^\circ02!2$		
b^{II}	-76°	-40°	-76°	-33°	
BM type		I (cD)	I (cD)	I (cD)	
Richness	(1)	(3)	(1)	4	Estimates in parentheses
z	.0278	.0603	.0487	.137	Table 5.3
1 arcsec	0.766kpc	1.560kpc	1.288kpc	3.083kpc	Scale at cluster
0.92 Mpc	1202 arcsec	590 arcsec	714 arcsec	298 arcsec	
N_{-19}	47	105	51	95	
$M^*_{B_{27}}$	-19.3	-19.6	-19.6	-19.9	
L_x (log W)	37.06	38.21	<37.5		Table 9.1
X source	2A2344-285	2A0430-615 =4U0427-61			Chap. 2
S km/s	775	1720	894		Table 5.3
$S_{el.}$ km/s	427	1289	425		" "

Notes:

z The heliocentric redshift adopted for the cluster. The value for S40/6, A1146 and 2354-35 is that of the cD galaxies in those clusters. The value for K44 is the mean of the redshifts of the 8 galaxies within 200kpc of the centre.

N_{-19} The number of galaxies, after correction for non-members, with $M_{B_{27}} \leq -19$ and within 0.92mpc of the cluster centre.

$M^*_{B_{27}}$ The magnitude of Abell's "knee" (Chap. 8). Eye estimate.

References

The following non-standard abbreviations are used:-

M.N. = Monthly Notices of the Royal Astronomical Society
A.&A. = Astronomy & Astrophysics
A.J. = Astronomical Journal
Ap.J. = Astrophysical Journal
P.A.S.P. = Publications of the Astronomical Society of the Pacific
Mem. = Memoirs of the Royal Astronomical Society
A.Nach. = Astronomische Nachrichten

Abell G O 1958 Ap.J.Supp. 3 211
--------- 1962 IAU Symp. 15 213
--------- 1965 Ann. Rev. Astron. & Ap. 3 1
--------- 1975 p601 in Sandage et al (1975)
Albert C E, White R A & Morgan W W 1977 Ap.J. 211 309
Alcaino G 1974 A.&A.Supp. 13 305
--------- 1976 A.&A.Supp. 26 261
Allen C W 1973 "Astrophysical Quantities" (Univ. London, Athlone Press)
Allen D A, Longmore A J, Hawarden T G, Cannon R D. & Allen C J
1978 M.N. 184 303
Austin T B & Peach J V 1974a M.N. 167 437
---------- 1974b M.N. 168 591
Avni Y & Bahcall N A 1976 Ap.J. 209 16

Baade W 1928 A.Nach 233 67
Bahcall N A 1974 Ap.J. 193 529
---------- 1977a Ann. Rev. Astron. & Ap. 15 505
---------- 1977b Ap.J. 217 L77
---------- 1977c Ap.J. 218 L93
Baker E A 1957 J. Phot. Sci. 5 94
Balkowski C, Bottinelli L, Gouguenheim L & Heidmann J 1972 A.&.A. 21 303
Bautz L P & Morgan W W 1970 Ap.J. 162 L149
Binney J 1977 M.N. 181 735
-------- 1978 M.N. 183 501
Bolton J G & Ekers J 1966 Austral. J. Phys. 19 559

Braid M K & MacGillivray H T 1978 M.N. 182 241
Brecher K & Burbidge G R 1972 Nature 237 440
Bucknell M J 1977 D.Phil. thesis Univ. Oxford
Bucknell M J, Godwin J G & Peach J V 1979 M.N. (submitted)
Bucknell M J & Peach J V 1976 Observatory 96 61
Burbidge G R & Burbidge E M 1959 Ap.J. 130 629
Butcher H & Oemler A 1978 Ap.J. 226 559

Cannon R D, Hawarden T G, Sim M E, Tritton S B 1978 Occ. Rep. Royal Obs. Edinburgh 4: "The UK 1.2m Schmidt Telescope and the Southern Sky Survey. II - Photographic Techniques"
Carter D 1978 M.N. 182 797
Carter D & Dixon K L 1978 A.J. 83 574
Carter D & Godwin J G 1979 M.N. (accepted)
Carter D & Metcalfe N 1979 in preparation
Chandrasekhar S 1943 Ap.J. 97 255
Chincarini G & Rood H J 1971 Ap.J. 168 321
---------- 1977 Ap.J. 214 351
Chincarini G, Tarenghi M & Bettis C 1978 Ap.J. 221 34
Clark B G 1973 Proc. I.E.E.E. 61 1654
Coleman G D, Hintzen P, Scott J S & Tarenghi M 1976 Nature 262 476
Cooke B.A, Ricketts M J, Maccacaro T, Pye J P, Elvis M, Watson M G, Griffiths R E, Pounds K A, McHardy I, Maccagni D, Seward F D, Page C G & Turner M J L 1978 M.N. 182 489 (2A Catalogue)
Cousins A W J 1973 Mem. 77 223
---------- 1974 Mon. Not. Astr. Soc. S. Africa 33 149
Cowie L L & Binney 1977 Ap.J. 215 723

Davis M & Peebles P J E 1977 Ap.J.Supp. 34 425
de Vaucouleurs G 1959 Handbuch der Physik 53 311
---------- 1968 Applied Optics 7 1513
---------- 1977 Occ. Rep. Royal Obs. Edinburgh 2: "Topics in Extragalactic Astronomy"
de Vaucouleurs G & de Vaucouleurs A 1964 "Reference Catalogue of Bright Galaxies" (Univ. Texas, Austin)
---------- 1972 Mem. 77 1
de Vaucouleurs G, de Vaucouleurs A & Corwin H G 1976 "Second Reference Catalogue of Bright Galaxies" (Univ. Texas, Austin)

de Vaucouleurs G & Malik G M 1969 M.N. 142 387
De Young D S 1978 Ap.J. 223 47
Dickens R J & Moss C 1976 M.N. 174 47
Doroshkevich A G, Shandarin S F & Saar E 1978 M.N. 184 643
Dressler A 1976 Ph.D. thesis Univ. California, Santa Cruz
---------- 1978a Ap.J. 223 765
---------- 1978b Ap.J. 226 55
Dreyer J L E 1888 Mem. 49 1
---------- 1910 Mem. 59 105
Duus A & Newell B 1977 Ap.J.Supp. 35 209

Ekers R D & Ekers J A 1973 A.&A. 24 247

Faber S M, Burstein D & Dressler A 1977 A.J. 82 941
Faber S M & Dressler A 1977 A.J. 82 187
Faber S M & Jackson R E 1976 Ap.J. 204 668
Felten J E & Morrison P 1966 Ap.J. 146 686
Finlay E A & Jones B B 1973 Austral. J. Phys. 26 389
Forman W, Jones C, Cominsky L, Julien P, Murray S, Peters G,
Tananbaum H & Giacconi R 1978 Ap.J.Supp. 38 (4U Catalogue)

Gallagher J S & Ostriker J P 1972 A.J. 77 288
Geller M J & Peebles P J E 1976 Ap.J. 206 939
Giacconi R, Murray S, Gursky H, Kellogg E, Schreier E, Matilsky T,
Koch D & Tananbaum H 1974 Ap.J.Supp. 27 37 (3U Catalogue)
Giacconi R, Murray S, Gursky H, Kellogg E, Schreier E &
Tananbaum H 1972 Ap.J. 178 281 (2U Catalogue)
Godwin J G 1976 D.Phil. thesis Univ. Oxford
---------- 1977 Rep. Dept. Astrophysics Univ. Oxford 1
Godwin J G & Peach J V 1977 M.N. 181 323
---------- 1979a Nature (accepted)
---------- 1979b M.N. (submitted)
Gollnow H 1961 M.N. 123 391
Gott J R & Turner E L 1977 Ap.J. 213 309
Gregory S A & Thompson L A 1978 Ap.J. 222 784

Gregory S A & Tifft W G 1976 Ap.J. 206 934

Groth E J & Peebles P J E 1977 Ap.J. 217 385

Gull S F & Northover K J E 1975 M.N. 173 585

Gunn J E & Gott J R 1972 Ap.J. 176 1

Gursky H & Schwartz D A 1977 Ann. Rev. Astron. & Ap. 15 541

Hausman M A & Ostriker J P 1978 Ap.J. 224 320

Hintzen P, Scott J S & Tarenghi M 1977 Ap.J. 212 8

Hoffman A W & Crane P 1977 Ap.J. 215 379

Holmberg E 1950 Lund Obs. Medd. II 128

---------- 1958 Lund Obs. Medd. II 136

---------- 1969 Archiv för Astronomi 5 305

---------- 1975 p123 in Sandage et al 1975

Holmberg E, Lauberts A, Schuster H-E, West R M 1975 A.&A.Supp. 22 327

Honeycutt R K & Chaldu R S 1970 A.A.S. Photo-Bulletin 2 14

Hooley T 1978 Observatory 98 105 (Report of 21st Herstmonceux Conference)

Howe H A 1899 M.N. 60 130

Hubble E 1936 Ap.J. 84 158

Humason M L, Mayall N U & Sandage A R 1956 A.J. 61 97

Jôeveer M, Einasto J & Tago E 1978 M.N. 185 357

Johnson H L & Morgan W W 1951 Ap.J. 114 522

Jones C & Forman W 1978 Ap.J. 224 1

Jones J E & Jones B J T 1978 M.N. 184 327

Jones W B, Gallet R M, Obitts D L & de Vaucouleurs G 1967 Pub. Dept. Astr. Univ. Texas Ser. II Vol I No. 8

Karachentsev I D & Kopylov A I 1977 Soviet Astr. Letts. 3 130

Katz J I 1976 Ap.J. 207 25

Kellogg E, Murray S, Giacconi R, Tananbaum H & Gursky H 1973 1973 Ap.J. 185 L13

Kiang T 1961 M.N. 122 263

King I R 1966 A.J. 71 64

Klemola A R 1969 A.J. 74 804

Lea S M 1977 Highlights of Astronomy 4 329
Lea S M & Holdman G D 1978 Ap.J. 222 29
Leir A A & van den Bergh S 1977 AP.J.Supp. 34 381
Lindegren L & Dravins D 1978 A.&A. 67 241
Lynden-Bell D 1967 M.N. 136 101

MCG = Vorontsov-Velyaminov B A et al 1962-8
Maccacaro T, Cooke B A, Ward M J, Penston M V & Haynes R F 1977 M.N. 180 465
Maccagni D, Tarenghi M, Cooke B A & Maccacaro T, Pye J P, Ricketts M J & Chincarini G 1978 A.&A. 62 127
MacGillivray H T, Martin R, Pratt N M, Reddish V C, Seddon H, Alexander Alexander L W G, Walker G S & Williams P R 1976 M.N. 176 265
McHardy I 1978 M.N. 184 783
Malina R F, Lea S M, Lampton M & Bowyer C S 1978 Ap.J. 219 795
Martin W L 1976 M.N. 175 633
Massey P L 1975 A.J. 80 778
Materne J 1974 A.&A. 33 451
Matthews T A, Morgan W W & Schmidt M 1964 Ap.J. 140 35
Matthews T A & Sandage A R 1963 Ap.J. 138 30
Mattila K 1977 A.&A. 60 425
Melnick J & Quintana H 1975 Ap.J. 198 L97
Melnick J & Sargent W L W 1977 Ap.J. 215 401
Melnick J, White S D M & Hoessel J 1977 M.N. 180 207
Mills B Y, Slee O B & Hill E R 1960 Austral. J. Phys. 13 676
Mitchell R J, Culhane J L, Davison P J N & Ives J C 1976 M.N. 175 29P
Moore C E 1959 "Atomic Energy Levels" (Nat. Bureau of Standards)
Morgan W W, Kayser S & White R A 1975 Ap.J. 199 545
Morgan W W & Lesh J R 1965 Ap.J. 142 1364
Moss C 1976 Ph.D. thesis, Univ Sussex

Neyman J, Scott E L & Shane C D 1954 App.J. Supp. 1 269
Nilson P 1973 "Uppsala General Catalogue of Galaxies" (Roy. Sci. Soc. Uppsala)

Oemler A 1973 Ap.J. 180 11
-------- 1974 Ap.J. 194 1
-------- 1976 Ap.J. 209 693
Ostriker J P & Hausman M A 1977 Ap.J. 217 L125
Ostriker J P & Tremaine S D 1975 Ap.J. 202 L113

Palmer D R & Milsom A S 1972 Adv. in Electronics & Electron Phys. 33b 769
Partridge R B 1974 I.A.U Symp. 63 157
Pence W 1976 Ap.J. 203 39
Perek L & Kohoutek L 1967 "Catalogue of Galactic Planetary Nebulae"
(Czechoslovak Acad. Sci.)

Richstone D O 1976 Ap.J. 204 642
Rood H J 1965 Ph.D. thesis, Univ. Michigan
Rood H J & Dickel J R 1976 Ap.J. 205 346
Rood H J, Page T, Kintner E & King I 1972 Ap.J. 175 627
Rood H J & Sastry G N 1971 P.A.S.P. 83 313
Rose J A 1976 A.&A.Supp. 23 109
Rubin V C, Thonnard N, Ford W K & Roberts M S 1976 A.J. 81 719

RCBG1 = de Vaucouleurs G & de Vaucouleurs A 1964
RCBG2 = de Vaucouleurs G et al 1976

SAO = Smithsonian Astrophysical Observatory Star Catalog
Sandage A 1973 Ap.J. 183 711
--------- 1975a p761 in Sandage et al (1975)
--------- 1975b Ap.J. 202 563
--------- 1976a A.J. 81 954
--------- 1976b Ap.J. 205 6
--------- 1978 A.J. 83 904
Sandage A, Kristian J & Westphal J A 1976 Ap.J. 205 688
Sandage A, Sandage M & Kristian J 1975 Stars and Stellar Systems XI:
"Galaxies and the Universe" (Univ. Chicago)
Sandage A & Visvanathan N 1978a Ap.J. 223 707
---------- 1978b Ap.J. 225 742

Sargent W L W 1972 Ap.J. 176 581
---------- 1973 P.A.S.P. 85 281
Sastry G N 1968 P.A.S.P. 80 252
Schechter P 1976 Ap.J. 203 297
Serlemitsos P J, Smith B W, Boldt E A, Holt S S & Swank J H
1977 Ap.J. 211 L63
Sérsic J L 1974 Astrophysics & Space Sci. 28 365
Shane C D & Wirtanen C A 1967 Pub. Lick Obs. 22 1
Shapley H 1933 Proc. Nat. Acad. Sci. 19 591
Shapley H & Ames A 1926 Harvard Coll. Obs. Circ. 294
---------- 1932 Harvard Coll Obs. Ann. 88 43
Shobbrook R R 1966 M.N. 131 351
Silk J 1976 Ap.J. 208 646
Simkin S M 1977 A.&A. 55 369
Smith S 1936 Ap.J. 83 23
Snow T P 1970 A.J. 75 237
Solinger A B & Tucker W H 1972 Ap.J. 175 L107
Spinrad H 1977 P.A.S.P. 89 116
Spitzer L & Baade W 1951 Ap.J. 113 413
Stock J & Schueking E 1957 A.J. 62 98
Strom S E & Strom K M 1978 Ap.J. 225 93
Sullivan W T & Johnson P E 1978 Ap.J. 225 751
Swift L 1898 A.Nach. 147 209

Tarter J C 1978 Ap.J. 220 749
Thomas J C & Batchelor D 1978 A.J. 83 1160
Tifft W G 1978 Ap.J. 220 418
Totsuji H & Kihara T 1969 Pubs. Astr. Soc. Japan 21 221
Tremaine S D & Richstone D O 1977 Ap.J. 212 311
Tritton K P 1972 M.N. 158 277
---------- 1977 Revised list (privately circulated)
Turner E L 1976 Ap.J. 208 304
Tytler D & Vidal N V 1978 M.N. 182 33P

van den Bergh S 1976 Ap.J. 206 883
---------- 1977a Vistas in Astronomy 21 71
---------- 1977b P.A.S.P. 89 746

Vidal N V 1975 P.A.S.P. 87 625
--------- 1977 Highlights of Astronomy 4 291
von Humboldt A 1866 "Cosmos" XI p25 (quoted in Zwicky 1957, p81)
Vorontsov-Velyaminov B A, Krasnogorskaja A & Arkipova V P 1962-8
"Morphological Catalogue of Galaxies" (Moscow)

Wegner G 1978 Astrophysics & Space Sci.
West R M 1977 A.&A.Supp. 27 73
Westerlund B E & Wall J V 1969 A.J. 74 335
White S D M 1976 M.N. 174 19
---------- 1977 M.N. 177 717
White S D M & Sharp N A 1977 Nature 269 395
Whiteoak J B 1972 Australian J. Phys. 25 233
Wilson R E 1953 "General Catalogue of Stellar Radial Velocities"
(Carnegie Institute Washington)
Wolf M 1901 A.Nach. 155 127

Yahil A 1974 Ap.J. 191 623
Yahil A & Ostriker J P 1973 Ap.J. 185 787
Yahil A & Vidal N V 1977 Ap.J. 214 347

Zaidel' A N, Prokof'ev V K, Raiskii S M, Slavnyi V A, Schreider E Ya
1970 "Tables of Spectral Lines" (Plenum)
Zwicky F 1933 Helv. Phys. Acta 6 110
-------- 1937 Ap.J. 86 217
-------- 1957 "Morphological Astronomy" (Springer-Verlag)
Zwicky F, Herzog E, Wild P, Karpowicz M & Kowal T C 1961-8 "Catalogue
of Galaxies and Clusters of Galaxies" (C.I.T)

Acknowledgements

This thesis was supervised by Dr J.V. Peach and I thank him and Prof. D.E. Blackwell for their help and support during these 39 months at the Department of Astrophysics. I am grateful to the Science Research Council for a 3 year Studentship and their allocation to me of telescope time and the necessary funds to make use of it. Additional financial help has been provided by the Scott Fund, Corpus Christi College, the Oxford University Committee for Graduate Studies and the Johnson Memorial Fund.

I have relied on the knowledge of the galaxy workers, past and present at Oxford: Jon Godwin, John Peach, Keith Dixon, Tim Austin, Martin Bucknell, Dave Carter and James Binney. In particular, much of the credit for the photographic photometry must lie with Jon Godwin, and I thank him too for his criticisms of my dud astronomy and dud English. Dave Carter has allowed me to make use of his work on the alignment of cD galaxies with their clusters.

Tim Austin and Keith Dixon helped at the telescopes and I thank them for their fortitude in the long, cold nights when things didn't always go as planned. Keith Dixon also helped with the photoelectric reductions. I am grateful to the Directors and staff of the S.A.A.O. for their assistance and hospitality during my observing periods.

My thanks also to the Oxford University Computer Lab., the R.G.O. and the U.K. Schmidt Telescope Unit for their various services. Finally, I would like to thank the Oxford University Parks Department for providing such a splendid view, without which this thesis would have been finished some months ago.